

**Investigation of new candidate genes in a cohort of
patients with familial congenital hypopituitarism and
associated disorders**

Louise Cheryl Gregory

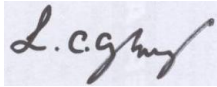
UCL

Doctor of Philosophy

Thesis

Declaration

I, Louise Cheryl Gregory confirm that the work presented in this thesis is my own. Where information has been derived from other sources, I confirm that this has been indicated in the thesis.

A handwritten signature in black ink on a light blue background, reading "L.C. Gregory".

Publication arising from this thesis:

Gregory, L.C., Humayun, K.N., Turton, J.P., McCabe, M.J., Rhodes, S.J., Dattani, M.T. 2015. Novel Lethal Form of Congenital Hypopituitarism Associated With the First Recessive LHX4 Mutation. J Clin Endocrinol Metab. 100(6): 2158-64.

Abstract

Congenital hypopituitarism is a complex variable genetic disorder that is known to be caused by multiple mutated genes, both in isolation and in variably penetrant cases of digenic inheritance. In only <10% of cases, a mutation in a known causative gene has been identified in the patient, leaving the vast majority of patients yet to have a genetic mutation detected that is responsible for the pathogenicity and that has functional significance to their condition. This study investigates novel genes and pathways involved in hypothalamo-pituitary development. Our large cohort of consanguineous and non-consanguineous pedigrees with hypothalamo-pituitary disease are routinely screened for variants in the known causative genes. In pedigrees where there are no variants in these particular genes, exome sequencing in collaboration with GOSgene is carried out to uncover novel genes and regions of interest that are abnormal in the individual. Upon the identification of any novel variant in known or novel genes, functional assays are conducted to further show the significance of the change. Firstly this study identifies the first novel homozygous mutation in the *LHX4* gene, p.T126M, in two deceased brothers from a pedigree with combined pituitary hormone deficiency with subsequent fatal consequences. Functional luciferase assays showed that there was no significant difference between mutant p.T126M and WT constructs in transactivating the α GSU and prolactin promoters, and that mutant LHX4 could synergise with POU1F1 similar to WT LHX4. Secondly, six new candidate genes; *CTPS2*, *RNPC3*, *PRMT6*, *FASN*, *APEX2* and *EIF2S3*, were identified in phenotypically unique pedigrees submitted to GOSgene for exome sequencing. The human embryonic expression profiles of these novel candidate genes were analysed in this study in a hypothalamo-pituitary context, as well as in related tissues that are affected in the individuals. Thirdly, the role of eIF2 γ , encoded by *EIF2S3*, which was found to be mutated in an X-linked pedigree with congenital hypopituitarism, hypothyroidism and hyperinsulinism causing

hypoglycaemia, was investigated in this study. A lentiviral shRNA knock out of the *EIF2S3* gene in human pancreatic cells resulted in significantly higher apoptosis compared to WT cells. This study has used both a Sanger sequencing and an exome sequencing approach to identify novel variants in known and novel candidate genes respectively.

Acknowledgements

I would like to say a huge thank you to Professor Mehul Dattani for employing me in my first science job as his research assistant back in 2009, and for keeping me on all this time. The experience in molecular biology and genetics that I gained from 2009 – 2012 led me to want to undertake a PhD in this interesting subject. My working life would not have been the same, or half as good as it would have been, unless you gave me that lucky break straight after I finished university. I am very grateful for the many opportunities you have given me within this job, especially to travel to all parts of the world to present my data. I would also like to thank Dr Daniel Kelberman for being my second supervisor, who has helped me and given me advice throughout my PhD. I would like to thank a great colleague and friend, Dr Mark McCabe, who in my opinion is one of the best molecular and genetic scientists there is. Thank you for helping me throughout my career and for teaching me many techniques in the lab. Even after you moved back to Australia you have continued to help me on numerous occasions with advice on experiments and I owe a great deal to you. You are the most approachable person I have ever met throughout my whole career, and have never made me feel stupid for asking a question, even if you've thought I was! I would like to thank Dr Sandy Alatzoglou for all her help over the past few years. Thank you for your advice and encouragement, and for educating me in clinical endocrinology, especially for my first oral presentation as a research assistant at the BSPED London meeting in 2011. I think I succeeded in fooling the audience for a whole fifteen minutes that I had been clinically trained!

I would like to thank my Mum and Dad for their constant encouragement, support, love and friendship. You have always inspired me and believed in me, and I am forever grateful. I would like to thank my husband Dave for his love and support over the last ten years. How very lucky I am to have you.

Table of Contents

Abstract	3
Acknowledgements	5
Table of Contents	6
List of Figures	12
List of Tables	15
List of Appendices	17
Abbreviations	18
Chapter 1: Introduction	24
1.1. Hypothalamo-pituitary development	25
1.1.1. The intermediate lobe and posterior lobe	27
1.1.2. The anterior pituitary hormones	28
1.2. Human conditions arising from disordered hypothalamo-pituitary development	32
1.2.1. Isolated growth hormone deficiency	32
1.2.2. Other isolated hormone deficiencies and abnormalities	34
1.2.3. Combined pituitary hormone deficiency	36
1.2.4. Holoprosencephaly	38
1.2.5. Septo-optic dysplasia	42
1.2.6. Hypogonadotropic hypogonadism	44
1.3. Genes implicated in human hypothalamo-pituitary disorders	47
1.3.1. Genetic analysis and known causative genes	47
1.3.2. HESX1	48
1.3.3. SOX2 and SOX3	49
1.3.4. OTX2	52
1.3.5. ARNT2	53

1.3.6.	LHX3 and LHX4	53
1.3.7.	POU1F1 and PROP1	55
1.4.	Investigating the genotype of patients	57
1.4.1.	Genetic analysis	57
1.4.2.	Expression studies	60
1.4.3.	Cohort of patients	61
1.5.	Aims and objectives	62
Chapter 2: Materials and methods		63
2.1.	Primer Design	64
2.2.	PCR and direct sequencing analysis	64
2.3.	Functional Studies for LHX4 variants	66
2.3.1.	Cell culture	66
2.3.2.	Preparation of constructs for qualitative analysis	66
2.3.3.	Western Blot for LHX4 protein	67
2.3.4.	Transfection of constructs for qualitative analysis	67
2.4.	Functional studies for <i>EIF2S3</i>	71
2.4.1.	Cell culture	71
2.4.2.	Constructs containing shRNA cassettes	71
2.4.3.	Lentiviral packaging	73
2.4.4.	Transduction of 1.1B4 cells using packaged LV vectors for stable gene knockdown	73
2.4.5.	Cell lysis and RNA extraction	74
2.4.6.	Reverse transcription	75
2.4.7.	qPCR primer design and analysis	76
2.4.8.	Western Blot analysis – Method used for both LHX4 and EIF2S3 protein analysis	78
2.4.8.1.	Protein extraction	78
2.4.8.2.	Running the gel	78
2.4.8.3.	Transfer	80
2.4.9.	Insulin Secretion Assay	82

2.4.10.	Apoptosis assay	84
2.4.11.	Single site-directed mutagenesis	85
2.4.12.	LV-IRES vector digest	88
2.4.13.	Alkaline Phosphatase treatment	88
2.4.14.	Gel extraction	89
2.4.15.	Amplification of the <i>EIF2S3</i> insert	89
2.4.16.	Polyadenylation	91
2.4.17.	TA-Cloning: Ligation of the cDNA <i>EIF2S3</i> _WT insert into the pGEM-T Easy vector	92
2.4.18.	Transformation of pGEM-T Easy vector	93
2.4.19.	Enzyme digest to cut out inserts from p.GEM-T vector	95
2.4.20.	Ligation of <i>EIF2S3</i> into LV-IRES vector	96
2.4.21.	Multi-site-directed mutagenesis	96
2.4.22.	Transfection of the <i>EIF2S3</i> constructs	101
2.4.23.	Cell sorting	101
2.5.	<i>In situ</i> hybridization	102
2.5.1.	Linearizing plasmids	102
2.5.2.	DIG probe transcription	102
2.5.3.	Human embryonic sections	104
2.5.4.	Pre-hybridisation treatment	104
2.5.5.	Hybridisation	104
2.5.6.	Post-hybridisation washing	105
2.5.7.	Antibody detection	105
Chapter 3: Novel lethal form of congenital hypopituitarism associated with the first recessive <i>LHX4</i> mutation		107
3.1.	Introduction	108
3.1.1.	Pedigree 1	108
3.2.	Results	115
3.2.1.	Mutational analysis	115
3.2.2.	Western blot analysis	118

3.2.3.	Protein prediction modelling	119
3.2.4.	Gene activation assays	121
3.2.4.1.	Non-parametric tests: Part 1	121
3.2.4.2.	Non-parametric tests: Part 2	122
3.2.4.3.	Non-parametric tests: Part 3	124
3.2.4.4.	Parametric tests: Two tailed unpaired T-tests	127
3.3.	Discussion	130
3.4.	Conclusion	135

Chapter 4: New candidate genes identified through exome sequencing and their expression profiles in a phenotype-related context **136**

4.1.	Introduction	137
4.2.	CTPS2	139
4.2.1.	Pedigree 2	139
4.2.2.	Exome sequencing results: <i>CTPS2</i>	139
4.2.3.	<i>CTPS2</i> function	140
4.2.4.	<i>CTPS2</i> expression results	142
4.3.	RNPC3 and PRMT6	145
4.3.1.	Exome sequencing results of Pedigrees 3-6	145
4.3.2.	RNPC3 function	149
4.3.3.	<i>RNPC3</i> expression results	153
4.3.4.	PRMT6 function	157
4.4.	FASN and APEX2	160
4.4.1.	Pedigree 7	160
4.4.2.	Exome sequencing results: <i>FASN</i> and <i>APEX2</i>	161
4.4.3.	<i>FASN</i> function	163
4.4.4.	<i>FASN</i> expression results	164
4.4.5.	<i>APEX2</i> function	166
4.4.6.	<i>APEX2</i> expression results	167
4.5.	Discussion	170
4.5.1.	Pedigree 2: Discussion	170

4.5.2.	Pedigree 3-6: Discussion	171
4.5.3.	Pedigree 7: Discussion	172
4.6.	Summary of expression profiles	174
4.7.	<i>EIF2S3</i>/eIF2γ	175
4.7.1.	Exome sequencing of the X chromosome in Pedigree 8	175
4.7.2.	<i>EIF2S3</i> expression results	177
Chapter 5: A Novel Mutation in Eukaryotic Translation Initiation Factor 2 Subunit 3		
(<i>EIF2S3</i>) Associated with Severe Hypoglycaemia and X-Linked Hypopituitarism		
		180
5.1.	Introduction	181
5.1.1.	Patients in Pedigree 8	183
5.1.1.1.	The three affected males	183
5.1.1.2.	Patient IIIc	183
5.1.1.3.	Twin brothers: patients III d and III e	184
5.1.2.	<i>EIF2S3</i>	192
5.2.	Results	201
5.2.1.	Cohort screening	201
5.2.2.	<i>EIF2S3</i> knock down	201
5.2.3.	qPCR analysis	203
5.2.4.	Western Blot Analysis	206
5.2.5.	Insulin secretion ELISA assay	208
5.2.6.	Apoptosis Caspase 3/7 Assay	211
5.2.6.1.	Non-parametric tests	213
5.2.6.2.	Two-way ANOVA test	215
5.2.6.3.	Parametric tests: Two tailed unpaired T-tests	216
5.2.7.	The <i>EIF2S3</i> (p.P432S) mutant	217
5.3.	Discussion	221
5.3.1.	Cell line choice and insulin secretion assay	221
5.3.2.	<i>EIF2S3</i> expression	223
5.3.3.	<i>EIF2S3</i> /eIF2 γ	224
5.4.	Future work investigating the function of eIF2γ	229

5.4.1. Transfection assays	229
5.4.2. Luciferase assays	230
5.4.3. Binding assays	232
5.4.4. Mouse-models	233
Chapter 6: General discussion	235
6.1. Summary of findings	236
6.2. Future work	237
6.3. Genetic screening methods	243
6.4. Control databases	246
6.5. Variable penetrance	249
6.6. Human embryonic sections	250
6.7. Genetic counselling	251
Appendices	255
References	269

Figures

Figure 1.1: The pituitary gland and its position within the brain

Figure 1.2: Development of the murine pituitary gland

Figure 1.3: A basic overview of the temporal expression of different genes during embryonic murine pituitary development

Figure 1.4: MRI scans of holoprosencephaly patients

Figure 1.5: A summary of the gene screening process

Figure 2.1: Constructs transfected into HEK293T cells

Figure 2.2: A summary of the cloning process

Figure 3.1: Pedigree 1 harbouring the *LHX4* (p.T126M) variant

Figure 3.2: The MRI scan of patient IIIb and chest X-rays of patients IIIa and IIIb from Pedigree 1

Figure 3.3: The electropherogram and conservation of the *LHX4* (p.T126M) variant

Figure 3.4: A schematic diagram of the *LHX4* protein

Figure 3.5: *LHX4* western blot analysis

Figure 3.6: A protein prediction model of the *LHX4* (p.T126M) variant

Figure 3.7: Transient transfection gene activation assays in HEK293T cells using the *LHX4* (p.T126M) variant

Figure 4.1: Pedigree 2 with the patient harbouring the *CTPS2* (p.F166L) variant

Figure 4.2: Conservation of the substituted *CTPS2* residue

Figure 4.3: *CTPS2* expression in the developing hypothalamic-pituitary axis, eyes and lungs during human embryogenesis

Figure 4.4: *CTPS2* expression in the developing ear

Figure 4.5: Pedigrees 3-6 harbouring the *RNPC3* (p.L483F) and *PRMT6* (p.P350R) variants

Figure 4.6: Conservation of the substituted *RNPC3* and *PRMT6* residues

Figure 4.7: A comparison of the steps during the formation of the U2- and U12-type spliceosome

Figure 4.8: Human embryonic tissue sections from the ovary and developing kidney

Figure 4.9: *RNPC3* expression in the developing hypothalamic-pituitary axis and the ovary during human embryogenesis

Figure 4.10: *PRMT6* transcriptional repression

Figure 4.11: Pedigree 7 with the patient harbouring the *FASN* (p.A2132V) and *APEX2* (p.M422V) variants

Figure 4.12: Conservation of the substituted *FASN* and *APEX2* residues

Figure 4.13: *FASN* expression in the hypothalamo-pituitary axis and the eye in the developing human embryo

Figure 4.14: *APEX2* expression in the hypothalamo-pituitary axis, oral cavity and the eye in the developing human embryo

Figure 4.15: *APEX2* expression in developing human embryonic tissues

Figure 4.16: Conservation of the substituted eIF2 γ residue

Figure 4.17: Human *EIF2S3* expression in the hypothalamo-pituitary axis, eye and pancreas in the developing human embryo

Figure 5.1: Pedigree 8 harbouring the *EIF2S3* (p.P432S) variant

Figure 5.2: The growth charts from the three affected males from Pedigree 8, IIIc, IIIId, IIIe

Figure 5.3: The MRI scans from the three affected males, IIIc, IIIId, IIIe

Figure 5.4: Domain structure of human eIF2 α -, β -, and γ -subunits

Figure 5.5: Eukaryotic initiation factor 2 (eIF2): The role of eIF2 in the initiation of mRNA translation

Figure 5.6: Formation of the eIF2 ternary complex stimulated by insulin

Figure 5.7: qPCR *EIF2S3* expression results in cDNA populations

Figure 5.8: Western blot analysis using the anti-EIF2S3 primary antibody

Figure 5.9: Insulin secretion assay in MIN6 cells

Figure 5.10: A pilot apoptosis assay performed on WT untransduced MIN6 and 1.1B4 cells

Figure 5.11: Apoptosis assay comparing caspase activity in *EIF2S3* KO cells compared to controls, with and without cytokine treatment

Figure 5.12: Amplification of the *EIF2S3* cDNA insert

Tables

Table 1.1: Genetic causes of isolated hypogonadotropic hypogonadism (IHH) and Kallmann syndrome (KS)

Table 2.1: RNA concentrations derived from transfected cells

Table 2.2: The volume of RNA and reagents used in reverse transcription

Table 2.3: Volumes and concentrations of reagents and primers used in qPCR

Table 2.4: The calculation of protein samples used in the pilot western blot assay

Table 2.5: How to make KRB buffer

Table 2.6: Insulin secretion assay test agents

Table 2.7: The volume of reagents used to digest the LV-IRES vector

Table 2.8: Amplification of the *EIF2S3* cDNA insert

Table 2.9: *EIF2S3* ligation into the pGEM-T Easy vector

Table 2.10: Enzyme digest reaction

Table 2.11: Multi-site directed mutagenesis

Table 2.12: Details of IMAGE cDNA clones used in *in situ* experiments

Table 3.1: Endocrinology and phenotypes of the three patients in Pedigree 1

Table 3.2: Protein prediction models used for the LHX4 (p.T126M) variant

Table 5.1: Clinical data from the three affected males in Pedigree 8; IIIc, IIIId, IIIe

Table 5.2: Clinical data following gonadotrophin tests from the three affected males in Pedigree 8, IIIc, IIIId, IIIe

Table 5.3: Glucose tolerance test in patient IIIId

Table 5.4: qPCR *EIF2S3* expression results in cDNA populations

Table 5.5: BCA assay quantification

Appendices

Appendix 1: Transactivation assays investigating the *LHX4* (p.T126M) variant

Appendix 2: Flowchart showing the exome sequencing data filtering process

Appendix 3: Exome sequencing filtering results from Pedigrees 2-7

Appendix 4: Genotypes and phenotypes of patients in Pedigrees 2-7

Appendix 5: Raw mean average data and statistical tests of apoptosis assays

Appendix 6: Clinical phenotypes of male patients with *EIF2S3* mutations from three separate studies

Abbreviations

1L-1 β	Interleukin 1 beta
5FU	5-fluorouracil
α GSU	Glycoprotein hormones alpha subunit
ACTH	Adrenocorticotrophic hormone
Akt/c-Met	v-akt murine thymoma viral oncogene homolog/ MET proto-oncogene,
AP	Anterior pituitary
APH	Anterior pituitary hypoplasia
ARNT2	Aryl-hydrocarbon receptor nuclear translocator 2
AVP	Arginine vasopressin
AVPD	Arginine vasopressin deficiency
BCA	Bicinchoninic acid assay
BCIP	Bromo-chloro-indolyl-phosphate
BER	Base excision repair
BSA	Bovine Serum Albumin
CACH	Central nervous system hypomyelination
CC	Corpus callosum
CF	Cystic fibrosis
CGH	Comparative genomic hybridization
CH	Congenital hypopituitarism
CIAP	Calf intestinal alkaline phosphatase
CMV	Cytomegalovirus
CNS	Central nervous system
CNV	Copy number variant
CPHD	Combined pituitary hormone deficiency
CRF	Corticotrophin-releasing factor
CRISPR	Clustered regularly interspaced short palindromic repeats

CS	Carnegie stage
CXR	Chest X-ray
DEPC	Diethylpyrocarbonate
DIG	Digoxigenin
DMEM	Dulbecco's Modified Eagle Medium
DMSO	Dimethyl sulfoxide
DNA	Deoxyribonucleic acid
DNA-PK	DNA-dependent protein kinase
dNTPs	Deoxyribonucleotide triphosphate
E	Embryonic day
EDTA	Ethylenediaminetetraacetic acid
eEF	Eukaryotic elongation factors
EIF2S3	Eukaryotic translation initiation factor 2 subunit 3
EPP	Ectopic posterior pituitary
ER	Estrogen receptor
ES	Embryonic stem
EV	Empty vector
FASN	Fatty acid synthase
FCS	Fetal calf serum
FSH	Follicle-stimulating hormone
GA	Gestation age
GH	Growth hormone
GHRHR	Growth hormone-releasing hormone receptor
GLI2	GLI-family zinc finger 2
GnRH	Gonadotrophin-releasing hormone
GTP	Guanosine triphosphate
HBSS	Hanks Balanced Saline Solution
HC	Head circumference

HCG	Human chorionic gonadotrophin
HDBR	Human Developmental Biology Resource
HEK	Human embryonic kidney
HH	Hypogonadotropic hypogonadism
HMG	High mobility group
HPE	Holoprosencephaly
HRP	Horseradish peroxidase
HSV-TK	Herpes simplex virus thymidine kinase
IAD	Isolated Adrenocorticotrophic hormone deficiency
IBMX	Isobutylmethylxanthine
ICH	Institute of Child Health
ID	Intellectual disability
IGF1	Insulin-like growth factor
IGFBP3	Insulin-like growth factor-binding protein 3
IgG	Immunoglobulin G
IGHD	Isolated growth hormone deficiency
IHH	Isolated hypogonadotropic hypogonadism
IL-6	Interleukin-6
INF- γ	Interferon gamma
IPTG	Isopropyl β -D-1-thiogalactopyranoside
KRB	Krebs Ringer Bicarbonate
KS	Kallmann syndrome
LB	Liquid broth
LH	Luteinizing hormone
LV	Lentiviral
M	Molar
Met-tRNAi	Initiator methionyl-tRNA
MGI	Mouse genome informatics

MIN6	Mouse insulinoma pancreatic beta cells
Mins	Minutes
MO	Morpholino
MOI	Multiplicity of infection
MPHD	Multiple pituitary hormone deficiency
MRI	Magnetic resonance imaging
MSH	Melanocyte-stimulating hormone
NADPH	Nicotinamide adenine dinucleotide phosphate
NBT	Nitro-blue-tetrazolium-chloride
N-COR	Nuclear corepressor
NF- κ B	Nuclear factor-kappa B
NHLBI	National Heart, Lung, and Blood Institute
NSPC	Neural stem and progenitor cells
ONH	Optic nerve hypoplasia
OTX2	Orthodentic homeobox 2
PBS	Phosphate buffered saline
PCR	Polymerase chain reaction
pcw	Post conception week
PFA	Paraformaldehyde
pGIPZ	GFP-IRES-Puromycin-Zeomycin plasmids
PHE	Public Health England
PK	Protein kinase
POMC	Proopiomelanocortin
POU1F1	POU Class 1 Homeobox 1
POU-H	POU homeodomain
POU-S	POU-specific domain
PRLD	Isolated prolactin deficiency
Prl-Luc	Prolactin-luciferase

PRMT6	Protein arginine methyltransferase 6
PVA	Polyvinyl alcohol
RDS	Respiratory distress syndrome receptor tyrosine kinase
rGH	Recombinant growth hormone
rhGH	Recombinant human growth hormone
RLT	RNeasy lysis buffer
RNA	Ribonucleic acid
RNPC3	RNA-binding region (RNP1, RRM) containing 3
RPMI	Roswell Park Memorial Institute
RQ	Relative quantification
RRM	RNA recognition motifs
S.O.C	Super optimal broth with catabolite repression
SD	Standard deviation
SDS	Sodium dodecyl sulfate (practical scientific definition)
SDS	Standard deviation score (clinical definition)
SHBG	Sex hormone-binding globulin
SHH	Sonic hedgehog
shRNA	Short hairpin ribonucleic acid
SNP	Single nucleotide polymorphisms
snRNA	Small nuclear RNA
SNV	Single-nucleotide variant
SOD	Septo-optic dysplasia
SSC	Saline-sodium citrate
SV	Structural variant
T ₃	Triiodothyronine
T ₄	Thyroxine
TLE1	Transducing-like enhancer of split 1

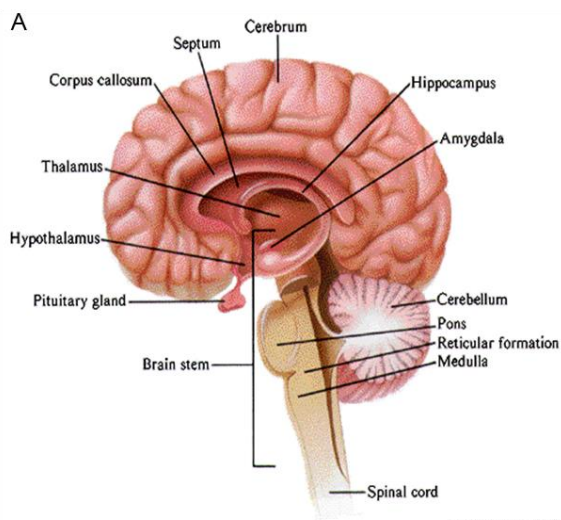
Tm	Temperature
TNF- α	Tumour necrosis factor alpha
TRH	Thyrotrophin releasing hormone
Tris HCl	Trizma hydrochloride
tRNA	Transfer RNA
TSH	Thyroid-stimulating hormone
TSHD	Thyroid-stimulating hormone deficiency
V	Volts
VA	Ventricular asymmetry
VWM	Vanishing white matter
WML	White matter loss
WT	Wild-type
XSCID	X-linked severe combined immune deficiency

Chapter 1

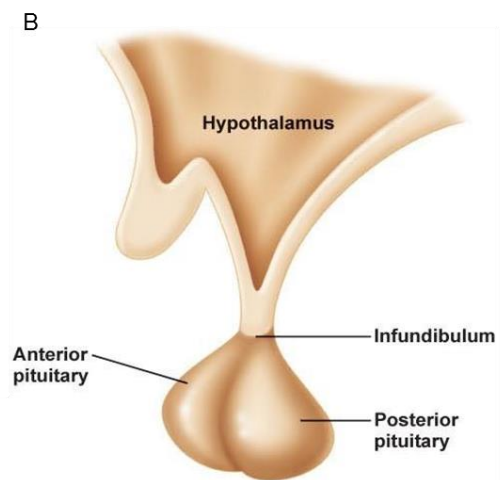
Introduction

1.1. Hypothalamo-pituitary development

The pituitary gland is a major endocrine gland, also known as the hypophysis, the function of which is to control growth, metabolism, reproduction and development. It regulates the function of other endocrine glands in the body. The pituitary gland is situated within the sella turcica recess of the sphenoid bone at the base of the brain and is made up of three lobes; the anterior, intermediate and posterior (Figure 1.1) that have a dual embryonic origin. The anterior and intermediate derive from the oral ectoderm, whilst the posterior originates from the neural ectoderm (see Figure 1.2 for murine pituitary development, similar to human embryogenesis) (Cohen, 2012, Bancalari et al., 2012). Hypothalamo-pituitary development is determined by the communication between the oral and overlying neural ectoderm. This occurs through a complex spatio-temporal genetic cascade of transcription factors and signalling molecules that may be either intrinsic or extrinsic to the developing Rathke's pouch, the primordium of the anterior pituitary (AP) (Kelberman et al., 2009), which when fully developed will become a central regulator of growth, reproduction and homeostasis (Davis et al., 2010).



www.usmanscience.com



www.Emaze.com

Figure 1.1: The pituitary gland and its position within the brain. Diagrams taken and adapted from two different web pages respectively; (www.usmanscience.com, www.Emaze.com). **(A)** A schematic diagram showing the location of different segments of the brain. **(B)** An enlarged diagram of the pituitary gland showing the anterior and posterior lobes, and their link to the hypothalamus via the infundibulum.

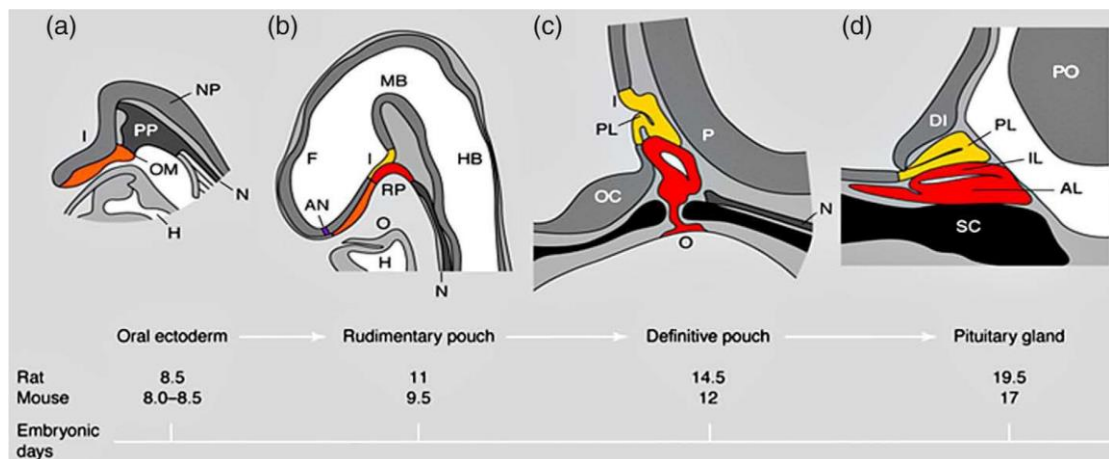


Figure 1.2: Development of the murine pituitary gland. Taken from Sheng *et al.* (Sheng *et al.*, 1997), animated sagittal sections during mouse embryonic development. **(a)** At E8.5 the thickening of the oral ectoderm signifies the onset of pituitary organogenesis. **(b)** Twenty four hours later the rudimentary pouch invaginates towards the overlying ventral diencephalon. **(c)** The definitive Rathke's pouch is formed as its connection to the oral ectoderm is severed. The posterior pituitary forms by the infundibulum evaginating from the ventral diencephalon. **(d)** Progenitors of the hormone-secreting cell types proliferate and terminally differentiate to produce the mature pituitary gland consisting of the anterior lobe, intermediate lobe and posterior lobe. E = Embryonic day; I = infundibulum; NP = neural plate; N = notochord; PP = pituitary placode; OM = oral membrane; H = heart; F = forebrain; MB = midbrain; HB = hindbrain; RP = Rathke's pouch; AN = anterior neural pore; O = oral

cavity; PL = posterior lobe; OC = optic chiasm; P = pontine flexure; PO = pons; IL = intermediate lobe; AL = anterior lobe; DI = diencephalon; SC = sphenoid cartilage.

1.1.1: The intermediate lobe and posterior lobe

The intermediate lobe contains a group of endocrine cells called the melanotrophs that essentially synthesise a precursor protein called proopiomelanocortin (POMC). This in turn generates biologically active peptides, such as adrenocorticotrophic hormone (ACTH), endorphins and melanocyte-stimulating hormone (MSH), through proteolytic cleavage (Lamacz et al., 1991). In humans, by adulthood the intermediate lobe is either very small or totally absent. The posterior lobe of the pituitary contains neuronal axon projections which stem from magnocellular neurosecretory cell bodies that reside in the hypothalamus. Two main hormones are synthesised in these hypothalamic nuclei; arginine vasopressin (AVP) in the supraoptic nuclei and oxytocin in the paraventricular nuclei, which in turn travel via the hypothalamo-neurohypophyseal tract and short portal vessels to the posterior lobe of the pituitary where they are released (Zimmerman and Antunes, 1976, Duncan and Shipston, 2016).

A series of tightly regulated steps that result in cell proliferation and differentiation, give rise to the five different specialized AP cell types that secrete six different hormones: somatotrophs [growth hormone (GH)], thyrotrophs [thyroid-stimulating hormone (TSH)], gonadotrophs [luteinizing hormone (LH) and follicle-stimulating hormone (FSH)], lactotrophs [prolactin (PRL)] and the corticotrophs [adrenocorticotrophic hormone (ACTH)] (Figure 1.3) (Alatzoglou and Dattani, 2009).

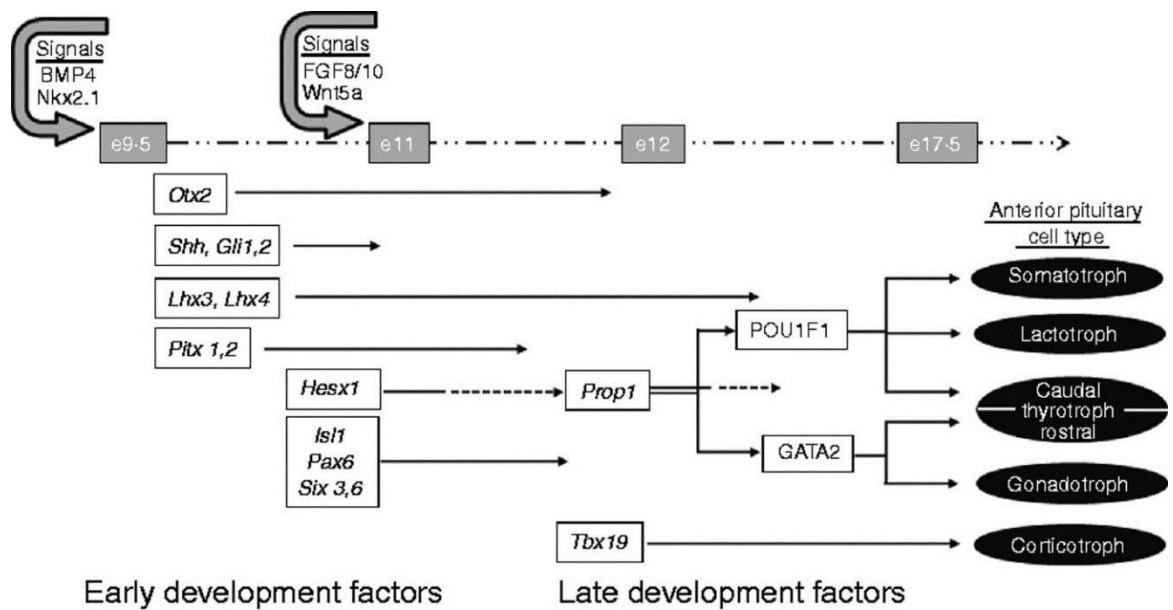


Figure 1.3: A basic overview of the temporal expression of different genes during embryonic murine pituitary development. A spatio-temporal genetic cascade of transcription factors and signalling molecules, culminating in the differentiation of the five anterior pituitary cell types. Image taken from Romero CJ *et al* (Romero *et al.*, 2011).

1.1.2. The anterior pituitary hormones

The synthesis of each one of the six anterior pituitary hormones is stimulated by specific ligands. Many of these ligands are released from the hypothalamus that then travel via the hypophyseal portal system into the bloodstream, a transport system that allows rapid communication and migration of hormones to the anterior pituitary. The ligands bind to their respective receptors on each specific anterior pituitary cell type, giving rise to the six hormones that have distinct roles in endocrine regulation elsewhere in the body. The stimulation of each anterior pituitary cell type, the hormones secreted, and their role in the maintenance of growth, reproductive development and homeostasis, are discussed in this section.

The growth hormone-releasing hormone receptor (*GHRHR*), expressed on somatotroph cells, binds its ligand GHRH that is released from the hypothalamus. Binding to the receptor results in the synthesis and release of GH, in the presence of the transcription factor POU1F1 (Iguchi et al., 1999). GH then binds to its receptors on target tissues, primarily the liver, leading to the release of insulin-like growth factor 1 (IGF1) and its binding protein, IGFBP3, which in turn form a ternary complex with the acid-labile subunit (ALS), to promote cell growth through mitosis, with inhibition of apoptosis (Boisclair et al., 2001, Baxter and Dai, 1994). In addition to the promotion of growth, IGF1 stimulates glucose uptake from the blood, enhances glucose utilization by peripheral tissues, and suppresses hepatic glucose production in a similar manner to insulin (Boulware et al., 1992). Hypothalamic thyrotrophin releasing hormone (TRH) binds to its receptor on the thyrotroph cells of the pituitary. It stimulates gene expression of the TSH β subunit, and the conjugation of TSH α and β subunits to form TSH molecules, as well as regulating its glycosylation which results in TSH secretion from the thyrotrophs. TSH then binds with receptors on the thyroid gland to stimulate the production of the thyroid hormone, thyroxine (T₄), which can feed back to the hypothalamus and pituitary to inhibit the production and secretion of TRH and TSH. Additionally, T₄ is converted into triiodothyronine (T₃) via deiodinase enzymes, type I and II (D1 and D2), and enters cell nuclei to bind to thyroid receptor α and β isoforms that are differentially expressed in tissues, thereby regulating gene transcription (Yamada and Mori, 2008). The thyroid hormones are essentially required for normal development, the regulation of metabolism, linear growth and bone maintenance.

During embryogenesis, gonadotrophin-releasing hormone (GnRH) neurons migrate with olfactory neurons from the olfactory placode to their normal position in the hypothalamus (Wierman et al., 2004). GnRH is secreted from the hypothalamus in a pulsatile fashion, to bind to its receptors (GnRHR) on the gonadotroph cells, thereby

stimulating the release of the gonadotrophins, LH and FSH. Following the withdrawal of placental steroids at birth, gonadotrophins rise and remain elevated for the first 1–2 years in girls, and first 6 months in boys, with a subsequent decrease during the remainder of childhood. Pulsatile gonadotrophin secretion then resumes again at puberty, with pulses occurring approximately every two hours in adult males. In females, the pulses are more variable, depending on the time of the menstrual cycle (McCartney, 2010, Ehlers et al., 2013). LH and FSH bind to receptors on the reproductive organs, the testes and the ovaries, stimulating sex steroid production. In men, LH stimulates Leydig cells to produce testosterone, which in turn provides negative feedback to both the anterior pituitary and the hypothalamus. FSH release stimulates the Sertoli cells in men to produce sex hormone-binding globulin (SHBG) and inhibin, thereby stimulating spermatogenesis and giving negative feedback to the anterior pituitary to decrease FSH secretion, respectively (Jin and Yang, 2014). In women, there is a surge of LH and FSH that triggers ovulation during the mid-cycle of menstruation, where the oocyte lives for up to only 24 hours without fertilisation. FSH stimulates the ovaries to produce oestrogen, with the most potent and prevalent oestrogen being oestradiol, during the follicular phase, and LH stimulates progesterone from the corpus luteum during the luteal phase of the menstrual cycle. Oestrogen is part of a negative feedback loop to the hypothalamus that inhibits gonadotrophin release (Hillier, 2001).

In contrast to the other anterior pituitary hormones so far discussed, the production of prolactin is normally suppressed by a hypothalamic hormone, dopamine, rather than stimulated by one. Dopamine binds to its receptors on the lactotroph cells and thus inhibits prolactin secretion. Therefore when this suppression is interrupted by specific hormones, which interfere with dopamine secretion or receptor binding, it leads to an enhanced secretion of prolactin (Torre and Falorni, 2007). Thus, if transcription factors and signalling molecules involved in prolactin regulation are

mutated, then respective disorders more often elicit an increase in prolactin, diagnosed in patients as hyperprolactinaemia (Turankar et al., 2013), rather than a decrease as seen in most other anterior pituitary hormone abnormalities. Prolactin is positively regulated by TRH, GnRH, vasoactive intestinal polypeptide, and oestrogen. The latter increases in the blood stream in late pregnancy, elevating concentrations of prolactin, thus preparing the mammary glands at the end of gestation for lactation after delivery of a baby. Furthermore, prolactin has a multitude of roles in reproduction other than lactation, in addition to possessing multiple homeostatic roles (Freeman et al., 2000, Guclu et al., 2015).

The release of ACTH, also known as corticotrophin, from corticotroph cells, is stimulated by vasopressin and catecholamines, but most potently by corticotrophin-releasing factor (CRF) released from the hypothalamus. CRF activates both adenylate cyclase and cAMP-dependent protein kinase to stimulate ACTH secretion. CRF also upregulates *POMC* expression, the precursor of ACTH within the anterior pituitary (Reisine et al., 1985). In contrast ACTH secretion in the corticotrophs is negatively regulated by serum glucocorticoids (Birnberg et al., 1983). The main essential role of ACTH is to stimulate cortisol production and release from the cortex of the adrenal gland in a circadian rhythm. Thus, concentrations of ACTH are generally higher in the morning and fall throughout the day, in conjunction with cortisol release. Moreover, ACTH has additional roles in the production of various chemical compounds that trigger an increase in other hormones, such as adrenaline and noradrenaline. As cortisol concentrations rise in the bloodstream, a negative feedback loop to the hypothalamus slows CRF release, thereby decreasing ACTH production and its stimulating abilities on cortisol. This is counteracted by physical or psychological stress, which inhibits this feedback, thus stimulating cortisol secretion once again (Dallman, 2005).

1.2. Human conditions arising from disordered hypothalamo-pituitary development

Congenital hypopituitarism (CH) is a syndrome with a wide variation in severity, which may present early in the neonatal period or later in childhood. CH is characterized by deficiencies in one or more of these 6 hormones mentioned above, with GH being the predominant hormone deficiency, often seen in isolation (Kelberman et al., 2009). Midline and craniofacial structural abnormalities are often associated with CH, giving rise to a range of characterized disorders; from incompatibility with life, to holoprosencephaly (HPE), septo-optic dysplasia (SOD) and hypogonadotropic hypogonadism (HH) (McCabe et al., 2011b). Thus disordered embryogenesis can cause variable phenotypes involving a range of craniofacial midline defects, associated with hypothalamo-pituitary disorders. The isolated and combined deficiencies, and the spectrum of these disorders are discussed in this chapter.

1.2.1. Isolated growth hormone deficiency

The most common isolated deficiency is congenital isolated GH deficiency (IGHD) with an incidence varying between 1/4000 to 1/10,000 live births. The majority of cases are sporadic with a small percentage (3-30%) of familial cases, although for most patients its aetiology remains unknown (Alatzoglou et al., 2015, Alatzoglou et al., 2014b). IGHD essentially involves short stature ranging from moderate to severe, delayed growth velocity, and delayed skeletal maturation. Children with GHD are treated with recombinant human GH (rhGH), and generally respond well to this treatment (Alatzoglou et al., 2014b). Heterozygous dominant negative mutations in the *GH1* gene usually affect splicing and lead to the most common autosomal dominant form of GHD, known as type II GHD. Exon skipping occurs as a result of such mutations, in which one exon is essentially missed out of the transcript. For example one such shorter GH isoform of 17.5kDa has been reported to exert a dominant negative effect on GH secretion, of which expression levels directly relate

to the severity of the disorder (Ryther et al., 2003). GHD type II patients have variable height deficit and severity of GHD, and may develop additional pituitary hormone deficiencies over time, including ACTH, TSH and gonadotrophin deficiencies (Alatzoglou et al., 2015). Autosomal recessive IGHD type IA present with severe growth failure in the first 6 months of life with undetectable GH concentrations, and patients frequently develop anti-GH antibodies after receiving exogenous GH. These antibodies can prevent the growth response that is usually expected after patients receive rhGH therapy (Cogan and Phillips, 2006). Patients with IGHD type IA were first described to have homozygous *GH1* deletions (Wagner et al., 1998); however, other severe loss of function *GH1* gene mutations have since been described in such cases. Patients with severe autosomal recessive type IB GHD, also known as Sindh dwarfism (Baumann and Maheshwari, 1997), often have mutations in the *GHRHR* gene, which is more common in pedigrees from Brazil or the Indian subcontinent (Baumann, 1999), that are often consanguineous. This GHD type IB elicits a phenotype that is not of the classic IGHD phenotype, in that these patients have minimal facial hypoplasia and no microphallus, but do manifest anterior pituitary hypoplasia (APH) on their magnetic resonance imaging (MRI) (Shohreh et al., 2011). The vast majority of *GHRHR* mutations have a complete loss of function that usually affects cAMP production, such as p.K329E which failed to show any cAMP response following GHRH treatment in *in vitro* studies (Salvatori et al., 2002). However a recent study performed by myself and colleagues described a novel partial loss of function homozygous *GHRHR* mutation, p.P79L, which gives rise to an unusually mild form of IGHD in two unrelated families. The patients were compound homozygous, with the second homozygous variant in *GHRHR*, p.R4Q, suggesting a possible founder effect of these variants in patients with IGHD that originates from a certain area of South-East Asia (Gregory et al., 2016). In addition to *GH1* and *GHRHR*, mutations have occasionally been described in IGHD patients in genes encoding early (*HESX1*,

SOX2, *SOX3* and *OTX2*) or late (*PROP1* and *POU1F1*) transcription factors (Alatzoglou et al., 2014b, Ashkenazi-Hoffnung et al., 2010, Thomas et al., 2001)

1.2.2. Other isolated hormone deficiencies and abnormalities

Congenital functional failure of a single lineage has been reported for all pituitary cell types, giving rise to isolated hormone deficiencies other than IGHD, such as isolated TSH deficiency (TSHD), isolated gonadotrophin (LH and FSH) deficiency; namely isolated HH (IHH) (discussed in section 1.2.6), isolated ACTH deficiency (IAD) and very rarely isolated PRL deficiency (PRLD) (Douchi et al., 2001). As briefly mentioned, abnormalities associated with prolactin are more often due to an increase as opposed to a decrease in the hormone. Hyperprolactinaemia may emanate from a prolactinoma, a benign prolactin-secreting tumour in the lactotroph cells, or is sometimes apparent in pregnancy when production of prolactin is above the normal threshold. There is a higher prevalence for this condition in women, not only due to problems during pregnancy, but also due to the fact that most prolactinomas are present in women rather than men. Phenotypic features of this disorder include sexual dysfunction and infertility, neurological and visual problems, and headaches (Hayes et al., 2000). Interestingly, hyperprolactinaemia has also been reported in some patients with primary hypothyroidism (Bahar et al., 2011). Patients with the latter have elevated TRH concentrations, which are therefore directly thought to be the cause of the prolactin upregulation (Croissandeau et al., 1994). Although rare, isolated PRLD may occur and clinically manifests only in women as a failure in puerperal alactogenesis; namely the production of milk in breastfeeding (Kauppila, 1997). There have been very few reports of this, one such familial case involved a mother and daughter who between them had eight pregnancies all followed by puerperal alactogenesis that resulted from isolated PRLD (Zargar et al., 1997). The etiology of isolated PRLD is yet unknown and candidate genes often screened are those found to be mutated in patients with PRLD as part of combined pituitary hormone deficiency

(CPHD) that are known to be involved in the lineage differentiation of lactotroph cells, such as *POU1F1*, *PROP1*, *LHX3*, *LHX4*, *HESX1*, and *OTX2* transcription factors (Iwama et al., 2013). PRLD, also termed hypoprolactinaemia, may also result from a hypophysectomy; surgical removal of the pituitary gland often performed to treat craniopharyngiomas, or from pharmacological suppression of the pituitary, which in turn have been reported to adversely affect the luteal phase of the menstrual cycle (Kauppila et al., 1988). A recent report identified elevated autoantibodies in an isolated PRLD patients' serum that specifically recognized a subset of PRL-secreting cells but not PRL itself or any other pituitary cells or hormones, thus uncovering a new autoimmune etiology for the condition (Iwama et al., 2013).

In TSHD inadequate thyroid hormone biosynthesis occurs, due to defective stimulation of the thyroid gland by TSH, therefore causing central, or secondary, hypothyroidism in the patient. In some rare cases, mutations in genes controlling the TSH biosynthetic pathway, *TSHB*, *TRHR*, *IGSF1*, have been described in patients with isolated TSHD (Garcia et al., 2014). *IGSF1* mutations have been reported to be responsible for an X-linked type of central hypothyroidism associated with macroorchidism (Sun et al., 2012); however this latter phenotypic feature is not present in all patients with such mutations (Hughes et al., 2016). Interestingly, parental heterozygous female carriers of these *IGSF1* mutations may sometimes manifest mild hypothyroidism (Joustra et al., 2013). Lastly, IAD is a very rare heterogeneous condition making diagnosis very difficult, due to the varied clinical presentation. It can be a lethal condition due to the hypocortisolism, and has in turn been known to cause neonatal hypoglycaemia, convulsions, hypercalcaemia and/or cholestasis that can reach a 20% mortality rate in the latter if unrecognised (Alsaleem et al., 2016) (Bigos and Carnes, 1982). IAD patients have also presented with an empty sella and severe hyponatraemia. Usually patients with an empty sella remain asymptomatic, however in those who develop IAD, corticosteroid treatment should be

commenced to avoid fatal consequences (Doroftei et al., 2016). The *TBX19* gene has a critical role in the terminal differentiation of the corticotroph and melanotroph cell types, the pituitary POMC lineages. Mutations in *TBX19* have been associated with IAD, and been found in up to 2/3 of neonatal cases, with complete or severe loss of function in DNA binding and/or transactivation (Lamolet et al., 2001). These *TBX19* mutations are most often substitutions in the DNA binding Tbox domain, thus producing impaired DNA binding or protein-protein interaction. However premature stop codons, aberrant splicing and chromosomal deletions have also occurred in this gene (Couture et al., 2012). Mutations in the *POMC* gene have also been reported in IAD, in which patients usually have the distinct phenotypic hallmarks of early-onset obesity and red hair pigmentation, in addition to adrenal insufficiency (Krude et al., 1998). In contrast to IAD, excess amounts of ACTH may be secreted from a benign pituitary tumour namely an adenoma within the corticotroph cells, termed Cushing's disease. This disease may cause a wide variety of non-specific symptoms such as abnormal weight gain, polycystic ovary syndrome, deep vein thrombosis, localized adiposity amongst many others, thus often making the diagnosis delayed and highly challenging (Broder et al., 2016).

1.2.3. Combined pituitary hormone deficiency

Combined pituitary hormone deficiency (CPHD) is the presence of at least two or more pituitary hormone deficiencies including GH, TSH, PRL, ACTH and gonadotrophin deficiencies. Depending on which deficiencies are present in the patient, the phenotypic features may include hypothyroidism, delayed or absent puberty which may lead to infertility, intellectual disability, midline defects such as cleft lip or palate, short stiff neck (specifically caused by *LHX3* mutations), and underdeveloped optic nerves. Mutations in transcription factors *PROP1*, *POU1F1*, *LHX3*, and *LHX4* underlie CPHD, and as they act at different stages of pituitary development, they often result in unique patterns of hormonal deficiencies that reflect

their differential expression during organogenesis (Pfaffle and Klammt, 2011). For example, the early acting transcription factors LHX3 and -4, as opposed to the later acting PROP1 and POU1F1, cause deficiencies of most, if not all, pituitary hormones, often referred to as panhypopituitarism or multiple pituitary hormone deficiency (MPHD). All four genes, when mutated, are known to affect somatotroph cell development and therefore can all give rise to severe forms of short stature, thus reasoning that GHD is the most prevalent deficiency to occur. Additionally, mutations in *HESX1*, *SOX3* and *OTX2* may occasionally give rise to CPHD with different combinations of endocrine deficits (Thomas et al., 2001, Woods et al., 2005, Diaczok et al., 2008). Mutations in the Kallmann syndrome (KS) genes, discussed in section 1.2.6, have also been described in such cases, once again demonstrating the genetic overlap that diseases related to hypopituitarism can have. For example, a CPHD patient with right microphthalmia, right renal aplasia and severe developmental delay had a hemizygous variant in *KAL1* that was predicted to cause functional damage by *in silico* analysis (Takagi et al., 2014). The known *PROKR2* p.R85H mutation previously identified in KS, was also found in a patient diagnosed with CPHD. This patient manifested GH, TSH, ACTH, LH and FSH deficiencies with a microphallus, with the latter suggesting neonatal GnRH deficiency (Raivio et al., 2012) and thus features that overlap with HH and KS in this case. In addition a recent report described a novel *PROKR2* variant, p.R248W, predicted to be deleterious, in a patient with CPHD. This substituted residue at this highly conserved region had previously been mutated to glutamine in a patient with HH (Asakura 2015). Mutations in *FGFR1*, another Kallmann gene, have also been implicated in this disorder, for example a novel loss of function mutation, p.R448W, was recently identified in a patient with GH and TSH deficiency (Correa et al., 2015). Despite these reports implying a genetic overlap in CPHD and HH/KS cases, digenic inheritance cannot be ruled out here. There may be an unidentified additional mutation in another gene other than the mutation in the Kallmann gene described in these patients that is involved in the

etiology of one of the deficiencies in their CPHD. Despite the genes reported in the aetiology of this heterogeneous disease, the majority of CPHD cases remains unexplained, suggesting the involvement of other genes yet to be identified.

1.2.4. Holoprosencephaly

HPE is a complex heterogeneous brain malformation resulting from incomplete cleavage of the prosencephalon, the two hemispheres of the brain, affecting both the forebrain and the face (Dubourg et al., 2004). The 3 classic types of HPE include alobar (virtually no forebrain division) with the most severe cases resulting in cyclopia, semilobar (some degree of hemispheric cleavage), and lobar HPE (more complete separation) (Figure 1.4). Mildly affected patients may have a normal central nervous system (CNS) but often have microform features of HPE, with microcephaly, hypotelorism, a single central maxillary incisor, and cleft lip and/or palate being among the most common (Solomon et al., 2010). Several recurrent chromosomal anomalies, termed cytogenetic abnormalities, are estimated to be present in ~25-50% of HPE patients (Bendavid et al., 2010). These have implicated a spectrum of candidate genes in the aetiology of HPE, many of which are components of the Sonic Hedgehog (SHH) signalling pathway. SHH signalling is required during multiple stages of rostroventral midline development, and many heterozygous mutations in its pathway have been identified in HPE patients (Hong and Krauss, 2013). Previous studies have shown that mutations in the *SHH* gene affect distinct steps of SHH biogenesis to attenuate its activity to variable levels. Thus contributing to the phenotypic variation seen in HPE patients (Singh et al., 2009). Haploinsufficiency of the *SHH* gene represents the most frequent genetic cause identified in these patients, with most being loss-of-function mutations (Lami et al., 2013). The *GLI family zinc finger 2 (GLI2)* transcription factor is a component of the SHH signalling pathway and is a known causative gene that when mutated is widely known to cause holoprosencephaly (Roessler et al., 2003). Unlike mutated *SHH* which fundamentally

causes HPE in the hypothalamo-pituitary spectrum, mutated *GLI2* is also associated with CH without the presence of midline brain defects (Gregory et al., 2015a, Arnhold et al., 2015). Mutated *ZIC2*, *SIX3* and *TGIF1* genes are other SHH pathway components implicated in HPE on rare occasions (Gripp et al., 2000, Wallis et al., 1999, Brown et al., 1998). These have in turn led to the identification of a larger array of causative genes that include *PTCH1*, *DISP1*, *TDGF1*, *GAS1*, *EYA4*, and *FOXH1* (Bendavid et al., 2010). Mutations in the *FGF8* gene, important for GnRH neuronal development, are usually associated with Kallmann syndrome (KS). However, a homozygous *FGF8* mutation has been implicated in a consanguineous family with semilobar HPE, diabetes insipidus, and TSH and ACTH insufficiency (McCabe et al., 2011b), making this Kallmann gene a new candidate for HPE. Digenic inheritance has recently been described in cases of HPE, where two mutations in different genes have given rise to the phenotype (Mouden et al., 2016). Furthermore, sub-microscopic deletions at a number of loci believed to be implicated in HPE have been identified in a number of patients (Rosenfeld et al., 2010), suggesting that there are many more mutations that need to be defined and characterized for this disease.

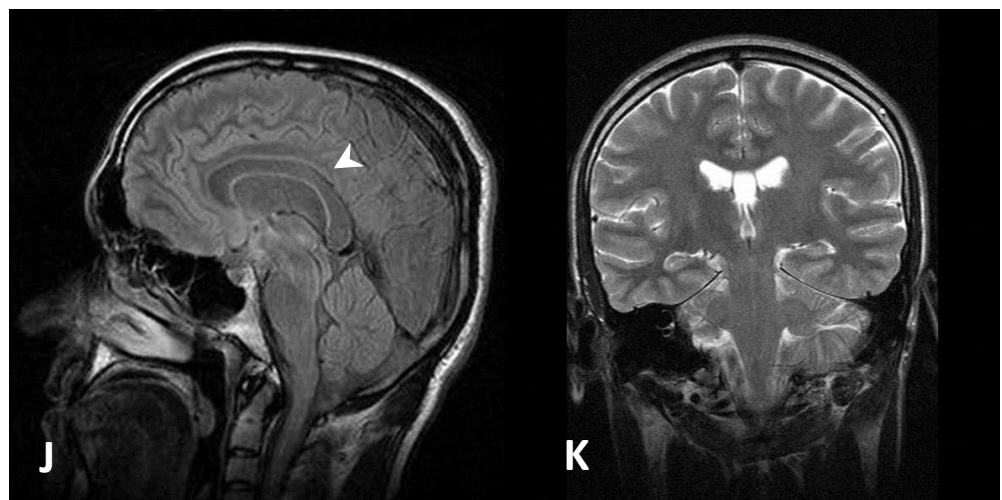
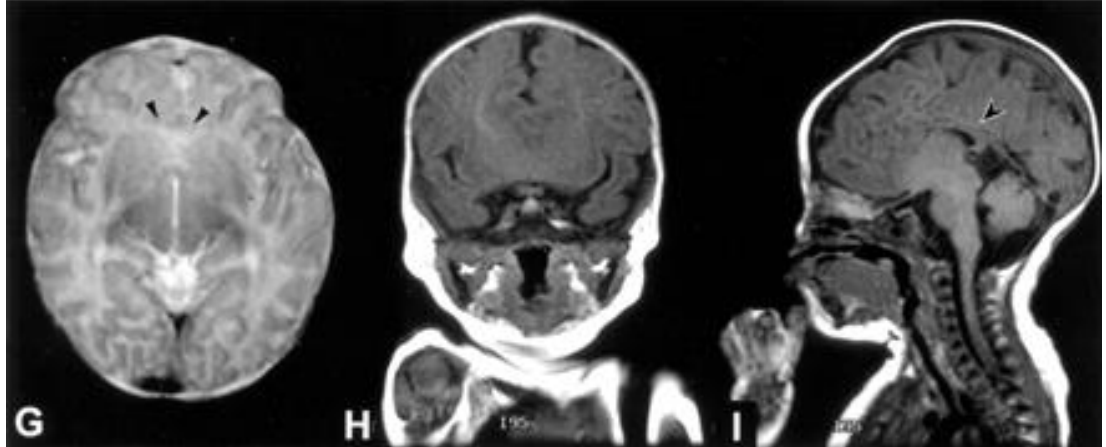
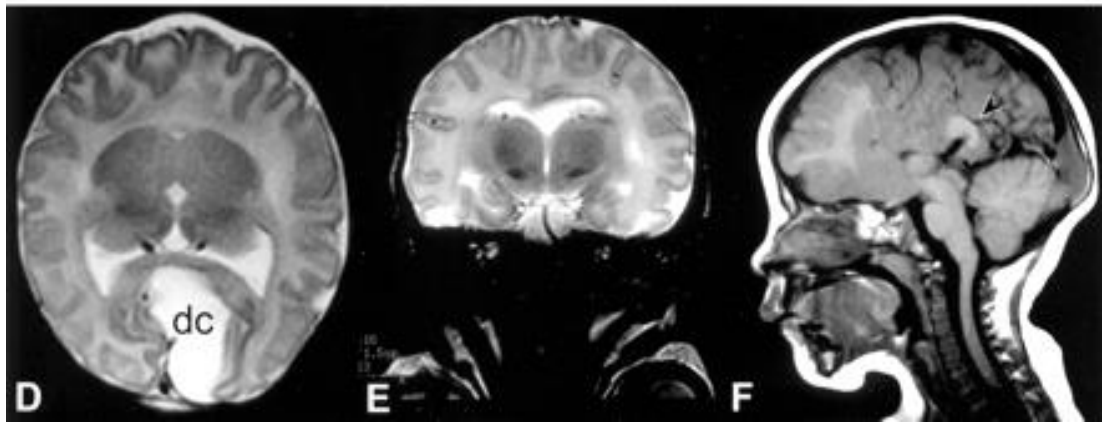
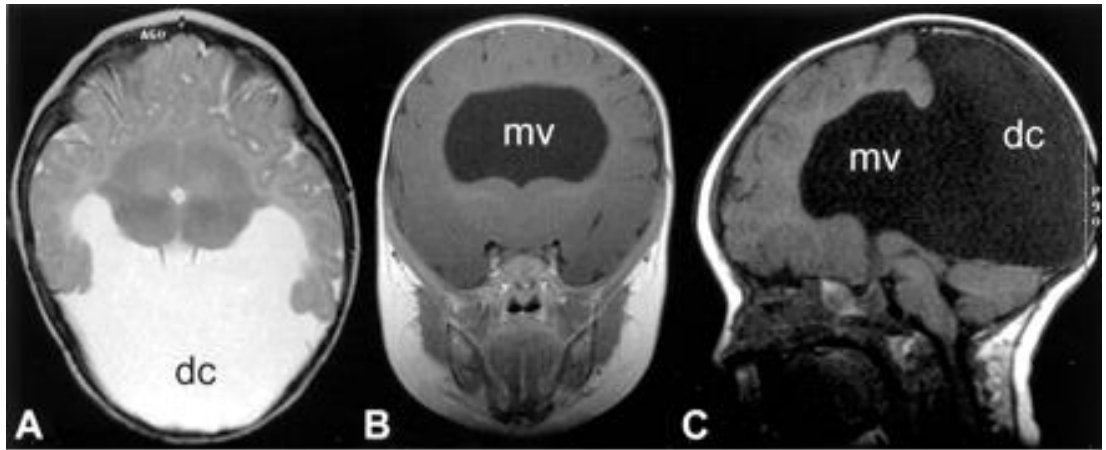


Figure 1.4: MRI scans of holoprosencephaly patients. Taken and adapted from Plawner *et al.* (Plawner *et al.*, 2002). (A, B and C) MRI of a patient with alobar holoprosencephaly (HPE). **(A)** A transverse image with incomplete separation of the two hemispheres, striatum, and thalami, and a large dorsal cyst (dc). **(B)** Coronal image showing continuity of grey matter over the two hemispheres without an interhemispheric fissure. The ventricular system is composed of a single midline ventricle, monoventricle (mv). **(C)** Sagittal image with absence of the corpus callosum and a monoventricle that communicates freely with the dorsal cyst. **(D, E and F)** MRI of two patients with semilobar HPE. **(D-E)** Transverse and coronal images respectively, from the same patient. Posterior portions of the hemispheres are well separated, however the anterior cerebral hemispheres are not cleaved and there is presence of a dorsal cyst (dc). Posterior horns of the lateral ventricles are well formed but frontal horns are poorly developed. **(E)** Posteriorly there is a monoventricle demonstrated on a coronal image. **(F)** Sagittal image showing that the posterior portion of the corpus callosum is formed (arrowhead), however the anterior portion is not developed; highly characteristic of semilobar or lobar HPE. **(G, H and I)** MRI of a patient with lobar HPE. **(G)** Transverse image of the cerebral hemispheres showing fair separation both anteriorly and posteriorly. There is some development of the frontal horns (arrowheads). **(H)** Coronal image showing failure of complete cleavage of the frontal lobe. **(I)** Sagittal image showing that the posterior portion of the corpus callosum (arrowhead) is formed, however the anterior portion is not developed. **(J-K)** MRI scans from a normal control individual for comparison to all other images A - I. **(J)** A sagittal image showing a normal fully formed corpus callosum (arrowhead). **(K)** A coronal image showing normal separation of the two hemispheres of the brain.

1.2.5. Septo-optic dysplasia

SOD, also known as de Morsier Syndrome, occurs in 1/10,000 live births with equal prevalence in males and females. It is a heterogeneous disorder with a variable phenotype, loosely defined by any combination of the triad of optic nerve hypoplasia (ONH), midline neuroradiological abnormalities (such as agenesis of the corpus callosum and absence of the septum pellucidum), and pituitary hypoplasia with consequent endocrine deficits (De Morsier, 1956, Brodsky and Glasier, 1993). Although an absent septum pellucidum is usually associated with endocrine deficits, around 40% of SOD patients may actually present with normal endocrinology. Intriguingly SOD is associated with a younger maternal age compared with isolated defects of the hypothalamo-pituitary axis (McNay et al., 2007). The reason for this SOD maternal age bracket has remained unknown, but has been suggested to be associated with increased maternal drug and alcohol abuse. (Webb and Dattani, 2010, Lippe et al., 1979). Approximately 75–80% of patients exhibit ONH, which may be unilateral or more commonly bilateral (88% as compared with 12% unilateral cases), and may be the first presenting feature with later onset of endocrine dysfunction (Kelberman and Dattani, 2007a). In rare cases, the eye abnormality may be more severe, resulting in microphthalmia or anophthalmia (Kelberman and Dattani, 2008); where one or both of the eyes are abnormally small or completely absent respectively. The association of midline abnormalities with hypopituitarism has long been established, suggesting a common developmental origin (Mehta et al., 2009). Mutated *HESX1*, a transcriptional repressor, is known to play a role in the pathogenesis of rare cases of SOD (McCabe et al., 2011a, Dattani et al., 1998). Significant insights into the pathogenesis of the disorder were provided by the original studies, whereby murine transgenesis resulted in murine phenotypes highly reminiscent of SOD. Thereafter, human mutations have been cloned into mouse models and studied in depth; such as the first *HESX1* mutation p.R160C ever identified (Sajedi et al., 2008b). The *SOX2*, *SOX3* and *OTX2* genes have been shown

to be mutated in rarer forms of SOD, often involving bilateral eye defects including microphthalmia or anophthalmia in patients harbouring *SOX2* and *OTX2* mutations, and often abnormalities in the infundibulum and the corpus callosum in patients with *SOX3* mutations (Woods et al., 2005). Mutations in the Kallmann genes have also been linked with SOD, such as two heterozygous *KAL1* mutations that were identified in three females from two unrelated families with SOD, through work undertaken by my colleagues and I (McCabe et al., 2015). Prior to this, three SOD patients were reported to have heterozygous mutations in *FGFR1* that altered receptor signalling, with one predicted to affect splicing (Raivio et al., 2012). The same report also identified the heterozygous loss of function mutation, p.R268C, in the *PROKR2* gene in a Caucasian and African SOD proband respectively, that had previously been implicated in normosmic HH and KS. In addition they identified a *PROKR2* variant in a third proband that was predicted to be a loss of function mutation (Raivio et al., 2012). Thus broadening the spectrum of candidates to span the Kallmann genes associated with this rare disorder. Aside from mutations in the Kallmann genes, two *TCF7L1* missense variants were identified in two unrelated SOD patients in a very recent report (Gaston-Massuet et al., 2016). SOD can be associated with a wide range of phenotypic variability, highlighting the complexity of the disorder and suggesting the impact of both genetic and environmental factors involved in the aetiology of the disease (Polizzi et al., 2006). Other associated features include developmental delay, seizures, visual impairment, sleep disturbance, precocious puberty, obesity, anosmia, sensorineural hearing loss and cardiac anomalies (Webb and Dattani, 2010).

1.2.6. Hypogonadotropic hypogonadism

Congenital HH and KS are rare disorders with an occurrence rate of 1-10 in 100,000 births (Fraietta et al., 2013). The major underlying cause is a failure to activate pulsatile secretion of GnRH, causing deficiencies in gonadotrophins (LH and FSH), and thus sex hormones; namely oestrogen in girls and testosterone in boys. This in turn causes a delay in the onset or a complete/partial failure of puberty in patients (Layman, 2007). HH is difficult to differentiate from a diagnosis of constitutional delay in puberty, making it challenging for clinicians to make a diagnosis. GnRH testing can be useful, and may be used in combination with human chorionic gonadotrophin (hCG) testing to discriminate between the two and to make a reliable diagnosis (McCabe et al., 2014, Segal et al., 2009). It is associated with genital abnormalities such as micropenis (Bin-Abbas et al., 1999), and/or systemic abnormalities such as cleft lip/palate, renal agenesis, synkinesis (Conrad et al., 1978) and hearing defects (Bianco and Kaiser, 2009). Additionally, anosmia; a total or partial loss of olfaction (sense of smell), often accompanies HH and occurs in approximately 60% of HH patients. It results from incomplete embryonic migration of GnRH-synthesizing neurons, and when present in patients is termed KS (Cariboni and Maggi, 2006). Isolated HH (IHH) and KS are both clinically and genetically heterogeneous, with over 25 known causative genes implicated to date (Boehm et al., 2015). All such genes encode proteins that have a role in regulating GnRH neuronal development, their migration from the nasal placode to the hypothalamus, and GnRH secretion and/or action. The genes that have been found to be most frequently mutated in IHH/KS patients are: *KAL1* in approximately 5% of cases, *PROKR2* or *PROK2* in ~9%, *FGFR1* in ~10% and *FGF8* in ~2%, which are known as the Kallmann genes. *GnRHHR* is the most commonly mutated gene in IHH; in approximately ~11% of cases (Topaloglu and Kotan, 2016). However these only account for <37% of cases cumulatively. Many other mutated genes have been reported in a few cases respectively, with an increasing number of novel candidate genes constantly being

identified (known causative genes associated with HH are listed in Table). For example, a recent next generation sequencing study has implicated an additional 19 new candidate genes in IHH/KS patients (Quaynor et al., 2016) not listed in Table 1.1. This heterogeneity indicates that IHH/KS can arise from a multitude of different genetic sources to give rise to a variable phenotype. This signifies great difficulty in identifying a genotype in these patients and makes genetic screening a timely and costly ordeal. Exome sequencing would be beneficial in such cases to uncover mutations that are bespoke to each particular patient, enabling future personalised treatments that can be suited to the individual's need. Furthermore, the optimal timing of treatment in these individuals is critical to their sexual development and progression through puberty, as well as for their bone and metabolic health, which can otherwise result in debilitating consequences both physically and psychologically for the patient.

Hypogonadotropic hypogonadism known causative genes

<u>Mechanism affected</u>	<u>Mutated</u>
Disorders of the embryonic migration of GnRH neurons (KS)	KAL1, FGFR1, PROK2, PROKR2, FGF8, HS6ST1, CHD7, WDR11, SEMA3A, FGF17, IL17RD, DUSP6, SPRY4, FLRT3, NELF, FEZF1
Disorders of the GnRH pulse generator	TAC3 (IHH) , TACR3 (IHH) , KISS1 (IHH) , KISS1R (IHH) , GNRH1 (IHH)
Disorders of the pituitary gonadotrophs	GNRHR (IHH) , FSHB, LHB
Developmental disorders of the hypothalamo-pituitary region	DAX1, HESX-1, LHX3, PROP-1, SOX2, OTX2
Disorders of IHH associated with obesity	LEP, LEPR, PC1
Disorders of IHH associated with neurodegenerative syndromes	POLR3A, POLR3B, PNPLA6, RNF216, OTUD4, STUB1, RAB3GAP1, RAB3GAP2, RAB18, TBC1D20

Table 1.1: Genetic causes of isolated hypogonadotropic hypogonadism (IHH) and Kallmann syndrome (KS). Adapted from Topaloglu *et al.* (Topaloglu and Kotan, 2016). The six genes highlighted in red are the most common genes to be mutated in patients in the known IHH/KS population. All other genes listed have occurred less frequently in reported cases. The four genes that have been found to be mutated in IHH only and not KS patients are denoted with '(IHH)'.

1.3. Genes implicated in human hypothalamo-pituitary disorders

1.3.1. Genetic analysis and known causative genes

The majority of CH cases are sporadic, although familial cases have been described. The latter have led to the identification of mutations in key developmental genes that are involved in normal pituitary development; including *HESX1*, *SOX2*, *SOX3*, *OTX2*, *ARNT2*, *LHX3*, *LHX4*, *POU1F1* and *PROP1* (Alatzoglou and Dattani, 2009). These genes are commonly screened for mutations, and many are functionally deleterious in the form of missense point mutations, frameshifts, insertions and deletions that have been identified and shown to most likely account for hypothalamo-pituitary phenotypes (Reynaud et al., 2012). Variable penetrance is often apparent where a patient has a heterozygous mutation with functional consequences that is also present in the unaffected parent (Ming and Muenke, 2002). Additionally, digenic inheritance may account for the variable penetrance in some cases, as is well established in KS (Falardeau et al., 2008), where more than one mutation in the Kallmann genes has been known to be inherited from either parent causing the phenotype (Dode et al., 2006). The apparent overlap in KS, CPHD and SOD genotypes opens up a new source of potential genetic associations (Bancalari et al., 2012, Raivio et al., 2012).

A vast array of genes, which is constantly increasing, encoding transcription factors and signalling molecules, have been reported to be mutated and give rise to the different hypothalamo-pituitary disorders that have been discussed. The known causative genes are among the most prevalent to be mutated, and thus the ones routinely screened in our laboratory. These genes are discussed in the following section.

1.3.2. HESX1

The transcription factor HESX1 is a member of the paired-like class of homeodomain proteins which acts as a transcriptional repressor essential for pituitary organogenesis (Dattani et al., 1998). Binding partners of human HESX1 such as transducing-like enhancer of split 1 (TLE1) (ortholog of Groucho in *Drosophila*), the nuclear corepressor (N-COR) and DNA methyltransferase 1 (DNMT1), can all form complexes to enable it to exert this repressive activity (Dasen et al., 2001, Sajedi et al., 2008a). *Hesx1* is one of the earliest markers of murine pituitary development, expressed initially during gastrulation in the region fated to form the forebrain and ventral diencephalon, and is then restricted to Rathke's pouch by embryonic day (E) 9.0 (Thomas and Beddington, 1996). *Hesx1* continues to be expressed in the developing AP until E12, when it then disappears in a spatio-temporal sequence that corresponds to progressive pituitary cell differentiation (Kelberman and Dattani, 2009). *Hesx1* transcripts have totally disappeared from the entire ventral portion by E13, giving rise to the anterior lobe of the pituitary (Hermesz et al., 1996). A homozygous null mutation in mice results in a phenotype that resembles SOD, with 5% of *Hesx1* null mice exhibiting a severe phenotype with no AP (Dasen et al., 2001). This is consistent with an insertion mutation in exon 3 in the 'Alu' element; a sequence that encodes the major part of the homeodomain of *HESX1*, which was identified in a retinal coloboma patient with aplasia of the AP. Thus patients have subsequent undetectable concentrations of all AP hormones (Sobrier et al., 2005). Patients with *HESX1* mutations have phenotypes ranging from evolving hypopituitarism in the absence of midline and eye defects, through to SOD and pituitary aplasia (Kelberman and Dattani, 2007b). *Hesx1* null mice show great variability with features that include a reduction in forebrain tissue, craniofacial dysplasia with a short nose and absence of developing optic vesicles. These mice also have significantly decreased head size, absence of telencephalic vesicle or infundibulum development, absence of olfactory placodes, hypothalamic abnormalities and irregular morphogenesis of Rathke's

pouch (Dattani et al., 1998). Rathke's pouch formation was variably affected, and abnormal bifurcations were apparent resulting in multiple pituitary glands, due to multiple invaginations in the oral ectoderm in a proportion of the mice (Newbern et al., 2013, McCabe et al., 2011a, Dattani et al., 1998). Although of variable severity, both neonatal and adult homozygous mutant mice manifested phenotypes that presented with eye defects such as microphthalmia and anophthalmia, with abnormalities of the septum pellucidum and corpus callosum, closely resembling SOD in humans (section 2.5).

1.3.3. SOX2 and SOX3

SOX2 and SOX3 are members of the *SOXB1* subfamily of 'SRY-related HMG box' transcription factors. They have an N-terminal domain of unknown function, a DNA-binding High Mobility Group (HMG) box domain and a longer C-terminal domain involved in transcriptional activation (Stevanovic et al., 1993). Members of the *SOXB1* subfamily are expressed throughout the CNS and are among the earliest neural markers that play a role in neuronal determination (Hutton et al., 2009). Murine *Sox3* is shown to be involved in neurogenesis through its expression in actively dividing undifferentiated neural progenitor cells, and is maintained throughout development (Bylund et al., 2003). Expression of *Sox3* is also seen in the ventral diencephalon, infundibulum and presumptive hypothalamus, a similar expression pattern to that of *Wnt5a* expression (Solomon et al., 2004). Due to the importance of inductive signals from these areas in the normal formation of the AP, hypopituitarism with consequent endocrine dysfunction may be associated with *Sox3* mutations. *Sox3*, as well as *Tcf4* and *Wnt5a*, deficient mice exhibit expanded BMP and FGF signalling domains as well as abnormalities in Rathke's pouch (Rizzoti et al., 2004), suggesting a possible mechanism underlying the hypopituitary phenotype in these mutants (Potok et al., 2008). The mutant mice exhibited variable complex phenotypes including craniofacial abnormalities, midline CNS defects and a reduction in size and fertility (Rizzoti et al.,

2004). Duplications as well as loss-of-function mutation expansions of the polyalanine tract in *SOX3* have been described in a number of patients with hypopituitarism (Woods et al., 2005). Mutations such as these are usually associated with infundibular hypoplasia and an ectopic or undescended PP, and have been shown to result in aggresome formation (a mass of misfolded proteins in the cell) and impaired transactivation (Wong et al., 2007). Submicroscopic duplications on chromosome Xq27.1, which include *SOX3*, are associated with variable hypopituitary phenotypes including CPHD, absence or hypoplasia of the infundibulum, and an abnormality of the corpus callosum (Woods et al., 2005). Additionally, a 2.31-Mb deletion on Xq27 incorporating *SOX3*, was identified in a patient with CH and the unusual phenotype of a persistent craniopharyngeal canal (Alatzoglou et al., 2014a). Furthermore, an 18bp deletion in the polyalanine tract of *SOX3* was identified in a CH patient, resulting in an increase in transcriptional activation (Alatzoglou et al., 2011b). These data highlight the critical gene dosage of *SOX3* in normal development of the diencephalon and infundibulum, and consequently the AP.

SOX2 is expressed in neural progenitor populations throughout the developing and adult CNS, and is necessary to maintain their progenitor identity (Hutton and Pevny, 2011). After gastrulation, murine *Sox2* expression is restricted to the presumptive anterior neuroectoderm and by E9.5 is expressed throughout the CNS, brain, sensory placodes, branchial arches, gut endoderm, oesophagus and trachea. Homozygous null *Sox2* mice fail to survive and die shortly after implantation (Avilion et al., 2003), whereas heterozygous mice have hypoplasia and abnormal morphology of the AP, with subsequent reduction in GH, LH, ACTH and TSH concentrations (Kelberman et al., 2006). Other studies have shown that retinal progenitor cells with conditionally ablated *Sox2* lose competence to both proliferate and terminally differentiate. Additionally, *Sox2* hypomorphic/null mice, with a 40% reduction of *Sox2* expression compared to wild-type (WT) mice, present with variable microphthalmia as a result of

aberrant neural progenitor differentiation. Furthermore, this study suggests that *Sox2*/*SOX2* activity functions in a dose-dependent manner in retinal progenitor cell differentiation (Taranova et al., 2006). The first description of *SOX2* mutations in humans was in a cohort of individuals with severe eye phenotypes. *De novo* mutations were associated with bilateral anophthalmia, or severe microphthalmia, with accompanying developmental delay, learning difficulties, oesophageal atresia and genital abnormalities (Williamson et al., 2006). Conclusively, the majority of males with *SOX2* mutations had abnormalities in genital development. *SOX2* expression in humans is observed throughout the human brain, including the developing hypothalamus, as well as Rathke's pouch, and the eye (Kelberman et al., 2008). Following on from these studies, *SOX2* mutations have also been associated with AP hypoplasia and HH (Kelberman et al., 2006), and are usually loss of function mutations. These result in a loss of DNA binding, nuclear localisation or transcriptional activation, suggesting that the phenotypes arise as a result of haploinsufficiency of *SOX2* in development. In the murine pituitary, conditionally deleted *Sox2* mutant mice have abnormal gonadotrophin secretion as well as TSH and GH deficiencies. This suggests a likely role for *Sox2* in the hypothalamus and/or the developing pituitary, particularly with respect to GnRH neurons (Jayakody et al., 2012), which reflects the *SOX2* mutations described in HH patients. In addition, loss of function *SOX2* haploinsufficiency mutations have been implicated in the generation of slow progressing pituitary tumours of early onset in patients (Alatzoglou et al., 2011a). Furthermore, a very recent study (Goldsmith et al., 2016) has implicated a role for *SOX2* in melanotroph cell fate acquisition, independent of its early role in promoting progenitor proliferation. This study showed that *SOX2* is maintained at low levels in melanotrophs (Goldsmith et al., 2016) where its expression is likely regulated by P27 (Li et al., 2012).

1.3.4. OTX2

OTX2 (Orthodentic homeobox 2) is a transcription factor that is required for the formation of anterior structures and maintenance of the forebrain, and has been implicated in 2–3% of anophthalmia/microphthalmia related syndromes in humans (McCabe et al., 2011a). In mice, the expression of *Otx2* is localised to developing neural and sensory structures of the brain such as the cerebellum, the eye, nose and ear, and is required at multiple steps in brain development and neuronal differentiation (Frantz et al., 1994). Mice homozygous for mutations die from severe brain abnormalities after exhibiting malformations in both the forebrain and the eye due to impaired gastrulation. Heterozygous mice can display a range of phenotypes from normal to severe forms of eye/brain abnormalities such as anophthalmia and holoprosencephaly (Ang et al., 1996). During retinal development, *Otx2* regulates retinal pigment epithelium specification, and photoreceptor and bipolar cell differentiation and maturation, with expression being maintained in these three cell types throughout life (Housset et al., 2013). *Otx2* transcripts and protein are normally detectable at E10.5 in both the ventral diencephalon and Rathke's pouch. By E12.5 *Otx2* transcripts are undetectable in Rathke's pouch, but persist in the ventral diencephalon until E14.5, and by E16.5 no *Otx2* transcripts are detected in either structure (Mortensen et al., 2011). A previous study showed that *Otx2* expression in Rathke's pouch in *Prop1*-mutant mice continued until E16.5; four days after *Prop1* peak expression, and two days after any pituitary defects become apparent (Mortensen et al., 2011). This study suggests that *Prop1* regulates expression of other factors that suppress *Otx2*; implying a role for *Otx2* in murine pituitary development. Another study reported an HH phenotype in GnRH-neuron-*Otx2* knockout mice (Diaczok et al., 2011). These murine data are consistent with OTX2 human mutations, where phenotypes exhibit highly variable pituitary defects ranging from IGHD, panhypopituitarism through to HH. All of which commonly include the accompanying severe ocular malformations discussed (Gorbenko Del Blanco et al., 2012). Despite

this knowledge, the role of *OTX2* in hypothalmo-pituitary development still remains largely unclear (Bancalari et al., 2012).

1.3.5. ARNT2

ARNT2 (aryl-hydrocarbon receptor nuclear translocator 2) is a member of the basic-helix-loop-helix-Per-Arnt-Sim (bHLH-PAS) superfamily of transcription factors. This protein forms heterodimers with sensor proteins from the same family that then bind regulatory DNA sequences. *Arnt2*(-/-) embryos die perinatally and exhibit impaired hypothalamic development (Keith et al., 2001). Recent studies showed expression of *ARNT2* within the CNS, including the hypothalamus, as well as the renal tract during human embryonic development. A homozygous frameshift *ARNT2* mutation has been associated with congenital hypopituitarism, progressive neurological abnormalities, renal tract abnormalities and post-retinal visual pathway dysfunction in certain individuals. This is an example of how ARNT2 is essential in hypothalmo-pituitary development, post-natal brain growth, and visual and renal function in humans (Webb et al., 2013).

1.3.6. LHX3 and LHX4

LHX3 and LHX4 are members of the 'LIM homeobox' protein family, containing the characteristic two LIM domains; unique cysteine-rich zinc-binding domains known to play a role in transactivation and protein-protein interaction (Pfaeffle et al., 2008, Tajima et al., 2010, Takagi et al., 2012). These proteins are multifunctional as they act as scaffolds and adaptors to mediate interactions that modulate target gene transactivation. LHX3/LHX4 are transcription factors that possess overlapping but distinct functions during the establishment of the specialized cells of the mammalian pituitary gland and the nervous system (Colvin et al., 2009). In mice, *Lhx3* and *Lhx4* are expressed at embryonic day 9.5 (E9.5) in Rathke's pouch. By E12.5, *Lhx4* is concentrated in the tissue that will become the anterior lobe of the pituitary gland

whereas *Lhx3* expression continues throughout the pouch. Later transcription from the *Lhx4* gene is reduced and transcripts are found at lower levels than *Lhx3* in the mature gland (Sheng et al., 1997). Both *Lhx3/4* work in conjunction to form a definitive Rathke's pouch and regulate proliferation and differentiation of pituitary lineages; pituitary development halts at the rudimentary pouch stage in mice lacking both of these genes. In humans and rodents, *LHX4/Lhx4* expression is in the developing hindbrain, cerebral cortex, pituitary gland and spinal cord (Liu et al., 2002). *Lhx3* null mutant pituitary precursor cells cease to proliferate before differentiation, whereas in *Lhx4* null mutants, these cells differentiate albeit in reduced numbers. A lack of cellular proliferation in *Lhx4* mutants causes failure to respond to inductive signals and subsequent misregulation of other transcription factor genes e.g. *Lhx3*, which inevitably leads to increased cell death. Following on from this, mouse studies have shown that *Lhx4* is required for the correct temporal expression of regulatory genes such as *Lhx3* (Pfaeffle et al., 2008). Therefore patients with *LHX4* mutations may have a partial loss of LHX3 function. Mutations in *LHX3* may give rise to CPHD, and in specific cases loss of neck rotation resulting in a short stiff neck, considered to result from nervous system abnormalities (Netchine 2000). Mice homozygous for *Lhx4* mutations die shortly after birth with immature lungs that fail to inflate, whereas heterozygous mice appear normal (Li et al., 1994). Additionally, *Lhx4* null mice exhibit incomplete pituitary gland development. Heterozygous *LHX4* mutations in humans are usually associated with variable and variably penetrant CPHD (Pfaeffle et al., 2008), and are usually due to haploinsufficiency rather than having a dominant-negative effect.

1.3.7. POU1F1 and PROP1

POU Class 1 Homeobox 1 (POU1F1), formally known as PIT1, is a pituitary-specific transcription factor characterised by the presence of a highly conserved bi-partite DNA binding domain, comprising the POU-specific domain (POU-S) and the POU homeodomain (POU-H) (Herr and Cleary, 1995). *POU1F1* is expressed during differentiation steps that take place at later stages in the development of the AP gland, and its expression is restricted to the somatotroph, thyrotroph and lactotroph cell lineages. This is consistent with functional studies of this protein which show that expression of the *GH*, *PRL*, *TSH-β* subunit and *GHRHR* genes is regulated by POU1F1 (Dattani, 2004). Furthermore, studies have also shown that *Pou1f1/POU1F1* binds to its own proximal promoter and upregulates its own expression (Delhase et al., 1996). Homozygous loss-of-function mutations in a lesion in the *Pou1f1* gene have been reported to give rise to the Snell dwarf mouse model phenotype (Camper et al., 1990), which results in the absence of the three cell types in which *Pou1f1* is expressed, as mentioned above. Mutations in *POU1F1*, that are usually homozygous recessive, have been implicated in CPHD, with the spectrum of hormone deficiency varying considerably in patients. Patients usually manifest with GH and PRL deficiencies initially, often with the development of secondary hypothyroidism (Pfaffle et al., 1992), although some maintain a normal TSH concentration (Turton et al., 2005). In addition, a recent study has described an autosomal dominant heterozygous missense *POU1F1* mutation in a large family with IGHD (Sobrier et al., 2016). Thus presenting a novel aetiology for IGHD and demonstrating further variability in patients with *POU1F1* mutations. The first *POU1F1* mutation; a homozygous nonsense mutation, resulted in a severely truncated protein of 171 amino acids, lacking half of the POU-S and all of the POU-H domain (Tatsumi et al., 1992). This first novel mutation was identified in a patient with GH, PRL and TSH deficiencies, due to the mutant POU1F1 protein being completely incapable of binding to the GH and prolactin promoters and resulting in loss of transcription. The Prophet of Pit-1 (PROP1)

pituitary-specific paired-like homeodomain transcription factor is important for the production and secretion of GH, PRL, TSH and gonadotrophins, and is believed to be required for the expression of *POU1F1*. This was first characterized in the Ames dwarf mouse model, which harbours a homozygous missense *Prop1* mutation (p.S83P) causing a lack of *Pou1f1* gene activation and absence of progression to mature cells (Andersen et al., 1995, Dattani, 2004). It is known that mutant PROP1 causes failure of cells to differentiate, due to retained progenitor cells in the periluminal area (Ward et al., 2005). In addition, recent studies have shown that PROP1 stimulates stem cells to undergo an epithelial to mesenchymal transition-like process, which is essential for cell migration and differentiation (Perez Millan et al., 2016). Thus suggesting that PROP1 is a central transcriptional component of pituitary stem cell differentiation. Mutations in *Prop1/PROP1* can elicit a CPHD phenotype commencing initially with GH, PRL and TSH deficiencies, often with evolution of secondary hypogonadism, although this may also be present at birth (Pfaffle et al., 1999). Other phenotypic features include evolving ACTH deficiency (Bottner et al., 2004), as well as an enlarged anterior pituitary suggestive of a tumour (Mendonca et al., 1999), that can regress with time and lead to complete pituitary involution and an empty sella syndrome. POU1F1 and PROP1 are the best characterized intrinsic signalling molecules in terms of function in both humans and mice (Dattani, 2004).

1.4. Investigating the genotype of patients

1.4.1 Genetic analysis

CH patients are routinely screened for mutations in respective known causative genes in the laboratory via a polymerase chain reaction (PCR) and direct sequencing analysis approach, also known as Sanger sequencing. Instead of screening one gene at a time in this way, which can be a time consuming process, with low frequency hit rates due to a large number of genes with many exons, panel screening is often the preferred choice. Multi-gene panel tests use next-generation sequencing to screen several known causative genes simultaneously, which enables variants to be identified, or for mutations in all these known genes to be excluded, more rapidly and cost effectively than Sanger sequencing provokes (Slavin et al., 2015). Despite these known genes implicated in CH and related phenotypes, the potential genetic cause remains unknown in the majority of cases (80% according to our unpublished data). This signifies the need for further investigation into genes involved in pituitary development and that may be potentially responsible for the phenotypic manifestation of the disease. A range of different genetic strategies are now used in the search for novel candidate genes, and these include homozygosity mapping and exome sequencing. Homozygosity mapping uses single nucleotide polymorphisms (SNPs) to compare the DNA of affected individuals from a consanguineous pedigree, to find regions that are homozygous by descent, reflecting potential loci of interest (Bocquet et al., 2013). Identified areas of homozygosity can then be further sequenced using next generation sequencing, to identify novel genes of interest related to a particular disease. Exome sequencing can be used to sequence the entire coding region of the genome, identifying any variants in the affected patients. Following any variants identified, comparisons are made within the family and online control databases are consulted for their presence, such as 1000 Genomes, dbSNP, EVS and the ExAC Browser. Variants found in genes or regions that are known to be involved in pituitary

development, or genes that are expressed in specific areas of the midline brain structures that are affected in the individual, can then be identified and studied further. The flowchart below illustrates the filtering process of how patient genotypes were analysed in this study (Figure 1.5).

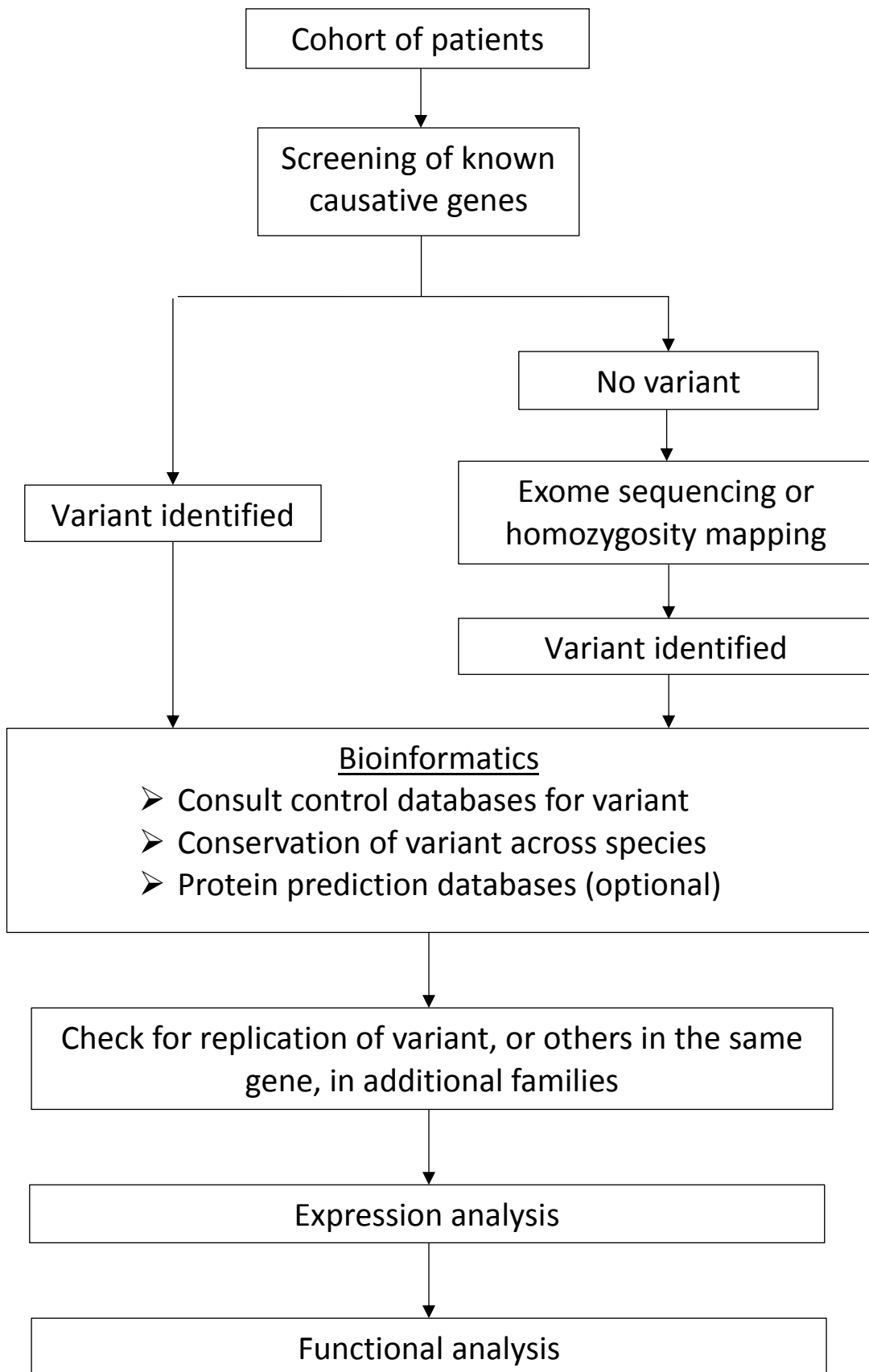


Figure 1.5: A summary of the gene screening process. The flowchart illustrates how the patients in our cohort are screened for mutations in genes, and how unknown genes and regions of interest associated with hypothalamo-pituitary development are identified and characterised.

1.4.2. Expression studies

Upon the identification of a mutated novel gene of unknown function in an individual, expression will initially be analysed in relevant tissues in mice. If the expression pattern is already known, this information will be available on the mouse genome informatics (MGI) database (www.informatics.jax.org). The expression pattern can then be verified in human embryonic tissue, if available. We have access to human embryonic tissue that forms part of a unique resource at the ICH with the Institute of Genetic Medicine in Newcastle, organised by the MRC Wellcome Trust Human Developmental Biology Resource (HDBR). This resource provides valuable human embryonic tissue sections for *in situ* hybridisation analysis of new candidate genes. A detailed hypothalamo-pituitary expression profile for the gene is then established before any functional analysis is undertaken. It is important to perform this first to see whether the gene is expressed in the hypothalamo-pituitary axis, as well as in tissues that are affected in the patient phenotype, before designing an appropriate functional assay that can potentially allow for comparison between the WT and mutated gene. These would include, for example, luciferase reporter transactivation assays or DNA-binding assays in the case of transcription factors. This particular procedure is executed through the generation of genetic constructs, involving the insertion of relevant variants into a specific plasmid via site-directed mutagenesis. Changes in the function induced by the mutated allele can then be assessed via a functional assay, such as a dual-luciferase reporter assay, which is just one of the many assays described in this thesis. However, one needs to bear in mind that if expression is

absent from a particular tissue it should not be completely excluded from further study, as the secreted protein in which the gene encodes may act on target tissues that do not express the relevant gene. Therefore the expression profile determined should act as a guide and not an absolute criterion for further study of a gene.

1.4.3. Cohort of patients

We have a large cohort of patient DNA (>2000) here at Great Ormond Street Hospital (GOSH) and the UCL ICH, consisting of both consanguineous and non-consanguineous pedigrees from many different ethnic backgrounds around the world. These patients have a variety of different hypothalamo-pituitary phenotypes that range in severity. Essentially these patients have forms of congenital hypopituitarism, with phenotypes ranging from IGHD, CPHD/MPHD, HPE, SOD and HH/KS. Endocrine dysfunction includes different combinations of deficiencies; GH, TSH, ACTH, FSH, LH, PRL deficiencies, and sometimes arginine vasopressin deficiency (AVPD), with GHD occurring in the majority. Accompanying craniofacial midline defects and other associated abnormalities are present in many of the individuals, including cleft lip and/or palate, anophthalmia/microphthalmia, blindness, micropenis, microcephaly, hydrocephalus, obesity and developmental delay amongst many others. Usually, a number of known causative genes are initially screened for mutations in the CH patients in our cohort. If no mutations are identified we then, in selected familial cases, proceed to perform exome sequencing analysis to potentially uncover novel variants in new genes that are not previously implicated in the aetiology of congenital hypopituitarism. However, some pedigrees within our cohort have a very unique phenotype, including hypopituitarism in combination with an additional phenotype, e.g. hyperinsulinism, that has not been previously reported in the literature. Pedigrees such as these may be more efficiently analysed by exome sequencing in the first instance due to there being no clear known genes that are implicated in congenital hypopituitarism that could account for these new and unusual

phenotypes. Patients such as these are also often likely to have more than one, or multiple, mutations that are contributing to their unique phenotype, which exome sequencing analysis would be able to identify.

1.5. Aims and objectives

This thesis describes novel genetic variants leading to novel phenotypes in pedigrees within this large cohort, using both a Sanger sequencing approach (Chapter 3) and an exome sequencing approach (Chapters 4, 5) respectively. The first aim of this study is to investigate the functional significance of the homozygous LHX4 (p.T126M) variant identified by Sanger sequencing, in two deceased siblings that had CPHD. Protein modelling, western blot analysis and luciferase assays were used to investigate the p.T126M mutation, and its effect on the transactivation of α GSU (glycoprotein hormones alpha subunit) and prolactin reporters, as well as its ability to synergise with POU1F1, compared to WT LHX4. Additionally, novel variants in new candidate genes that have not been previously associated with CH, have been identified in a subset of phenotypically unique pedigrees submitted to GOSgene for exome sequencing. An expression profile in human embryonic tissue is established in this study for each of these potential novel candidate genes, in a hypothalamo-pituitary context, as well as in tissues that are known to be affected in the respective patients. Patients from one of these pedigrees (Pedigree 8) with severe short stature and GHD, central hypothyroidism and hyperinsulinism causing hypoglycaemia, harboured a novel variant in the *EIF2S3* gene, p.P432S. The role of this mutation in this potential novel candidate gene has been functionally analysed in this study in a hypothalamo-pituitary and pancreatic context.

Chapter 2

Materials and Methods

2.1. Primer Design

Primers for PCR were designed using the Ensembl Genome Browser (<http://www.ensembl.org/index.html>), the UCSC genome browser (<https://genome.ucsc.edu/>) and the Primer3 input (version 0.4.0) (<http://bioinfo.ut.ee/primer3-0.4.0/>) databases. Specifications were entered and altered from the default within Primer3 as follows: product size ranges: 150 - 1000, number of primers to return in output: 25, primer temperature (T_m): 55°C - 65°C, maximum T_m difference: 2°, GC%: minimum 30, optimum 45, maximum 60, maximum self-complementarity: 5, maximum poly X (number of same bases in a row): 4.

2.2. PCR and direct sequencing analysis

DNA was extracted from blood samples taken from our patients and was screened for variants in known causative genes, namely *HESX1*, *PROP1*, *POU1F1*, *LHX3*, *LHX4*, *SOX2*, *SOX3*, *OTX2*, *SHH*, *GLI2*, *KAL1*, *PROK2*, *PROKR2*, *FGFR1*, *FGF8*, *WDR11* and *NELF*, in accordance with the patient phenotype. The coding regions of these genes were amplified by PCR using the BIOTAQ™ DNA Polymerase kit (Bioline, BIO-21060) and exon flanking primers, on an Eppendorf Thermocycler; initially heating the reaction to 95°C for 2 minutes (mins) followed by 35 cycles of: 95°C for 30 seconds (denaturation step), 55°C - 62°C for 30 seconds (annealing step) and 72°C for 45 seconds (extension step). PCR products were treated with MicroClean reagent (Web Scientific, 2MCL-10) in order to clean the product, spun on a centrifuge at 4000rpm, and subsequently upside down on tissue paper at 600rpm to remove liquid. The precipitate was sequenced with either the forward or reverse respective primer at any one given time, using the BigDye® Terminator v1.1 Cycle Sequencing Kit (Life Technologies Ltd., 4337450). The sequencing plate was put into an Eppendorf Thermocycler and heated to 95°C for 2 mins, followed by 39 cycles of 95°C for 30 seconds, 55°C for 15 seconds and 60°C for 4 mins. The sequencing

products were washed by spinning with 100% ethanol containing 3 molar (M) sodium acetate for 40 mins, followed by 70% ethanol for 5 mins, and upside down on tissue paper to remove liquid for 1 min, on a centrifuge at 3050, 3000 and 300rpm respectively. The precipitate was then resuspended in 1M TE buffer before analysis on a 3730XL DNA Analyzer (Applied Biosystems/Hitachi, Japan, cat # 625-0020). Detailed PCR conditions for each exon in each gene are available upon request including primer sequences, amplicon sizes, annealing temperatures, which range from 55°C to 62°C, and whether dimethyl sulfoxide (DMSO) was added to the PCR reaction or not. For any variants identified, control databases were consulted; 1000 Genomes (www.1000genomes.org), dbSNP NCBI National Institutes of Health (www.ncbi.nlm.nih.gov/SNP/), Exome Variant Server (EVS) (www.evs.gs.washington.edu/EVS/), and The Exome Aggregation Consortium (ExAC) Browser (www.exac.broadinstitute.org) which includes approximately 100,000 reference alleles per gene alone.

Aside from screening many patients for mutations in the known causative genes listed above, specific to this study, I have screened the following: 103 patients for variants in the *EIF2S3* gene and 95 patients for *RNPC3* variants (please refer to Chapters 4-5 for more details on each cohort screening respectively).

2.3. Functional Studies for *LHX4* variants

2.3.1. Cell culture

Human embryonic kidney (HEK293T) cells were maintained in a humidified CO₂ incubator at 37°C in Dulbecco's Modified Eagle Medium (DMEM) (Sigma, Cat: D5796) supplemented with 5% penicillin/streptomycin (penstrep) (Invitrogen) and 10% fetal calf serum (PAA). Media was replaced every 2 days, cells were washed with x1 phosphate buffered saline (PBS) (VWR International) and passaged when 80% confluent. The cells were tested for mycoplasma and cell identity before use.

2.3.2. Preparation of constructs for qualitative analysis

Variants were introduced by site-directed mutagenesis (2.4.11) into full length human *LHX4*, in the mammalian expression vector pc.DNA3.1 that contained a FLAG-tag (Invitrogen), using the following primer pairs respectively:

LHX4_R84C_F: GGACTTCTTCAAGT**T**GCTTCGGC

LHX4_R84C_R: GCCGAAGC**A**CTTGAAGAAGTCC

LHX4_T126M_F: GGCAGCTGGCCAT**T**GGGGGACGAATTC

LHX4_T126M_R: GAATTCGTCCCC**A**TGGCCAGCTGCC

These PCR products were then transformed using XL10 ultracompetent cells. Colonies from each reaction were then picked and grown overnight in liquid broth (LB) at 37°C on a shaker, and amplified via miniprep the following day (QIAprep Spin Miniprep Kit, Qiagen, Cat: 27106). An aliquot of each miniprep was sent to Source Bioscience for the whole *LHX4* cDNA inserts to be verified by direct sequencing analysis, to check that the correct bases and that no unwanted errors had been introduced. Maxipreps were then made for each verified construct using the HiSpeed

Plasmid Maxi Kit (Qiagen, Cat: 12662) to yield enough DNA for multiple transfections and other subsequent experiments.

2.3.3. Western Blot for LHX4 protein

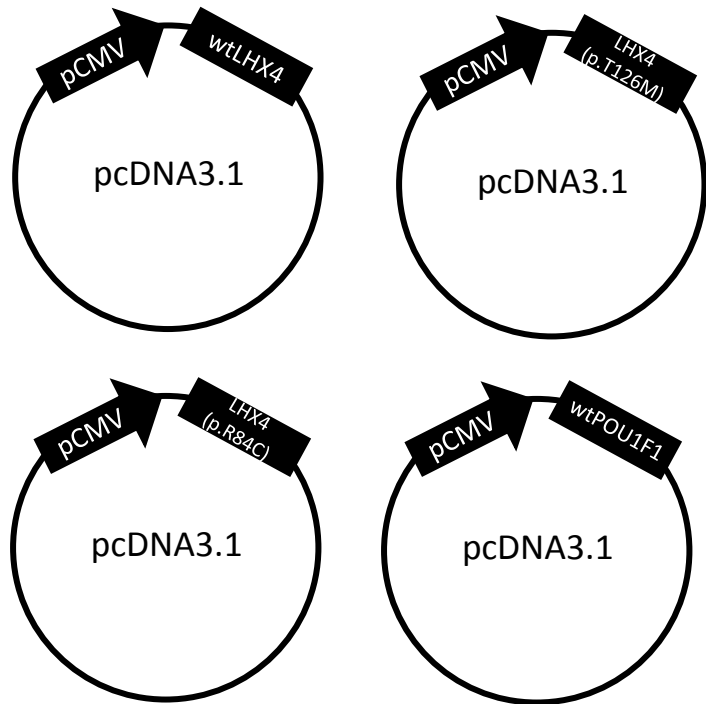
Protein extracts were taken from 80% confluent T25 flasks of HEK293T cells transfected with the constructs expressing WT *LHX4* (*wtLHX4*), *LHX4* (p.R84C) and *LHX4* (p.T126M) mutants respectively. Protein extracts were quantified using a bicinchoninic acid assay (BCA assay) (Pierce, Thermo Scientific, Cat: 23225) and a total of 10µg of each was added to each well. The negative control used in this assay was a pcDNA3.1 empty vector. Rabbit anti-FLAG Tag polyclonal primary antibody (SIGMA, Cat: SAB4301135) and goat anti-rabbit Immunoglobulin G (IgG) Horseradish Peroxidase (HRP)-conjugated secondary antibody (Cell Signaling, Cat: #7074S) were used to stain for LHX4. Please refer to the protocol used for the EIF2S3 western blot analysis (Chapter 2.4.8), including the antibodies used to stain for GAPDH, as this is the same method used for the LHX4 western blot.

2.3.4. Transfection of constructs for qualitative analysis

HEK293T cells were seeded into 24-well plates at 1×10^6 cells/well 48 hours prior to transfection. Transient transfection of mutant and *wtLHX4* constructs were conducted using Fugene-6 transfecting reagent (Promega, Cat: E2691). The cells were co-transfected with 125ng/well of firefly-luciferase reporter plasmid with either an α GSU or prolactin promoter, and 62.5ng/well of expression plasmid; these values were consistent with the reporter/expression vector concentrations/ratios used in previous established *LHX4* transfection studies (Pfaeffle et al., 2008). In addition, the cells were transfected with 50ng/well of *Renilla*-luciferase reporter vector (pRL-TK from Promega) and 10ng of mCherry vector (Cherry-N1 from Clontech) as a control and to visualise transfection efficiency under the microscope during the 24 hours after transfection respectively. All wells contained the same DNA concentration. In assays

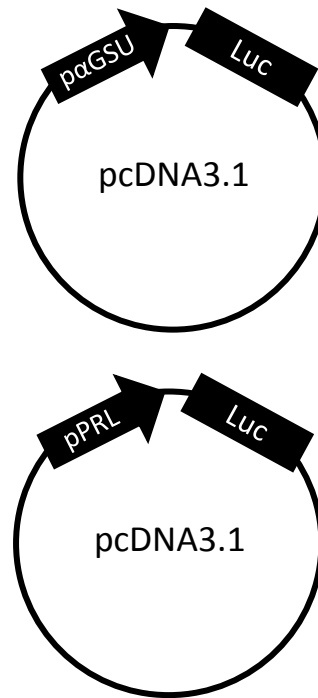
analysing synergy between LHX4 and POU1F1, a lower dose of 31.25ng/well of expression vector was also applied in addition to the described value (62.5ng/well) to look at dose dependency; pcDNA3.1 empty vector was added to the wells containing the lower dosage to maintain the same concentration of DNA per well. Cells were lysed 24 hours after transfection using Passive Lysis Buffer (Promega) and measurement of luciferase activities was performed using the Dual-Luciferase Reporter Assay System (Promega) on a luminometer (FLUO star, Optima, BMG Labtech). Two-sample Wilcoxon rank-sum (Mann-Whitney) non-parametric statistical tests, and two-tailed unpaired parametric T-tests were performed on the data generated from these assays. Results are shown as means \pm SD of 3 independent experiments in triplicate.

Expression
plasmids

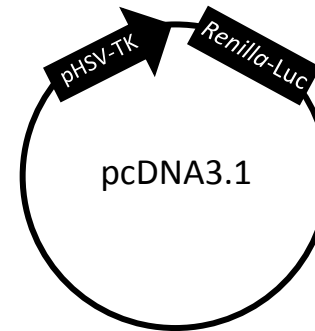


62.5ng/well
or
31.25ng/well

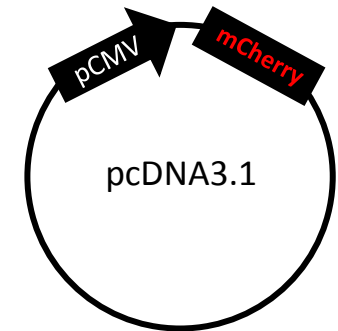
Reporter
plasmids



125ng/well



50ng/well



10ng/well

Figure 2.1: Constructs transfected into HEK293T cells. Four different expression plasmids containing mutant and WT LHX4 genes and the WT POU1F1 gene respectively, were transiently transfected into wells seeded with HEK293T cells in a 24-well plate. These were either transfected alone at a concentration of 62.5ng/well, or in combination with another at 31.25ng/well, as noted in the diagram. A firefly luciferase reporter plasmid containing either an α GSU or a prolactin promoter that directly drives luciferase was also transfected at 125ng/well. In addition a *Renilla*-luciferase reporter plasmid (pRL-TK from Promega) at 50ng/well driven by the HSV-TK promoter, and an mCherry reporter plasmid (Cherry-N1 from Clontech) at 10ng/well driven by the CMV promoter, were both added to every well. The black arrow-headed shapes with labelling beginning with 'p' in the constructs represent the plasmid promoter that drives expression of the gene noted in the respective adjacent labelled black shape in that construct. HSV-TK, herpes simplex virus thymidine kinase; CMV, cytomegalovirus.

2.4. Functional studies for *EIF2S3*

2.4.1. Cell culture

A hybrid cell line (1.1B4 cells) formed by the electrofusion of a primary culture of human pancreatic islets with PANC-1, a human pancreatic ductal carcinoma cell line, were obtained from Public Health England (PHE) (Cat: 10012801). The cells were maintained in a humidified CO₂ incubator at 37°C in Roswell Park Memorial Institute (RPMI) medium 1640 containing L-glutamine (Life Technologies, Cat: 21875-034), supplemented with 10% fetal calf serum (PAA-The Cell Culture Company) and 5% penstrep (Invitrogen). The cells were washed in x1 Hanks Balanced Saline Solution (HBSS) bought in as x10 stock (Gibco, Cat: 14185045) and diluted with autoclaved water, and trypsinised with x1 trypsin bought in as x10 stock (Gibco, Cat: 15400054) and diluted with x1 HBSS in line with manufacturer's instructions. Mouse insulinoma pancreatic beta cells (MIN6) were obtained from Professor Peter Jones' laboratory at Kings College, London. The cells were maintained in a humidified CO₂ incubator at 37°C in DMEM supplemented with 15% fetal calf serum (PAA), 5% penstrep (Invitrogen) and 5% L-Glutamine. Cells were washed in x1 PBS (VWR International) and trypsinised with x1 trypsin containing phenol red (Life Technologies, Cat: 25300054). All cells were passaged when >80% confluent. All cells were tested for mycoplasma and cell identity before use.

2.4.2. Constructs containing shRNA cassettes

Four different GFP-IRES-Puromycin-Zeomycin plasmids (pGIPZ) (11,744bp) referred to in this study as Clone 1-4 respectively, were obtained from the UCL Cancer Institute that contained small hairpin RNA (shRNA) cassettes targeting the *EIF2S3* human gene. The shRNA cassette sequence of each had been validated by the UCL Cancer Institute prior to being obtained and matched 100% with the expected hairpin

sequence according to the Open Biosystems library database. An additional pGIPZ plasmid containing a scrambled shRNA sequence was also obtained that was non-silencing and used as a control in transduction experiments. All five plasmids had a lentiviral (LV) backbone, which essentially consists of two long terminal repeats (LTR's) and a packaging signal that allow the genome to be packaged into LV particles. In the LV vectors used in this study, one of these repeats contains a deletion to prevent the LV particles replicating, making this virus self-inactivating and therefore a safer option to use in the laboratory. There is a promoter in front of the transgene (in this case the *EIF2S3* shRNA cassette) to drive expression, and also a woodchuck post-transcriptional regulatory element (WPRE) that is known to improve translation of the protein in mammalian cells (Zufferey et al., 1999). In addition to the shRNA cassette, the pGIPZ plasmids also contained green fluorescent protein (GFP) and a puromycin-resistance cassette. This co-expression enabled the cells to be monitored for GFP expression and puromycin selected following transduction (the standard map of the pGIPZ plasmid is available upon request). A maxiprep of each plasmid was prepared and used in LV packaging and transduction assays.

2.4.3. Lentiviral packaging

LV packaging was carried out in the Immunology lab in the ICH with a trained licensed member of staff, due to this procedure being classed as a Safety Activity Class 2, which requires specific Health Safety Executive project notifications. LV particles were produced by transient co-transfection of HEK293T cells (4.0×10^5 cells/well of a 6 well plate seeded 24h prior transfection) with 500ng of the pGIPZ vector constructs, 333ng of encapsidation plasmid (p8.9) and 333ng of VSV-G envelope expressing plasmid (pMDG2). The transfecting agent used was Fugene HD (3.5 μ l/well) (Promega, Cat: E2311) and the total volume pipetted into each well was 80 μ l made up with opti-mem media (Thermo Fisher Scientific, Cat: 31985070). Mastermixes were made for each pGIPZ plasmid for ease when pipetting, and each was transfected as above, in duplicate. The cells were then incubated at 37°C for 24 hours, after which the medium was changed and incubated for an additional 24 hours before harvesting the viable lentiviruses. Infectious titres were determined by doing limiting dilution of LVs on HEK293T cells. Titres were comprised between 10^5 and 10^6 transducing units/ml.

2.4.4. Transduction of 1.1B4 cells using packaged LV vectors for stable gene knockdown

1.1B4 cells were seeded into 6-well plates and transduced at a multiplicity of infection (MOI) of 5, using the previously generated lentivirus under strict sterile and contained conditions. MOI refers to the number of transducing LV particles per cell. Cells were then incubated at 37°C for 72 hours, after which the media was removed from each well. Fresh RPMI medium containing 10% serum and 5% penstrep that was also used on non-transduced cells, was supplemented with puromycin and added to the cells to positively select the transduced cells expressing the respective shRNA. The cells were monitored and kept under puromycin selection for a further 10 days, trypsinised

when confluent and expanded into T25cm² flasks respectively. The cells were washed in x1 HBSS, the media was changed when appropriate, and the cells were visualised under an Olympus IX71 inverted Fluorescence microscope for the presence of GFP until ready for lysing.

2.4.5. Cell lysis and RNA extraction

Media was removed from all wells and 1.1B4 cells were washed with HBSS. An aliquot of RNeasy lysis buffer (RLT) was prepared by adding β -mecaptoethanol at a ratio of 10 μ l/1ml. The β -mecaptoethanol is added to completely inactivate the activity of RNases. RLT buffer mix was then added to each well (350 μ l/well in a 12-well plate). A cell scraper was used followed by pipetting the buffer up and down for 2-3 mins to lyse the cells. Lysates were transferred into fresh labelled Eppendorf tubes on ice. RNA was then extracted from the lysate using an RNeasy MiniKit (Qiagen, Cat: 74104). The standard protocol from this kit was followed with the addition of a DNase digestion step using the RNase-Free DNase Set (Cat: 79254 Qiagen). Aliquots of RNA were then stored at -80°C until use.

<u>Population of RNA</u>	<u>RNA concentration in ng/μl</u>
Non transduced	652
Scrambled non-silencing	1700
Clone 1	300
Clone 2	1575
Clone 3	1310
Clone 4	99

Table 2.1: RNA concentrations derived from transfected cells. The concentration of RNA derived from 1.1B4 cells transduced with shRNA cassette-containing pGIPZ LV constructs. These values were used to calculate the reverse transcription quantities (Table 2.2). LV, lentiviral.

2.4.6. Reverse transcription

The High Capacity RNA-to-cDNA Kit (Cat: 4387406 Applied Biosystems, Life Technologies LTD) was used to yield cDNA from each RNA population. 891ng of each RNA (protocol suggests using up to 2 μ g) was used to make the cDNA due to Clone 4 having the lowest RNA concentration (99ng/ μ l) (Table 2.1) and needing the whole 9 μ l volume allowance in the protocol, which was equal to 891ng in total. The standard concentration of components were added to each reaction consistent with the supplied kit, please see Table 2.2.

<u>Reaction component</u>	<u>Constructs used in transduction on 1.1B4 cells</u>					
	<u>Non transduced</u>	<u>Scrambled</u>	<u>Clone 1</u>	<u>Clone 2</u>	<u>Clone 3</u>	<u>Clone 4</u>
<u>2X RT buffer</u>	10	10	10	10	10	10
<u>20X RT Enzyme Mix</u>	1	1	1	1	1	1
<u>Sample (891ng of RNA)</u>	1.37	0.52	2.97	0.57	0.68	9
<u>Nuclease-free water</u>	7.63	8.58	6.03	8.43	8.32	0
<u>Total per reaction</u>	20	20	20	20	20	20

Table 2.2: The volume of RNA and reagents used in reverse transcription. The values are calculated based on the RNA concentrations in Table 2.1. All volumes are in μ l. Scrambled: non-silencing shRNA.

2.4.7. qPCR primer design and analysis

The Fast SYBR Green Master Mix (Life Technologies, Cat: 4385612) was used in the qPCR reactions in this study and the standard protocol was followed, as demonstrated in Table 5 below. Primers for qPCR were designed using the Universal Probe Library database by Roche (lifescience.roche.com/shop/CategoryDisplay?identifier=Universal+Probe+Library), which generate intron flanking primers in the default setting. This database was used for the target gene (*EIF2S3*) and the three housekeeping genes (*GAPDH*, β -*ACTIN* and *HPRT*), as the primers generated bind to complementary bases within the exon/DNA coding region (cDNA), and not within introns which are absent at the qPCR stage due to the DNase digestion step performed during the RNA extraction

procedure. This ensures that complete complementary binding will occur during the qPCR reaction.

A pilot qPCR was performed initially with serial dilutions of the non-transduced cDNA as follows: undiluted, 1:5, 1:10, 1:20, 1:50 and 1:100, to define which dilution of cDNA began exponential growth at the appropriate cycle number and thus which would be used in future qPCR experiments with all cDNA populations.

The cDNA derived from the reverse transcription was diluted 1:5 in all further qPCR reactions. Nuclease-free water was used as the blank for each gene in all qPCR assays.

<u>SYBR green Real time PCR</u>	<u>x1 reaction (per well) in μl</u>	<u>x18 reactions (Mastermix) in μl</u>
SYBR green 2X	10	180
Forward primer (10 μ M) stock = 100uM	1	18
Reverse primer (10 μ M) stock = 100uM	1	18
Nuclease-free water	7	126
cDNA (1:5)	1	-
<u>TOTAL</u>	20	

Table 2.3: Volumes and concentrations of reagents and primers used in qPCR.

The table contains volumes for 1 well/reaction and volumes for 18 wells/reactions, a mastermix. The forward and reverse primer volumes in the table are from 1:10 dilutions of the stock primer aliquots respectively.

2.4.8. Western Blot analysis – Method used for both LHX4 and eIF2 γ protein analysis

2.4.8.1. Protein extraction

Human 1.1B4 cells were trypsinised respectively in a 15ml falcon tube by spinning for 5 mins at 1000rpm and supernatant was removed carefully leaving the smallest volume of media possible. The cell pellet was then washed with x1 HBSS by re-suspending the pellet in 5ml and by spinning as before. The HBSS buffer was carefully removed and the pellet resuspended in as small amount of RIPA buffer (Sigma, Cat: R0278-50ML) containing a protease inhibitor (Complete™, Mini, EDTA-free Protease Inhibitor Cocktail. Roche Cat: 11836170001), as possible; e.g. for a pellet derived from a confluent T25 flask, 200-350 μ l of RIPA buffer was added. The resuspended pellet was vortexed and put on ice for 60 mins. It was then vortexed briefly and centrifuged for 20 mins at 4°C at 13,000rpm (top speed). The supernatant was transferred into a fresh tube, being careful not to disturb the pellet containing the insoluble substance, and aliquots were snap frozen on dry ice and stored at -80°C until use. A BCA protein assay (Pierce, Thermo Scientific, Cat: 23225) was conducted on these lysates using manufacturer's instructions, to quantify the total protein concentrations of each population.

2.4.8.2. Running the gel

The x20 stock of NuPAGE MOPS SDS Running Buffer (Life Technologies Ltd, Cat: NP0001) was diluted to x1 using MilliQ H₂O. The green protective strip was removed from the bottom of a Mini-PROTEAN TGX Stain Free gel (4-20%) (Biorad, Cat: 4568094) and placed into a gel clamp inside a tank, with another gel or plastic balance on the opposing side. The middle chamber of the holder was filled with the x1 running buffer, and the combs were carefully removed, before topping up the tank with x1 running buffer to the bottom of the gel, to enable the electric current to pass through.

The wells were washed out by pipetting up and down with an empty pipette before the samples were loaded.

The BCA values generated were used to normalize the protein quantity thus determining the volume of lysate needed to total the desired protein concentration (5µg, 10µg, 30µg). Please refer to Table 2.4 for the samples that were loaded into wells in the pilot assay performed. This pilot assay used total protein derived from HeLa cells and human 1.1B4 non-transduced cells. The HeLa cell lysate was used as a positive control for the anti-EIF2S3 antibody as recommended by the manufacturer.

Cell population	Protein lysate concentration (µg/µl)	Total protein added into well (µg)	Protein lysate volume added to well (µl)	ddH2O added to well (µl)	x4 Laemmli buffer added to well (µl) (Total volume 40µl)
Hela (1:10)	1.39	5	3.60	26.40	10
Hela (1:10)	1.39	10	7.19	22.81	10
Hela (1:10)	1.39	30	21.58	8.62	10
1.1B4 WT	1.34	5	3.73	26.27	10
1.1B4 WT	1.34	10	7.46	22.54	10
1.1B4 WT	1.34	30	22.38	7.62	10

Table 2.4: The calculation of protein samples used in the pilot western blot assay. The pilot western blot assay used HeLa cell lysate and 1.1B4 WT cell lysate at three different concentrations respectively. 1:10, 1 in 10 dilution of the stock lysate was used in the HeLa protein calculation. WT, wild-type.

Following preparation of the samples calculated in Table 2.4, 2µl of DTT (10%) was added to each sample aliquot and then denatured at 95°C for 5 mins using a heat block.

10µl of PAGERuler prestained protein ladder (Generon, Cat: 26616) was loaded into the first well and up to 40-50µl of each sample respectively into subsequent wells. The gel was run at ~100 volts (V) until the blue dye was only ~5 mm from the bottom of the gel; approximately 45 mins depending on protein size.

2.4.8.3. Transfer

A Trans-Blot Turbo Transfer Pack, PVDF, 7 x 8.5 cm (BioRad, Cat: 1704156) was used for transfers. The side labelled 'bottom' was laid into the Trans Blot Turbo machine tray, with the attached membrane facing up. The supplied roller was used to roll over the membrane to remove any bubbles. The gel was then prised out of the plastic after it had finished running using the supplied green device and placed onto the membrane manually. The roller was used again to smooth out the gel, and the side labelled 'Top' was placed on top of the gel (either side can face up). The tray applicator was closed, making sure all 4 edges were clipped in before slotting into the Trans Blot Turbo machine. To operate this machine the following options were pressed: 'Turbo', '1 mini gel' (or however many gels are transferring), 'A run' 'B run' or both, depending on which draw (A or B) had the gel in. The gel took 7 mins to transfer completely. Whilst the above was transferring, blocking agent was prepared in a 50ml falcon tube: 2.5g of milk powder in 50ml of x1 TBS/TWEEN detergent (Calbiochem, Cat: 524753-1EA).

When transferred, the transfer 'sandwich' was separated and the membrane placed in approximately 20ml of blocking agent in a falcon tube and put on a rotator for 1 hour at room temperature.

The membrane was incubated with the primary antibody; 10ml of blocking agent containing 20µl of anti-EIF2S3 rabbit polyclonal antibody (Proteintech Europe, Cambridge Bioscience, Cat: 11162-1-AP) to result in a 1:500 dilution and rotated on a roller at 4°C overnight. The supplier of the antibody used the gene name for the antibody rather than the protein name, therefore it is termed as 'anti-EIF2S3', as opposed to 'anti-eIF2γ', throughout this study. A monoclonal mouse anti-GAPDH (Merck Millipore, Cat: MAB374) primary antibody, diluted to 1:4000, was used as the control.

The next day, the membrane was taken out and washed in 40ml of x1 TBS/TWEEN for 10-15 mins x4 times in a rotating 50ml falcon tube.

The membrane was incubated with a secondary antibody; 10ml of blocking agent containing 2µl (1:5000 dilution) of goat anti-rabbit IgG HRP-conjugated antibody (Cell Signaling, Cat: #7074S), and rotated on a roller for 1 hour at room temperature. For the GAPDH control, a polyclonal goat anti-mouse IgG HRP-conjugated secondary antibody (Dako, Cat: P0447) diluted to 1:4000 was used. The membrane was then washed at least x4 times in the x1 TBS/TWEEN as before (the washing is essential at this stage).

The developing mix was prepared using Clarity Western ECL substrate (Biorad, Cat: 1705061) at a 1:1 ratio and 2ml was pipetted onto the membrane. It was incubated for 5 mins and developed on the ChemiDoc via the following settings: 'single channel', 'Blot', 'Higher Chemi sensitivity', 'Setup': start at 1 second, end at ~30 seconds and set to take 5 images. Manual exposure at 0.5 was set for the first analysis and the exposure time was adjusted if no image emerged.

2.4.9. Insulin Secretion Assay

Krebs Ringer Bicarbonate (KRB) Buffer (1x) was prepared in a final volume of 1 Litre of MilliQ water (store at 4°C) using the volumes in Table 2.5. A magnetic stirrer was used to dissolve the powder into solution and the pH was adjusted to 7.4 using a pH meter.

Solution	Volume in grams	Concentration mM
NaCl	7.95	34
KCL	2.5	1.175
KH ₂ PO ₄	0.163	0.3
NaHCO ₃	0.42	1.25
MgSO ₄ (7H ₂ O)	0.295	0.3

Table 2.5: How to make KRB buffer. The volume and concentration of chemicals used to make the KRB buffer for use in an ultrasensitive insulin ELISA assay. KRB, Krebs Ringer Bicarbonate.

Pre-incubation buffer was prepared by adding 0.5g of bovine serum albumin (BSA) powder and 2mM of glucose (0.18g) to 500ml of the 1x KRB buffer. This was then aliquoted into 50ml falcons and stored at 4°C in cold room.

Day 1

MIN6/1.1B4 cells were plated at 3×10^5 per well in a 6-well plate, in a total volume of 2ml of each cell types respective media, and left overnight in an incubator at 37°C until cells grew to 80-90% confluency (usually 24 hours).

Day 2

The media was removed and 2ml of the pre-incubation buffer was added and left for 60 mins before turning the plate upside down onto tissue paper to remove the solution. Test agents were added (1ml/well) (Chapter 2, Table 2.6) and incubated at 37°C for 24 hours. Media was aspirated carefully so as not to blow holes in the cells, aliquoted and frozen at -20°C until use.

1x KRB buffer only (0% glucose)	Make as Table 2.5 states
1x KRB buffer with 10mM glucose (0.09g in 50ml)	Measure 0.09g glucose and dissolve in 50ml of the 0% glucose 1x KRB buffer to make 10mM glucose buffer
Forskolin 10µM (with 10mM glucose)	Stock powder comes at 10mg. Dissolve all in 2.44ml of DMSO to make a 10mM stock and dilute this 1:1000 by adding 10µl into 10ml of 1x KRB buffer with 10mM glucose
IBMX 100µM (with 10mM glucose)	Stock IBMX is 100mM. Dilute this 1:1000 by adding 10µl into 10ml of 1x KRB buffer with 10mM glucose

Table 2.6: Insulin secretion assay test agents. A simple guide to calculate test agent concentrations, used in insulin secretion assays. IBMX, 3-isobutylmethylxanthine.

Insulin secretion was then measured in each sample using an ultrasensitive insulin Elisa kit (MERCODIA, Cat: 10-1132-01) using the standard protocol. MIN6 cells were used in this insulin secretion assay as a control and were plated at the same density as 1.1B4 cells.

2.4.10. Apoptosis assay

MIN6/1.1B4 cells were seeded into white 96-well sterile tissue culture treated microplates with clear bottoms (PerkinElmer, Cat: 6005181), at 10,000 cells/well in a total volume of 200µl of cell-type specific media, and incubated overnight at 37°C. Media was removed by inversion of the plate and 100µl of cytokine mix containing the following was added to respective triplicate wells: 1L-1β (50 U/ml), TNF-α (1000 U/ml), INF-γ (1000 U/ml); diluted in media and incubated for 16 hours at 37°C.

Caspase-Glo 3/7 reagent (Promega, Cat: G8090) was added at a 1:1 ratio of reagent:sample (100µl) to each well and incubated for 1 hour at room temperature before reading the luminescent signal generated on the luminometer. There were triplicate wells of each of the following:

- Blank wells: had no cells but had cytokine mix added. These wells emitted background luminescence associated with Caspase-Glo reagent. This value was subtracted from experimental values.
- Basal caspase activity: wells containing cells with media not containing cytokine mix.
- Cytokine-stimulated caspase activity: wells containing cells with respective cytokine mix added.

Two-sample Wilcoxon rank-sum (Mann-Whitney) non-parametric statistical tests, two-way ANOVA tests, and two-tailed unpaired parametric T-tests were performed on the data generated from these apoptosis assays.

2.4.11. Single site-directed mutagenesis

The QuikCHANGE II XL site-directed mutagenesis kit (Agilent Technologies, Cat: 200521) was used to alter the BamHI site that was within the *EIF2S3* insert in the pCMV-SPORT6 vector containing the full cDNA *EIF2S3* sequence (Source Bioscience). This is the same vector that was used to make RNA probes for the *in situ* hybridization studies (Chapter 2.5). The BamHI site already within the *EIF2S3* cDNA had to be mutated so that the insert would not be cut in half during the BamHI digestion step. This BamHI site had one nucleotide substituted during this step without changing the amino acid, thus keeping the WT protein sequence intact and unaltered. Therefore when adding the BamHI enzyme at a later stage to cleave the *EIF2S3* insert out of this pCMV-SPORT6 vector it would only cut at the ends of the insert yielding the full *EIF2S3* sequence. The *EIF2S3* insert had to have BamHI sites at either end, as the cloning site within the host LV-IRES vector that the inserts have to ligate into was within two BamHI sites. The primers used in this reaction to alter one base of the BamHI sequence (GAATCC) were as follows, with the altered nucleotide highlighted in red:

BamHI_alter_F: GCTCATGGTGAACATAGG**GCT**CCTGTCAACAGGAGG

BamHI_alter_R: CCTCCTGTTGACAGGG**AGC**CTATGTTACCATGAGC

The above primers were diluted to 125ng/μl and the vector to 10ng/μl. 1μl of this diluted vector was pipetted into a tube on ice and the following was added:

1μl of each diluted primer

1μl of dNTPs

5μl of x10 buffer

3μl Quikchange

38μl of double distilled water

Lastly, 1µl of *pfu* enzyme (2.5 U/µl) was added to each well to total 50µl/well and the Thermocycler machine was set to run the following protocol:

STAGE 1	STAGE 2 (x12)			STAGE 3
95c	95c	60c	68c	68c
1min	50secs	50secs	6mins *	7mins

*This time length relates to 1 min per kb of DNA, reflecting the size of the vector containing the insert, which in this case was 5.815kb.

Following the above PCR reaction, the wells were put on ice to cool slightly before 1µl of *Dpn* I restriction enzyme was added into each well and mixed thoroughly with a pipette. The plate was then put into an incubator at 37°C for 1 hour to dissolve the parental supercoiled DNA.

XL10 ultracompetent cells (provided in kit) were thawed on ice and 45µl of cells were aliquoted into labelled tubes. 2µl of β-mecaptoethanol (provided in kit) was added into each tube and left on ice for 10 mins whilst being flicked occasionally to mix. 2µl of the PCR product was pipetted into the respective tube, stirred with a pipette tip and left for approximately 30 mins on ice. During this time, S.O.C medium (Invitrogen, Cat: 15544034) was warmed to 42°C.

After the 30 mins, the cells were heat shocked at exactly 42°C in a water bath for precisely 30 seconds and put back on ice immediately for 2 mins. Then 500µl of the pre-warmed S.O.C medium was pipetted into the tubes and shaken at 37°C for 1 hour, during which time, ampicillin-resistant agar plates were warmed to 37°C.

The transformed cells were pipetted into the middle of their respective plate (250µl/plate) and a sterile spreader was used to equally spread them before incubation at 37°C overnight (not on a shaker). The following day ~4-6 colonies from each plate were picked using a pipette tip and dropped into ~3ml of ampicillin supplemented liquid broth (LB) in a 15ml falcon tube respectively. The tubes were incubated overnight at 37°C on a shaker and minipreps were carried out for each on the following day, using manufacturer's instructions.

Four primers were used to verify the full cDNA sequence of *EIF2S3*, (the *EIF2S3_1R* covered the beginning of the gene):

EIF2S3_1F: 5' GATCTTGTGGGAGCAGTACACC 3'

EIF2S3_2F: 5' CCAAGAGACTTTACTTCAGAGCC 3'

EIF2S3_3F: 5' CCGGGCTGACAGAATGGTGGGG 3'

EIF2S3_1R: 5' CCGTTCAGCATAGTAGCCATC 3'

2.4.12. LV-IRES Vector digest

The LV backbone host vector was obtained from the Immunology lab (ICH) (see Chapter 2.4.2 for details on LV vectors such as this). An unwanted insert was removed from this vector using the BamHI restriction enzyme (Promega, Cat: R6021) by adding the reagents listed in Table 2.7 to a sterile tube, briefly spinning down in a centrifuge and incubating at 37°C for <4 hours.

<u>Reagent</u>	<u>Volume (µl)</u>
Nuclease-free water	83
Restriction enzyme 10x Buffer E	10
BSA (10µg/µl)	1
Vector DNA (1680ng/µl)	3
Mix by vortex at this stage	
BamHI enzyme (10U/µl)	3
	Total volume = 100 µl

Table 2.7: The volume of reagents used to digest the LV-IRES vector. Reagents were added into a sterile Eppendorf tube in the order listed.

2.4.13. Alkaline Phosphatase treatment

The linearized BamHI cut LV-IRES vector was dephosphorylated by treatment with calf intestinal alkaline phosphatase (CIAP) (Promega, Cat: M1821) to prevent the BamHI cut vector ends ligating back together. As per manufacturer's instructions, the digested DNA was purified before dephosphorylation by ethanol precipitation: 10µl of sodium acetate (3M) and 250µl of 100% ethanol was added to the 100µl of digested

DNA, and centrifuged at 13,000rpm for 10 mins. The supernatant was removed and 200µl of 70% ethanol was added and spun as before, to wash the pellet. The supernatant was removed and the pellet was allowed to air dry for >10 mins at room temperature. Nuclease-free water (43 µl) was added to resuspend the pellet, followed by 5µl of 10x CIAP buffer and 1µl of stock CIAP enzyme (Promega, Cat: M1821), and incubated at 37°C for 30 mins. A further 1µl of CIAP stock enzyme was added to make a final volume of 50µl, and was incubated at 37°C for a further 30 mins.

2.4.14. Gel extraction

The dephosphorylated cut vector was run over 2 wells on a 20-well 1% agarose gel at 100V for 1 hour before being excised using a scalpel under UV light. The weight of an empty Eppendorf tube was subtracted from the weight of the gel and tube together to give the weight of the gel. A QIAquick Gel Extraction Kit protocol (Qiagen, Cat: 28704) was then followed as by manufacturer's instructions to yield purified vector DNA, which was then stored at -20°C.

2.4.15. Amplification of the *EIF2S3* insert

The full coding region of the *EIF2S3*_WT insert was amplified out of the original pCMV-SPORT6 plasmid (Source Bioscience, IRATp970H0941D, IMAGE ID: 4419438). Primers were designed with the BamHI sequence flanking the *EIF2S3* coding region (highlighted in red):

EIF2S3_BAMHI_F: 5' GGACTCGGATCCATGGCGGGCGGAGAAGCTGG 3'

EIF2S3_BAMHI_R: 5' CGCTTAGGATCCTCAGTCATCATCTACTGTTGG 3'

An AccuPrime *pfx* Supermix (Invitrogen, Cat: 12344-040) containing a proofreading 3' to 5' exonuclease activity with a higher fidelity than the *pfu* proof reading polymerase enzyme, was used in the PCR reaction.

Reagent	Volume (μ l)
10ng of DNA maxiprep (diluted stock to 10ng/ μ l)	1
Accuprime <i>pfx</i> supermix (containing MgSO ₄ , dNTPs and polymerase enzyme)	22.5
Forward and reverse primer (diluted 100uM stock 1:10 to give 10uM)	1 of each primer
	Total volume: 25

Table 2.8: Amplification of the *EIF2S3* cDNA insert. Reagents and volumes used in the PCR reaction to amplify the *EIF2S3* gene out of the pCMV-SPORT6 vector.

The above PCR reaction was prepared on ice in a 96-well sequencing plate, put into a Thermocycler and run using the following protocol:

Step1 (x1 cycle)

95°C for 5 mins

Step 2 (x35 cycles)

95°C for 15 seconds

60°C for 30 seconds

68°C for 2 mins (~1 min for every kb in insert: *EIF2S3* = 1.419kb)

Step 3 (x1 cycle)

Cool to 4°C for >10 mins

5µl was then run on a 1% agarose gel slowly at 90 V for 90 mins next to a 1kb DNA ladder (Hyperladder I, Biorun, Cat:33053), to verify that the *EIF2S3* insert was the correct size and had been amplified.

2.4.16. Polyadenylation

The addition of adenine bases (a Poly(A) tail) on the 3' end of the amplified *EIF2S3_WT* PCR product was necessary for ligation of the inserts into the pGEM-T Easy vector (TA-cloning). This was achieved using Terminal Transferase (New England Biolabs LTD (NEB), Cat: M0315S). Manufacturer's instructions were followed:

Adenine tailing reaction

5µl 10X Terminal Transferase buffer (TdT)

5µl 2.5mM CoCl₂ solution (provided in kit)

20µl *EIF2S3* PCR product

0.5µl 10mM dATP (from dNTP set, 100mM, Biorun, Cat: 39025)

0.5µl Terminal Transferase (20units/µl)

Deionized (nuclease-free) water up to 50µl total volume (19µl)

Incubate at 37°C for 30 mins and then stop the reaction by heating the mix to 70°C in a heat block for 10 mins. The PCR product was then column purified using the QIAquick PCR Purification Kit (Qiagen, Cat: 28104).

2.4.17. TA-Cloning: Ligation of the cDNA *EIF2S3 WT* insert into the pGEM-T

Easy vector

The polyadenylated *EIF2S3_WT* PCR product was cloned into the pGEM-T Easy vector (pGEM-T Easy Vector System II, Promega Cat: A1380) using the following standard equation for ligation of insert into vector:

$$\frac{\text{ng of vector} \times \text{kb size of insert}}{\text{kb size of vector}} \times \text{insert:vector molar ratio} = \text{ng of insert}$$

The pGem-T Easy vector kit recommends to use 50ng of the vector at a 3:1 insert:vector ratio. Therefore the following values were put into the above equation to calculate how many ng's of insert (*EIF2S3* PCR product) were needed in the ligation reaction:

$$\frac{50\text{ng of vector} \times 1.419\text{kb insert}}{3.0\text{kb vector}} \times \frac{3}{1} = 70.95\text{ng of insert}$$

The following table (Table 2.9) presents the volumes of DNA and reagents that were pipetted into sterile 0.5ml tubes for the ligation of the *EIF2S3_WT* insert into the pGEM-T Easy vector. The reactions were mixed by pipetting and incubated at room temperature for 1 hour.

Reagent	<i>EIF2S3</i> WT ligation	Positive control
2X Rapid ligation buffer for T4 ligase	5	5
pGEM-T Easy vector *(50ng)	1	1
Respective <i>EIF2S3</i> insert PCR product *(70.95ng)	1.48 (stock DNA = 48ng/μl)	-
Control insert DNA	-	2
T4 DNA ligase (3U/μl)	1	1
Nuclease-free water to a final concentration of 10μl	1.52	1

Table 2.9: *EIF2S3* ligation into the pGEM-T Easy vector. The volumes of reagents used in the ligation of the *EIF2S3* amplified insert into the pGEM-T Easy vector. All volumes are in μl. *The concentration of DNA needed in the final reaction to give a 3:1 ratio of insert:vector.

2.4.18. Transformation of pGEM-T Easy vector

The two products from the ligation reactions above; *EIF2S3*_WT and the positive control, were transformed in duplicate, respectively, on LB agar/ampicillin/IPTG/X-GAL plates with ampicillin. JM109 High Efficiency Competent Cells (supplied in the pGEM-T Easy vector II kit) were thawed on ice (5 mins) and mixed by gently flicking. 2μl of each ligation reaction was pipetted into sterile 1.5ml tubes on ice (x2 for each ligation), and 50μl of the JM109 cells were added to each. The tubes were gently

flicked to mix and placed on ice for 20 mins. The cells were then heat-shocked for 45 seconds in a heat block at exactly 42°C and immediately returned to ice for 2 mins. 950µl room temperature S.O.C medium was added to each tube and incubated for 1.5 hours at 37°C on a shaker (~150rpm). During the last 30 mins of this incubation, x6 LB agar plates containing ampicillin were spread with 100µl of 100µM IPTG and 50µl of 20µg/µl X-GAL to enable blue/white staining, and incubated at 37°C (without shaking). 100µl of each transformation culture in duplicate was plated onto labelled LB agar/ampicillin/IPTG/X-GAL plates and incubated overnight (16 hours) at 37°C. (The positive control ligation was diluted 1:10 with S.O.C medium before 100µl was plated in duplicate.)

The following day white colonies were picked from each ligation and incubated in 3ml of LB with ampicillin in 15ml falcon tubes overnight (~16 hours) at 37°C on a shaker. The x8 tubes were then amplified via miniprep following manufacturer's instructions. An aliquot from the *EIF2S3*_WT pGEM-T Easy plasmid miniprep was sent to Source Bioscience for the complete cDNA *EIF2S3* insert to be sequenced (using the same four primers listed in Chapter 2.4.11) to check for unwanted errors.

JM109 competent E.Coli cells were used in the transformation of the *EIF2S3* insert into LV-backboned vectors as these cells contain mutations in the genes *recA1* and *endA1*. These mutations aid in minimizing recombination and ensuring plasmid stability, therefore these cells are a better choice than DH5 alpha E.Coli cells when transforming LV-backboned vectors especially, as they yield a high quality plasmid DNA (Sigma).

2.4.19. Enzyme digest to cut out inserts from p.GEM-T vector

Upon sequence verification of the *EIF2S3_WT* insert within the pGEM-T Easy vector, the insert was digested with BamHI, using the following protocol:

<u>Reagent</u>	<u>Volume (µl)</u>
Nuclease-free water	17.5
Restriction enzyme 10x Buffer E	5
BSA (10µg/µl)	0.5
p.GEM-T vector containing insert	25
Mix by vortex at this stage	
BamHI enzyme (10U/µl)	2
	Total volume = 50µl

Table 2.10: Enzyme digest reaction. The volume of reagents used to digest the *EIF2S3_WT* insert out of the pGEM-T Easy vector using the BamHI restriction enzyme. Reagents were added into a sterile Eppendorf tube in the order listed.

The above reagents were briefly spun down in the tube in a centrifuge and incubated at 37°C for <4 hours. These were all run on a 1 % agarose gel and purified by gel extraction as previously described, using the QIAquick Gel Extraction Kit (Qiagen, Cat: 28704).

2.4.20. Ligation of *EIF2S3* into LV-IRES vector

The *EIF2S3_WT* purified insert was ligated into the linearized dephosphorylated LV-IRES vector using T4 DNA ligase and 100ng of the vector at a 3:1 ratio of insert:vector as per manufacturer's instructions (Promega, Cat: M1801):

$$\frac{100\text{ng of vector} \times 1.419 \text{ kb insert}}{10.5 \text{ kb vector}} \times \frac{3}{1} = 40 \text{ ng of insert}$$

The reaction was incubated overnight on a Thermocycler at 15°C for 16 hours. The ligation product was then transformed with JM109 cells overnight using the same method used in transforming the pGEM-T Easy vector (Chapter 2.4.18). Colonies were picked and minipreps were made. Aliquots of each miniprep (x6) from six different colonies were sent to Source Bioscience with one primer (*EIF2S3_1R*) to verify that the insert had ligated into the LV-IRES vector in the correct orientation. The miniprep containing the *EIF2S3* insert in the correct orientation was then taken forward for multi-site-directed mutagenesis.

2.4.21. Multi-site-directed mutagenesis

The patient *EIF2S3* (p.P432S) mutation was introduced into the *EIF2S3_LV-IRES* ligated vector, in addition to correcting the altered BamHI site (as discussed in section 2.4.11) within the *EIF2S3* insert sequence. This was carried out to yield the final *EIF2S3* (p.P432S) mutant construct used in further studies. The two primers used in this reaction were:

EIF2S3_P432S_F: GTTTTGACCAATTCAGTGTGCACAGAGG

BamHI correct_F: GCTCATGGTGAACATAGGATCCCTGTCAACAGGAGG

The protocol for this multi-site-directed reaction differs to the single site-directed reaction and is described in Table 2.11.

<u>Reaction component</u>	<u>For templates >5kb</u>
10x Quikchange Multi reaction buffer	2.5 µl
Double-distilled water	X µl to final volume of 25 µl
QuikSolution	0–0.75 µl (titrate for each template)
Ds-DNA template	X µl of (100ng)
Mutagenic primers	X µl (112ng of <i>EIF2S3_P432S_F</i> primer, 144 ng of <i>BamHI_correct_F</i> primer)
dNTP mix	1 µl
Quikchange multi enzyme blend	1 µl

Table 2.11: Multi-site directed mutagenesis. Both primers used in this reaction are forward primers only (one for each mutation introduced), the ng's of these primers added are relative to the number of nucleotides in them e.g. 25 bases = 100ng of primer is needed in the reaction, therefore a primer with 36 bases = 144ng of primer needed. This is consistent with the multi-site-directed mutagenesis protocol instructions.

The reaction in Table 2.11 was run on the Thermocycler machine as follows:

Segment	Cycles	Temperature	Time
1	1	95	1 min
2	30	95	1 min
		55	1 min
		65	2 mins/kb of plasmid length (<i>EIF2S3</i> -LV-IRES = ~12kb)

A single site-directed mutagenesis reaction using the described method (Chapter 2.4.11) was performed on the *EIF2S3*-LV-IRES plasmid to revert the single nucleotide back to give the original BamHI site within the *EIF2S3* insert. This yielded the exact original *EIF2S3*_WT cDNA sequence and thus the final *EIF2S3*_WT construct used in further studies. This reaction corrected the previously altered BamHI site within the *EIF2S3* cDNA by using the following primer pair:

BamHI correct_F: GCTCATGGTGAACATAGGATCCCTGTCAACAGGAGG

BamHI correct_R: CCTCCTGTTGACAGGGATCCCTATGTTACCATGAGC

Both PCR products from both the single and multi-site-directed mutagenesis reactions above were transformed in JM109 cells as previously described (Chapter 2.4.18). Colonies were picked and minipreps were made. An aliquot of a miniprep from both *EIF2S3*_WT and *EIF2S3* (p.P432S) constructs respectively was sent to Source Bioscience for sequencing with the same four primers as before (Chapter 2.4.11). This was to verify the whole cDNA *EIF2S3* insert sequence to check if the site-directed reactions above had introduced the correct bases and that no unwanted

errors had occurred. Upon verification that the sequences in both constructs were correct, maxipreps of these plasmids were then generated.

These final constructs: *EIF2S3_WT* and *EIF2S3* (p.P432S) in the LV-IRES vector, were constructed in order to be packaged into viable LV particles and transduced into 1.1B4 cells using the previously described method (Chapter 2.4.3 – 2.4.4).

Cloning flowchart

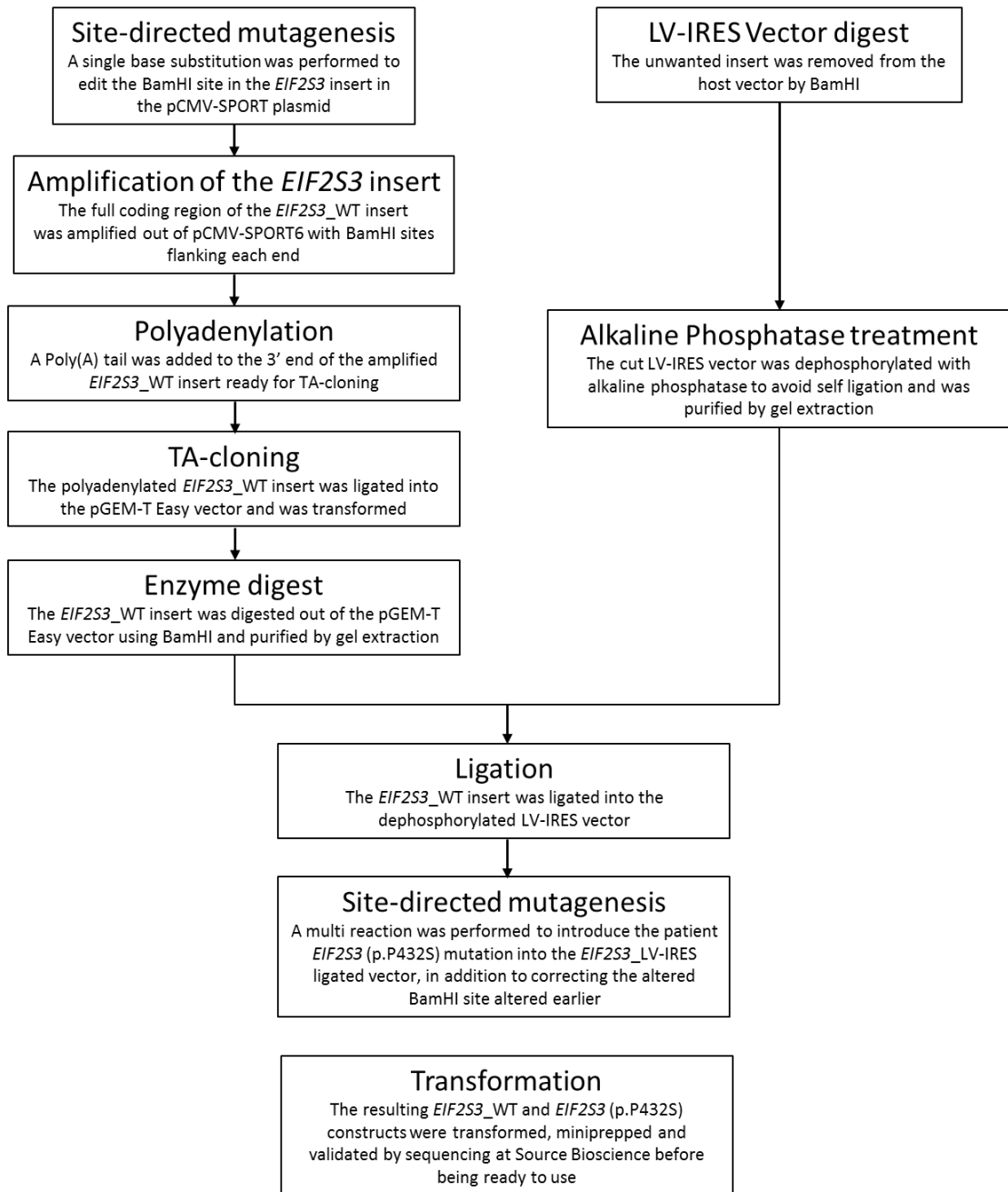


Figure 2.2: A summary of the cloning process. The steps performed in cloning the *EIF2S3* insert into the LV-IRES vector and yielding the two constructs: *EIF2S3*_WT and *EIF2S3* (p.P432S) used in further studies.

2.4.22. Transfection of the *EIF2S3* constructs

Both 1.1B4 and MIN6 cells were seeded at 3×10^5 per well in a 6-well plate in their specific complete media (10% FBS and 5% penstrep) and incubated (Chapter 2.4.1). The LV-IRES empty vector, *EIF2S3_WT* and *EIF2S3* (p.P432S) constructs were transfected into cells using both Fugene-6 as previously described (Chapter 2.3.4) and lipofectamine 2000 (Life Technologies Ltd, Cat: 11668027) transfecting agents respectively on separate occasions, using standard manufacturer protocols. When using lipofectamine, 4 μ g of DNA and 10 μ l of lipofectamine in a total of 250 μ l opti-mem media (Thermo Fisher Scientific, Cat: 31985070) was added to each well. Media was changed 24 hours after transfection and cells were observed for GFP 48 and 72 hours after transfection.

2.4.23. Cell sorting

Seventy-two hours after transfection, cells were trypsinised and suspended in 1ml of respective media containing 1.5% FBS in 15ml falcon tubes and transported on ice. The cells were put into a BD FACS Aria III cell sorter, which has four different lasers: 405nm, 488nm, 561nm and 633nm. The 530/30 filter from the 488nm laser was used in detecting the green fluorescing cells from each population: empty vector, *EIF2S3_WT* and *EIF2S3* (p.P432S) LV-IRES transfected cells, which were collected in 1ml of complete media in 15ml falcon tubes. These green fluorescing cells were then plated into culture plates for expansion.

2.5. In situ hybridization

2.5.1. Linearizing plasmids

Fully sequenced human purified cDNA clones containing the full coding sequence of their respective gene, were obtained from Source Bioscience (<http://sourcebioscience.com/>). They were digested with specific restriction enzymes (Promega) (see Table 2.12 for all clones and enzymes used) that did not cut within our gene of interest, via the following protocol:

10µg DNA (circular plasmid)

1 × restriction enzyme buffer (10µl of the x10 stock)

20-50U restriction enzyme (5µl of the 10U/µl stock)

Make up to 100µl with double distilled water (ddH₂O)

The reactions were then incubated for 2 hours at the enzymes' optimum temperature, which in each case was 37°C. 1µl of the original circular plasmid was run next to the linearized clone on a 1.5% agarose gel with 5µl of 1kb ladder. The linearized plasmids were cleaned using a QIAquick PCR purification kit (Qiagen, Cat: 28104).

2.5.2. DIG probe transcription

The purified linearized plasmids (Table 2.12) were labelled with digoxigenin (DIG), using 1µg of DNA, 2µl of DIG RNA labelling mix (stock at x10) (Roche, 11277073910), 1µl of transcription buffer (stock X10), 1µl of protector RNA inhibitor (Roche, 03335399001), 1µl of either T3, T7 or SP6 RNA polymerase (Roche), made up to a final volume of 20µl with RNase and DNase free water and incubated for 2 hours at 37°C. 2µl of RNA probe was run for 5 mins at 150V on a 1% agarose gel to assess the efficiency of transcription. Good probes are usually ten-fold brighter than the DNA band in the 1kb ladder. The DIG probes were diluted with DEPC-water up to a total of 100µl and purified using spin columns (Chroma-spin, Clontech-100).

Gene Name	Source Bioscience reference	Plasmid	Cloning site	Restriction enzyme and polymerase used for <u>sense</u> probe	Restriction enzyme and polymerase used for <u>antisense</u> probe
<i>EIF2S3</i>	IRATp970H0941D IMAGE ID: 4419438	pCMV- SPORT6	5s: Sall 3s: NotI	XhoI, SP6	AgeI, T7
<i>CTPS2</i>	IRATp970A0631D IMAGE ID: 5268973	p.BluescriptR	5s: Sall- XhoI 3s: BamHI	KpnI, T7	EcoRI, T3
<i>RNPC3</i>	IRATp970A029D IMAGE ID: 3873751	pCMV- SPORT6	5s: Sall 3s: NotI	XhoI, SP6	AgeI, T7
<i>PRMT6</i>	IRATp970A0595D IMAGE ID: 5212478	pCMV- SPORT6	5s: EcoRV 3s: NotI	XhoI, SP6	AgeI, T7
<i>FASN</i>	IRATp970A1078D IMAGE ID: 6172538	pCMV- SPORT6	5s: Sall 3s: NotI	XhoI, SP6	AgeI, T7
<i>APEX2</i>	IRAU969F1116D IMAGE ID: 3537317	pOTB7	5s: EcoRI 3s: XhoI	BglII, SP6	EcoRI, T7

Table 2.12: Details of IMAGE cDNA clones used in *in situ* experiments.

Restriction enzymes that were used to linearize plasmids, deciphered from plasmid maps supplied with the respective IMAGE clone from Source Bioscience. The RNA polymerase used during transcription of sense and antisense probes.

2.5.3. Human embryonic sections

Slides with sections of human embryonic tissue were selected at different stages of development: Carnegie stage (CS) 16, 19, 20, 23 and at late 8 post conception week (pcw) and prepared and obtained from the Human Developmental Biology Resource (HDBR). Slides were treated with RNase as an extra control to avoid non-specific binding/hybridisation and were subject to the following steps:

2.5.4. Pre-hybridisation treatment

The sections were placed into solutions in different sterilized troughs (all equipment was RNase-free), beginning with HistoClear solution (Agar Scientific), which helps preserve and clean wax from the tissue, followed by a series of washing steps with decreasing dilutions of ethanol to hydrate the tissue. Following this; 4% paraformaldehyde in 1x PBS (PFA) to 'fix' the sections, PBS to wash them, Proteinase K (PK) for precisely 8 mins to perforate the tissue, PFA to re-fix, a second PBS wash, 0.1M Triethanolamine with acetic anhydride to break up the bonds and make RNA accessible, a third PBS wash ending with a dehydration step with increasing ethanol concentrations and subsequent air drying on the bench.

2.5.5. Hybridisation

A solution of Hybmix, of which ingredients are listed below, RNase inhibitor, tRNA and the *EIF2S3* probe made earlier was added to each slide (100ul to each), then covered with a clean cover slip avoiding bubbles and placed into a humid chamber overnight at 65°C.

Hybmix solution:

50% formamide

0.3M sodium chloride

20mM Tris HCL at pH7.0

5mM EDTA

10% Dextran sulphate

1x Denhardt's solution (a mixture of blocking agents)

2.5.6. Post-hybridisation washing

All following steps and solutions were at 65°C and not RNase-free. The cover slips were removed from the slides which were placed into a rack, in a trough containing pre-warmed 2x saline-sodium citrate (SSC) (a hybridisation buffer) in a 65°C water bath. The following washes then took place:

- Rack of slides was washed in fresh 2x SSC solution for 30 mins.
- Washed with formamide twice for 30 mins.
- Washed twice in 2x SSC for 30 mins.
- Washed in 0.2x SSC for 30 mins.
- The trough was then emptied and filled with 0.2x SSC and allowed to cool to room temperature.

2.5.7. Antibody detection

The slides were transferred into a rack and washed twice in buffer 1 (0.1M Tris pH 7.6, 0.15M sodium chloride), followed by a blocking step for 1 hour in buffer 1 containing 10% fetal calf serum (FCS). After draining the slides, the antibody solution; anti-DIG fab antibody at 1:1000 in buffer 1, was added and covered with parafilm before being incubated in a humid chamber overnight at 4°C. The fragment antigen-binding (Fab) fragment is the region on the antibody that binds to the antigen, which in this case is DIG. Therefore the anti-DIG fab antibody recognises and binds to the DIG-labelled probe that is bound to the respective RNA transcripts in the section. The following day the parafilm was removed and slides were washed in buffer 1. Finally the developing solution (polyvinyl alcohol (PVA), Nitro-blue-tetrazolium-chloride (NBT) and Bromo-chloro-indolyl-phosphate (BCIP) separating solution) (Roche) was added to each slide and allowed to develop, resulting in a purple colour change

reaction detectable by eye showing the presence of the anti-DIG antibody and thus where the RNA transcripts are located.

Chapter 3

Novel lethal form of congenital hypopituitarism
associated with the first recessive *LHX4* mutation

3.1. Introduction

Due to our laboratory screening patients on such a large scale, other hospitals across the world contact and send us DNA from patients with hypothalamo-pituitary related phenotypes for us to screen. One such case, was a hospital in Karachi, Pakistan where Dr Humayun, an endocrinologist from the Aga Khan University Hospital, sent us DNA from two male deceased siblings from a pedigree (Pedigree 1) that had had CPHD related symptoms with fatal consequences.

3.1.1. Pedigree 1

A non-consanguineous Pakistani pedigree consisted of three siblings (Pedigree 1, Figure 3.1); one female and two males. The first child, a daughter (IIIa), was born with a birth weight of 2.4kg and a birth length of 46cm (DNA not available). She had poor tone and respiratory effort with grunting, persistent hyponatraemia, mid-facial hypoplasia, small nose with depressed nasal bridge, antimongoloid slant of eyes and low set crumpled ears. She had no cleft of lip or palate. She was started on nasal continuous positive airway pressure followed by ventilation. The second child, a son (IIIb), was born with a birth weight of 2.44kg and a birth length of 51cm. He presented with poor tone and respiratory distress marked by grunting, upon which he was started on ventilation. Examination showed signs of panhypopituitarism, normal tone and reflexes, low set crumpled ears, small upturned nose with depressed nasal bridge, mid-facial hypoplasia, hypoplastic nipples and nails, micropenis (1.7cm) and absent scrotal rugae with undescended testes. His free thyroxine was 200µg/L, TSH 0.01mU/L, basal cortisol 2.9µg/dL and ACTH was undetectable. The third child, a male (IIIc), was born with a birth weight of 2.6kg and a birth length of 37.5cm (Table 3.1). He had poor tone, low blood glucose, respiratory distress with grunting, and was started on ventilation. Examination showed signs of panhypopituitarism, normal tone and reflexes, low set crumpled ears, small upturned nose with depressed nasal bridge, mid-facial hypoplasia, micropenis (1.5cm), absent scrotal rugae, and a

palpable right testis with a left undescended testis. Persistent hyponatraemia and intestinal perforation complicated the clinical phenotype. His free thyroxine was 350µg/L, basal TSH 0.004mU/L, basal PRL <0.5µg/L, peak GH <0.05µg/L, basal cortisol <1.1µg/dL with an undetectable ACTH (Table 3.1). In spite of the rapid commencement of hydrocortisone and thyroxine, all three children died within the first week of life with what was presumed as fulminant sepsis, with klebsiella sepsis confirmed as the cause of death only in the first born male.

Pedigree 1

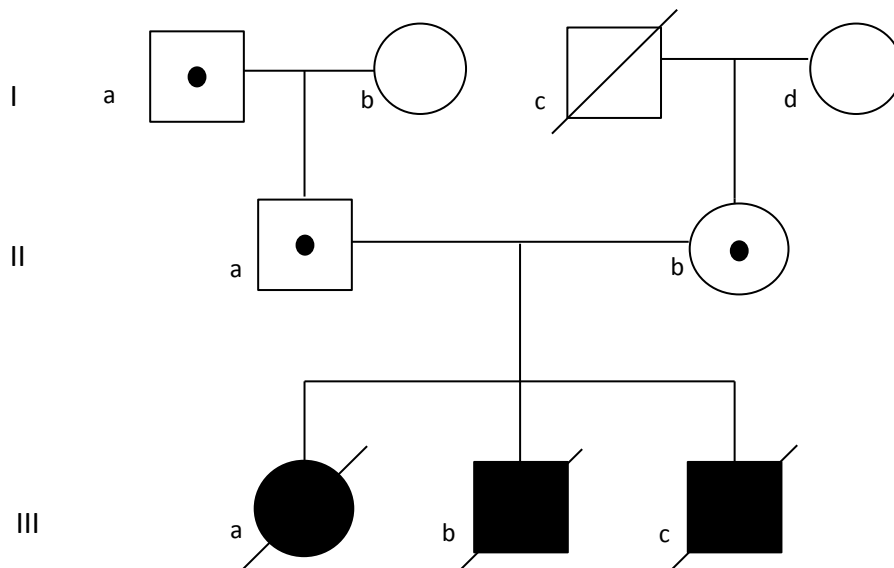


Figure 3.1: Pedigree 1 harbouring the *LHX4* (p.T126M) variant. The three affected sibling, female and two males, are represented by the fully shaded circle and squares respectively; the two affected brothers harboured the homozygous *LHX4* (p.T126M) variant. The shapes containing a dot represent heterozygous asymptomatic carriers. Un-shaded shapes indicate normal control individuals, and shapes crossed with a diagonal line indicate that the individual is deceased.

<u>Patient</u>	<u>IIIa</u>	<u>IIIb</u>	<u>IIIc</u>
Sex	Female	Male	Male
GA	35	35	38
Birth weight SDS (kg)	-2.3 (2.4)	-2.4 (2.44)	-2 (2.6)
Birth length SDS (cm)	-2.2 (46)	-0.02 (51)	-1.8 (47.5)
FT4 (ng/dL) (NR)	-	0.20 (NR 0.93-1.7)	0.35 (NR 0.93-1.7)
Basal TSH (mU/L)	-	0.01	<0.01
Basal Cortisol (µg/dL)	-	2.9	<1.1
ACTH	-	Undetectable	Undetectable
Peak GH (µg/L)	-	-	<0.05
Basal Prolactin (µg/L)	-	-	<0.5

Other features	<ul style="list-style-type: none"> - Antimongoloid slant of eyes - Persistent hyponatraemia - Poor muscle tone - Poor respiratory effort, grunting (started on ventilation) - CXR: atelectasis and RDS-like picture - Low set crumpled ears - Small upturned nose with depressed nasal bridge - Mid-facial hypoplasia 	<ul style="list-style-type: none"> - Poor muscle tone - Small phallus (1.7cm) and absent scrotal rugae - Undescended testes - Poor respiratory effort, grunting (started on ventilation) - CXR: atelectasis and RDS-like picture - Low set crumpled ears - Small upturned nose with depressed nasal bridge - Mid-facial hypoplasia 	<ul style="list-style-type: none"> - Poor tone and reflexes - Small phallus (1.5cm) and absent scrotal rugae - Left undescended testis - Low blood glucose - Persistent hyponatraemia - Poor respiratory effort, grunting (started on ventilation) - CXR: atelectasis and RDS-like picture - Low set crumpled ears - Small upturned nose with depressed nasal bridge - Mid-facial hypoplasia
----------------	---	--	--

Table 3.1: Endocrinology and phenotypes of the three patients in Pedigree 1. *GA, gestational age; SDS, standard deviation score; NR, normal range; TSH, thyroid-stimulating hormone; ACTH, adrenocorticotrophic hormone; GH, growth hormone; CXR, chest X-ray; RDS, respiratory distress syndrome.

MRI of patient IIIb from Pedigree 1 showed a complete absence of the anterior pituitary and an ectopic posterior pituitary (EPP) gland (Figure 3.2 C-D). A comparison between a normal control individual and patient IIIb MRI scans are presented in Figure 3.2 where a different position and size of the pituitary gland is noted in the patient. The two other patients; IIIa and IIIc did not have an MRI available. The three siblings were reported to have atelectasis of the lungs, with chest X-rays of patients IIIa and IIIb showing a ground-glass appearance (a hazy increased attenuation of the lungs) typical of hyaline membrane disease, which is now more commonly known as classical respiratory distress syndrome (RDS) (Figure 3.2 E-F). Chest X-ray images were not available for patient IIIc.

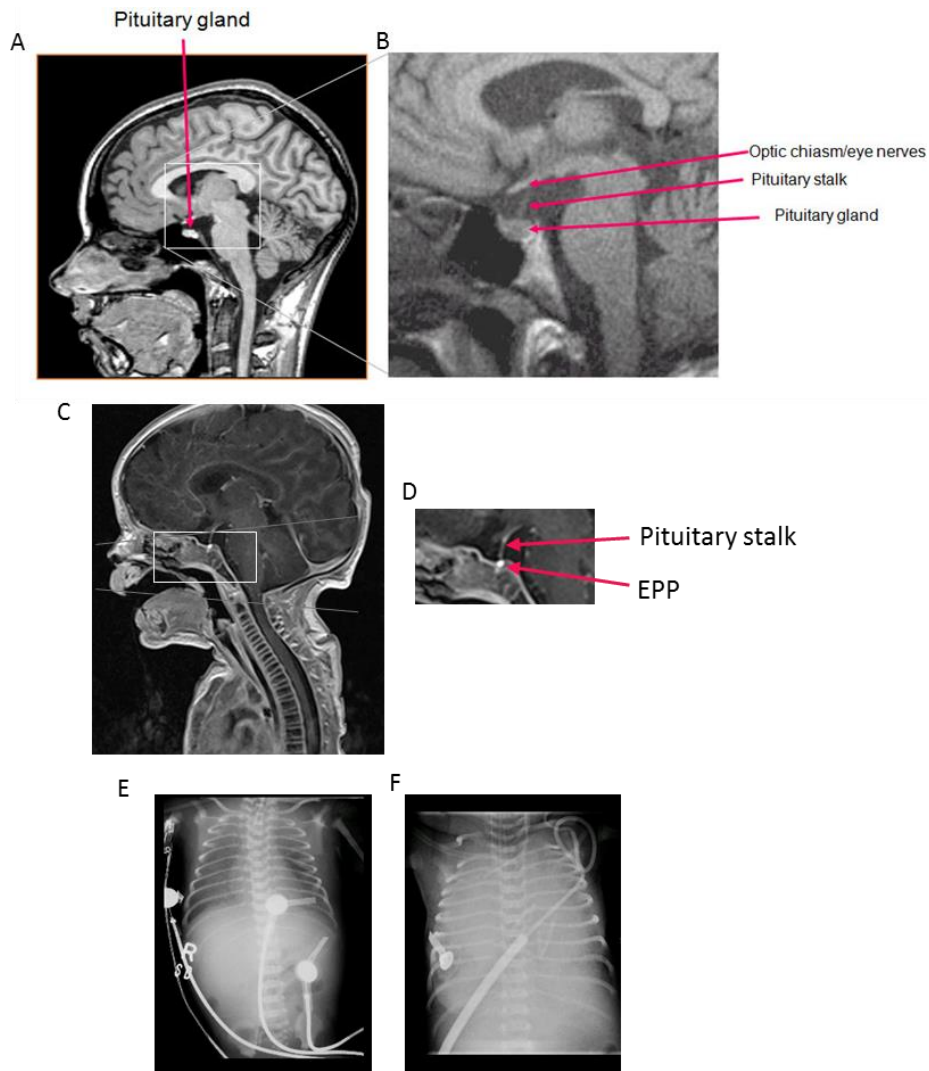


Figure 3.2: The MRI scan of patient IIIb and chest X-rays of patients IIIa and IIIb from Pedigree 1. (A-B) Taken from the Fipa patients database (www.fipapatient.org). **(A)** A sagittal MRI view of a normal control individual showing the correct size and position of both the anterior and posterior lobes of the pituitary gland. **(B)** A magnified image of the area of the brain highlighted by the white box in 'A', however the image is taken from a different normal control individual. **(C)** A sagittal MRI view of patient IIIb showing complete absence of the AP and an EPP gland. **(D)** A magnified image of 'C' in the area highlighted by the white box. **(E-F)** Chest X-rays of patients IIIa and IIIb respectively, showing a ground-glass opacity typical of hyaline membrane disease, also known as classical RDS. AP, anterior pituitary; EPP, ectopic posterior pituitary; RDS, respiratory distress syndrome.

3.2. Results

LHX4 is a member of the LIM/homeobox protein family which are multifunctional. Please refer to Chapter 1.3.6 for a detailed account of LHX4 and its past association with hypopituitarism. Heterozygous *LHX4* mutations in humans are usually associated with variable and variably penetrant CPHD (Pfaeffle et al., 2008), making *LHX4* a known causative gene and thus why it is routinely screened in our cohort of CPHD patients. The proband and his younger brother from Pedigree 1 sent to us from Pakistan were therefore screened for variants in the *LHX4* gene by direct sequencing analysis (Chapter 2.1 – 2.2).

3.2.1. Mutational analysis

Direct sequencing analysis revealed a novel homozygous missense variant in exon 3 of *LHX4* (ENST00000263726), c.377C>T, p.T126M, in the two deceased brothers (Pedigree 1) (Figure 3.3 A). The variant was not present in 1000 Genomes, dbSNP, EVS or the ExAC Browser databases, with the latter including a total of >100,000 control alleles of which >16,000 were of a South Asian background and thus more relevant to refer to for this variant in Pedigree 1. The mutated residue is located within a highly conserved region across multiple species as well as with other members of the LHX-family (Figure 3.3 B). Causative genes *LHX3*, *HESX1*, *PROP1*, *POU1F1* and *SOX3* were also screened for mutations in the patients in Pedigree 1, but were negative for mutations.

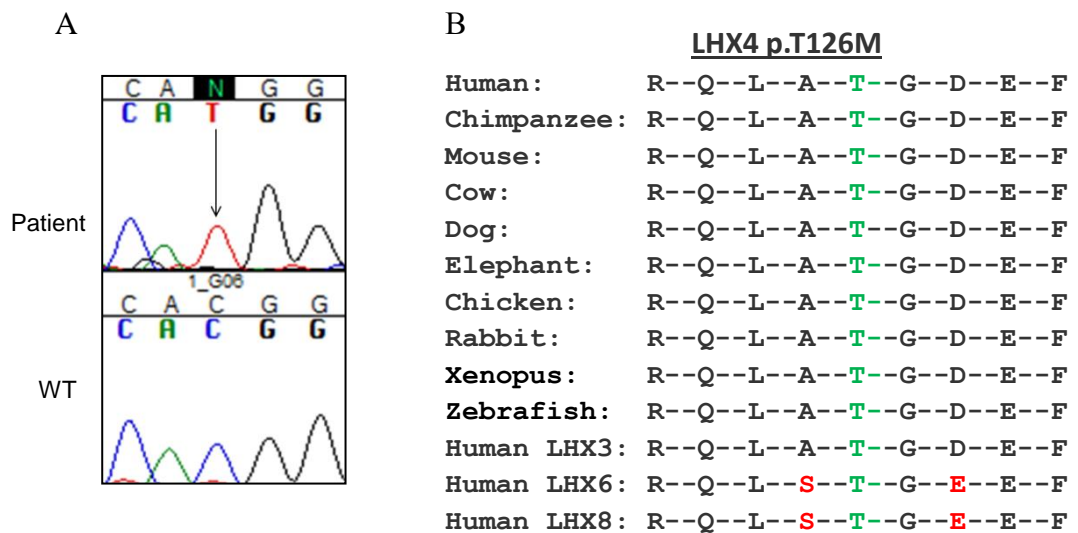


Figure 3.3: The electropherogram and conservation of the LHX4 (p.T126M) variant. (A) An electropherogram showing the homozygous missense variant, c.377C>T (p.T126M), in exon 3 of *LHX4* in pedigree 1 (indicated by the arrow) with the WT sequence shown below the patient coding sequence. **(B)** The conservation of the *LHX4* residue that is mutated. The threonine residue (represented by the green 'T') at location p.T126 is highly conserved between multiple species and other members of the LHX-family of proteins. This residue is substituted by methionine in the proband and his sibling in pedigree 1. WT, wild-type.

This detected LHX4 (p.T126M) variant is located within the LIM2 domain where previous reported mutations in LHX4 have been located. Other mutations have also been identified in the LIM1 and homeodomain, as well as along the whole protein (Figure 3.4).

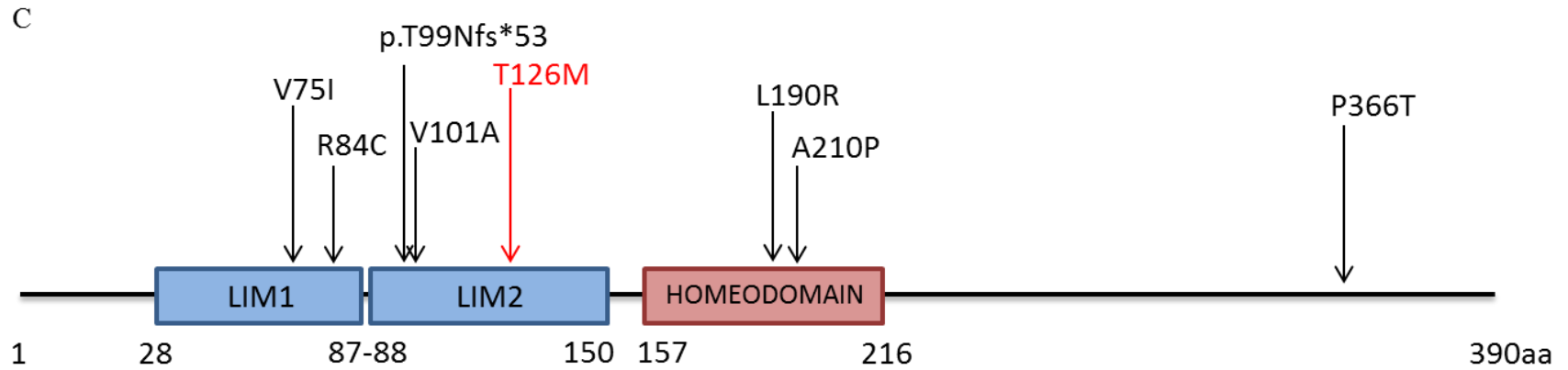


Figure 3.4: A schematic diagram of the LHX4 protein. Previously published exonic heterozygous mutations in LHX4 and the novel homozygous variant, T126M, located in the LIM2 domain (highlighted in red). The numbers depict the protein position of the mutated residue, and at what residue the domains begin and end respectively.

3.2.2. Western blot analysis

In the first instance, western blot analysis was performed on total protein extracted from cell lysates following transfection with wtLHX4, LHX4 (p.T126M) and LHX4 (p.R84C) constructs respectively to investigate the amount of LHX4 protein that was being produced in each population. The known partial loss of function mutation LHX4 (p.R84C) was used as a control in the transfection assays in this study, and therefore was also run on the western blot. This LHX4 (p.R84C) mutated protein is known to be of comparable size to wtLHX4 protein (Pfaeffle et al., 2008). Total protein was quantified using a BCA assay and a western blot was performed as described in Chapter 2.3.3, with GAPDH used as a control. Results indicated that protein extracted from LHX4 (p.T126M) transfected cells produced a protein product of comparable size to wtLHX4 and LHX4 (p.R84C) transfected cells (Figure 3.5).

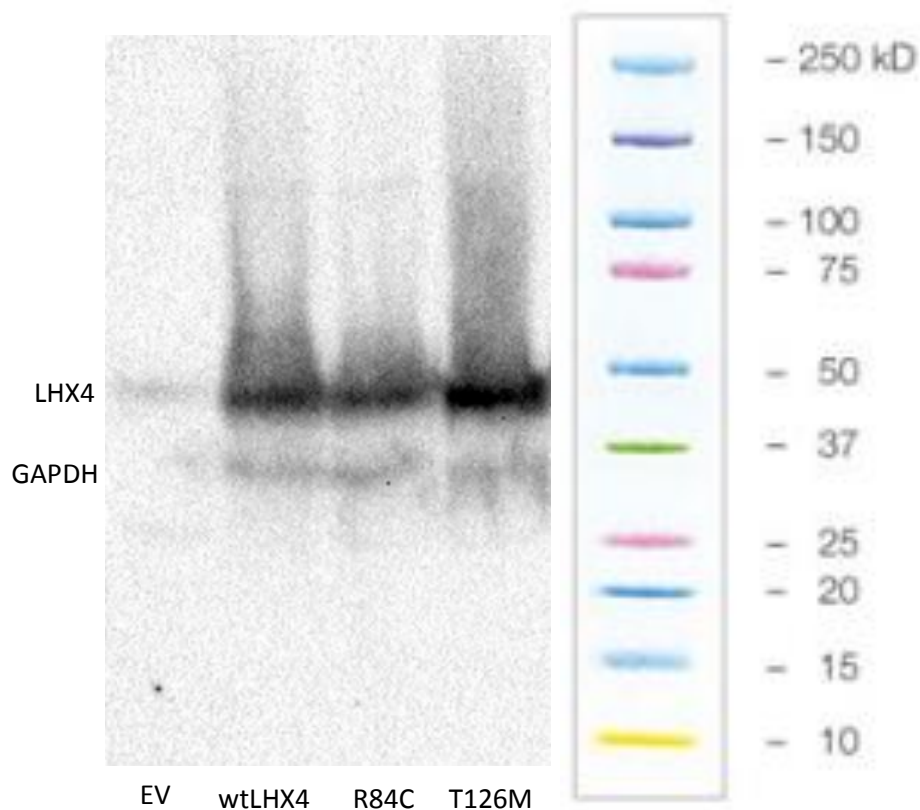


Figure 3.5: LHX4 western blot analysis. Western blot analysis using an anti-LHX4 antibody showing a specific band at 42kDa, indicative of LHX4, at the same significant intensity in wtLHX4, LHX4 (p.R84C) and LHX4 (p.T126M). An anti-GAPDH antibody was used to stain GAPDH as a control, which is shown in the specific band at 38kDa. 'EV'; empty vector, 'wtLHX4'; wild-type LHX4.

3.2.3. Protein prediction modelling

Online prediction models Polyphen2 and SIFT were initially consulted for the LHX4 (p.T126M) variant, showing a score of 1.000 on Polyphen2 termed 'possibly damaging' and a score of 0 on SIFT interpreted as 'damaging'. An actual protein prediction model was created by our collaborator; Dr Jose Saldanha from the Division of Mathematical Biology, National Institute for Medical Research, Mill Hill, using the RasMol software (www.RasMol.Org) database. He is an expert in this field and interpreted the model to give the prediction discussed here. This was carried out in order to analyse what happens to the structure of the LHX4 protein when the p.T126M variant is introduced. The model showed that normally the threonine at position 126 in LHX4 likely interacts with arginine at position 103 (Figure 3.6). Substitution of this threonine by methionine, as seen in the patients in Pedigree 1, is predicted to disrupt this interaction by affecting stability of the protein. Additionally, the threonine is on the surface within a turn of the protein structure (Figure 3.6), suggesting direct involvement in protein-protein interaction.

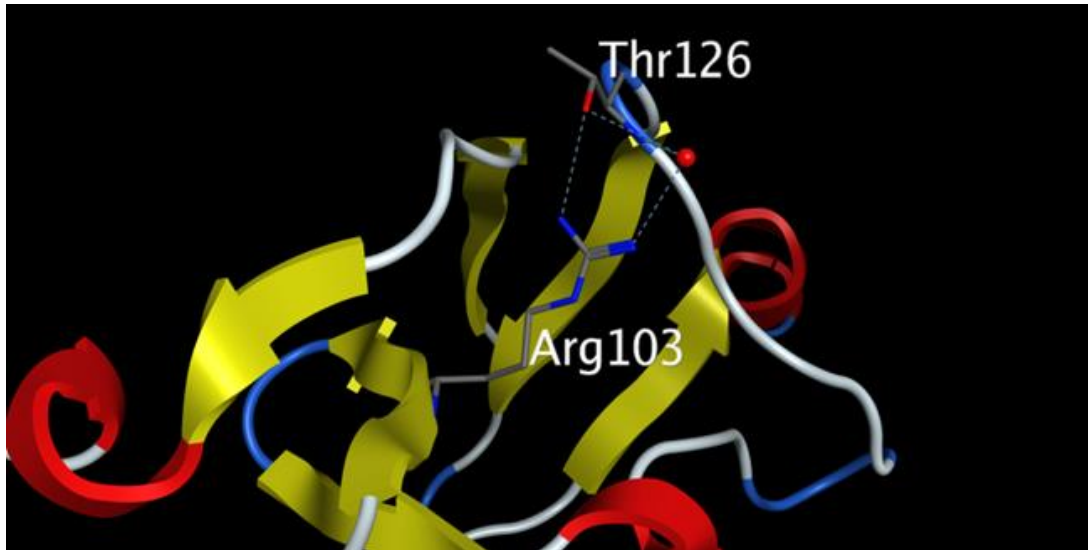


Figure 3.6: A protein prediction model of the LHX4 (p.T126M) variant. The RasMol software (www.RasMol.Org) database; a computer program commercially used for molecular visualization of protein models, was used to create the LHX4 (p.T126M) protein model. The threonine at p.T126 is on the turn of the protein. The threonine interacts with an arginine residue at p.R103, labelled. This interaction is predicted to be disrupted when this threonine is substituted for methionine (p.M126) as seen in Pedigree 1. The yellow shapes signify beta-strands, thus p.R103 is in a beta strand. The light blue represents a turn region in the protein and therefore T126 is on a turn. The dotted lines depict hydrogen-bonds and the red spheres represent water molecules. Thr; threonine, Arg; arginine.

3.2.4. Gene activation assays

The LHX4 (p.T126M) variant identified in Pedigree 1 is located in the LIM2 domain; known to play a role in transactivation and protein-protein interaction. This knowledge led me to perform transactivation assays to investigate whether the p.T126M variant would affect the activation of known LHX4 downstream targets; α GSU and prolactin (PrI). In these assays, luciferase (Luc) was used as the reporter that was measured to compare activation of the mutant LHX4 (p.T126M) against the WT LHX4 (wtLHX4), at two different doses (Chapter 2.3.4). The constructs transfected into cells is illustrated in Figure 2.1.

3.2.4.1. Non-parametric test: Part 1 (data refers to Figure 3.7 A and Appendix 1

A)

A two-sample Wilcoxon rank-sum (Mann-Whitney) test was used to test the hypothesis that the two independent samples (WT group and T126M group) come from populations with identical luciferase/protein (luciferase normalised to total protein values) distribution (in other words, to compare WT luciferase/protein values to T126M luciferase/protein values). There was no significant difference in luciferase/protein between WT LHX4 and T126M ($p = 0.4015$).

Group (Cell population?)	N	Rank sum	Expected
WT	9	76	85.5
T126M	9	95	85.5
Combined	18	171	171

Both wtLHX4 and LHX4 (p.T126M) similarly activated the α GSU-Luc reporter (Figure 3.7 A), showing that the LHX4 (p.T126M) variant does not result in a change of function in the context of activating the α GSU-Luc promoter. Thereafter, the synergistic activity of wtLHX4 and LHX4 (p.T126M) with POU1F1, a known protein

partner of LHX4 (Pfaeffle et al., 2008) were compared respectively on the Prl promoter.

Mann-Whitney tests were used to compare the normalised luciferase values (each raw measurement divided by the average EV for that particular assay).

3.2.4.2. Non-parametric tests: Part 2 (data refers to Figure 3.7 B and Appendix

1 B)

A significant difference was found between LHX4 and lhx4 ($p = 0.0003$).

Group (Cell population?)	N	Rank sum	Expected
LHX4	9	126	85.5
lhx4	9	45	85.5
Combined	18	171	171

A significant difference was found between lhx4 and lhx4+pou1f1 ($p = 0.0003$).

Group (Cell population?)	N	Rank sum	Expected
lhx4	9	45	85.5
lhx4+pou1f1	9	126	85.5
Combined	18	171	171

No evidence of a difference between lhx4 and t126m ($p = 0.2332$).

Group (Cell population?)	N	Rank sum	Expected
lhx4	9	99	85.5
t126m	9	72	85.5
Combined	18	171	171

There was evidence to suggest that T126M and lhx4 are significantly different ($p = 0.0007$).

Group (Cell population?)	N	Rank sum	Expected
T126M	9	124	85.5
lhx4	9	47	85.5
Combined	18	171	171

Evidence to suggest that there is a difference between *lhx4* and *t126m+pou1f1* ($p = 0.0003$).

Group (Cell population?)	N	Rank sum	Expected
<i>lhx4</i>	9	45	85.5
<i>t126m+pou1f1</i>	9	126	85.5
Combined	18	171	171

No evidence to suggest a difference between LHX4 and T126M ($p = 0.4529$).

Group (Cell population?)	N	Rank sum	Expected
LHX4	9	94	85.5
T126M	9	77	85.5
Combined	18	171	171

Evidence of a difference between POU1F1 and *pou1f1* ($p = 0.0092$).

Group (Cell population?)	N	Rank sum	Expected
POU1F1	9	115	85.5
<i>pou1f1</i>	9	56	85.5
Combined	18	171	171

Evidence of a difference between *t126m* and T126M ($p = 0.0003$).

Group (Cell population?)	N	Rank sum	Expected
<i>t126m</i>	9	45	85.5
T126M	9	126	85.5
Combined	18	171	171

Significant difference between *t126m* and *t126m+pou1f1* ($p = 0.0003$).

Group (Cell population?)	N	Rank sum	Expected
<i>t126m</i>	9	45	85.5
<i>t126m+pou1f1</i>	9	126	85.5
Combined	18	171	171

No evidence to suggest a difference between *lhx4+pou1f1* and *t126m+pou1f1* ($p = 0.4015$).

Group (Cell population?)	N	Rank sum	Expected
<i>lhx4+pou1f1</i>	9	76	85.5
<i>t126m+pou1f1</i>	9	95	85.5
Combined	18	171	171

3.2.4.3. Non-parametric tests: Part 3 (data refers to Figure 3.7 C and Appendix

1 C)

Significant difference between LHX4 and lhx4 ($p = 0.0003$).

Group (Cell population?)	N	Rank sum	Expected
LHX4	9	126	85.5
lhx4	9	45	85.5
Combined	18	171	171

Significant difference between lhx4 and lhx4+pou1f1 ($p = 0.0003$).

Group (Cell population?)	N	Rank sum	Expected
lhx4	9	45	85.5
lhx4+pou1f1	9	126	85.5
Combined	18	171	171

Significant difference between lhx4 and r84c ($p = 0.0013$).

Group (Cell population?)	N	Rank sum	Expected
lhx4	9	122	85.5
r84c	9	49	85.5
Combined	18	171	171

Significant difference between lhx4 and lhx4+r84c ($p = 0.0071$).

Group (Cell population?)	N	Rank sum	Expected
lhx4	9	55	85.5
lhx4+r84c	9	116	85.5
Combined	18	171	171

Significant difference between lhx4 and r84c+pou1f1 ($p = 0.0003$).

Group (Cell population?)	N	Rank sum	Expected
lhx4	9	45	85.5
r84c+pou1f1	9	126	85.5
Combined	18	171	171

Significant difference between LHX4 and R84C ($p = 0.0003$).

Group (Cell population?)	N	Rank sum	Expected
LHX4	9	126	85.5
R84C	9	45	85.5
Combined	18	171	171

Significant difference between lhx4+pou1f1 and lhx4+r84c ($p = 0.0003$).

Group (Cell population?)	N	Rank sum	Expected
lhx4+pou1f1	9	126	85.5
lhx4+r84c	9	45	85.5
Combined	18	171	171

Significant difference between lhx4+pou1f1 and r84c+pou1f1 ($p = 0.0003$).

Group (Cell population?)	N	Rank sum	Expected
lhx4+pou1f1	9	126	85.5
r84c+pou1f1	9	45	85.5
Combined	18	171	171

Significant difference between r84c and R84C ($p = 0.0009$).

Group (Cell population?)	N	Rank sum	Expected
r84c	9	48	85.5
R84C	9	123	85.5
Combined	18	171	171

Significant difference between r84c and lhx4+r84c ($p = 0.0003$).

Group (Cell population?)	N	Rank sum	Expected
r84c	9	45	85.5
lhx4+r84c	9	126	85.5
Combined	18	171	171

Significant difference between r84c and r84c+pou1f1 ($p = 0.0003$).

Group (Cell population?)	N	Rank sum	Expected
r84c	9	45	85.5
r84c+pou1f1	9	126	85.5
Combined	18	171	171

Significant difference between pou1f1 and POU1F1 ($p = 0.0017$).

Group (Cell population?)	N	Rank sum	Expected
pou1f1	9	50	85.5
POU1F1	9	121	85.5
Combined	18	171	171

3.2.4.4. Parametric tests: Two-tailed unpaired T-tests

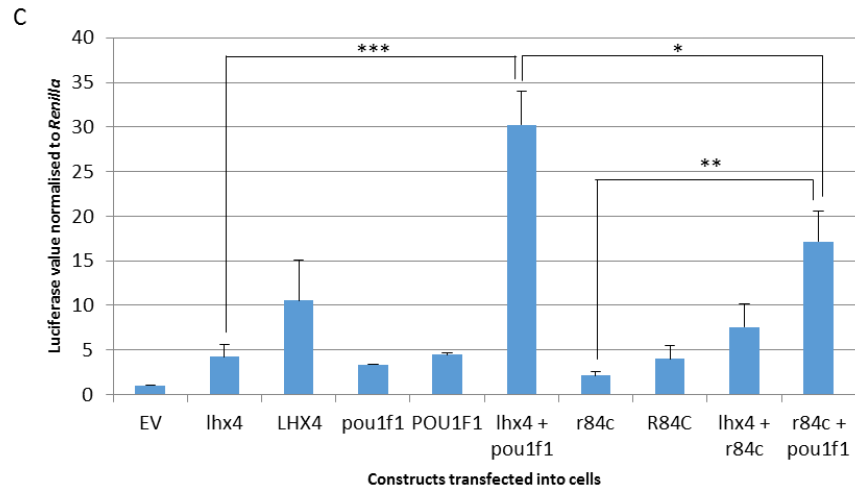
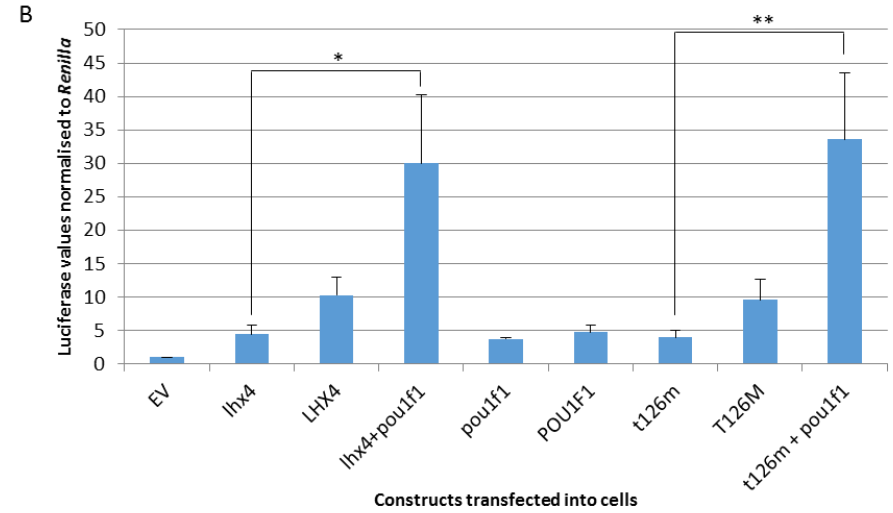
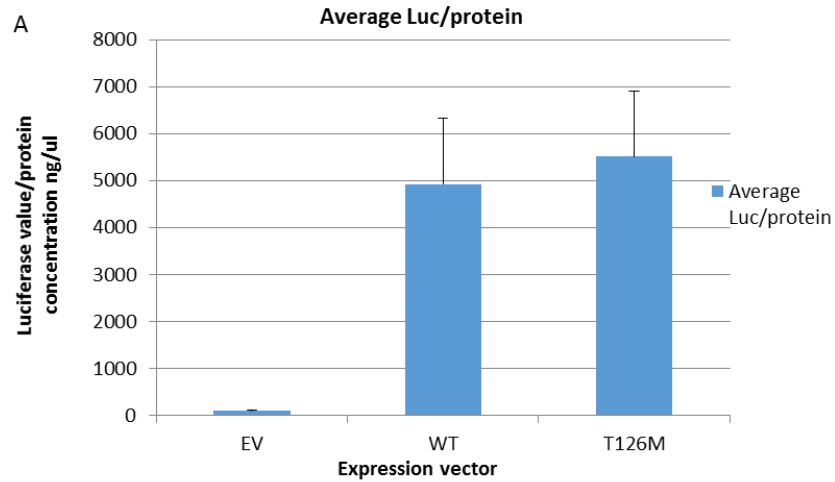


Figure 3.7: Transient transfection gene activation assays in HEK293T cells using the LHX4 (p.T126M) variant. (A-C) Results are shown as the mean \pm SD of 3 independent experiments with each assay performed in triplicate. The average mean values from each triplicate assay 1, 2, 3 are shown in Appendix 1. The error bars represent the standard deviation (SD) of the mean. Two-tailed unpaired T-tests were the statistical tests used here. **(A)** Luciferase activity on the α GSU promoter following transfection with wtLHX4 and LHX4 (p.T126M) expression constructs respectively, co-transfected with the α GSU-Luc reporter construct. Luciferase activity was normalized to the amount of total protein and showed no significant difference between wtLHX4 and LHX4 (p.T126M). EV: empty vector was used as a negative control. **(B)** Luciferase activity on the Prl-Luc following transfection with wtLHX4, wtPOU1F1 and LHX4 (p.T126M). The lower dose (31.25ng/well) is indicated by the lower case lettering (lhx4, pou1f1) and the higher dose (62.5ng/well), which is the concentration consistent with previous studies, is indicated by the upper case lettering (LHX4, POU1F1). Luciferase activity was normalized to Renilla-luciferase activity. There was a significant increase in luciferase activity between wtLHX4 transfected alone, and wtLHX4 co-transfected with wtPOU1F1 on activating the Prl-Luc ($p < 0.05$) indicated by *. In addition, there was significant difference in luciferase activity between LHX4 (p.T126M) alone, and LHX4 (p.T126M) co-transfected with wtPOU1F1 ($p < 0.01$) indicated by **. **(C)** Luciferase activity on Prl-Luc following transfection with two doses, as described in 'B', of each expression construct: wtLHX4, wtPOU1F1 and LHX4 (p.R84C) alone, in addition to wtLHX4 and LHX4 (p.R84C) (lower dose) co-transfected with wtPOU1F1 (lower dose). The significant increase in luciferase activity between wtLHX4 transfected alone, and wtLHX4 co-transfected with wtPOU1F1 was replicated in this assay on activating the prolactin promoter but to a higher degree ($p < 0.001$), indicated by ***. There was also a significant increase in activity between LHX4 (p.R84C) alone, and LHX4 (p.R84C) co-transfected with wtPOU1F1 ($p < 0.01$) indicated by **. There was a significant

difference in luciferase activity between wtLHX4 co-transfected with wtPOU1F1, and LHX4 (p.R84C) co-transfected with wtPOU1F1 ($p < 0.05$), indicated by *. Luc, luciferase; Pri-Luc, prolactin-luciferase.

When activating prolactin-luciferase (Pri-Luc), the individual constructs alone (wtLHX4 and LHX4 (p.T126M)) resulted in a dose-dependent increase in luciferase activity. When each of these constructs were co-transfected with wtPOU1F1, there was a significant increase in activity compared to transfection with LHX4 alone. Results are shown as the mean \pm SD of 3 independent experiments with each assay performed in triplicate; wtLHX4 with wtPOU1F1, 4.44 ± 1.28 vs 30.01 ± 10.23 ; $p = 0.013$ and LHX4 (p.T126M) with wtPOU1F1, 3.92 ± 1.01 vs 33.60 ± 9.95 ; $p = 0.007$. However, there was no significant difference in synergistic transactivation of the Pri-Luc reporter between wtLHX4 and LHX4 (p.T126M), co-transfected with and without wtPOU1F1 (Figure 3.7 B). The significant increase in activity between wtLHX4 transfection alone and wtLHX4 co-transfection with wtPOU1F1 was replicated, 4.22 ± 1.43 vs 30.26 ± 3.73 ; $p = 0.0004$ in another set of transfection assays that activated the Pri-Luc reporter (Figure 3.7 C). This is a higher significant difference in transactivation between wtLHX4, and wtLHX4 with wtPOU1F1, compared to what was observed the first time ($p = 0.0004$ vs $p = 0.013$) (Figure 3.7 B), showing variability between assays with a stronger transactivation in this final assay (Figure 3.7 C). In these final transfections, the known partial loss of function mutation, LHX4 c.250C>T, p.R84C (Pfaeffle et al., 2008), was used as a control. There was no significant difference in activation of the Pri-Luc reporter when transfecting the LHX4 (p.R84C), both alone and in the presence of wtLHX4, compared to wtLHX4 alone. Additionally, co-transfection of LHX4 (p.R84C) with wtPOU1F1 led to an increase in transcriptional activity compared to LHX4 (p.R84C) alone, 2.12 ± 0.45 vs 17.13 ± 3.44 ; $p = 0.002$, however, activation was significantly lower than that achieved by co-expression of

wtLHX4 with wtPOU1F1, 30.26 ± 3.73 vs 17.13 ± 3.44 ; $p=0.011$ (Figure 3.7 C), demonstrating the reported partial loss of function of LHX4 (p.R84C). The use of this reported mutant construct, indicates that the assays performed in this study work well and that the results are a true representation. As the wtLHX4 and the LHX4 (p.T126M) showed similar positive activities, it is suggested that both are well expressed, thus complementing the western blot analysis (Figure 3.5).

3.4. Discussion

The homozygous *LHX4* variant identified in the three siblings from Pedigree 1 causes a change in a highly conserved region of the LIM2 domain of the protein (Figure 3.3 B), and has outcomes that parallel the *Lhx4* homozygous null mutant mouse model (Li et al., 1994). This is the first homozygous *LHX4* mutation to be described in humans in association with hypopituitarism, I therefore wished to further test the impact of the mutation on LHX4 function. Mutations affecting LIM domains have been known to affect transactivation as well as interaction of protein partners, however functional studies have been performed in a relatively small number of mutant LHX4 proteins. Previous functional studies on the partial loss of function mutation, LHX4 (p.R84C), showed reduced activation of the α GSU and TSH β reporters and inactivity on the *POU1F1* promoter reporter gene (Pfaeffle et al., 2008). Another study looked at the LHX4 (p.V101A) mutant which was completely unable to activate the *POU1F1* and FSH β subunit gene promoters (Tajima et al., 2010). Additionally, the LHX4 (p.V75I) mutation located in the LIM1 domain was associated with a partial impairment of the capacity to transactivate *POU1F1* and *α GSU*, without any dominant-negative effects (Takagi et al., 2012).

As transactivation of both the α GSU-Luc and Prl-Luc promoters were not affected by LHX4 (p.T126M), it is suggested that gene activation is perhaps not the mechanism affected by this variant. It is understood that there are other promoters to explore in this context such as *TSH β* , *POU1F1* and *FSH β* ; however it cannot be certain that these are genuine physiological targets of LHX4 as they may be expressed at different developmental stages and at very particular doses. Thus the lower and higher doses used in the transactivation assays in these studies may not be mirroring the *in vivo* doses that occur in the body. In addition, LHX4 and POU1F1 may not be present in equal doses *in vivo*, as they have been in the analysis of these assays; the quantities of both proteins most likely vary within the biological system making it extremely difficult to mimic what occurs physiologically in *in vitro* studies. Essentially, the complete target gene set of LHX4 is unclear and many mechanisms taking place *in vivo* might underlie the defect associated with this mutation. Therefore controversially it cannot be ignored that the possibility of the LHX4 (p.T126M) substitution may be effecting an as yet undetermined function of the protein. It should also be noted that as this variant was identified via a Sanger sequencing approach, it cannot be excluded that another undetected genetic abnormality or deletion elsewhere in the genome may be contributing to the phenotype as only the known causative genes were screened in this Pedigree: *LHX3*, *HESX1*, *PROP1*, *POU1F1* and *SOX3*.

Mutations located in the *LHX4* homeodomain often cause a loss of DNA-binding, as seen in reported mutations p.L190R and p.A210P (Pfaeffle et al., 2008). A heterozygous frameshift mutation, p.T99Nfs*53, was previously identified in LIM2 of *LHX4* in two brothers with GH and TSH deficiencies, pituitary hypoplasia and a poorly developed sella turcica. The youngest also had corpus callosal hypoplasia and an EPP. This mutation led to a loss of transcriptional activity on the *POU1F1*, *PRL* and *GH* promoters due to abolished DNA-binding, which was a result of complete

truncation of the homeodomain (Castinetti et al., 2008). As the p.T126M substitution is not located and does not affect transcription of the homeodomain, it is not predicted to affect DNA-binding. Therefore it would not be necessary to perform an experiment such as an electrophoretic mobility shift assay (EMSA) for example, which is a common affinity electrophoresis technique used to study protein–DNA or protein–RNA interactions, as the homeodomain in our patients is intact and should have a normal DNA-binding ability.

LIM domains are involved in protein-protein interaction, as observed in both LHX3 and LHX4. Sloop et al. (Sloop et al., 2001) previously analysed the binding abilities of purified LHX3 protein (mutant and WT) with partners Ldb1/NLI and POU1F1. Through *in vitro* binding assays, they tested whether the LHX3 (p.Y1111/116C) substitution, located in the LIM2 domain, disrupts structure and binding to putative partner proteins. Interaction of LHX3 (p.Y1111/116C) with POU1F1 was reduced compared to wtLHX3, which may explain the reduction in the ability of LHX3 (p.Y1111/116C) to activate the Prl promoter in the presence of POU1F1 (Sloop et al., 2001). Studies such as this led me to investigate the protein-protein interaction of LHX4 and POU1F1 and its synergistic ability to activate the Prl promoter. Despite no significant difference being apparent in these synergistic assays, the LHX4 (p.T126M) may be affecting other such interactions with partner proteins even though interaction with POU1F1 seems to be unaffected. One needs to bear in mind that the partners with which LHX4 interacts are largely unknown, therefore the LHX4 (p.T126M) mutation may affect interaction with a partner yet to be identified. Alternatively likely partners such as Ldb1 for example may demonstrate impaired complex formation and be a possible mechanism whereby LHX4 (p.T126M), especially in its homozygous state, leads to the phenotype seen in Pedigree 1. Furthermore, the RasMol protein prediction model concluded that the threonine that is substituted by methionine in Pedigree 1, is on the surface within a turn of the protein (Figure 3.6), suggesting an

involvement in protein-protein interaction. Moreover, online prediction models Polyphen2 and SIFT predict the p.T126M variant to be damaging (Table 3.2).

<u>Protein prediction model software used</u>	<u>Website reference to software</u>	<u>Score generated from model if applicable</u>	<u>Result determined from model</u>
Polyphen2	genetics.bwh.harvard.edu/pph2/	1	Possibly damaging
SIFT	sift.jcvi.org/	0	Damaging
RasMol	www.RasMol.Org	N/A	Predicted to alter stability and protein-protein interaction

Table 3.2: Protein prediction models used for the LHX4 (p.T126M) variant. Two that generate a score reflecting the level of pathogenicity; Polyphen2 and SIFT, and one that illustrates a molecular model of the p.T126M variant; Rasmol.

The p.T126M variant was present in both brothers (IIIb, IIIc) in Pedigree 1. Unfortunately the daughter's (IIIa) DNA was not available; however, her clinical presentation suggests that it was highly likely that she carried the same homozygous variant in addition to her brothers. Previously, patients carrying heterozygous *LHX4* mutations have manifested variable CPHD incorporating GH +/- TSH, PRL, ACTH, LH and FSH deficiencies. Phenotypes have included dysmorphic features, a small AP, an EPP, a poorly developed sella turcica, Chiari malformation, respiratory distress syndrome and corpus callosal hypoplasia (Castinetti et al., 2008, Pfaeffle et al., 2008, Dateki et al., 2010, Tajima et al., 2007). Both brothers in Pedigree 1 presented with severe panhypopituitarism (Table 3.1) and showed anterior pituitary atrophy and an EPP, similar to previously reported carriers of *LHX4* mutations. One

such previous report describes a maternally inherited heterozygous 1.5-megabase microdeletion in 1q25.2-q25.3, which spans *LHX4* (q25.2), in a CPHD patient with minor physical anomalies, suggestive of a midline defect, and heart failure (Filges et al., 2012). Additionally, a *de novo* interstitial deletion of chromosome 1q24.3q31.1, again incorporating *LHX4*, was defined by array-comparative genomic hybridization (array-CGH) in a patient with pituitary hormone deficiencies, severe cognitive impairment, bilateral cleft lip/palate and other associated abnormalities. The deletion of *LHX4* was considered to be largely causative of the diminished growth and CPHD in this patient (Capra et al., 2014). The CPHD observed in Pedigree 1 is consistent with these previous data, however the fact that all three patients died supports the hypothesis that the presence of a homozygous *LHX4* mutation elicits fatal consequences.

3.5. Conclusion

To date, described *LHX4* mutations have been heterozygous, and often variably penetrant with outcomes likely caused by haploinsufficiency (McCabe and Dattani, 2014) (Figure 3.4). This is the first report describing a homozygous variant in a patient identified through Sanger sequencing. Exome sequencing was not performed in this pedigree. Given the lethality of recessive mutations in rodents (Li et al., 1994), the homozygous p.T126M variant is likely to be responsible for this pedigree's lethal phenotype, although the presence of another genetic abnormality contributing to their fatal phenotype cannot be ruled out. All three siblings presented with respiratory distress due to atelectasis of the lungs, echoing the mouse model in which null mutants died within the first week of life from immature lungs that failed to inflate (Li et al., 1994). Based on the phenotypic characterization of this mutant, this previous study concludes that *Lhx4* plays a critical role in the development of early postnatal respiratory control mechanisms and in the normal growth and maturation of the lung in the mouse, as this study also suggests in humans. However the etiology of how mutant *Lhx4/LHX4* elicits this fatal lung phenotype is as yet unknown. The high conservation between murine *Lhx4* and human *LHX4* indicates the fundamental importance of this protein in maintaining life across species and that recessive mutations in *Lhx4/LHX4* are lethal.

Chapter 4

New candidate genes identified through exome sequencing and their expression profiles in a phenotype-related context

4.1. Introduction

At Great Ormond Street Institute of Child Health (ICH) we have access to over 2000 DNA samples from around the world, that have hypothalamo-pituitary related phenotypes in whom no genetic diagnosis has been made. Aside from screening the known causative genes in the quest to find the genotype responsible for certain CH patient phenotypes, an alternative strategy of exome sequencing is demonstrated in this study. Many pedigrees that are negative for mutations in the known hypopituitarism genes, and phenotypically unique pedigrees that do not have any obvious genes to be screened, have been put forward for exome sequencing, in collaboration with GOSgene, to potentially highlight regions of interest in the exome that can be investigated further. The phenotypically unique cohort includes consanguineous and non-consanguineous families with varying hypothalamo-pituitary disorders that have unusual accompanying phenotypes that have not been described in collaboration with the CH spectrum in the literature before. This chapter describes seven different unrelated Pedigrees (Pedigrees 2-8) with unusual phenotypes of this nature, that have had novel variants in novel genes revealed through exome sequencing as potential targets for hypothalamo-pituitary related phenotypes. An example of how exome sequencing data is filtered is illustrated in Appendix 2. How each exome sequencing project (Pedigrees 3-7) was filtered is displayed in Appendix 3, and a summary table of the phenotypes and identified variants of Pedigrees 2-7 is shown in Appendix 4. Albeit the final pedigree (Pedigree 8) discussed in this chapter, these novel variants will be functionally investigated in future projects through various analyses that are specific to each gene and the pathway in which it is involved. In this study, expression analysis has been conducted for each of the genes in which potentially causative variants have been identified, focusing on the hypothalamo-pituitary axis in human embryonic development, and any related tissues relevant to the patient phenotype. Initially following identification of a novel gene, it is very important to establish an expression profile in the context

of the tissues affected in the pedigree. If no expression is apparent in these areas there is less evidence to say that the gene is contributing towards the phenotype. As well as their expression profile, an introduction to the potential function of each respective gene and the phenotype of the patients that harbour these potential pathogenic variants, is reviewed in this chapter. Each gene appears to be unique in terms of expression pattern, function and impact on the phenotype. Establishing the exact hypothalamo-pituitary expression as in these data, will potentially benefit and complement future functional studies enabling delineation of the role of the relevant gene in development and disease.

A total of six potential novel CH candidate genes have been identified through exome sequencing in these seven different families (Pedigrees 2-8). These genes, that were found to be mutated in the patients from these pedigrees, are: *CTPS2*, *RNPC3*, *PRMT6*, *FASN*, *APEX2* and *EIF2S3*. An antisense and sense DIG-labelled RNA probe was generated from IMAGE clones for each gene, and *in situ* hybridisation was performed on human embryonic tissue at different stages of development as described in Chapter 2.5. All control sense probes for the genes were negative for any mRNA transcript staining; presenting with no visible colour image under the microscope, thus confirming that the expression data generated from this study are reliable.

4.2. CTPS2

4.2.1. Pedigree 2

A 23 year old female patient of Afro-Caribbean non-consanguineous background presented with congenital panhypopituitarism; GH, TSH, ACTH, LH and FSH deficiencies. Her complex phenotype additionally included left microtia; an absent pinna, with severe conductive hearing loss, ciliary dyskinesia, complete situs inversus with dextrocardia, hypoplasia of the mandible, severe eczema, learning difficulties, left facial nerve palsy with left sided hemiparesis and learning difficulties (Pedigree 2, Figure 4.1).

Pedigree 2

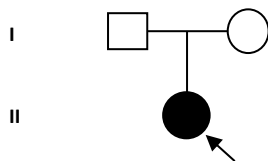


Figure 4.1: Pedigree 2 with the patient harbouring the *CTPS2* (p.F166L) variant.

The Afro-Caribbean non-consanguineous Pedigree 2 with the affected daughter, indicated by the shaded circle and arrow, that harbours the heterozygous *de novo* *CTPS2* (p.F166L) variant. The roman numerals on the left of the image refer to the generation within the pedigree. The unshaded square and circle represent that the parents are unaffected.

4.2.2. Exome sequencing results: *CTPS2*

A heterozygous missense *de novo* variant in *CTPS2* (ENST00000443824), c.498C>A, p.F166L, was identified in this patient (Pedigree 2). This is in a highly conserved region across multiple species (Figure 4.2) and is not present on any

control database, including 1000 Genomes, dbSNP, EVS or the ExAC Browser, with the latter including over >87,000 control alleles; with >52,421 alleles from an African origin, which is a more relevant control cohort to this patient.

CTPS2 (p.F166L)

Human: A--F--R--Q--F--Q--F--K--A
Mouse: A--F--R--Q--F--Q--F--K--A
Chimpanzee: A--F--R--Q--F--Q--F--K--A
Cow: A--F--R--Q--F--Q--F--K--A
Dog: A--F--R--Q--F--Q--F--K--A
Chicken: A--F--R--Q--F--Q--F--K--A
Xenopus: A--F--R--Q--F--Q--F--K--A

Figure 4.2: Conservation of the substituted CTPS2 residue. The extent of conservation across multiple species of the substituted amino acid (highlighted in green), and the spanning protein sequence, in CTPS2.

4.2.3. CTPS2 function

The coding region of Cytidine 5'-Triphosphate Synthase II (*CTPS2*) is 1.761kb in length, comprising of 19 exons on the X chromosome. CTPS2 catalyses the amination of UTP to CTP with the concomitant deamination of glutamine to glutamate (Bearne et al., 2001). It is the rate-limiting enzyme in the synthesis of cytosine nucleotides which play an important role in various metabolic processes and provide

the precursors necessary for the synthesis of RNA and DNA. CTPS2, like its family member CTPS1, regulates intracellular CTP levels through interactions with the four ribonucleotide triphosphates (Endrizzi et al., 2004). A recent report describes a loss-of-function homozygous mutation (rs145092287) in *CTPS1* in a patient with a novel life-threatening immunodeficiency, characterized by an impaired capacity of activated T and B cells to proliferate in response to antigen receptor-mediated activation (Martin et al., 2014). This mutation affected a splice donor site producing a transcript lacking exon 18 of *CTPS1*, of which expression was absent from lysates derived from Epstein-Barr Virus (EBV)-transformed B and T cells from patients. Functional assays performed in this previous study restored normal T-cell proliferation in *CTPS1*-deficient cells by expressing WT *CTPS1* or by the addition of CTP, or its nucleoside precursor cytidine (Martin et al., 2014). *CTPS2* may also be referred to as an oncogene, as cancer cells that exhibit increased cell proliferation also exhibit an increased activity of this encoded protein, making it a potential target for chemotherapy (www.ncbi.nlm.nih.gov). Previous studies have shown that a reduction in *CTPS2* expression increases resistance of colorectal cancer cell lines to the drug 5-fluorouracil (5FU). This was reflected in their study *in vivo*, where patients with low *CTPS2* did not gain a survival benefit from 5FU treatment, while those with high expression did (Tan et al., 2011).

Murine *Ctps2* is expressed in multiple systems including the reproductive, respiratory, nervous, olfactory, auditory and visual systems with many more listed as having transcript staining (MGI). Human *CTPS2* expression is highest in the prostate, ovarian follicles, testis, areas of the brain, lymph nodes, tonsils and the parathyroid gland as well as other areas of the body according to the Human Protein Atlas.

4.2.4. CTPS2 expression results

The hypothalamo-pituitary axis of the brain has not previously been studied for *CTPS2* in detail. Expression analysis conducted in this study show expression in the neural tube and Rathke's pouch (the primordium of the anterior pituitary) at CS16 and CS19 (Figure 4.3A-B, D). In the diencephalon, telencephalon (Figure 4.3C), trigeminal ganglia at CS19 (Figure 4.3D), spinal cord and spinal ganglia at CS19 (Figure 4.3E). In the developing neural retina of the eye at CS19 and at late 8 post conception week (pcw) (Figure 4.3F-G), and in the oesophagus and the lungs; bronchi at CS19 (Figure 4.3H-I). *CTPS2* expression was also noted in parts of the developing ear; in the cochlea at CS23 and in the semi-circular canal and the utricle, which is one of the vestibular sensory organs at CS19 (Figure 4.4A-D). Due to the patient having dextrocardia, sections of the heart at CS19 were also analysed in this study, however they showed no significant transcript expression.

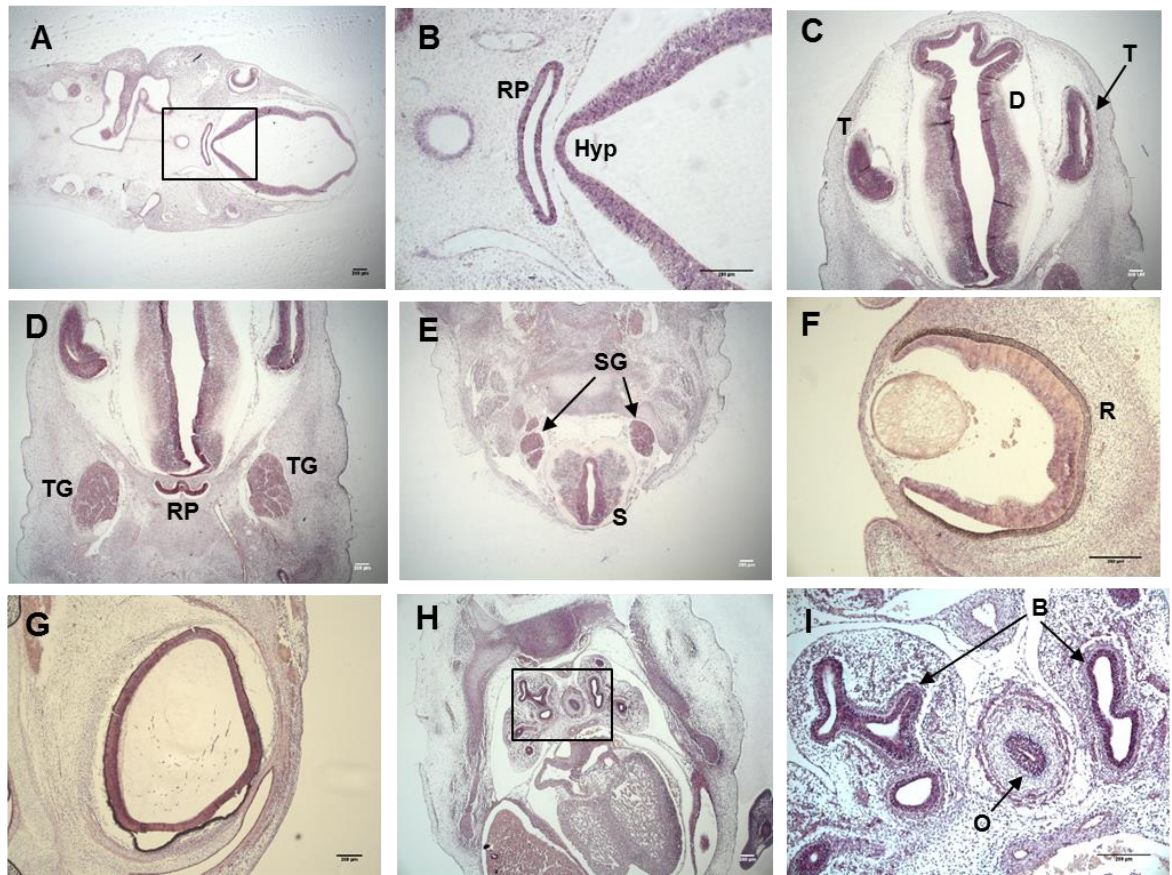


Figure 4.3: *CTPS2* expression in the developing hypothalamic-pituitary axis, eyes and lungs during human embryogenesis. *In situ* hybridization using the antisense probe against the human *CTPS2* mRNA transcript (*hCTPS2*) on human sections from different Carnegie stages (CS) during embryogenesis. Scale bars in each image depict 200 μ M. **(A-E)** Transverse sections, **(F-G)** sagittal sections, **(H-I)** transverse sections **(A) CS16:** expression is seen in the neural tube, Rathke's pouch and the eye. **(B) CS16:** Rathke's Pouch and the hypothalamus show high *CTPS2* expression. **(C) CS19:** expression in the telencephalon and diencephalon, **(D) CS19:** in the trigeminal ganglia and Rathke's pouch. **(E) CS19:** expression is observed in the spinal cord and spinal ganglia, **(F) CS19** a gradient of expression in the developing neural retina of the eye. **(G) Late 8 post conception week (pcw):** expression in the developing neural retina of the eye. **(H-I) CS19:** expression in the oesophagus and bronchi of the lungs. The black boxes in 'A' and 'H' reflect the section of the image that is magnified in 'B' and 'I' respectively. RP, Rathke's pouch; Hyp,

hypothalamus; T, telencephalon; D, diencephalon; TG, trigeminal ganglia; S, spinal cord; SG, spinal ganglia; R, retina; B, bronchi; O, oesophagus.

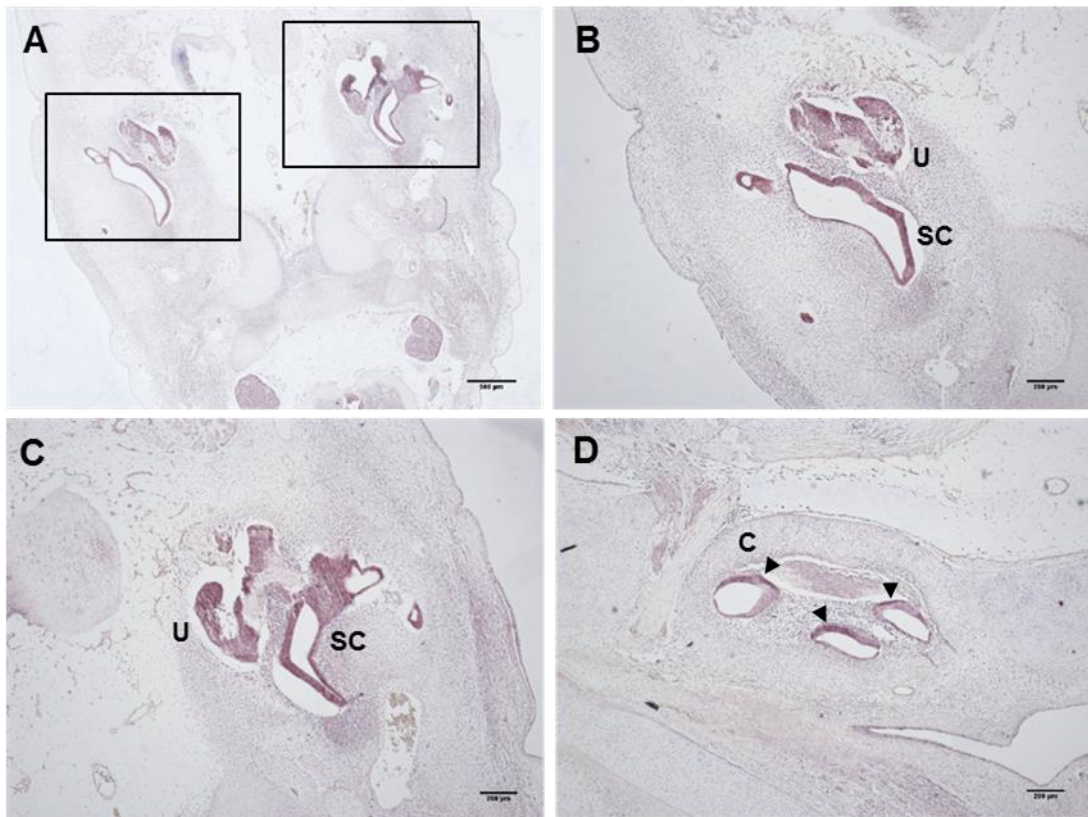


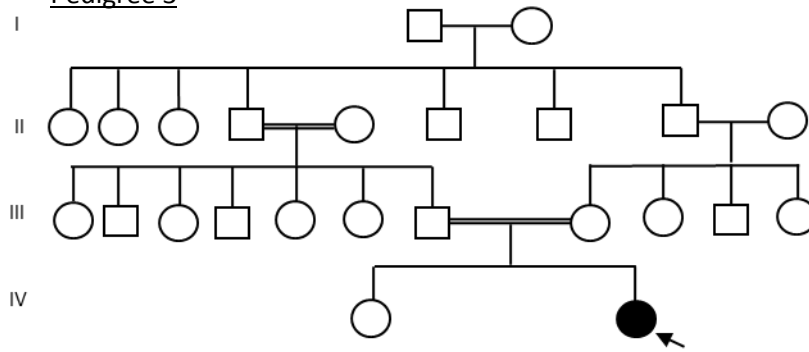
Figure 4.4: *CTPS2* expression in the developing ear. *In situ* hybridization performed on human transverse sections using the antisense probe against the human *CTPS2* mRNA transcript (*hCTPS2*). The scale bar in 'A' represents 500 μ M and the scale bars in 'B-D' depict 200 μ M. **(A-C) CS19:** expression is seen in the utricle (a vestibular sensory organ) and the semi-circular canal of the ear. The black boxes in 'A' are the sections of the image that are magnified in 'B' and 'C' respectively. **(D) CS23:** expression in the cochlea structure of the ear, highlighted by the arrowheads. U, utricle; SC, semi-circular canal; C, cochlea.

4.3. RNPC3 and PRMT6

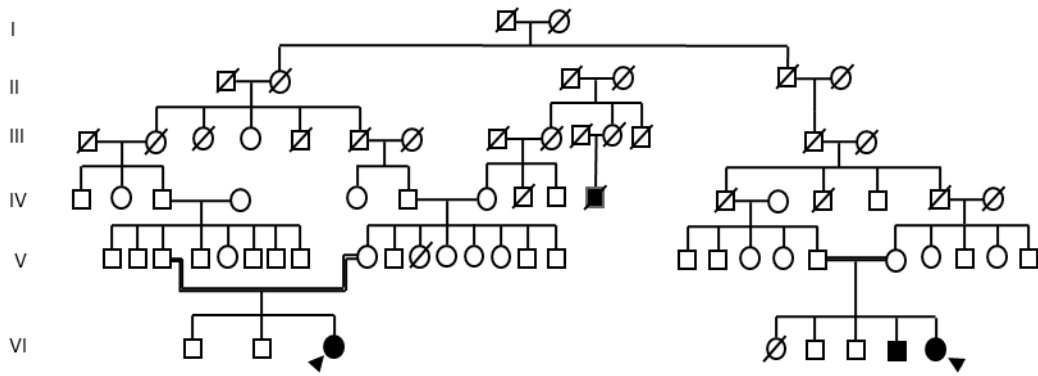
4.3.1. Exome sequencing results of Pedigrees 3-6

Exome sequencing revealed an area of homozygosity in four unrelated Turkish consanguineous pedigrees (Pedigrees 3-6, Figure 4.5) where the probands manifested a unique phenotype characterized by IGHD and primary ovarian failure in the affected females, with male patients manifesting IGHD. Six out of the seven affected individuals in Pedigrees 3-6; four females and two male patients, and the unaffected father of the female patient in pedigree 5, had exome sequencing performed (Figure 4.5). This area contained a novel homozygous missense variant in *RNPC3* (ENST00000423855), *c.1449A>T*, p.L483F, and a novel homozygous missense variant in *PRMT6* (ENST00000370078), *c.1049C>G*, p.P350R. The affected males have not been reported to have testicular problems, however limited detailed clinical information from these Turkish pedigrees are currently available.

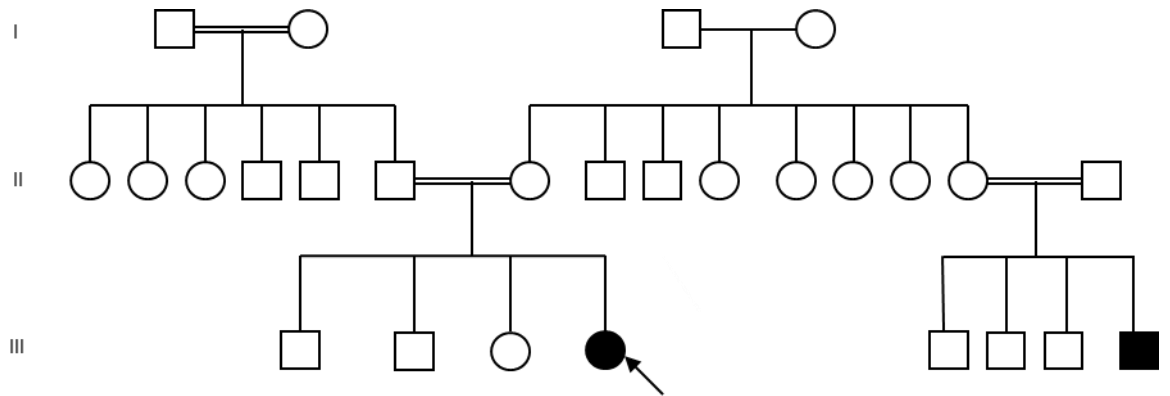
Pedigree 3



Pedigree 4



Pedigree 5



Pedigree 6

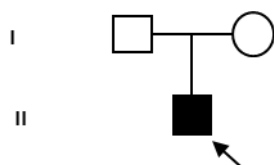


Figure 4.5: Pedigrees 3-6 harbouring the *RNPC3* (p.L483F) and *PRMT6* (p.P350R) variants. Four unrelated pedigrees (Pedigrees 3-6) from Turkish origin. Shaded squares and circles indicate affected family members, squares for males, circles for females. Shapes joined by two lines indicate consanguinity between those individuals. The arrows and arrowhead highlight the probands in each pedigree. A diagonal line through a shape indicates that the individual is deceased. The roman numerals down the left hand side refer to the generation within that Pedigree. All affected individuals illustrated in these pedigrees had exome sequencing performed, with the exception of the affected male patient in Pedigree 5. In addition, exome sequencing was also performed in the unaffected father of the female patient in Pedigree 5.

The novel missense substitution, *RNPC3* (p.L483F), is highly conserved across multiple species (Figure 4.6A) and is not present on control databases; 1000 Genomes, dbSNP, EVS or the ExAC Browser, with the latter including >111,000 alleles; incorporating >67,000 from a European background which is where any Turkish control alleles would be categorized and thus are more relevant controls to Pedigrees 3-6. The novel *PRMT6* (p.P350R) missense substitution is conserved across four species (Figure 4.6B) and is not present in homozygous form on control databases; 1000 Genomes, dbSNP, EVS or the ExAC Browser. However, a substitution of the Proline by a Threonine residue at position 350 is present in heterozygous form in two alleles from European origin on the ExAC Browser, out of a total of >66,000 control alleles; 60,174 of which were from the European cohort. The role of *PRMT6* is discussed in section 4.3.4 of this chapter.

A) RNPC3 (p.L483F)

Human: A--A--K--A--L--K--E--A--N

Mouse: A--A--K--A--L--K--E--A--N

Chimpanzee: A--A--K--A--L--K--E--A--N

Cow: A--A--K--A--L--K--E--A--N

Dog: A--A--K--A--L--K--E--A--N

Chicken: A--A--K--A--L--K--E--A--N

B) PRMT6 (p.P350R)

Human: S--R--D--N--P--R--R--L--R

Mouse: S--P--D--N--P--R--R--L--R

Chimpanzee: S--R--D--N--P--R--R--L--R

Elephant: A--R--D--N--P--R--R--L--R

Figure 4.6: Conservation of the substituted RNPC3 and PRMT6 residues. The extent of conservation across multiple species of each substituted amino acid, **(A)** RNPC3 and **(B)** PRMT6 (highlighted in green), and the spanning protein sequences. Any spanning amino acid residues that differ from the normal human reference sequence are highlighted in red.

4.3.2. RNPC3 function

There are two types of spliceosomes that catalyse splicing of pre-mRNAs: the major U2-type spliceosome removes U2-type introns (99% of pre-mRNA introns) and the minor U12-type spliceosome removes U12-type introns, which are rare with distinct splice consensus signals. Both the U2- and U12-type spliceosomes consist of several small nuclear RNAs (snRNAs) and associated proteins (Sharp and Burge, 1997) (Figure 4.7). The RNA-binding region (RNA recognition motifs [RRM]) containing 3 (*RNPC3*) coding region is 1.554kb in length, incorporating 16 exons on chromosome 1. *RNPC3* encodes a 65K protein that is a component of the U12-type spliceosome. It contains two bipartite nuclear targeting sequences important for nuclear targeting for proteins, especially those functioning in the cell nucleus itself (Zhao et al., 2003). *RNPC3* is located in the cell nucleus and is abundantly expressed in the kidney and pancreas (Zhao et al., 2003). This protein's two RRM's suggest that it may contact one of the small nuclear RNAs of the minor spliceosome (Zhao et al., 2003).

Defects in the U12-type splicing; via mutations in the U4atac snRNA component of the minor spliceosome, have been reported to be associated with the complex disorder Taybi-Linder syndrome (also known as microcephalic osteodysplastic primordial dwarfism 1), a severe developmental disorder involving brain and skeletal abnormalities, and tragically unexplained postnatal death (Edery et al., 2011) (He et al., 2011). This is an example of how poorly spliced endogenous U12-dependent introns, but not U2-dependent, can specifically cause life-threatening complex disorders. Defective U12-type splicing, via a mutation in the tumour suppressor gene *LKB1* intron, has also been linked to a hereditary intestinal polyposis condition, Peutz-Jeghers syndrome, which is associated with increased cancer risk (Hastings et al., 2005).

U2-type spliceosome and U12-type spliceosome

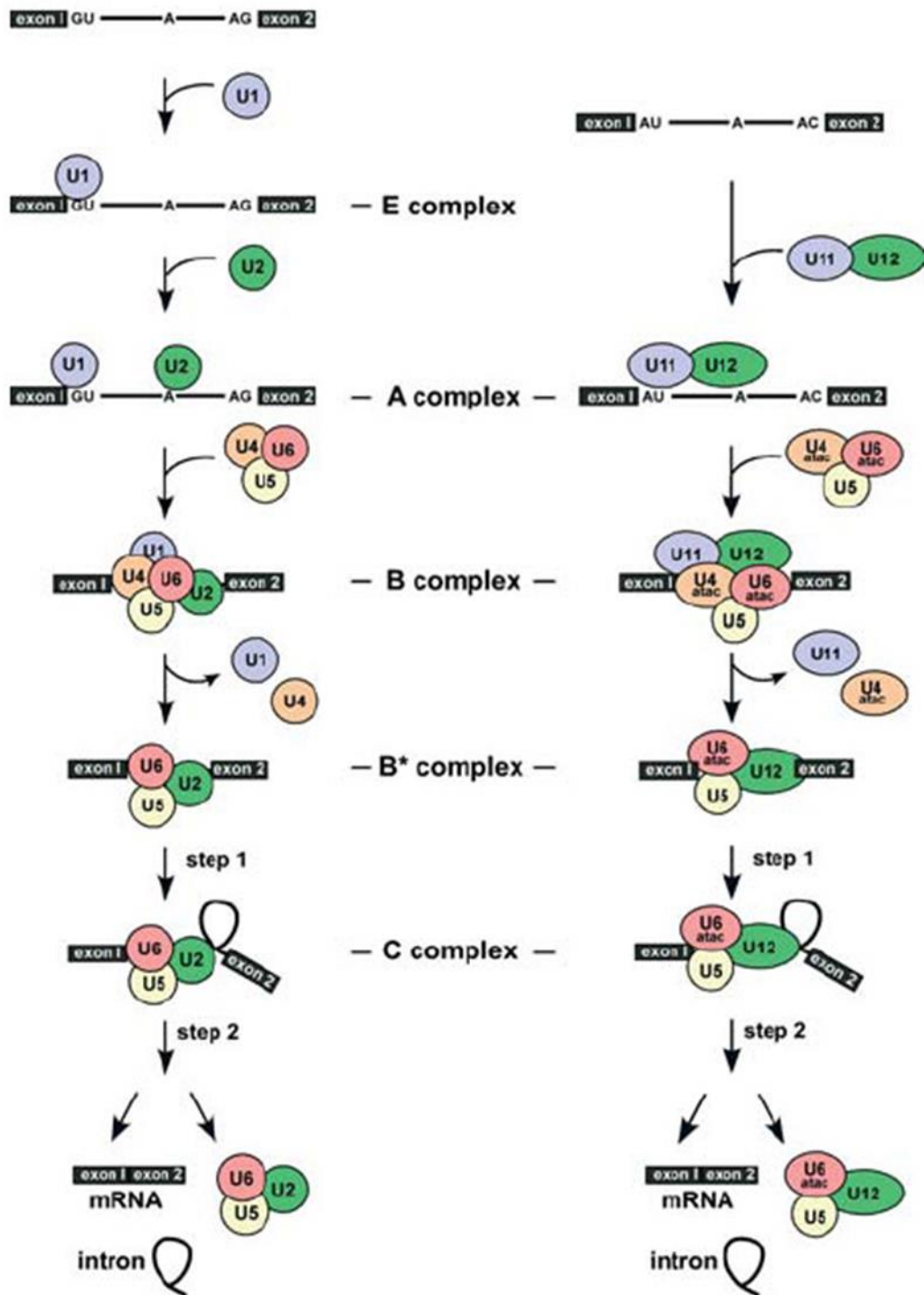


Figure 4.7: A comparison of the steps during the formation of the U2- and U12-type spliceosome. The U2-type major spliceosome forms at introns with a GU sequence at their 5' end and an AG sequence at their 3' end. The U12-type minor spliceosome forms at introns with an AU sequence at their 5' and an AC sequence at

their 3' end. Both the U2- and U12-type spliceosomes recognise an 'A' residue branch site in the intron. A series of different small nuclear RNA (snRNA) molecules e.g. U1, U2, U11, U12 etc, belonging to either the U2- or U12-type spliceosome, bind in succession to the intron to form the spliceosome complexes respectively, resulting in the cleavage and thus the splicing of introns. The U5 snRNA is the only common component between the U2- and U12-type spliceosome. This image was taken and adapted from Will CL, Luhrmann R. *Biol. Chem.* 2005 Aug; 386(8): 713-24.

Murine *Rnpc3* is expressed in the nervous and olfactory systems (MGI) yet, to date, there is no murine model for *Rnpc3* loss of function. However, a study using a zebrafish mutant model with an induced lethal point mutation in *rnpc3* resulted in arrested development of the digestive organs. This phenotype arose from the formation of aberrant U11- and U12-containing snRNAs that impaired the efficiency of U12-type splicing. This zebrafish model provided a useful and specific model of aberrant U12-type splicing *in vivo*. Analysis of its transcriptome revealed that efficient mRNA processing is a critical process for the growth and proliferation of cells during vertebrate development (Markmiller et al., 2014).

Biallelic mutations in *RNPC3* have previously been described in three sisters with severe IGHD and pituitary hypoplasia, where anomalies were identified in U11/U12 di-snRNP formation and the splicing of multiple U12-type introns in these patient cells (Argente et al., 2014). Through RNA sequencing (RNA seq) the authors identified a list of 21 genes with significantly decreased U12/U2 ratios in patient cells, as well as aberrant processing events including exon skipping and activation of cryptic U2-type splice sites (Argente et al., 2014). A subset of the 21 genes were found to encode proteins with relevant functions in pituitary development, such as *SPCS2* and *SPCS3* that encode subunits of the signal peptidase complex, implicated in posttranslational processing of preprohormones such as preproghrelin to proghrelin (Argente et al., 2014, Yin et al., 2009), thus themselves becoming candidates for the phenotype.

4.3.3. *RNPC3* expression results

Human expression analysis was performed on embryonic tissue from the hypothalamo-pituitary axis of the brain (Figure 4.9) in this study. Results showed high *RNPC3* expression in the telencephalon, diencephalon (Figure 4.9A), trigeminal ganglia, hypothalamus and Rathke's pouch at CS19 (Figure 4.9B-D). Furthermore, human embryonic ovarian sections were also requested from HDBR, however following staining of these sections it came to light that the tissue was not in fact fully ovarian, despite being referenced as so. Therefore the *RNPC3* mRNA transcript staining is observed in the mesonephros (ducts that later develop into the kidney), and in what is possibly the fallopian tube (Figure 4.9 F-K), at 9pcw, in tissue that was originally thought to be ovarian. The ovary and mesonephros are attached to each other during early female embryonic development, and by the 10pcw stage the mesonephros have disappeared as the true kidney is formed (HDBR specialists). Unfortunately, the large bulk of the ovary was not present in the 9pcw sections acquired in this study, only its smaller counterpart was intact, as demonstrated in the comparison below of our section and an image of what it should have looked like following sectioning (Figure 4.8) (recent unpublished information from HDBR). There are two pairs of genital ducts present in both male and female embryos, the mesonephric (wolffian) and paramesonephric (müllerian). In female embryogenesis at 9pcw, the mesonephric ducts degenerate but the paramesonephric ducts, by the process of fusion that starts caudally and progresses cranially, form the uterovaginal canal. This canal later develops into the upper portion of the vagina and uterus, while their non-fused portions become fallopian tubes (Grechukhina et al., 2016). In recent talks with HDBR, colleagues said that in transverse sections through the lower body at 10pcw stage or later, it would be possible to distinguish between the fallopian tubes and paramesonephric ducts, however it remains ambiguous here at 9pcw as it is too early to tell these structures apart. Therefore I will now acquire sections from at least

10pcw from HDBR, with intact ovarian tissue, in order to clarify where the *RNPC3* transcript staining is located.

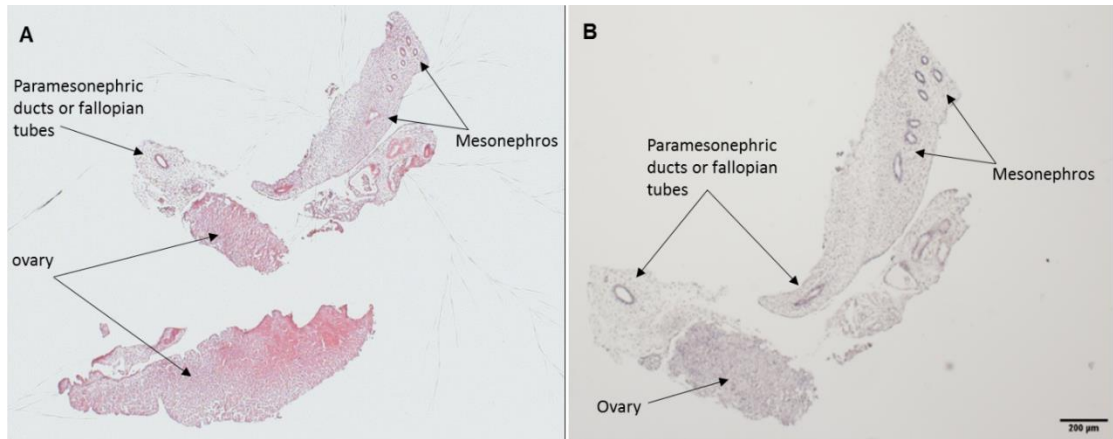


Figure 4.8: Human embryonic tissue sections from the ovary and developing kidney. (A) A sagittal section of human embryonic tissue taken from an ovary and developing kidney at 9pcw. **(B)** The 9pcw sagittal section that our study acquired with the large section of ovarian tissue missing, that is present in (A). Each specific tissue is indicated by the arrows. The scale bar in the image represents 200μM.

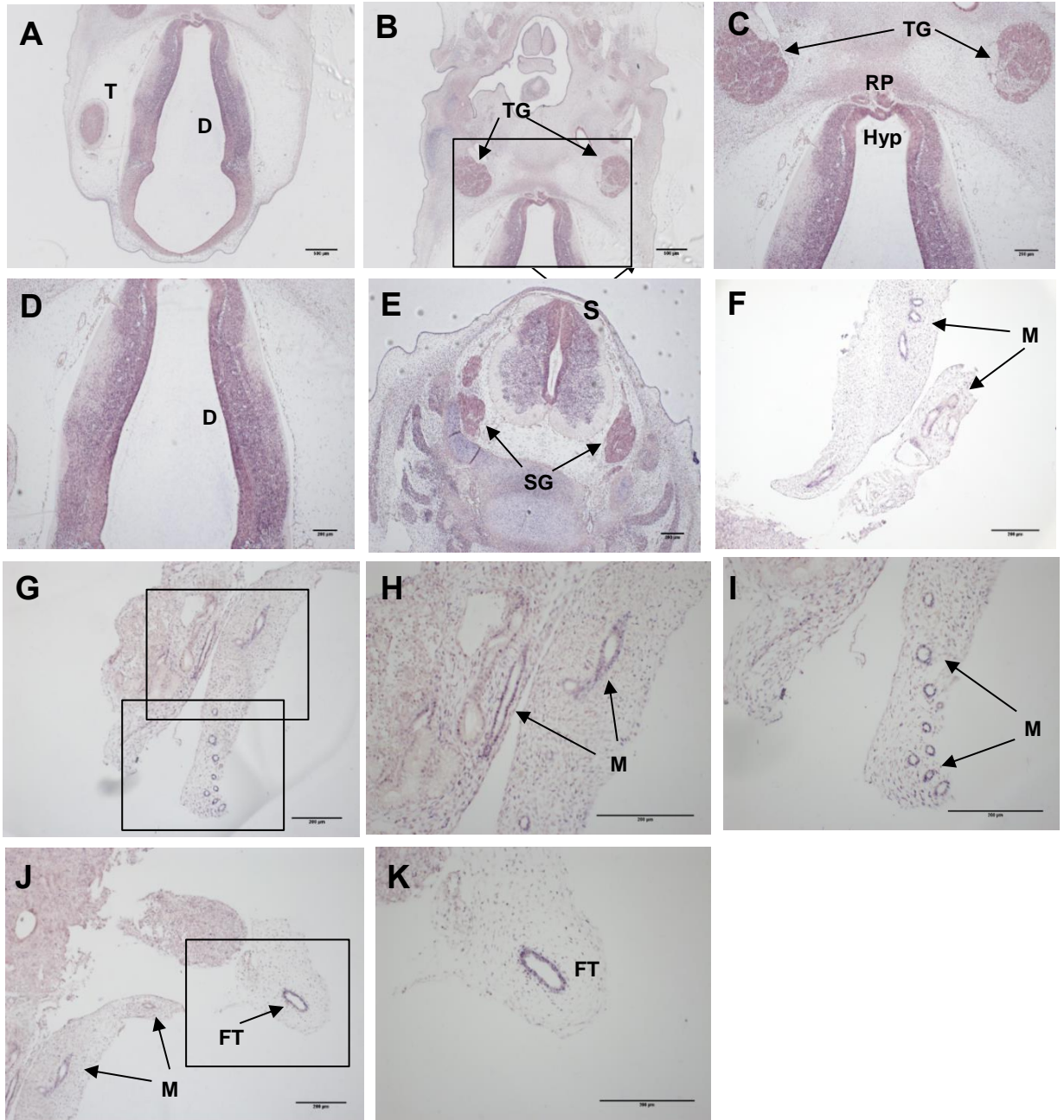


Figure 4.9: *RNPC3* expression in the developing hypothalamic-pituitary axis and the ovary during human embryogenesis. *In situ* hybridization using the antisense probe against the human *RNPC3* mRNA transcript (*hRNPC3*) on human sections from CS19 and 9pcw during embryogenesis. The scale bars in 'A-B' represent 500 μ M and the scale bars in 'C-K' represent 200 μ M. **(A-E)** Transverse sections, **(F-K)** sagittal sections. **(A-D) CS19:** high *hRNPC3* expression seen in the telencephalon, diencephalon, trigeminal ganglia and Rathke's pouch. **(E) CS19:**

expression can be seen in the spinal cord and spinal ganglia. **(F-J) 9pcw**: expression is noted in the mesonephros of the premature kidney, indicated by the arrows labelled 'M'. **(J-K) 9pcw**: expression is observed in what may be the paramesonephric duct or the fallopian tube, indicated by the arrows labelled 'FT' in this case. This structure is difficult to determine at this early stage of development. The black boxes in (B), (G) and (J) indicate the area in the image that has been enlarged in the adjacent image respectively. T, telencephalon; D, diencephalon; TG, trigeminal ganglia; RP, Rathke's pouch; Hyp, hypothalamus; S, spinal cord; SG, spinal ganglia; M, mesonephros; FT, fallopian tubes.

4.3.4. PRMT6 function

A homozygous missense variant in *PRMT6*, *c.1049C>G*, p.P350R, was identified in the same individuals from the four Turkish families (Pedigrees 3-6, Figure 4.5) that possess the *RNPC3* (p.L483F) variant, in the same area of homozygosity. Variants *RNPC3* (p.L483F) and *PRMT6* (p.P350R) are evidently inherited from the same allele from both asymptomatic heterozygous parents.

The coding region of Protein arginine methyltransferase 6 (*PRMT6*) is 1.128kb in length, consisting of only one exon on chromosome 1. It catalyses the sequential transfer of a methyl group from S-adenosyl-L-methionine to the side chain nitrogens of arginine residues within proteins, to form methylated arginine derivatives and S-adenosyl-L-homocysteine. *PRMT6* catalyses both the formation of Omega-N monomethylarginine and asymmetrical dimethylarginine (strongly) and specifically mediates the asymmetric dimethylation of Arg2 (R2) of histone H3 to yield its methylated form, giving it a specific tag for epigenetic transcriptional repression (Figure 4.10). *PRMT6* forms a complex with and methylates DNA polymerase beta, and brings about the stimulation of polymerase activity by enhancing DNA binding and processivity (El-Andaloussi et al., 2006).

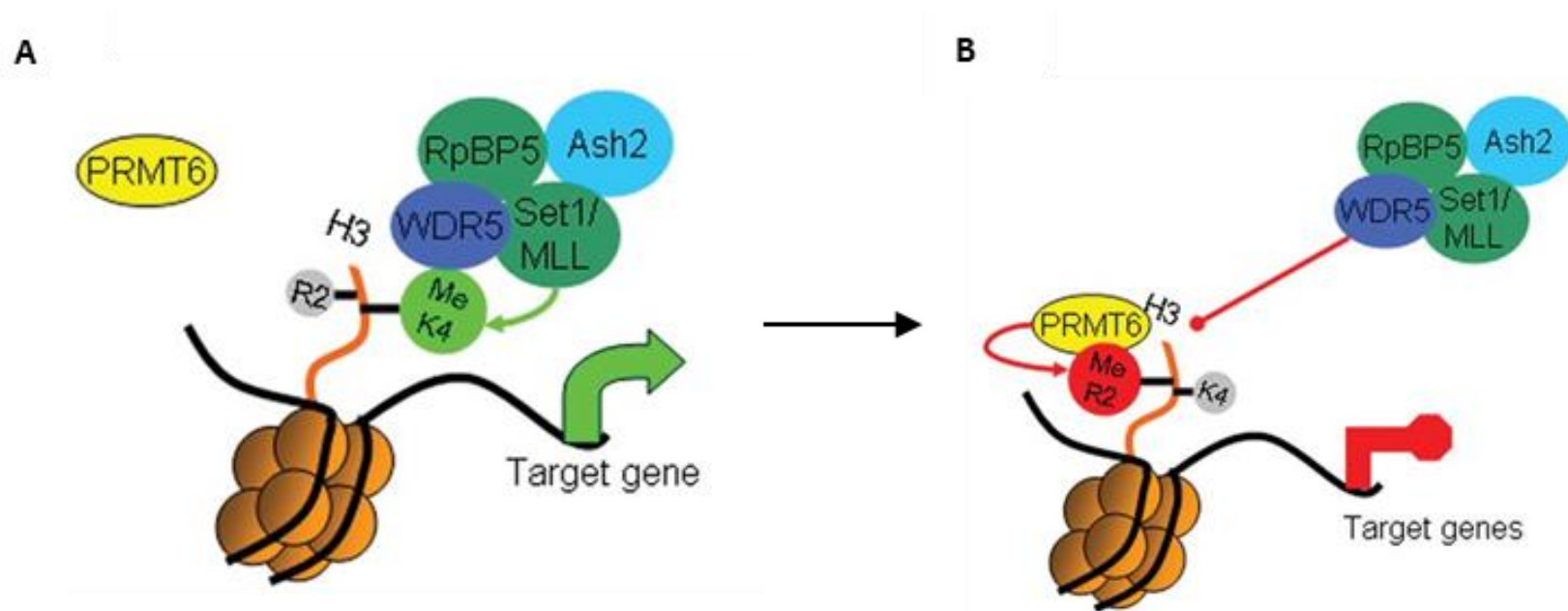


Figure 4.10: PRMT6 transcriptional repression. A model of the transcriptional repression of Hox genes and Myc-dependent genes by PRMT6. Taken and adapted from Litt *et al.* (Litt *et al.*, 2009). **(A)** Di and trimethyl of K4 is associated with the recruitment of MLL1 and WDR5 to chromatin and transcriptional activation. **(B)** PRMT6 recruitment and asymmetric dimethylation of R2 (Arg2) of H3 (H3R2) (denoted by the red circle labelled Me R2) results in the loss of the MLL complex, absence of H3 and K4 (H3K4) methylation (denoted by the green circle labelled Me K4), and decreased transcripts from target genes. The presence of asymmetrical dimethylation of H3R2 inhibited binding of the Ash2 (absent, small, or homeotic disc 2)/WDR5 (WD40 repeat-containing protein 5)/MLL (family methyltransferase complex) and methylation of H3K4. Brg1, BRM-related gene 1; mSin3A, mammalian SIN3A; HDAC2, histone deacetylase 2; RpBP5, retinoblastoma binding protein 5.

The Human Protein Atlas states that *PRMT6* is variably expressed throughout the human body, with high expression in the kidney (renal tubules), pancreas (exocrine glandular cells), oral mucosa, testes (Leydig cells), breast (myoepithelial cells), thyroid gland, tonsils and bronchi (respiratory epithelial cells). Medium expression is seen in the ovary, fallopian tubes, cervix, placenta, salivary glands and the gastrointestinal tract (stomach, small intestine). In this study, human embryonic whole ovarian sections for *in situ* hybridisation studies were not able to be obtained as discussed earlier, therefore we have not yet looked at *PRMT6* expression in the ovary.

Murine *Prmt6* is expressed in the nervous, olfactory and visual systems (MGI). A transgenic mouse model has been developed to ubiquitously express *Prmt6* fused to the hormone-binding portion of the estrogen receptor (ER). Upon systemic treatment with tamoxifen, it becomes stabilized and translocates into the nucleus. Induced ER-*Prmt6* activation results in increased interleukin-6 (IL-6) levels, with expression regulated by the nuclear factor-kappa B (NF- κ B) transcription factor and with *Prmt6* functioning as a coactivator of the pathway. *Prmt6* is recruited to chromatin at selective NF- κ B target promoters, where it likely impacts the histone code and/or methylates other chromatin-associated proteins to facilitate transcription (Di Lorenzo et al., 2014).

4.4. FASN and APEX2

4.4.1. Pedigree 7

A 19 year old male from a non-consanguineous family (Pedigree 7, Figure 4.11) presented at the age of 4 years with a unique complex phenotype characterized by panhypopituitarism; GH, TSH, ACTH, LH and FSH deficiencies, short stature, dysmorphic features, developmental delay, sensorineural deafness, hypoparathyroidism, retinal dystrophy, Reynaud's syndrome, splenomegaly and aortic regurgitation. He failed to respond to high doses of recombinant human growth hormone (rhGH) with low IGF1 concentrations. He measures 128 cm at the age of 19 years and is completely prepubertal.

Pedigree 7

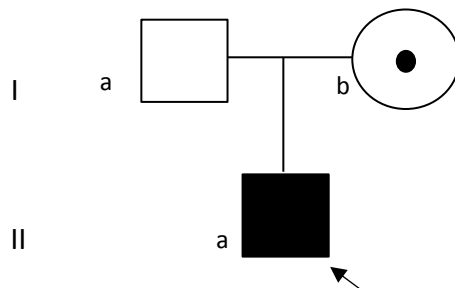


Figure 4.11: Pedigree 7 with the patient harbouring the *FASN* (p.A2132V) and *APEX2* (p.M422V) variants. The non-consanguineous Pedigree 7 with one affected male, indicated by the shaded square and arrow, that harbours both the heterozygous *de novo FASN* (p.A2132V) and the hemizygous *APEX2* (p.M422V) variant. The latter variant was inherited from the mother, indicated by the circle containing a dot. The roman numerals on the left of the image refer to the generation within the pedigree.

4.4.2. Exome sequencing results: *FASN* and *APEX2*

A novel heterozygous missense *de novo* variant in *FASN* (ENST00000306749) located on chromosome 17, c.6395C>T, p.A2132V, has been identified in this 19 year old male with a unique phenotype (Pedigree 7), via exome sequencing. This variant is highly conserved across multiple species (Figure 4.12A) and is not present on control databases, including 1000 Genomes, dbSNP, EVS or the ExAC Browser which includes a total of >100,000 control alleles; >10,000 of which are from an African origin the same as the mother, and >64,500 alleles which are from a European origin (including a mix of controls from different European countries) the same as the father, who is white European. These sub-cohorts were individually referenced as they are more directly relevant to the patients' ancestry. This patient also had a novel hemizygous missense variant in the *APEX2* gene (ENST00000374987) located on the X chromosome, c.1264A>G, p.M422V, at a residue conserved in three other species; chimpanzee, dog and dolphin (Figure 4.12B). This variant was inherited from the heterozygous asymptomatic mother. Furthermore this variant (p.M422V) was identified once on control databases; in the ExAC browser in an African heterozygous individual out of a total of 86,652 alleles, of which 8405 were from an African origin the same as the mother. The role of *APEX2* is discussed in section 4.4.5 in this chapter.

A) FASN (p.A2132V)

Human: V--E--A--V--**A**--H--I--L--G
Mouse: V--**K**--A--V--**A**--H--I--L--G
Chimpanzee: V--E--A--V--**A**--H--I--L--G
Chicken: V--E--A--V--**A**--H--I--L--G
Xenopus: V--E--A--V--**A**--H--I--L--G
Zebrafish V--E--A--V--**A**--H--I--L--G

B) APEX2 (p.M422V)

Human: M--S--A--L--**M**--T--P--K--T
Chimpanzee: M--S--**T**--L--**M**--T--P--K--T
Dog: M--**G**--A--L--**M**--T--P--K--T
Dolphin: **L**--**G**--**T**--L--**M**--T--P--K--T

Figure 4.12: Conservation of the substituted FASN and APEX2 residues. The extent of conservation across multiple species of each substituted amino acid (highlighted in green), and the spanning protein sequence, in both **(A)** FASN, and **(B)** APEX2. Any spanning amino acid residues that differ from the normal human reference sequence are highlighted in red.

4.4.3. FASN function

The coding region of Fatty Acid Synthase (*FASN*) is 7.536kb in length comprising of 43 exons on chromosome 17. *FASN* has long been identified as a crucial multienzyme composed of two identical 272 kDa polypeptides that have multiple functions in which substrates are transferred from one domain to another. More precisely, this complex enzyme essentially converts acetyl-CoA and malonyl-CoA into long-chain saturated fatty acids such as palmitate in the presence of NADPH, and has been reported to have as many as seven different catalytic activities (Wakil, 1989). Recent studies in mice have shown that hepatocarcinogenesis, induced by AKT/c-Met, is fully inhibited by *Fasn* ablation. Therefore suppression of *FASN* might be highly detrimental for the growth of human hepatocellular carcinoma subsets (Hu et al., 2016). In addition, Shh signalling induces *FASN*, which mediates metabolic processes such as proliferating neural progenitors to support rapid growth, which can induce lipogenesis and aerobic glycolysis; pathways that are increased in medulloblastoma metabolism (Tech and Gershon, 2015). *Fasn* is highly active in adult neural stem and progenitor cells (NSPCs) and conditional deletion of *Fasn* in mouse NSPCs impairs adult neurogenesis (Knobloch et al., 2013). Other studies have shown that murine null mutant *Fasn*^{-/-} embryos die before implantation, and *Fasn*^{+/-} heterozygotes die at various stages of development *in utero*, suggesting haploid insufficiency (Chirala et al., 2003).

Murine *Fasn* is expressed in the brain, parathyroids, liver and adrenal, as well as the high level of expression observed in adult NSPCs. It is expressed in numerous tissues including the limbs, the exocrine and endocrine systems, and the olfactory, reproductive, respiratory and connective tissue systems, to name a few (MGI). In humans, this multifunctional enzyme has been noted to be highly expressed in the glandular and adipocyte cells of the breast (Human Protein Atlas).

4.4.4. FASN expression results

In this study, human embryonic expression in a hypothalamo-pituitary context, revealed high *FASN* expression in the hypothalamus, and in Rathke's pouch at the early stage of CS16 (Figure 4.13A-C). At CS19, expression was noted in the spinal cord (Figure 4.13D), spinal ganglia and trigeminal ganglia (Figure 4.13E). However, despite expression being maintained in the diencephalon and telencephalon (Figure 4.13F), there appeared to be no *FASN* transcript expression in Rathke's pouch from this stage onwards in embryogenesis [shown by the lack of total expression in Rathke's pouch at CS20 (Figure 4.13I)]. Specific *FASN* expression was observed in the retina of the eye at CS20 (Figure 4.13G-H). No specific expression was observed in the developing ear, heart or spleen for this gene.

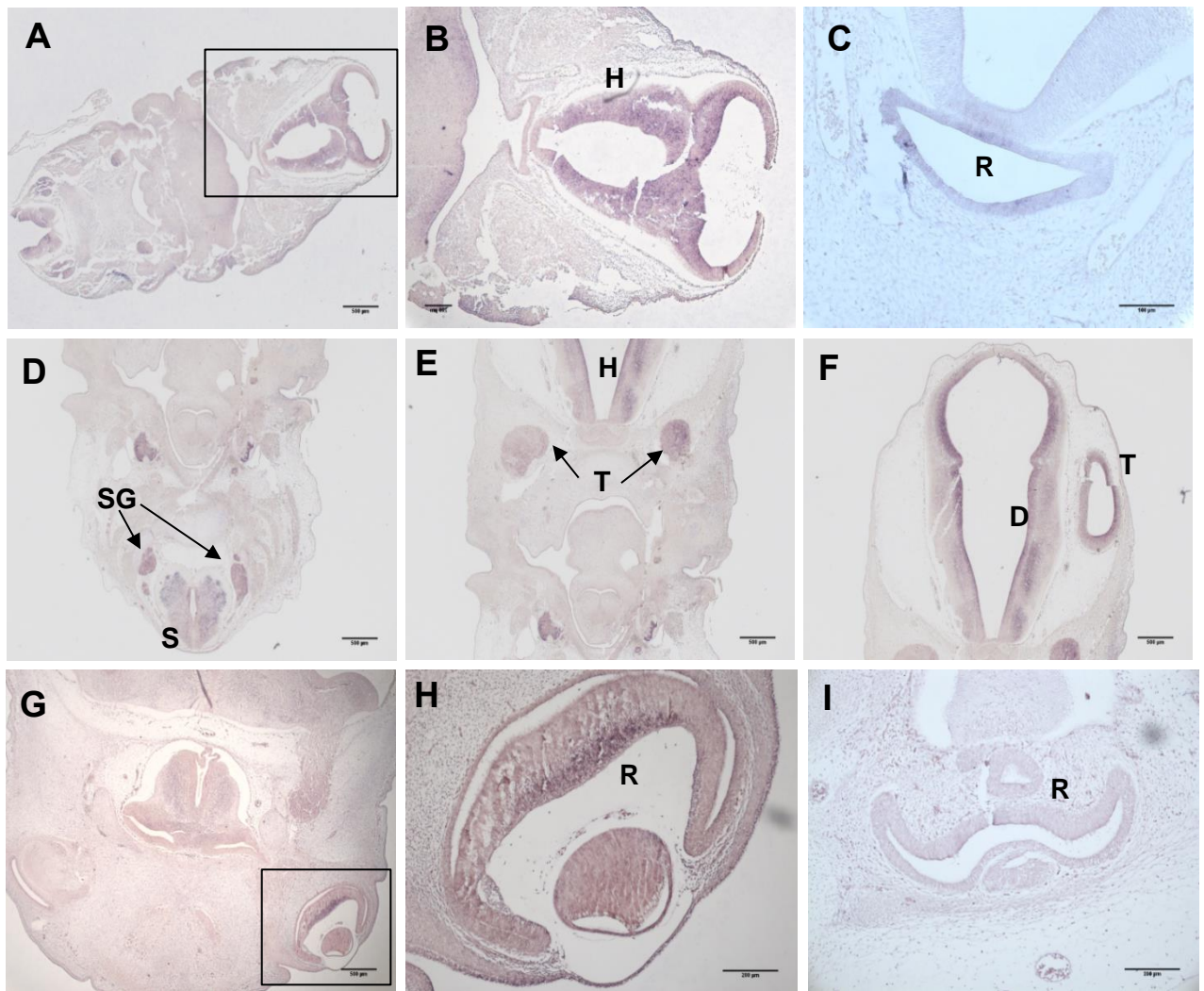


Figure 4.13: *FASN* expression in the hypothalamo-pituitary axis and the eye in the developing human embryo. *In situ* hybridization using the antisense probe against the human *FASN* mRNA transcript (*hFASN*) on human transverse sections from CS16, CS19 and CS20. The scale bars in the images are as follows: 500 μ M in 'A', 200 μ M in 'B', 100 μ M in 'C', 500 μ M in 'D-G' and 200 μ M in 'H-I'. **(A-B) CS16:** high *FASN* expression in the hypothalamus. **(C) CS16:** expression in Rathke's pouch. **(D) CS19:** expression seen in the spinal cord and spinal ganglia, **(E)** trigeminal ganglia and hypothalamus, **(F)** diencephalon and telencephalon. **(G-H) CS20:** expression in the retina of the eye, **(I)** Rathke's pouch shows no *FASN* expression at CS20. The

black boxes in 'A' and 'G' indicate the area of the sections that are magnified in images 'B' and 'H' respectively. H, hypothalamus; RP, Rathke's pouch; SG, spinal ganglia; S, spinal cord; TG, trigeminal ganglia; D, diencephalon; T, telencephalon; R, retina.

4.4.5. APEX2 function

The coding region of Apurinic/aprimidinic (AP) endonuclease 2 (*APEX2*) is 1.557kb in length comprising of 6 exons, on the X chromosome. It is a member of the endonuclease family that initiates the repair of AP sites formed by spontaneous hydrolysis of the N-glycosylic bond, mutagen-induced base release, or damaged-base excision caused by a DNA repair glycosylase (Hadi et al., 2002). Previous functional studies showed, through immunocytochemistry, that *APEX2* localises to the mitochondria due to the gene having a mitochondrial targeting sequence on its N-terminus (Tsuchimoto et al., 2001). These studies also showed evidence that *APEX2* participates in mitochondrial base excision repair (BER) as well as in nuclear BER (Tsuchimoto et al., 2001). Other studies revealed that *Apex2*-null mice exhibit a growth retardation phenotype (80% the size of WT littermates) with moderate dyshaematopoiesis and a severe defect in lymphopoiesis (Ide et al., 2004). In addition these mice showed significant accumulation of thymocytes and mitogen-stimulated splenocytes in G2/M phase compared to WT, which they concluded implicated *APEX2* as an essential regulator of efficient cell cycle progression of proliferating lymphocytes (Ide et al., 2004). Despite the name, *APEX2* exhibits weak AP endonuclease activity compared to its strong 3-5-prime exonuclease and 3-prime phosphodiesterase activities (Burkovics et al., 2006). According to the Human Protein Atlas, expression of the *APEX2* transcript is located in the myocytes of the heart.

4.4.6. APEX2 expression results

Human embryonic expression in this study interestingly revealed strong expression in areas of the developing oral cavity and throat as well as in the eye (Figure 4.14). At CS19 and 20, *APEX2* expression was seen in the laryngeal pharynx, laryngeal inlet, in the palatine shelf and the developing tongue of the oral cavity (Figure 4.14A-E, G-H), but is no longer expressed in these areas of the throat by CS23 (Figure 4.14J). Expression in the eye at CS19 appears to be specifically in the lens and around the front of the eye where the cornea will form (Figure 4.14F). By CS23, expression in the eye has become more defined and stronger around the developing cornea; distinctively in the conjunctival sacs of the eye, whilst remaining in the lens (Figure 4.14K). *APEX2* expression is also seen partially in the ear (Figure 4.15C-D), and in the gonads and the lining of the stomach (Figure 4.15B) in sections taken at CS19. Expression is also seen in the bronchi (Figure 4.15A, E-G), trachea (Figure 4.15F, H) and oesophagus (Figure 4.15F) at CS19 and CS22. Intriguingly at CS23, there is highly defined expression along the midline raphe glial system, located between the raphe nuclei in the brain (Figure 4.15I-J). The raphe nuclei are a moderate-sized cluster of nuclei with the main function of releasing serotonin to the rest of the brain. Serotonergic neurons in the raphe nuclei, situated in the brainstem, densely innervate the olfactory bulb where they modulate olfactory information (Brunert and Tsuno, 2016).

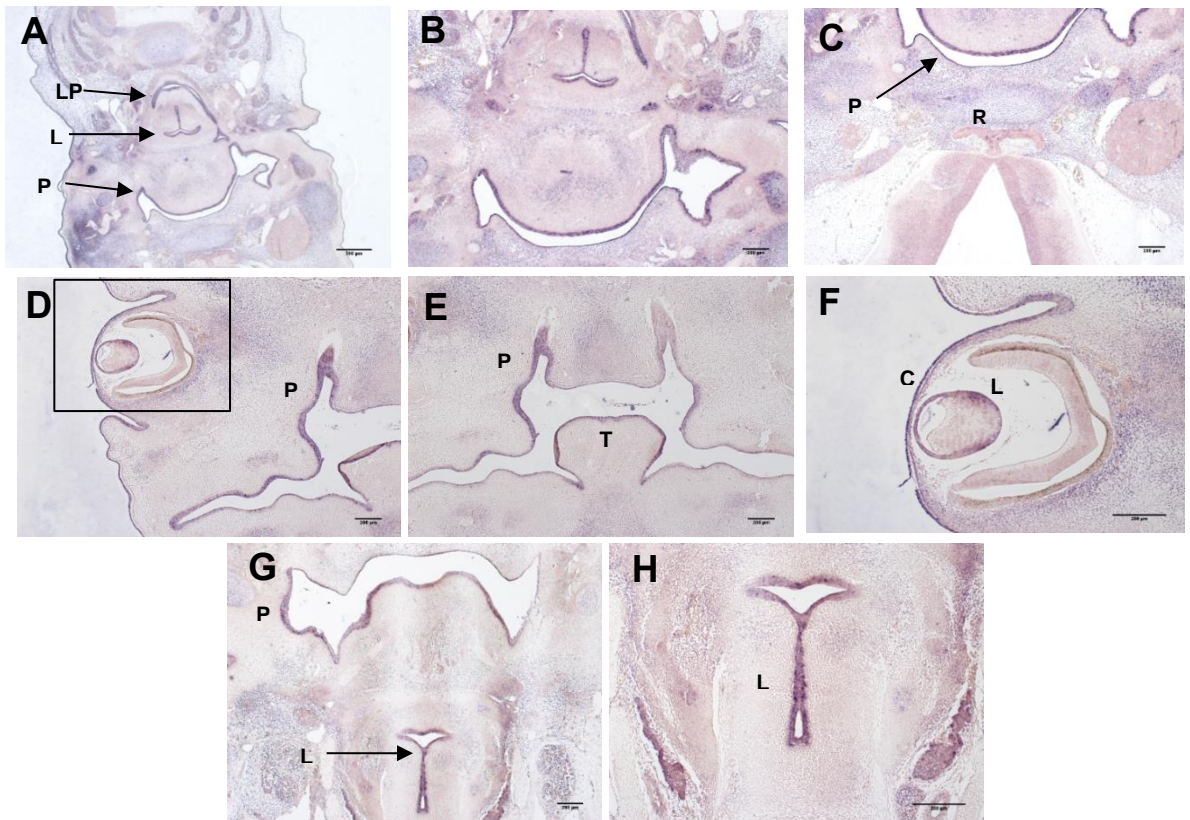


Figure 4.14: *APEX2* expression in the hypothalamo-pituitary axis, oral cavity and the eye in the developing human embryo. *In situ* hybridization using the antisense probe against the human *APEX2* mRNA transcript (*hAPEX2*) on human transverse sections from CS19 and CS20. The scale bar in 'A' represents 500 μ M and the scale bars in 'B-H' represent 200 μ M. **(A-B) CS19:** high *APEX2* expression in the oral cavity; LP, laryngeal pharynx; LI, laryngeal inlet; PS, palatine shelf. **(C) CS19:** expression is observed in the PS, however not in the hypothalamus or Rathke's pouch. **(D-E) CS19:** high expression in the PS from a different transverse section, expression in the body of the tongue can be seen in 'E'. **(F) CS19:** expression in the lens and the cornea of the eye (also visualised in 'D'). **(G-H) CS20:** expression remains high in the PS and LI areas of the oral cavity. RP, Rathke's pouch; Tn, tongue; C, cornea; L, lens.

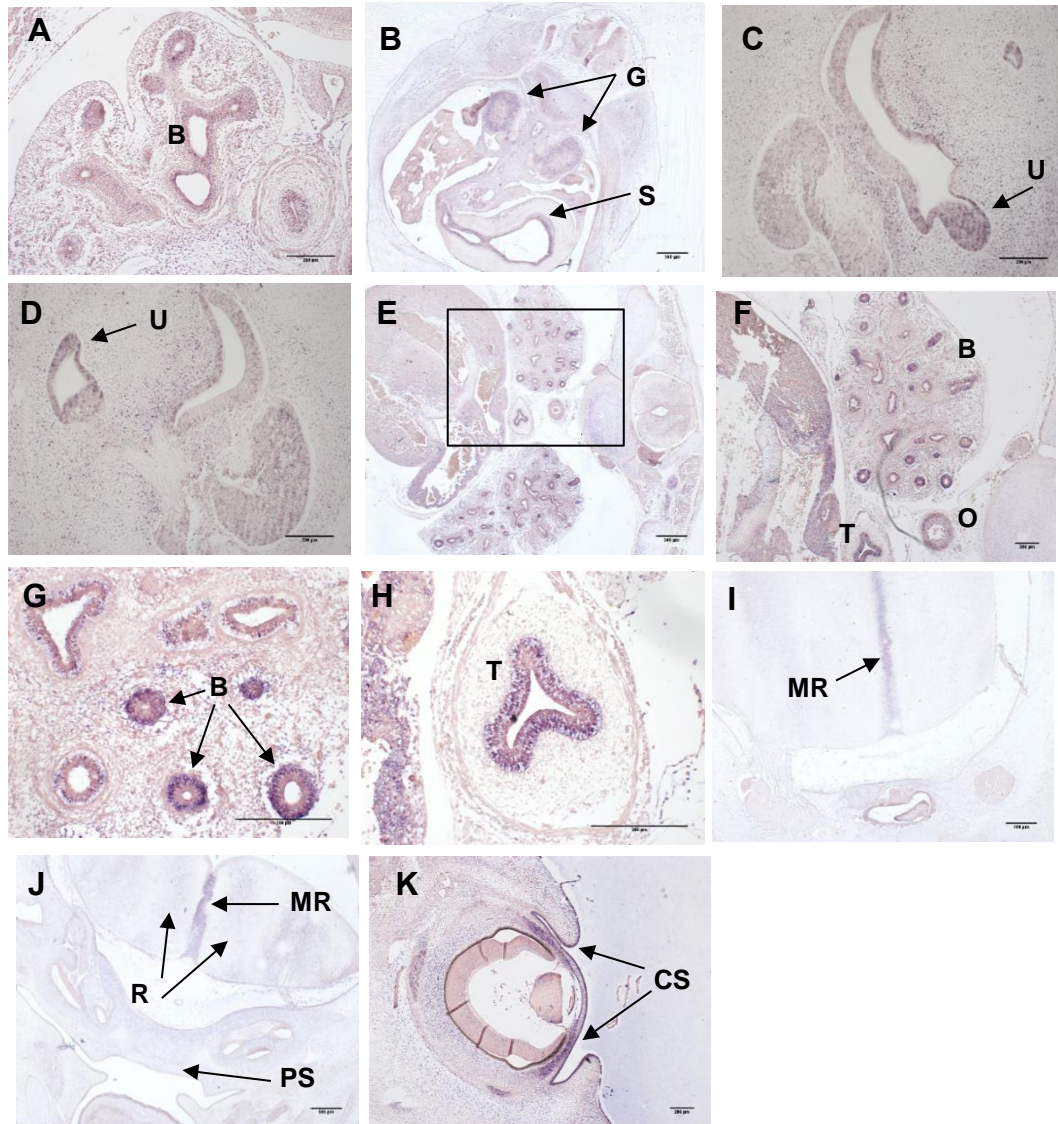


Figure 4.15: *APEX2* expression in developing human embryonic tissues. *In situ* hybridization using the antisense probe against the human *APEX2* mRNA transcript (*hAPEX2*) on human transverse sections from CS19, CS22 and CS23. **(A) CS19:** high *APEX2* expression in the bronchi of the lungs. The scale bars in the images are as follows: 200 μ M in 'A', 500 μ M in 'B', 200 μ M in 'C-D', 500 μ M in 'E', 200 μ M in 'F-H', 500 μ M in 'I-J' and 200 μ M in 'K'. **(B) CS19:** expression in the gonads and in the lining of the stomach. **(C-D) CS19:** expression in the ear; at the end of the utricle. **(E-H) CS22:** section of the torso showing *APEX2* expression in multiple bronchi, trachea and the oesophagus, **(H) CS22:** high expression in the trachea (image taken from

image 'E' in the area highlighted by the black box). **(I-J) CS23**: defined line of *APEX2* transcript expression noted in the midline raphe glial system. There is no expression in the palatine shelf at this stage. **(K) CS23**: high expression in the cornea of the eye; in particular the conjunctival sacs at the sides of the eye. B, bronchi; G, gonads; S, stomach; U, utricle; T, trachea; O, oesophagus; MR, midline raphe glial system; R, raphe nuclei; PS, palatine shelf; CS, conjunctival sac.

4.5. Discussion

4.5.1. Pedigree 2: Discussion

It should be noted that individuals from an African origin are known to have more genetic variation than those from the non-African population (Song et al., 2017). However as the *CTPS2* (p.F166L) variant is *de novo* there is a reasonable body of evidence to suggest that this heterozygous variant is likely to be associated with the striking phenotype of the proband in Pedigree 2. The strong *CTPS2* expression seen in the developing hypothalamus and Rathke's pouch, indicates a role for this gene in the formation of the midline forebrain; specifically the pituitary gland, during embryogenesis. The expression data make *CTPS2* a likely candidate in causing the panhypopituitarism seen in the patient carrying the *CTPS2* (p.F166L) variant (Pedigree 2), and it would therefore be worth taking the gene forward to conduct functional studies in this respect. In addition, the high expression of this gene seen in the ear is a strong indication that the variant may be contributing to the abnormal formation of the ear, with severe hearing loss seen in the patient. Although *CTPS2* is not expressed in the heart tissue specifically, this does not necessarily rule out a role for the gene in the phenotype of situs inversus with dextrocardia observed in the patient (Pedigree 2). Rather, this mutated gene may be involved in causing the asymmetry seen in the patient and thus would not be expressed in the heart tissue

itself. Looking at the phenotype, there are multiple signs of asymmetry diagnosed in the patient: the dextrocardia/situs inversus, left microtia, and the left-sided hemiparesis including left facial nerve palsy. Therefore it is proposed that *CTPS2* may well be involved in the determination of left-right asymmetry during development. Further functional studies need to be undertaken to delineate its role in human development.

4.5.2. Pedigree 3-6: Discussion

Due to the previously published data linking *RNPC3* mutations to the phenotype of IGHD and pituitary hypoplasia, together with the expression profile elucidated in this study, the novel *RNPC3* (p.L483F) variant is predicted to be responsible for the GHD observed in the patients in Pedigrees 3-6. Interestingly, and without intention, expression of *RNPC3* was noted in the mesonephros of the premature kidney, and in what is potentially the paramesonephric duct or the fallopian tube in 9pcw embryonic tissue. The cause of the ovarian failure in these patients remains to be established, and future work will begin by looking at the expression of both *RNPC3* and *PRMT6* in >10pcw ovarian sections when tissue is available. Interestingly Markmiller *et al* report that four genes, including the orthologs of the two mutated in Pedigrees 3-6: *col11A1*, *rnpc3*, *prmt6*, and *ntng1* (Markmiller et al., 2014), are contained within a region on chromosome 24 in the zebrafish. This region therefore appears to be syntenic to human chromosome 1, illustrating the close relationship between *RNPC3* (1p21) and *PRMT6* (1p13.3) in evolutionary terms. Thus evidently *RNPC3* and *PRMT6* are co-located across species, not just in humans, therefore the two mutations, *RNPC3* (p.L483F) and *PRMT6* (p.P350R), in Pedigrees 3-6 have co-segregated in all affected individuals. Due to all the patients in these consanguineous pedigrees having these variants, there is a strong possibility that these four pedigrees are distantly related as

they all originate from the same geographical isolated population in Turkey. However this is unknown and the families are therefore noted as unrelated. Therefore the co-segregation of these two variants may be termed as a founder effect. Further work is required to clarify the pathogenesis of the ovarian failure, and to understand the pathogenesis of IGHD in relation to the role of RNPC3 in pituitary development and function.

4.5.3. Pedigree 7: Discussion

The proband in Pedigree 7 has a unique phenotype with a multi-system disorder. The exciting finding of a *de novo* variant in *FASN* suggests that this patient's phenotype could at least in part be explained by a disorder of fatty acid synthesis. The role of the gene in NSPC proliferation could also suggest a role in hypothalamo-pituitary development, supported by the gene in the hypothalamus and developing pituitary. Further investigations are underway currently in this patient, and it is clear that the patient has consistently elevated fasting concentrations of triglycerides. *APEX2* does not appear to be expressed in the hypothalamus or in Rathke's pouch at any stage of embryogenesis, whereas *FASN* is strongly expressed in these areas at a very early stage during development (CS16). This indicates that it may be the *FASN* variant in this patient that may be causative of the panhypopituitarism. Additionally *FASN* is expressed in the retina, unlike *APEX2*, and again these data suggest a role for *FASN* in the aetiology of the retinal dystrophy rather than *APEX2*, which appears to be expressed in the conjunctival sacs near the lens of the eye. Previous studies have shown that hyperplastic parathyroids from patients with chronic renal failure strongly express fatty acid synthase, indicating that it may be a potential biological indicator of highly proliferating parathyroid cells (Alo et al., 1999). However our studies were unable to analyse whether parathyroids from a normal embryo express *FASN*.

Therefore we do not have enough evidence to conclude whether the FASN (p.A2132V) mutation is contributing to the hypoparathyroidism phenotype at this stage.

The proband in Pedigree 7 has been reported to have had many recurrent episodes of choking, which may possibly be linked via some unknown mechanism to the APEX(M422V) mutation, given its expression in the developing larynx. *APEX2* is also expressed in the developing ear (Figure 4.15 C-D) and therefore could be associated with the sensorineural hearing loss seen in the patient. It is unknown if the expression observed in the midline raphe glial system (Figure 4.15 I-J) is related to the phenotype in this patient. However due to serotonergic neurons, which derive from the raphe nuclei, densely innervating the olfactory bulb and modulating its information, the patients olfactory system should be monitored for any abnormalities, such as sense of smell and should perhaps be structurally analysed, if not done so with particular focus, by MRI. Given the presence of a *de novo* variant in a gene that is critical for embryonic survival (*FASM*), and a further variant in a gene that is on the X-chromosome (*APEX2*), there is a possibility of a digenic explanation for the highly complex phenotype in the patient in Pedigree 7. However further *in vivo/in vitro* functional investigation would need to take place for any clear conclusions to be drawn.

4.6. Summary of expression profiles

Expression of *CTPS2*, *RNPC3* and *FASN* in Rathke's pouch in the respective patients suggests that these three genes may be implicated in the early stages of embryonic development of the pituitary. The variants identified in these genes may be responsible for the endocrine deficits seen in the respective patients, through incomplete development of this primordium of the anterior pituitary in the embryo.

Expression is used as a strong indicator as to where a gene is active, however mutations may have a very different effect on the structure and function of the protein in which it encodes, and may differ from each other in pathogenicity, affecting one or many other tissues in addition to that showing expression. Thus, certain mutations may cause a downstream target effect and have an ultimate end result elsewhere. The complex genetic cascades of different multifunctional pathways within the body are intertwined and linked directly and indirectly, highlighting the need for manipulation and exploitation of these pathways through functional assays that help show the significance of a mutation, and shed light on what each individual mutation does. In the pedigrees described in this study, we have identified a number of genetic variants of interest, and in initial preliminary studies, have explored the expression patterns of the novel candidate genes in human embryonic tissue. The expression patterns of the genes seem to match the specific phenotypes observed in the patients, and act as a guide to functional studies, building evidence towards whether a mutation in that gene should be pursued. Given that functional studies are not only difficult to perform but also very expensive, we believe that the use of expression studies as an initial screen is essential. The expression studies could be performed in murine embryos, but given our access to human embryonic sections as part of the HDBR resource, I have pursued the route of human gene expression at this stage.

4.7. EIF2S3/eIF2γ

4.7.1. Exome sequencing of the X chromosome in Pedigree 8

Exome sequencing of the X chromosome was performed in a single X-linked non-consanguineous white European pedigree with GHD, severe hypothyroidism and an unusual pancreatic phenotype that fluctuates between hyperinsulinaemic hypoglycaemia and hyperglycaemia (Pedigree 8, Figure 5.1). At this time, the association of a pituitary and pancreatic phenotype had not been described in the literature previously, hence there was no clear defined known gene to screen in this unique family. Analysis revealed a novel hemizygous missense substitution in the *EIF2S3* gene (ENST00000253039.8): ChrX_24091319 C/T, *c.1294C>T*, p.P432S, located at a highly conserved residue across multiple species (Figure 4.16) in the C-terminal domain of unknown function. Protein prediction models predict this variant to be deleterious, Polyphen2: score 0.971, and SIFT: score 0, with SIFT inferring that this is most likely due to the loss of Proline, which is well known to be involved in protein folding. This variant was absent from control databases; 1000 Genomes, dbSNP, EVS and the ExAC Browser, with the latter incorporating a total of >87,000 control alleles with >52,000 being from a European background and thus ethnically relevant to Pedigree 8. GOSgene used their own internal data sets of the X-chromosome to filter for novel variants in Pedigree 8. The *EIF2S3* (p.P432S) was the only variant identified that was considered to be a potential pathogenic cause of the disease seen in the patients. Therefore this gene was taken forward for functional analysis in this study (Chapter 5).

eIF2 γ (p.P432S)

Human: V--L--T--N--P--V--C--T--E
Mouse: V--L--T--N--P--V--C--T--E
Chimpanzee: V--L--T--N--P--V--C--T--E
Cow: V--L--T--N--P--V--C--T--E
Dog: V--L--T--N--P--V--C--T--E
Chicken: V--L--T--N--P--V--C--T--E
Xenopus: V--L--T--N--P--V--C--T--E
Zebrafish V--L--T--N--P--V--C--T--E

Figure 4.16: Conservation of the substituted eIF2 γ residue. The conservation across multiple species of the substituted amino acid (highlighted in green), and the spanning protein sequence, in eIF2 γ .

It has already been established that the murine *EIF2S3* homologue, *Eif2s3x* on the X chromosome of the mouse, is highly expressed in the pancreas, hypothalamus and pituitary (MGI). However, human *EIF2S3* expression studies have not been previously performed in depth in a hypothalamo-pituitary context. I therefore performed *in situ* hybridisation to analyse the gene expression profile of the *EIF2S3* gene in human embryonic tissue taken from the brain and the pancreas.

4.7.2. EIF2S3 expression results

Human expression studies using the human *EIF2S3* DIG-labelled antisense probe showed *EIF2S3* mRNA transcript expression in the hypothalamus and Rathke's pouch at CS20, and in the anterior and posterior areas of the pituitary (AP and PP) at CS23, however not throughout the whole pituitary tissue (Figure 4.17 A-B). Expression was observed in the progenitor cells of the nasal epithelium (Figure 4.17 C), and in the retina of the eye at CS20 and 23 in the human fetus. At CS23 the retina is in the process of differentiating into different cell types, and the gradient of expression seen here appears to be within the developing inner nuclear layer, possibly in the developing ganglion cells (Figure 4.17 D). Expression seems to be excluded from the outer layer which is where cells that form the photoreceptors reside. The *EIF2S3* transcript was also present in the pancreas of a 13-week old fetus in the exocrine component and Islets of Langerhans, in the cells that will become beta cells (Figure 4.17 E-F). The *EIF2S3* DIG-labelled sense probe was negative for staining, in the areas in which the antisense probe stained positive, indicating that the expression profile generated from the antisense probe in this study is reliable.

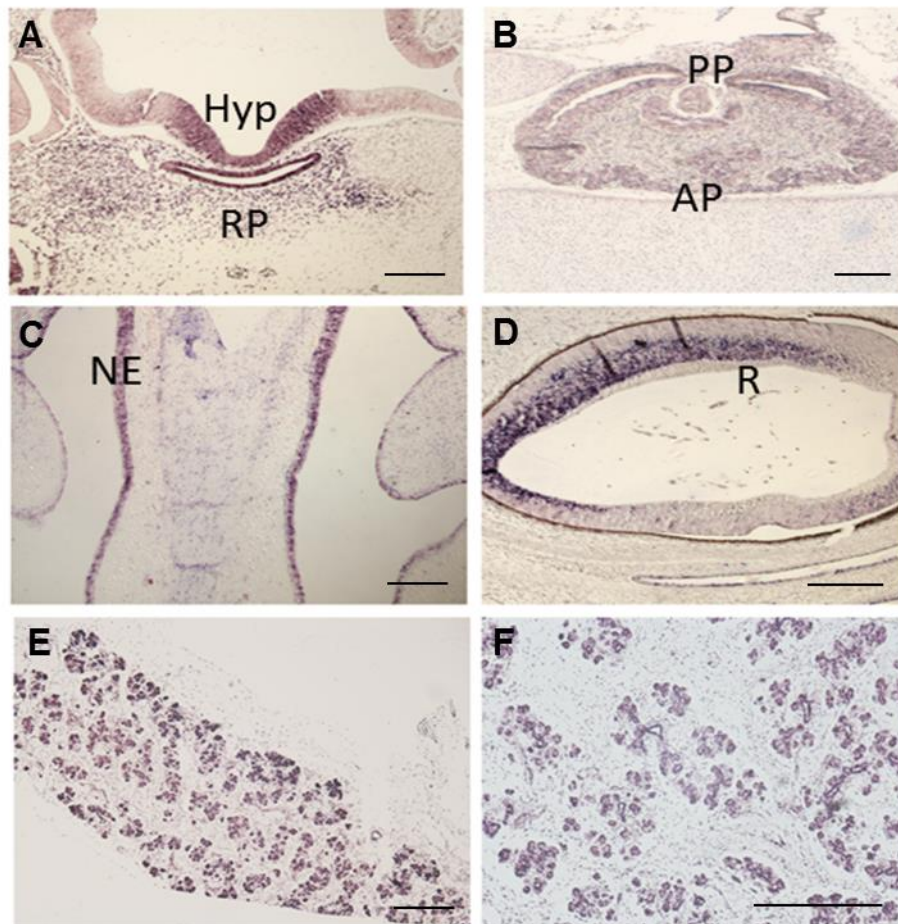


Figure 4.17: Human *EIF2S3* expression in the hypothalamo-pituitary axis, eye and pancreas in the developing human embryo. *In situ* hybridization using the antisense probe against the human *EIF2S3* mRNA transcript (h*EIF2S3*) on human sections. Expression is representative of two embryos. The scale bars in the images are as follows: 200µM in 'A', 100µM in 'B-C', 200µM in 'D' and 100 in 'E-F'. **(A-C)** Transverse sections of the brain, **(A)** mRNA *EIF2S3* transcripts were localised to the ventral hypothalamus and Rathke's pouch (CS20). **(B)** *EIF2S3* expression was seen in the AP and PP although not throughout the whole pituitary tissue (CS23). **(C)** Defined *EIF2S3* transcripts were seen in progenitor cells in the nasal epithelium (CS23). **(D)** Sagittal section of the eye. *EIF2S3* transcripts were localised in the retina (CS23). **(E-F)** Sagittal sections from a pancreas obtained from a 13 week old fetus, expressing the *EIF2S3* transcript in the exocrine component, in the Islets of

Langerhans and in the progenitors of beta cells; 'E'; X5 magnification, 'F'; X10 magnification. Abbreviations: Hyp, hypothalamus; RP, Rathke's pouch; AP, anterior pituitary; PP, posterior pituitary; NE, nasal epithelium; R, retina.

The expression profile performed in this study demonstrates the involvement of *EIF2S3* in early hypothalamo-pituitary and pancreatic development. These data support the hypothesis that the *EIF2S3* mutation identified in Pedigree 8 may be implicated in the phenotype observed in the patients, given the expression pattern of the gene in the relevant tissues. Therefore, after establishing this expression profile, this gene was taken forward and functionally assessed in this investigation in an attempt to understand its biological role, with particular focus on these tissues. Chapter 5 of this thesis investigates the role of *EIF2S3* and the effect of the p.P432S variant using a variety of assays.

Chapter 5

A Novel Mutation in Eukaryotic Translation Initiation Factor 2 Subunit 3 (EIF2S3) Associated with Severe Hypoglycaemia and X-Linked Hypopituitarism

5.1 Introduction

As discussed in Chapter 4 many novel potential candidate genes for hypopituitarism and related phenotypes have recently been identified through exome sequencing, in collaboration with GOSgene, of specific pedigrees with unique phenotypes. One such pedigree is Pedigree 8 (Figure 5.1), a non-consanguineous white European pedigree with affected male monozygotic (identical) twin brothers (IIId,e). Patients IIId and IIle have severe short stature and GHD, central hypothyroidism, hyperinsulinism causing hypoglycaemia and a small AP on MRI. They have maternal twin cousins; one male, one female, with the male manifesting a similar phenotype (IIIc). The exome sequencing performed on this single X-linked pedigree (Pedigree 8), revealed a novel hemizygous variant in the *EIF2S3* gene: ChrX_24091319 C/T, *c.1294C>T*, p.P432S, which segregates fully within the affected members of the family (Figure 5.1). The *EIF2S3* (p.P432S) variant was inherited from the heterozygous mothers who had presented with secondary amenorrhea.

Pedigree 8

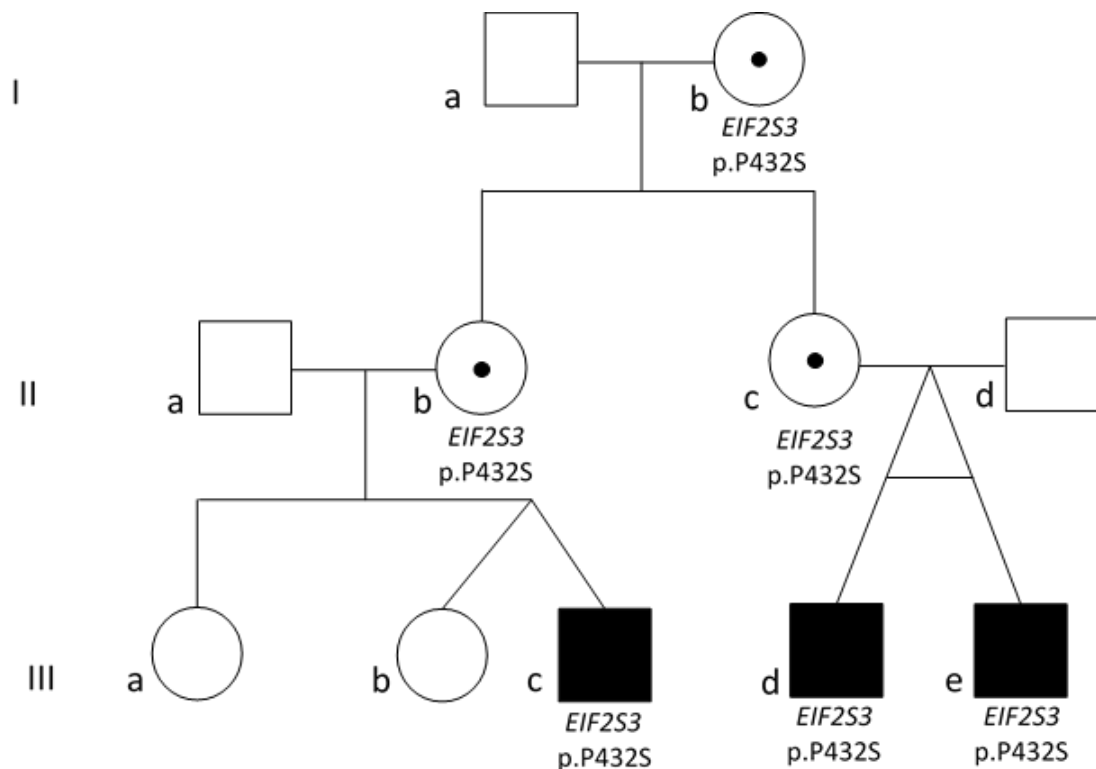


Figure 5.1: Pedigree 8 harbouring the *EIF2S3* (p.P432S) variant. This pedigree consists of three affected individuals that are hemizygous for the *EIF2S3* (p.P432S) variant, represented by the black shaded squares labelled with '*EIF2S3* p.P432S'. Patients III-d and III-e are monozygotic twins represented. The circles containing a dot highlight the females that carry the variant in heterozygous form. Un-shaded squares/circles represent males and females that were negative for the variant respectively. The roman numerals on the left of the image depict the generation within the pedigree. The letters 'a' – 'e' distinguish between each individual within that generation, which are referred to in the text.

5.1.1. Patients in Pedigree 8

5.1.1.1. The three affected males

The three males, IIIc, III d, III e, presented with severe recurrent hypoglycaemia, short stature and GHD (Figure 5.2), with a low IGF1 and low IGFBP3 concentration (Table 5.1). They have a unique pancreatic phenotype which fluctuates between hyperinsulinaemic hypoglycaemia and hyperglycaemia (Table 5.2). They were treated up to the age of 7 years with Diazoxide, and their blood glucose was adequately controlled during this time. To date, the cortisol and prolactin concentrations have been normal. Additional features in the three boys include intestinal lymphonodular hyperplasia and eosinophilic infiltration. MRI of the brain revealed a small AP, a normal posterior pituitary and stalk, and a thin corpus callosum, with patients IIIc and III d also having generalised white matter loss, and IIIc having ventricular asymmetry (Figure 5.3). Endocrine values for the three patients are presented in Tables 5.1 and 5.2.

5.1.1.2. Patient IIIc

Patient IIIc was the first born of twins via emergency caesarean at 38 weeks gestation, with a birth weight of 2.1kg. He presented with poor feeding and hypoglycaemia 18 hours after birth. Aside from the clinical phenotypes described above he presented with congenital heart disease; total anomalous pulmonary venous return, in which the four veins that take blood from the lungs to the heart do not attach normally to the left atrium. He also presented with a gastro-oesophageal reflux which required a Nissen's procedure with a complication of dumping syndrome. He has IGHD but is having his FT4 and TSH closely monitored, and is currently too young to have his gonadotrophins tested as he has not yet reached pubertal age. He had a blunted testosterone response to a 3-day HCG test, however he was only 3

years of age when this test was performed (Table 5.2). He has global developmental delay, behavioural problems and has hepatomegaly. His mother presented with secondary amenorrhoea.

5.1.1.3. Twin brothers: patients III d and III e

The monozygotic twin brothers were born via caesarean at 34 weeks gestation, patient III d had a birth weight of 2.15kg, and patient III e a birth weight of 1.93kg. Aside from the clinical phenotypes described in the above section (5.1.1.1), they developed central hypothyroidism at the age of 2 years and were treated with thyroxine (Table 5.1). They both presented with hypoglycaemia with seizures at this age, and had a microphallus, which increased in size following GH treatment. Patient III d had small pea-sized testes that were initially undescended, however they did descend spontaneously. His twin brother, III e, had normal descended testes on initial examination. The twins had feeding difficulties and poor weight gain, which may have been partly due to their dairy free diet, however their feeding is now normal. By the age of 4 years the brothers had delayed speech development, and by 6 years they had mild conductive hearing loss, global developmental delay, behavioural and learning difficulties. A microarray performed in both boys was normal. Patient III d presented with behavioural difficulties, although not as severe as his twin brother (III e), however he often had episodes of twitching, possibly related to his hypoglycaemia. Patient III d also had hepatomegaly, myopia and a squint, and now wears glasses. Both brothers underwent surgery at the age of 4 years to have their tonsils removed due to recurrent tonsillitis, their adenoids were removed due to recurrent upper respiratory infections and upper airway obstruction, and grommets were inserted due to glue ear. Their palates appeared normal on examination. At the age of 10 years the brothers had a glucose tolerance test which showed impaired

glucose tolerance; the glucose concentrations fluctuated between hypoglycaemia and hyperglycaemia. Table 5.3 shows these test results for patient III d. They have recently reached pubertal age and have had their gonadotrophin secretion tested, which appears reasonably normal (Table 5.2). Patient III d had a blunted testosterone response to a 3-day HCG test, with his brother III e having a borderline testosterone response (Table 5.2).

Their mother had osteoporosis due to secondary amenorrhoea, with menarche at 13 years and periods stopping at 16 years, after which she received oestrogen supplementation (CycloProgynova). In later life she had a hysterectomy. An MRI performed on the mother was reported to be normal. Their mother had a height of 162.9cm and their father a height of 169cm, with a mid-parental height of -0.34 SDS.

Patient	Birth weight kg (SDS) (gestation)	Age at presentation years	Height at presentation cm (SDS)	Peak GH to provocation µg/L	IGF1 ng/ml (NR)	IGFBP3 mg/L (NR)	Most recent cortisol nmol/L	FT4 (pre-treatment) pmol/L (NR)	TSH (pre-treatment) mU/L	PRL mU/L (NR)
IIlc	2.1 (-2.8) (38/40)	1.13	58.8 (-6.7)	<0.1 on profile	<25	<0.5	315	12.6 (12 - 22) Not treated	5	360 (40 - 555)
IIId	2.15 (-0.3) (34/40)	2.2	71.5 (-4.4)	1.1	9 (20 - 158)	0.67 (1.2 - 3.7)	183	11.4 (12 - 22)	2.9	225 (40 - 555)
IIle	1.93 (-1.5) (34/40)	2.2	69.5 (-5.2)	0.7	10 (20 - 158)	1.2 (1.2 - 3.7)	241	11.3 (12 - 22)	3.4	114 (40 - 555)

Table 5.1: Clinical data from the three affected males in Pedigree 8; IIlc, IIId, IIle. Patients presented with GH deficiency, and low IGF1 and IGFBP3 concentrations. Their cortisol and prolactin concentrations were normal. The twin brothers, IIId and IIle, developed central hypothyroidism and were treated with thyroxine. SDS, standard deviation score; NR, normal range.

Patient	Peak LH IU/L (GnRH at age 12)	Peak FSH IU/L (GnRH at age 12)	Peak testosterone to 3 day HCG nmol/L (age in years)	Most recent height SDS (age in years)	Glucose mmol/L (age in years)	Insulin mU/L (age in years)	HC SDS (age in years)	Diazoxide treatment (age in years)
IIIC	N/A	N/A	0.992 (3)	-1.03 (7)	3.3 (0.25)	5.9 (0.25)	-3.3 (2.4)	0.75 - 6.8
IIID	6.3	4.0	1.99 (12)	-2.04 (12.1)	3.4 (2.2)	6.8 (2.2)	N/A	2.5 - 6.7
IIIE	8.1	3.4	3.64 (12)	-2.23 (12.1)	3.2 (2.2)	4.9 (2.2)	N/A	2.5 - 6.7

Table 5.2: Clinical data following gonadotrophin tests from the three affected males in Pedigree 8, IIIC, IIID, IIIE. Values following a gonadotrophin secretion test and a 3-day HCG test. HCG, human chorionic gonadotrophin; SDS, standard deviation score; HC, head circumference.

Glucose tolerance test of patient IIIId off Diazoxide

Time (mins)	-75	0	30	60	90	120	150	180	210	240	270	300
Glucose (mmol/L)	3.6	3.2	10.2	12.1	8.8	8.4	7.8	6.2	5.5	5.5	4.0	2.7
Insulin (mU/L)	5.6	4.9	21.2	21.3	19.5	22	22	20.5	19.4	16.1	10.7	5.5

Table 5.3: Glucose tolerance test in patient IIIId. A prolonged glucose tolerance test was performed on patient IIIId at the age of 10 years, off Diazoxide treatment. At 0 mins the patient had a high basal glucose with detectable insulin. Glucose increased over time and after 2 hours (120 mins) the patient had a high blood glucose above the normal range. Glucose then decreased and by 5 hours (300 mins) the patient was hypoglycaemic with a detectable insulin.

Growth charts

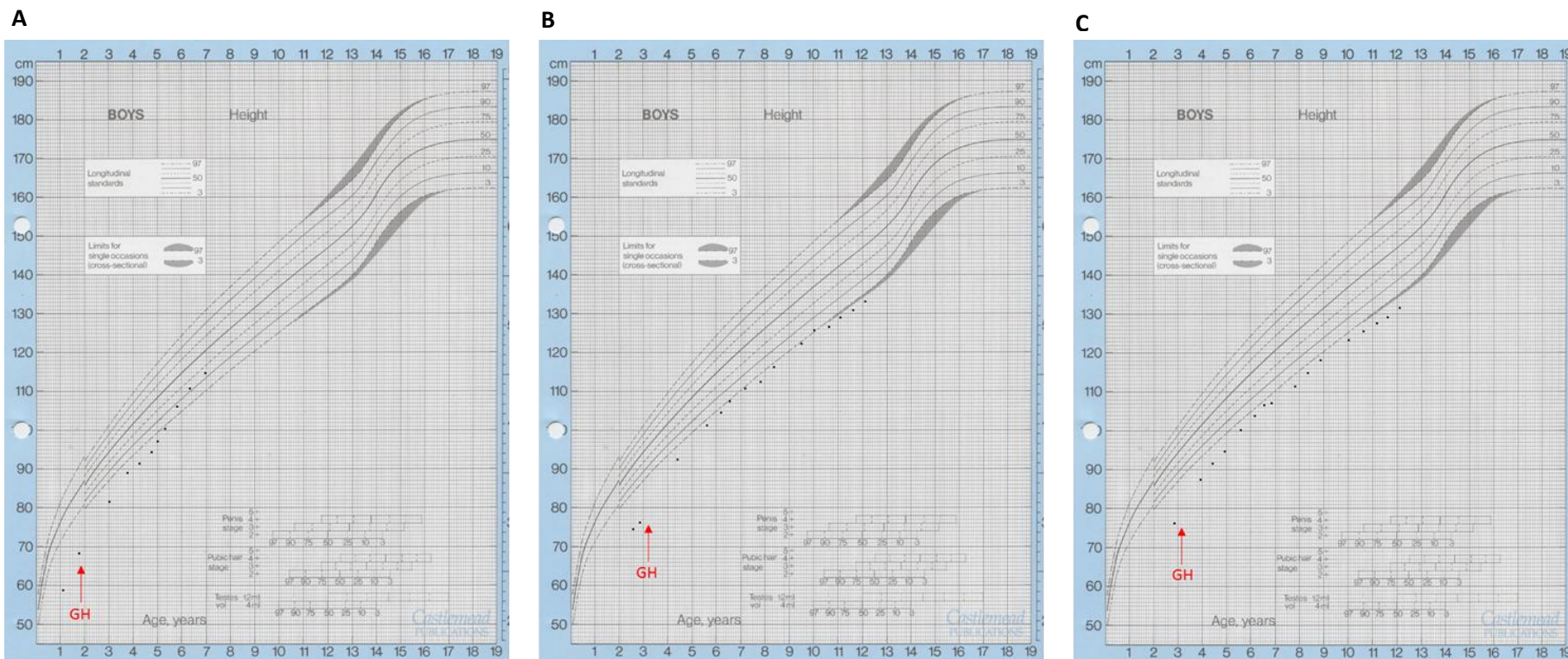


Figure 5.2: The growth charts from the three affected males from Pedigree 8, IIIc, IIId, IIIe. The labelled red arrows indicate when GH treatment was commenced in the three boys respectively.

MRI scans

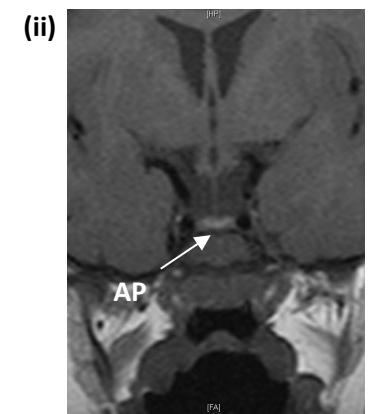
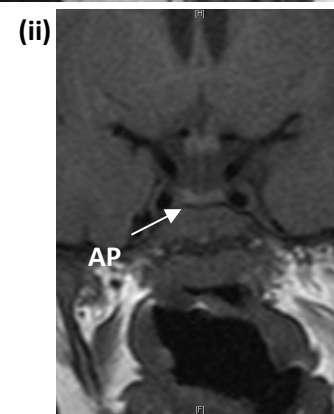
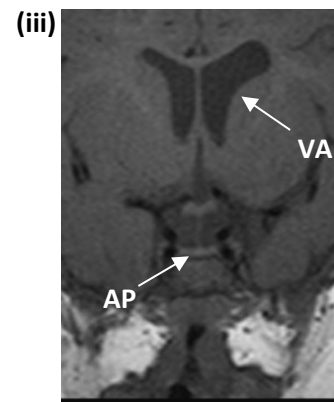
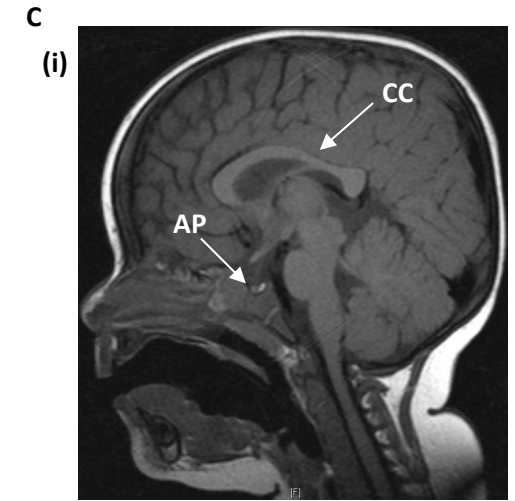
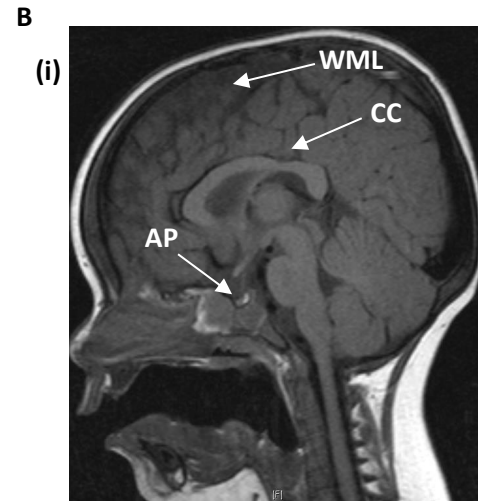
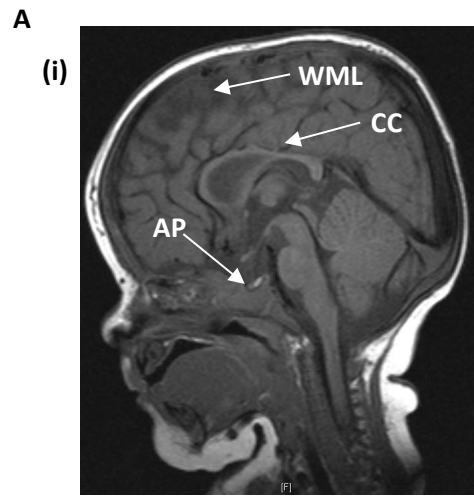


Figure 5.3: The MRI scans from the three affected males, IIIc, III d, IIIe. A-C: The patients have a small AP with an otherwise structurally normal pituitary gland, and a thin corpus callosum, indicated by the labelled white arrows respectively. **A (i-ii)** Sagittal images of patient IIIc showing generalised white matter loss, a small AP and a thin CC. **A (iii)** A coronal image of patient IIIc showing a small AP and ventricular asymmetry with the right ventricle being larger than the left. **B (i)** A sagittal image of patient III d showing generalised white matter loss, a small AP and a thin CC. **B (ii)** A coronal image of patient III d showing a small AP. **C (i)** A sagittal image of patient IIIe showing a small AP and a thin CC. **C (ii)** A coronal image of patient IIIe showing a small AP. CC, corpus callosum; AP, anterior pituitary; WML, white matter loss; VA, ventricular asymmetry.

5.1.2. EIF2S3

The Eukaryotic translation initiation factor 2 subunit 3 protein (*EIF2S3*) gene is located on the X chromosome at position p22.11 (ChrX: 24091319), and is 52kDa in size comprising 472 amino acids. eIF2 is a heterotrimeric G protein, also known as a guanine nucleotide-binding protein, composed of three subunits; alpha, beta and gamma, with *EIF2S3* coding for the eIF2 γ subunit protein (USCN Life Sciences). This is the largest subunit of this heterotrimeric guanosine triphosphate (GTP)-binding protein, containing all three consensus GTP-binding elements (guanine nucleotide binding domains) (Kimball, 1999) (Figure 5.4). When these domains are mutated, the binding of GTP/GDP to eIF2 γ is greatly decreased, suggesting that it is this subunit that contains the primary GTP-binding element (Naranda et al., 1995).

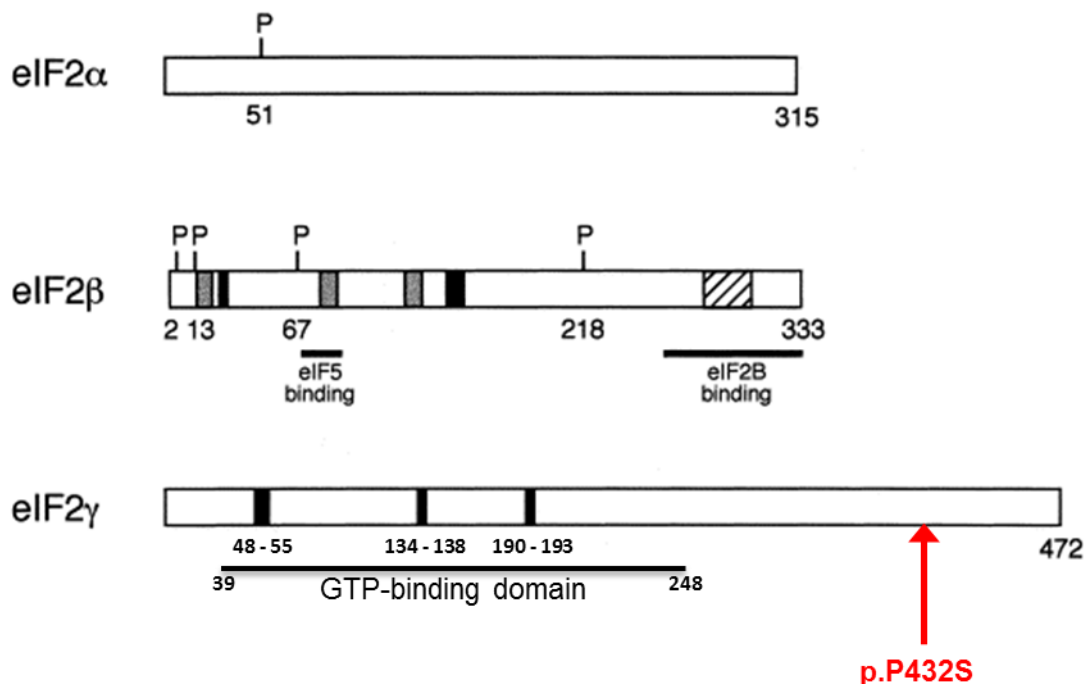


Figure 5.4: Domain structure of human eIF2 α -, β -, and γ -subunits. Taken and adapted from Kimball SR 1999 (Kimball, 1999). The number of amino acids in each eIF2 subunit is shown to the right and just below the open boxes representing the polypeptide chains. Known phosphorylation sites are represented by a 'P' above the

boxes with the residue number shown below it. Polylysine domains are shown as grey boxes, guanine nucleotide binding domains are shown as black boxes, and the putative 'zinc finger' motif in eIF2 β is shown as a box with cross hatching. The eIF2B and eIF5 binding domains in eIF2 β are denoted by black lines beneath the eIF2 β polypeptide. This figure has been modified from the original by the addition of the GTP-binding domain and the residue positions corresponding, with each guanine nucleotide binding region within the GTP-binding domain. In addition the location of the variant identified in this study has been added; indicated by the red arrow labelled 'p.P432S'.

eIF2 functions in the early steps of protein synthesis by forming a ternary complex with GTP and initiator methionyl-tRNA (Met-tRNA_i), in which cross-linking analysis has implicated the N-terminus of eIF2 γ in the binding of the latter (Kimball, 1999). This process mediates the association of Met-tRNA_i to the peptidyl-tRNA site, known as the 'P' site, on the 40S ribosomal subunit (Pain, 1996). Prior to this ternary complex binding to the 40S ribosomal subunit, another initiation factor (eIF3) binds to the ribosome first, whose role is to keep the ribosomal subunits, 40S and 60S, separate from each other at this early stage, thus allowing the ternary complex to associate with the 40S ribosomal subunit (Hershey, 2015). Following binding of eIF3 and the eIF2-GTP-Met-tRNA_i ternary complex, a third initiation factor binds (eIF4) to the ribosomal subunit, which guides the whole complex to the 5' end of mRNA where it binds to form the 43S pre-initiation complex (Flynn and Proud, 1996). This then scans mRNA to select the AUG start codon for protein synthesis (Figure 5.5) by using perfect complementarity with the anticodon of initiator tRNA to recognise the AUG (Hinnebusch, 2011).

eIF5 binds to eIF2 β and stimulates the hydrolysis of GTP; which is thought to be a very important step in this start site selection (Huang et al., 1997). The resultant eIF2-GDP inactive binary complex is then released from the ribosome (Figure 5.5). It is unclear where the GTPase activity that is responsible for catalysing this GTP-hydrolysis comes from, but it has been proposed to be eIF5 or the β - or γ -subunits of eIF2. It is apparent, however, that eIF5 can only stimulate GTP-hydrolysis when eIF2 is bound in its ternary complex (with GTP and Met-tRNA_i) to the 40S ribosome (Kimball, 1999), which shows how highly specific this action is.

eIF2 is then recycled and can participate in another round of translation initiation, only when the GDP is exchanged for GTP. It has been suggested that eIF2 transfer to the 60S ribosomal subunit, which in itself is bound to the 80S initiation complex, is important for recycling as eIF2 has been found to be associated with this structure (Chakrabarti and Maitra, 1992). However, it is the interaction with another translation initiation factor, eIF2B, that is directly involved in the recycling process of eIF2 ternary complex formation (Figure 5.5) (Kimball, 1999).

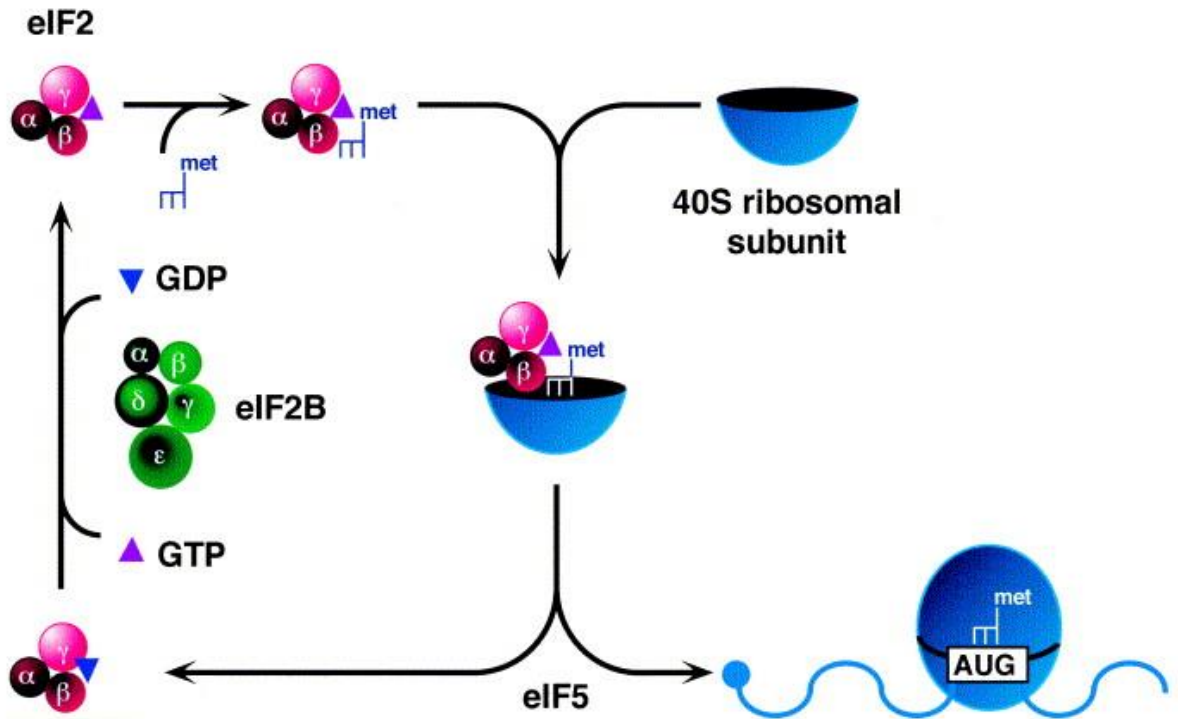


Figure 5.5: Eukaryotic initiation factor 2 (eIF2): The role of eIF2 in the initiation of mRNA translation. Taken from Kimball SR *et al.* 1999.

The eIF2B protein has been implicated in leukoencephalopathy, which essentially involves a neurological condition termed vanishing white matter (VHM), or childhood ataxia with central nervous system hypomyelination (CACH) (van der Knaap *et al.*, 2002). The GDP/GTP exchange reaction is therefore catalysed by eIF2B to reform the eIF2-GTP-Met-tRNAⁱ ternary complex (Pavitt and Proud, 2009).

Studies have shown that phosphorylation of eIF2 α regulates eIF2B activity (Pavitt *et al.*, 1998), but the actual interaction between these two proteins, eIF2 and eIF2B, occurs via eIF2 β (Kimball *et al.*, 1998). Therefore it is proposed that a structural change occurs from the phosphorylation of eIF2 α that alters the structure of eIF2 β in order to bind to eIF2B. The phosphorylation of eIF2 α is a highly conserved signal implicated in the cellular adaptation to numerous stresses, such as viral infection, apoptosis, cell transformation and amino acid limitation. Additionally it has been

shown that the sole phosphorylation of eIF2 α in the mediobasal hypothalamus is sufficient to regulate food intake (Maurin et al., 2014). Previous studies have shown that inhibition of the phosphorylated eIF2 α signalling in the liver leads to a decrease in hepatic glucose production, and in addition impairs insulin-stimulated muscle and adipose tissue insulin sensitivity. The authors concluded that the hepatic endoplasmic reticulum-stress eIF2 α signalling pathway affects hepatic glucose production, without altering hepatic insulin sensitivity (Birkenfeld et al., 2011). This association of protein synthesis and glucose production via eIF2 α signalling, suggests that impairments in other subunits of eIF2 such as the *EIF2S3* (p.P432S) variant may potentially be contributing to the glucose dysregulation seen in Pedigree 8. As described, eIF2B and eIF2 are protein partners that critically need to bind in order to permit translation initiation, which is a vital process routinely carried out *in vivo*. Insulin rapidly activates protein synthesis by activating components of the translational machinery including eIFs and eukaryotic elongation factors (eEFs), and interestingly it is insulin that indirectly regulates eIF2B activity and thus the recruitment of Met-tRNA_i to the 40S subunit (Figure 5.6) (Kimball, 1999).

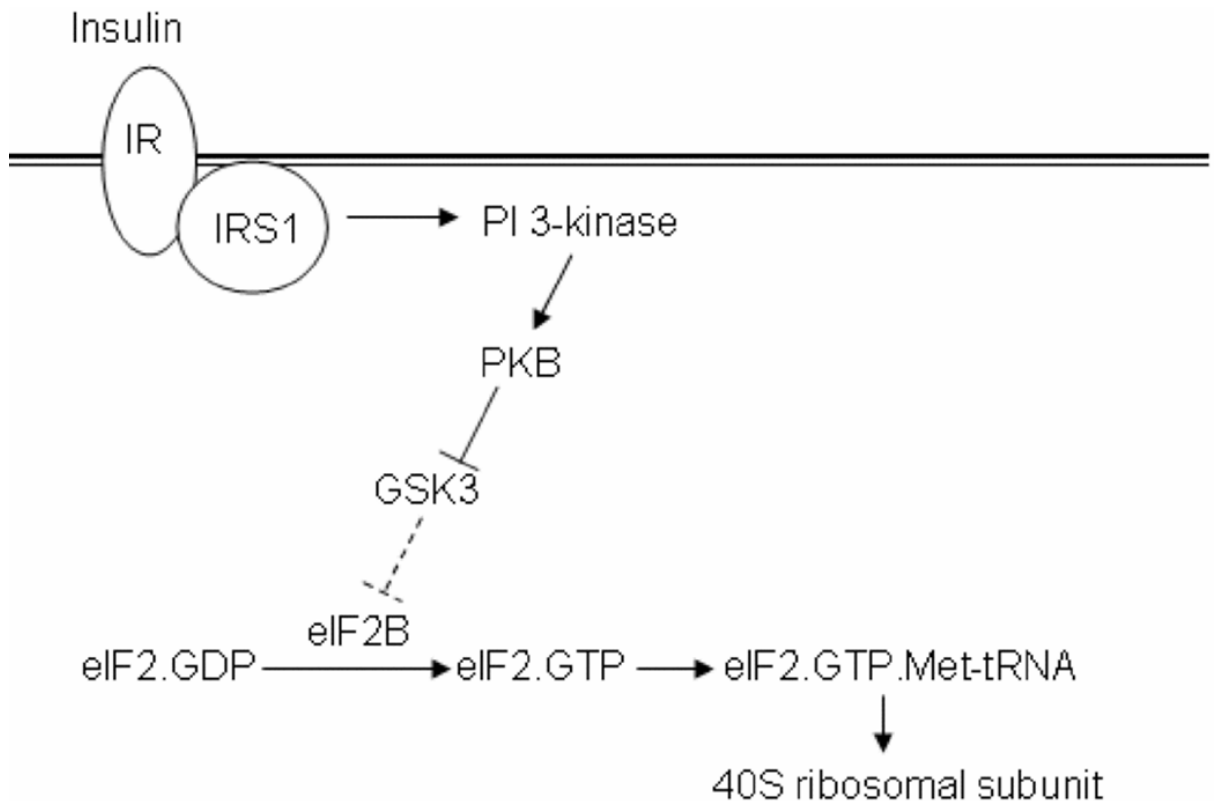


Figure 5.6: Formation of the eIF2 ternary complex stimulated by insulin. Taken from Proud CG (Proud, 2006). Insulin binds to its receptor on the cell membrane and signals through PI3K and PKB to phosphorylate GSK3, causing its inactivation. This allows eIF2B to dephosphorylate which promotes its GDP/GTP exchange activity and thus in turn the formation of the ternary complex; eIF2-GTP- Met-tRNAi. PI3K, phosphatidylinositol-4,5-bisphosphate 3-kinase; PKB, protein kinase B; GSK3, glycogen synthase kinase 3; eIF2B, eukaryotic initiation factor 2B.

Therefore as mutations in eIF2B have been shown to cause such drastic phenotypes, this suggests that a mutation in eIF2, such as p.P432S in eIF2 γ , may also do the same through disruption of translation initiation, and thus give rise to the complex phenotype observed in the hypopituitary related disease seen in our patients. Further evidence to support this theory is that patients IIIc and III d from Pedigree 8 in this study had generalised white matter loss, in addition to previous reported patients with

EIF2S3 patients that had global reduction in white matter on MRI in a recent study by Moortgat *et al*, later discussed in this chapter. As white matter loss is a main phenotypic finding in patients with eIF2B mutations, this suggests how mutations in these protein partners may yield a potential phenotypic overlap.

Despite the translation initiation role of eIF2 which takes place in the cytoplasm, studies by Ting *et al* have shown that eIF2 localises to the nucleus. In this previous study five polypeptides, three of which were the α -, β - and γ - subunits of eIF2, were found to interact with DNA-dependent protein kinase (DNA-PK), and stabilize formation of a complex containing DNA, DNA-PK and 'Ku' (a DNA binding protein). They found that eIF2 β was phosphorylated by DNA-PK. These analyses suggest that eIF2 may also have a physiological role in DNA repair through its interaction with DNA-PK, in addition to its role in translation initiation (Ting *et al.*, 1998).

A missense substitution in the highly conserved GTP-binding (G) domain of *EIF2S3*, p.I222T, has been previously described in three male individuals in the same pedigree with clinical features including; moderate-to-severe intellectual disability (ID), microcephaly, short stature, epilepsy and facial dysmorphic features (Borck *et al.*, 2012). Each affected individual had unique additional features consisting of cleft lip/palate and behavioural problems, generalised seizures, and postpubertal microgenitalism and obesity respectively. Two of the three patients had GHD, however no endocrine values or details of diagnosis were given by the authors, thus it was not the main phenotypic focus of their study. Therefore, due to the authors focusing on the neurological phenotype, they may have overlooked a more detailed pituitary phenotype in the patients. Through analysis of the homologous archaeal aIF2 γ complex, which can functionally replace eIF2 γ in binding Met-tRNA_i to the ribosome and scanning (Dmitriev *et al.*, 2011), this mutation lies within a hydrophobic cleft on the backside of the GTP-binding domain which forms the binding site for aIF2 β . Functional studies involved the corresponding yeast eIF2 γ residue being

mutated, p.V281T/p.V281K, which substantially impaired/abolished, respectively, eIF2 β binding to eIF2 γ . Overexpression of eIF2 β partially restored eIF2 γ binding to the mutants (Baumann, 1999). This group also showed that the equivalent mutation in yeast eIF2 γ also impaired translation start codon selection, of which the method is discussed in the future work section, 5.4.2, of this chapter. As stated, *EIF2S3* is located at Xp22.11, which is interestingly part of a region to which a rare X-linked ID disorder designated as MEHMO syndrome has previously been mapped by linkage analysis (Xp21.1-p22.13) (Steinmuller et al., 1998). MEHMO syndrome patients have a life expectancy of less than two years and the disorder is characterized by mental retardation, epileptic seizures, hypogonadism and hypogenitalism, microcephaly, and obesity, in which all are present in at least one affected individual from the family reported by Borck *et al.*

Very recently, two novel hemizygous variants in *EIF2S3* have been reported in three males from two unrelated pedigrees, two brothers and one unrelated male, that were inherited from their heterozygous mothers; a missense substitution p.I259M and a frameshift p.I465Sfs*4 (Moortgat et al., 2016). Contrastingly, these mutations are located within the C-terminal domain, as the p.P432S variant is, and are not within the GTP binding domain; as was the case with the p.I222T mutation reported in the previous study by Borck *et al.* These patients had a similar phenotype to the previously reported patient, in that they had severe ID, microcephaly, GHD and epilepsy with various unique additional features such as spastic quadriplegia, delayed puberty and genital abnormalities. However they also had hypoglycaemia (Moortgat et al., 2016), as observed in Pedigree 8, although the underlying pathogenesis for the hypoglycaemia was not clear in the patients described in their study. Unfortunately two unrelated patients from this recent report died, one at 17yrs from severe respiratory distress and multi-organ failure, and the other at 12 months from multisystemic failure. Moortgat *et al.* created a morpholino (MO)-based zebrafish

eif2s3, the human *EIF2S3* ortholog which shares 80.2% protein identity, knock down model, which they concluded recapitulated the human microcephaly and short stature phenotype, thus supporting the pathogenicity of their *EIF2S3* variants identified. Injected embryos and uninjected controls were analysed at 0, 1, 2, and 3 days post fertilization (dpf) for survival, motility, and morphology. In addition, 30 morphants and 30 controls were selected at 2 dpf for head width measurements. Their results showed that *eif2s3* morphants exhibited hypomotility and morphological deficits at 2 dpf and were shorter with a curved tail. These morphants also had a statistically significant reduction in head size (Kruskal–Wallis Test, $P < 0.0001$) with small eyes compared with control MO-injected embryos. Following the establishment of the knock down phenotype, they then performed rescue experiments by co-injection of *eif2s3* MO with 500 pg/egg of either WT zebrafish *eif2s3* RNA or human *EIF2S3* RNA, which partially restored the morphant phenotype. The authors also noted that there were no significant differences between the standard control MO and the uninjected embryos, and therefore concluded that the absence of total rescue was likely due to non-specific, or off-target effects of antisense technologies (Moortgat et al., 2016). These data, in addition to the phenotype of the patients manifesting both GHD and hypoglycaemia, support the hypothesis that the *EIF2S3* (p.P432S) is causative of the unique phenotype observed in Pedigree 8. Both previous reports describing *EIF2S3* mutations have had phenotypic focus on ID with microcephaly, of which the former is not prominent and the latter is not present in our patients. The males in Pedigree 8 differ vastly from these previous cases in having a much more severe hypopituitarism but a milder neurological phenotype. Therefore the *EIF2S3* (p.P432S) may have a different effect *in vivo* to previous *EIF2S3* mutations, giving rise to this different phenotype.

5.2. Results

5.2.1. Cohort screening

Upon identification of the *EIF2S3* (p.P432S) variant in Pedigree 8, I initially screened a cohort of patients within our database to see if any additional *EIF2S3* variants were present in other pedigrees. The full coding region of *EIF2S3* was analysed by PCR and direct sequencing analysis (Chapter 2.2) in 103 patients with variable hypopituitary-related phenotypes to identify any further *EIF2S3* variants in other patients in our cohort. The phenotype of patients ranged from mild to severe with and without structural midline brain defects on MRI: 16 had GHD with no details of further anterior pituitary deficiencies, 37 had SOD, 4 had HH/KS and 46 had variable MPHD. However no further variants were identified in the *EIF2S3* gene in any of these patients. No other eukaryotic initiation factors were screened for mutations in this cohort, only *EIF2S3*.

5.2.2. *EIF2S3* knock down

The expression pattern of *EIF2S3*/eIF2 γ in the pituitary, hypothalamus and the pancreas, and the unusual phenotype of the patients in Pedigree 8 led me to further investigate the role of *EIF2S3* in human development. An *EIF2S3* KO study on a human hybrid pancreatic beta cell line using a viable LV transduction approach was carried out in this study, with subsequent insulin secretion and apoptosis assays (Chapter 2.4), to compare insulin secretion and cell death in *EIF2S3* KO cells compared to controls respectively. These assays were performed to help characterize the functional role of this initiation factor of protein synthesis (*EIF2S3*/eIF2 γ), and its importance in sustaining cell viability.

The four different silencing, and the one non-silencing control, pGIPZ LV-backboned plasmids described in Chapter 2.4.2 were packaged into viable LV particles (Chapter 2.4.3) and, via transduction (Chapter 2.4.4), used to introduce *EIF2S3*-targeted shRNA cassettes into 1.1B4 human pancreatic cells in order to knock down the *EIF2S3* gene. These plasmids also encoded GFP and a puromycin resistance gene. Forty-eight hours after transduction was carried out on the 1.1B4 cells, the cells appeared to fluoresce green under the microscope, indicative of GFP expression and thus successfully transduced cells. These cells were then under puromycin selection, which killed the non-transduced cells therefore allowing for the expansion of transduced ones. This method of a stable knock down was used over a transient transfection method, so that a KO cell line could be grown and aliquots could be frozen over a longer time scale in order to be used in multiple assays and at a later date. Transient transfection wears off quicker and shRNA cassettes would have only interfered with the gene, and thus knocked it down, for only a fraction of the time that a LV vector permits. Following expansion of each cell population, RNA was extracted from cells, reverse transcribed and a qPCR was performed (Chapter 2.4.5 – 2.4.7) to verify which of the four *EIF2S3* shRNA cassette-containing pGIPZ plasmids was the most efficient in knocking down the gene. Initially a pilot qPCR assay was carried out on RNA derived from non-transduced WT 1.1B4 cells, to determine the most suitable dilution of cDNA to use, without using any cDNA samples from transduced cell populations. Following transduction using Clone 4, through visual observation the cells appeared to not survive for very long and cell viability looked extremely low, which would explain why very little RNA was able to be extracted (Chapter 2, Table 2.1).

5.2.3. qPCR analysis

The qPCR pilot assay concluded that the 1:5 dilution of stock cDNA began exponential expression of the genes tested at an appropriate cycle number (20 cycles) on the StepOne qPCR software. Therefore a 1:5 dilution of cDNA was used in further qPCR assays for the different 1.1B4 cell populations that had been transduced with the different shRNA-containing constructs described: Scrambled non-silencing clone, Clone 1, Clone 2, Clone 3 and Clone 4 shRNA respectively, in addition to the non-transduced cells used as a control in all assays (WT 1.1B4 cells).

Results from the qPCR showed that Clone 4 was the most successful construct in knocking down the *EIF2S3* gene. Clone 4 had a Relative Quantification (RQ) of 0.186 with a 95% Confidence Interval ranging between 0.127 - 0.274, when compared to non-transduced cells (RQ: 1, CI: 0.89 – 1.124) (Figure 5.7, Table 5.4), indicating that approximately 82% of *EIF2S3* was knocked down. Clone 1-3 were not as efficient in silencing the *EIF2S3* gene and only appeared to achieve a range between 15-40% knock down in the cells.

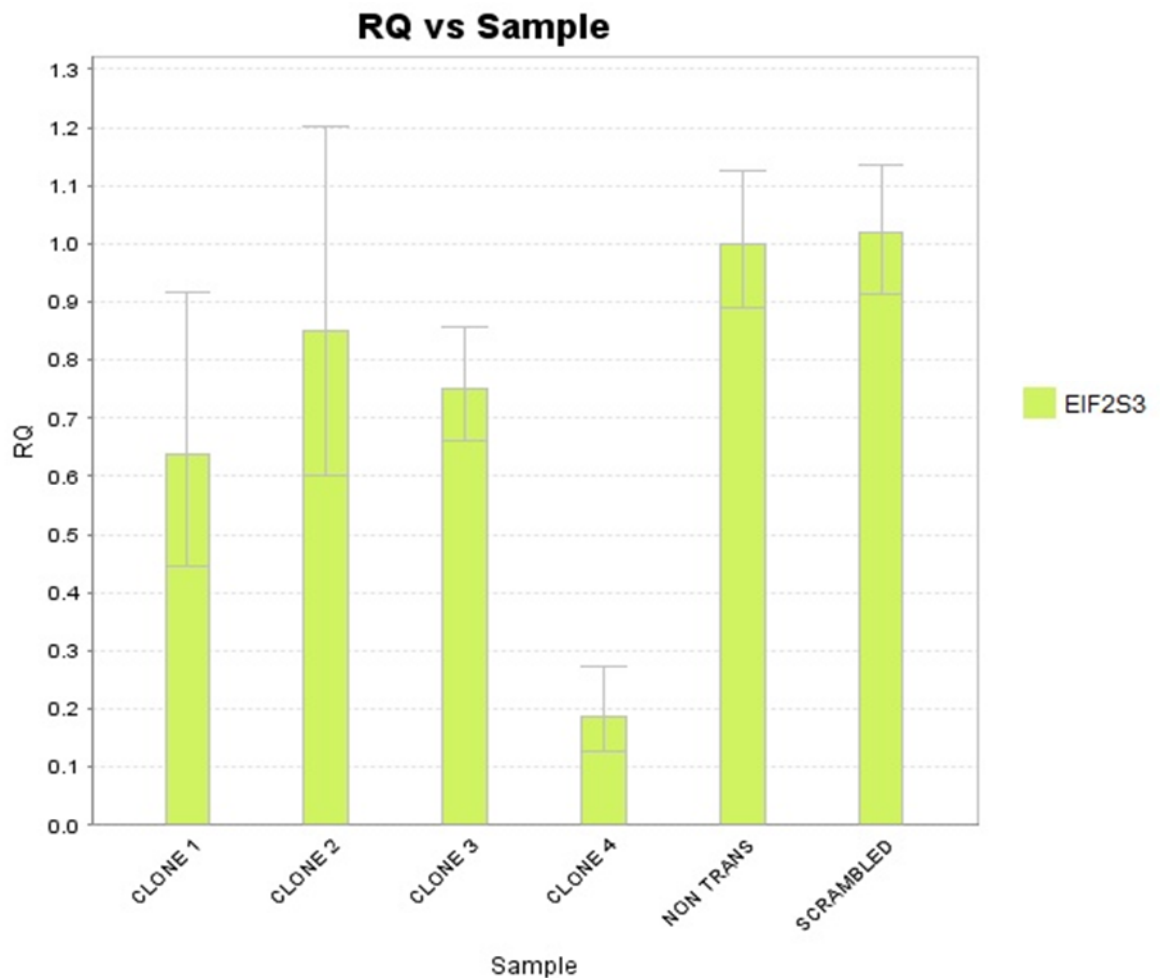


Figure 5.7: qPCR *EIF2S3* expression results in cDNA populations. Histogram showing the relative quantification of *EIF2S3* expression, against *GAPDH*, β -*ACTIN* and *HPRT* housekeeping genes in cDNA derived from transduced 1.1B4 cells, compared to non-transduced cells. Five different cDNA populations were derived from cells transduced with different shRNA cassette-containing constructs: Scrambled non-silencing and Clone 1, Clone 2, Clone 3, Clone 4 silencing. All were normalised to non-transduced cells.

cDNA population	Relative Quantification (RQ)	95% Confidence Interval	
		RQ Minimum	RQ Maximum
Non-transduced	1	0.89	1.124
Scrambled	1.019	0.913	1.137
Clone 1	0.638	0.444	0.915
Clone 2	0.85	0.601	1.201
Clone 3	0.752	0.66	0.856
Clone 4	0.186	0.127	0.274

Table 5.4: qPCR *EIF2S3* expression results in cDNA populations. qPCR Relative Quantification (RQ) values for *EIF2S3* expression against *GAPDH*, β -*ACTIN* and *HPRT* compared to non-transduced cDNA, with a 95% confidence interval range: minimum RQ and maximum RQ, for all five cDNA populations.

5.2.4. Western Blot Analysis

Following transduction as described, protein was extracted from cell lysates and a bicinchoninic acid assay (BCA) was performed to quantify the total concentration of protein in each sample (Table 5.5), in order to perform western blot analysis to detect eIF2 γ protein (Chapter 2.4.8). A polyclonal anti-EIF2S3 antibody was used for the detection of eIF2 γ in the different protein populations. A pilot western blot assay was performed on protein derived from HeLa cells, which were suggested to be used as a positive control by the antibody manufacturer, and non-transduced 1.1B4 cells respectively, at three different concentrations (Figure 5.8). This was to test the specificity of the antibody and to determine the optimal protein concentration to load into wells to obtain a clear eIF2 γ band.

BCA concentrations:

Protein lysate	Total protein lysate concentration ($\mu\text{g/ml}$)	Total protein lysate concentration ($\mu\text{g}/\mu\text{L}$)	Total protein yield ($\mu\text{g}/\mu\text{L}$)
HeLa (control)	696.667	0.697	209.1
1.1B4 WT NT	1339.313	1.339	401.7
Scrambled	1313.125	1.313	393.9
Clone 1	1173.375	1.173	351.9
Clone 2	1287.625	1.288	386.4
Clone 3	1173.375	1.173	386.4
Clone 4	134.375	0.134	26.8

Table 5.5: BCA assay quantification. Total protein lysate concentrations determined by a bicinchoninic acid assay (BCA) using a luminometer. WT, wild-type; NT, non-transduced.

The pilot western blot analysis showed strong unspecific binding of the primary anti-EIF2S3 antibody in both cell populations, HeLa and non-transduced protein, at all three total protein concentrations (5 μ g, 10 μ g and 30 μ g). Additionally, a band just above the 55kDa protein ladder band, at approximately 57kDa, was present on the blot (Figure 5.8), however I did not believe this to be specific to eIF2 γ and therefore did not perform a western blot on the extracted protein from Clones 1-4.

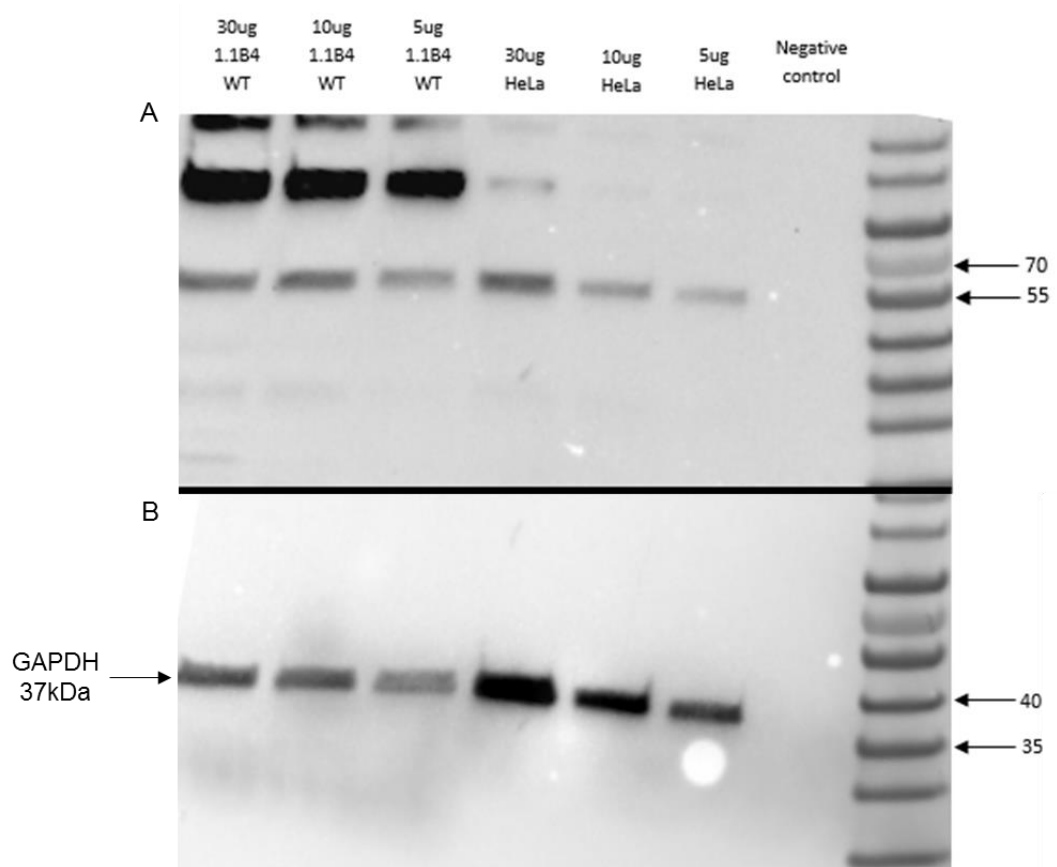


Figure 5.8: Western blot analysis using the anti-EIF2S3 primary antibody. (A-B)

Western blot membrane with WT human 1.1B4 cells and HeLa control protein lysate, each at three different concentrations; 5 μ g, 10 μ g and 30 μ g. Images A and B were taken from the same membrane. **(A)** An anti-EIF2S3 primary antibody was used to stain eIF2 γ at 52kDa, however there was no significant band on the membrane at this size. **(B)** An anti-GAPDH primary antibody was used to stain GAPDH (37kDa) indicated by the arrows. WT, wild-type.

5.2.5. Insulin secretion ELISA assay

As mentioned, the patients in Pedigree 8 had hyperinsulinism that caused hypoglycaemia. Due to this pancreatic phenotype observed in the patients, 1.1B4 cells (PHE) were chosen for this study as they are human pancreatic beta cells that have been reported to secrete insulin (McCluskey et al., 2011). Upon establishing a human *EIF2S3* KO cell line that had been verified by qPCR, I wanted to measure insulin secretion in these cells and compare it to WT cells, to see if there was a significant difference between the two. Initially, I wanted to confirm the insulin producing properties in this cell line myself as well as optimise the ultrasensitive insulin ELISA assay, before attempting to measure insulin secretion in the *EIF2S3* KO 1.1B4 cell line. Therefore a pilot assay was performed using non-transduced WT 1.1B4 cells.

Firstly, 10mM glucose alone was added to the cells, secondly Forskolin (10 μ M) was added in isolation to the cells, as it has been shown to stimulate insulin secretion in cell lines e.g. MIN6 cells (Luther et al., 2006). Thirdly, Forskolin (10 μ M) in combination with a phosphodiesterase inhibitor, IBMX (100 μ M), in a high glucose concentration (10mM) was added. IBMX is known to inhibit the breakdown of cAMP and thus further increase insulin secretion to a higher final concentration that can be more easily detectable (Al-Majed et al., 2004). However after subjecting the 1.1B4 cells to these treatments, the cells did not release any insulin above the background/lowest standard (Calibrator 0) from the ELISA kit. In further attempts, these test agent concentrations used as treatments on the cells were increased by 10 fold; 100mM glucose, 100 μ M Forskolin (in 100mM glucose), and 100 μ M Forskolin with 1000 μ M IBMX (in 100mM glucose), and yet still did not stimulate any insulin release from the human 1.1B4 cells.

At this later stage, I acquired MIN6 cells that were negative for mycoplasma from Professor Peter Jones, Kings College London, which up until this point had not been available. The original test agents made using the 10mM glucose KRB buffer used on the 1.1B4 cells (Chapter 2, Table 2.6) were then used to treat these MIN6 cells, with simultaneous treatment of 1.1B4 cells, and the solutions from all wells in the plate were collected and analysed for insulin secretion. The treatments successfully stimulated the MIN6 cells to release insulin (Figure 5.9), however the 1.1B4 remained unresponsive and had undetectable insulin secretion levels.

The MIN6 cells secreted insulin after being incubated with three different treatments: 10mM glucose, 10 μ M Forskolin (in 10mM glucose), and 10 μ M Forskolin with 100 μ M IBMX (in 10mM glucose) respectively, with the latter treatment combination being the most efficient at stimulating insulin secretion. The human 1.1B4 cells did not secrete insulin at a level above the 'Calibrator 0' standard after incubation with the same treatments.

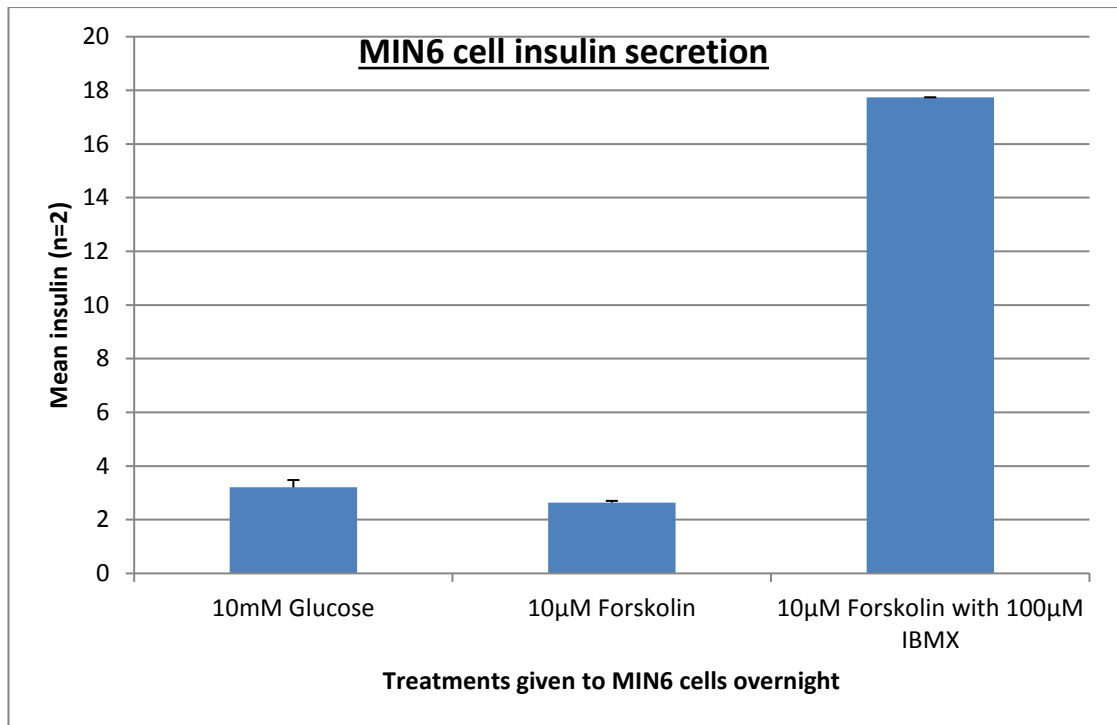


Figure 5.9: Insulin secretion assay in MIN6 cells. Graph showing the mean insulin secretion from MIN6 cells in a well from a 6-well plate after incubation with forskolin, and forskolin in combination with IBMX. The error bars represent the standard deviation of the mean. IBMX, 3-isobutylmethylxanthine.

These data suggest that these hybrid human 1.1B4 cells are not secreting insulin, as previously described in studies in Professor Peter Flatt's laboratory. Through helpful discussion with a collaborator, namely Professor Peter Jones from Kings College London, we hypothesised that the beta insulin-secreting cells in this hybrid may have been overtaken by rapid growth of the PANC-1 epithelial cells, and therefore no detectable measure of insulin can derive from this cell line as a whole. This revelation meant that we were unable to measure the effect of *EIF2S3* knock down on insulin secretion.

5.2.6. Apoptosis Caspase 3/7 Assay

As mentioned in section 5.2.2, during culturing the cells transduced with the Clone 4 shRNA cassette-containing construct were challenging to sustain and expand compared to the other cell lines (cells transduced with Clones 1-3). This may be due to a reduction in cell viability as a result of the highest percentage loss of normal *EIF2S3*, shown by qPCR (Figure 5.7). This led to the hypothesis that there is increased apoptosis in these cells due to the lack of eIF2 γ protein. Therefore Clone 4 was analysed for cell viability compared to WT 1.1B4 cells through conducting a cell apoptosis assay that measured caspase 3/7 activity in the cell, with and without the addition of a cytokine mix, which is known to stimulate caspase activity (Chapter 2.4.10).

Initially, a pilot apoptosis assay was performed using both MIN6 and 1.1B4 WT non-transduced cells. After treatment with cytokines, both cell lines showed an increase in caspase 3/7 compared to the cells untreated with cytokines; termed basal caspase activity (Figure 5.10).

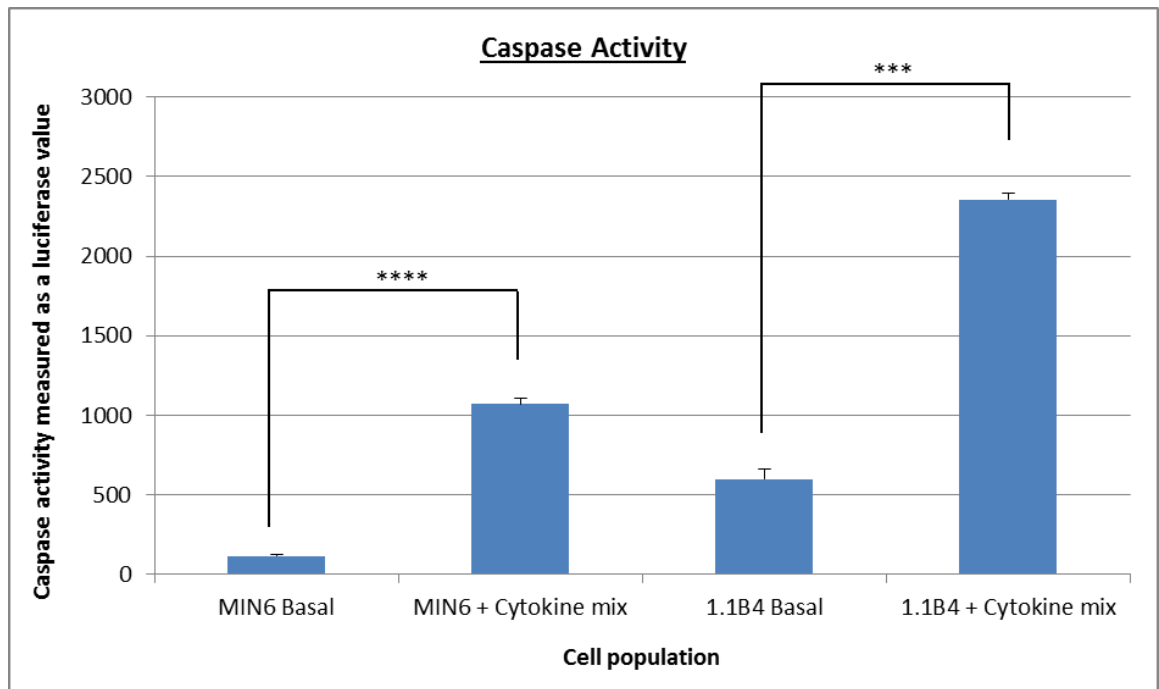


Figure 5.10: A pilot apoptosis assay performed on WT untransduced MIN6 and 1.1B4 cells. Cells were seeded 24 hours before a 16 hour incubation with a cytokine mix. Results are shown as the mean \pm SD from an assay performed in triplicate. There was a highly significant difference in caspase activity, measured as luciferase activity on a luminometer, in the cytokine-treated cells compared to basal activity in each cell line respectively; MIN6 cells (1070.33 ± 33.56 versus (vs) 116 ± 8.66) $p=0.0006$, 1.1B4 cells (2354.67 ± 40.7 vs 601.33 ± 62) $p=0.0001$). The error bars represent the standard deviation (SD) of the mean. WT, wild-type.

After establishing a working apoptosis assay, caspase activity in the human *EIF2S3* KO 1.1B4 cell population (Clone 4) was compared with 1.1B4 cells transduced with the scrambled non-silencing (NS) shRNA control construct, and the non-transduced (NT) cells respectively.

5.2.6.1. Non-parametric tests

Significant difference between Clone 4 cyto and Clone 4 basal ($p = 0.0003$).

Group (Cell population?)	N	Rank sum	Expected
Clone 4 cyto	9	126	85.5
Clone 4 basal	9	45	85.5
Combined	18	171	171

Significant difference between NS cyto and NS basal ($p = 0.0379$).

Group (Cell population?)	N	Rank sum	Expected
NS cyto	9	109	85.5
NS basal	9	62	85.5
Combined	18	171	171

Significant difference between NT cyto and NT basal ($p = 0.0003$).

Group (Cell population?)	N	Rank sum	Expected
NT cyto	9	126	85.5
NT basal	9	45	85.5
Combined	18	171	171

Significant difference between Clone 4 basal and NS basal ($p = 0.0003$).

Group (Cell population?)	N	Rank sum	Expected
Clone 4 basal	9	126	85.5
NS basal	9	45	85.5
Combined	18	171	171

Significant difference between Clone 4 basal and NT basal ($p = 0.0003$).

Group (Cell population?)	N	Rank sum	Expected
Clone 4 basal	9	126	85.5
NT basal	9	45	85.5
Combined	18	171	171

Significant difference between Clone 4 cyto and NS cyto ($p = 0.0003$).

Group (Cell population?)	N	Rank sum	Expected
Clone 4 cyto	9	126	85.5
NS cyto	9	45	85.5
Combined	18	171	171

Significant difference between Clone 4 cyto and NT cyto ($p = 0.0003$).

Group (Cell population?)	N	Rank sum	Expected
Clone 4 cyto	9	126	85.5
NT cyto	9	45	85.5
Combined	18	171	171

5.2.6.2. Two-way ANOVA test

This test was applied to the data to analyse whether there was a significant effect of cytokine treatment on caspase activity (represented through luciferase values) between the different cell populations: Clone 4, NS and NT. The data calculations are presented in Appendix 5B.

Table 1. Normalised to blank mean measurements by group

Cell line	Treatment group		Total
	cyto	basal	
Clone 4	2288.33	1202.67	1745.50
NS	467.78	257.44	362.61
NT	757.89	225.33	491.61
Total	1171.33	561.81	866.57

Table 2. ANOVA: group1: cell line and group2: treatment

Number of obs = 54		R-squared = 0.9483			
Root MSE = 177.663		Adjusted R-squared = 0.9429			
Source	Partial SS	df	MS	F	Prob>F
Model	27786935	5	5557386.9	176.07	<0.001
group1	21007560	2	10503780	332.77	<0.001
group2	5015423.1	1	5015423.1	158.90	<0.001
group1#group2	1763951.3	2	881975.63	27.94	<0.001
Residual	1515084.7	48	31564.264		
Total	29302019	53	552868.29		

There was a significant interaction between the two variable groups; cell populations, and with or without cytokine treatment ($F(2, 48) = 27.94, p < 0.001$) (Table 3), suggesting that the cytokine treatment has a different effect on caspase activity within each cell population.

5.2.6.3. Parametric tests: Two-tailed unpaired T-test

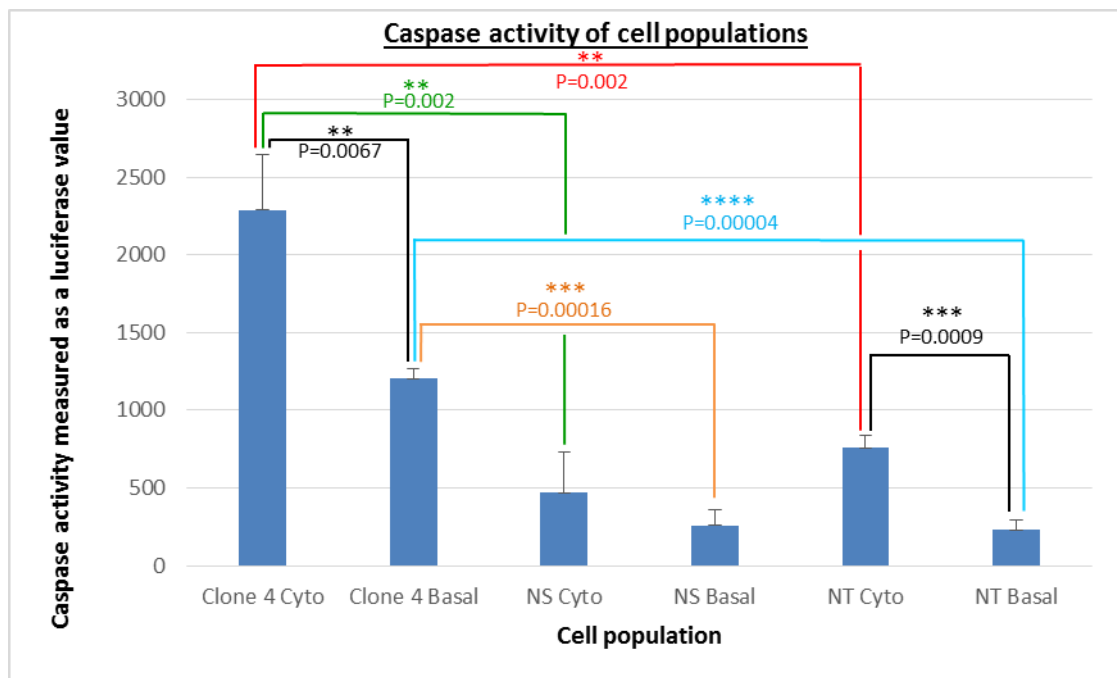


Figure 5.11: Apoptosis assay comparing caspase activity in *EIF2S3* KO cells compared to controls, with and without cytokine treatment. Results from an apoptosis assay shown as the mean \pm SD of 3 independent experiments with each assay performed in triplicate, on NT 1.1B4 cells, NS shRNA transduced 1.1B4 cells and *EIF2S3* knock-down (Clone 4) 1.1B4 cells. The average mean values from each triplicate assay 1, 2, 3 are shown in Appendix 5A. Caspase activity is measured as luciferase values on a luminometer. Caspase activity is significantly higher after cytokine treatment compared to the basal caspase activity in the Clone 4 (2288 ± 358.31 versus (vs) 1203 ± 63.52 $p=0.0067$) and NT (758 ± 84.06 vs 230 ± 59.76 $p=0.0009$) cell populations respectively. Basal caspase activity is significantly higher in Clone 4 compared with NS (1203 ± 63.52 vs 258 ± 100.49 $p=0.00016$; displayed in orange) and NT (1203 ± 63.52 vs 230 ± 59.76 $p=0.00004$; displayed in blue) respectively. Clone 4 cells treated with cytokine mix have a significantly higher caspase activity compared with NS (2288 ± 358.31 vs 468 ± 261.10 $p=0.002$; displayed in green) and NT (2288 ± 358.31 vs 758 ± 84.06 $p=0.002$; displayed in red)

cytokine-treated cell populations respectively. The error bars represent the standard deviation (SD) of the mean. NS, scrambled non-silencing; NT, non-transduced.

In line with the pilot assay, there was significantly higher caspase activity in both the Clone 4 and NT populations after the addition of cytokines, compared to basal. The NS population did not reach a statistically significant difference in caspase activity after the addition of cytokines. There was significantly higher caspase activity in Clone 4 compared to the two control populations, NS and NT, both after the addition of cytokines and in basal activity respectively (Figure 5.11).

5.2.7. The *EIF2S3* (p.P432S) mutant

A KO cell line with significant reduction in *EIF2S3* expression following transduction with Clone 4, showing a higher caspase activity (Figure 5.11) and thus increased apoptosis compared with WT cells, had now been established. I wanted to look at the effect of the specific mutation, *EIF2S3* (p.P432S), that was identified in the patients in Pedigree 8. Therefore the *EIF2S3*_WT and mutant *EIF2S3* (p.P432S) inserts were cloned into an LV-IRES (LV-backboned) vector, from their original pCMV-SPORT6, in order to be packaged into viable LV particles and transduced into cells using the same method (Chapter 2.4.3 – 2.4.4). The cloning procedure is illustrated in Figure 2.2.

The cloning site within the LV-IRES vector, that the inserts would have to ligate into, was within two BamHI sites. Therefore by site-directed mutagenesis (Chapter 2.4.11) the BamHI site already within *EIF2S3* cDNA had to be mutated so that the insert would not be cut in half during the BamHI digestion step. This BamHI site had one nucleotide substituted without changing the amino acid, thus keeping the WT protein

sequence intact and unaltered. The *EIF2S3*_WT insert was then amplified out of the pCMV-SPORT6 IMAGE clone vector by PCR, with the BamHI sequence on each end, using specific primers (Chapter 2.4.15) (Figure 5.12).

Amplification of *EIF2S3* insert

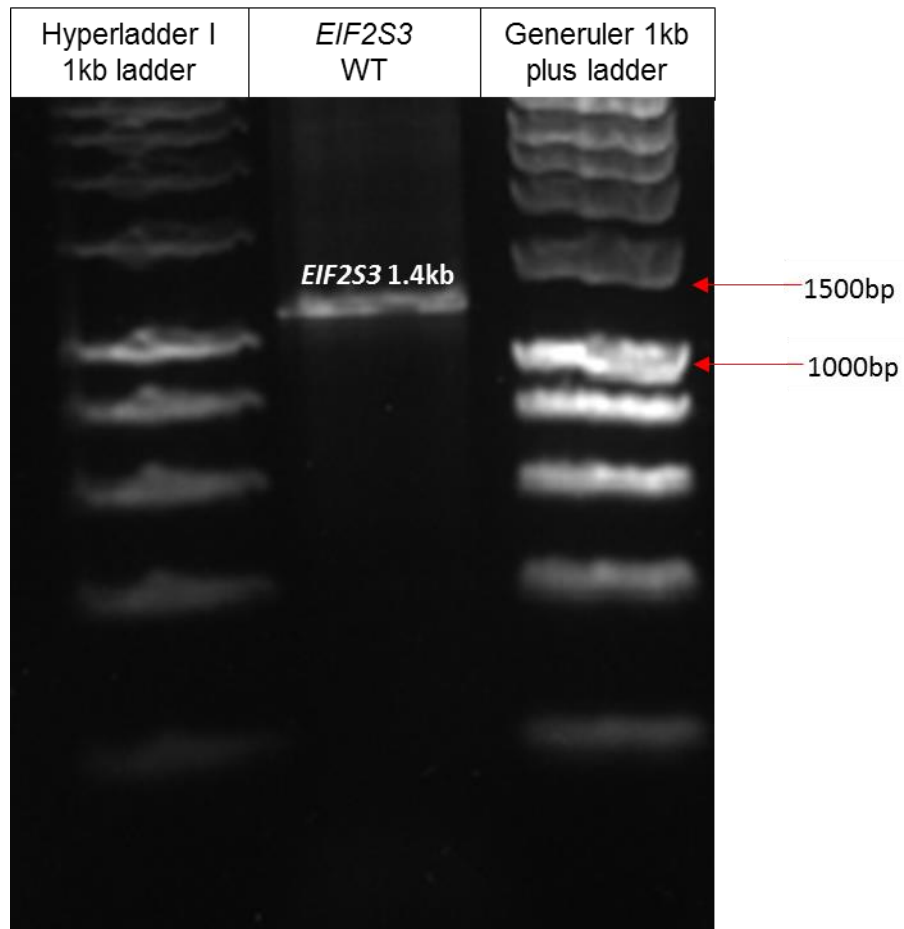


Figure 5.12: Amplification of the *EIF2S3* cDNA insert. Image showing the *EIF2S3* WT PCR product that was amplified from the pCMV-SPORT6 plasmid using specific primers, run on a 1% agarose gel next to different 1kb ladders. The arrows indicate the length of the ladder bands either side of the insert DNA band. The length of the *EIF2S3* insert corresponds to the correct length for *EIF2S3* cDNA; 1.4kb. 1kb ladders; Hyperladder I (Bioline) and GeneRuler 1kb plus (Thermo Scientific) respectively.

The PCR *EIF2S3* insert product was then purified through gel extraction (Chapter 2.4.14) and cloned into a pGEM-T Easy vector by TA-cloning (Chapter 2.4.16 – 2.4.17). The host LV-IRES vector was digested with BamHI enzyme and treated with alkaline phosphatase (Chapter 2.4.12 – 2.4.13), and the *EIF2S3* purified insert was cut out of the pGEM-T Easy vector, also with BamHI (Chapter 2.4.19), before the two were ligated (Chapter 2.4.20). Site-directed mutagenesis was then performed to revert the single nucleotide back to its original BamHI site within the insert, to yield the exact original *EIF2S3_WT* cDNA sequence and thus the final *EIF2S3_WT* construct. Alongside this, multi-site-directed mutagenesis (Chapter 2.4.21) was performed on another aliquot of LV-IRES_*EIF2S3_WT* ligated vector, to insert the p.P432S missense variant into the *EIF2S3_WT* sequence. This method simultaneously reverted the single altered nucleotide back to the original BamHI site at the same time, thus yielding the final *EIF2S3* (p.P432S) mutant construct.

Unfortunately, despite many attempts, the plasmids would not package into enough viable LV particles to be used in transduction assays. This LV packaging method appeared to work better for the shRNA cassette-containing pGIPZ plasmids used in the knockout studies. Therefore the *EIF2S3_WT* and *EIF2S3* (p.P432S) mutant constructs were transiently transfected into cells rather than transduced.

However, despite several attempts to transfect both 1.1B4 and MIN6 cells using both Fugene-6 and lipofectamine transfecting agent methods respectively (Chapter 2.4.22), there were not enough green fluorescing cells visualised following transfection to be able to proceed to functional assays, only ~5% green cells were present at 48 hours after transfection. Seventy-two hours after transfection, this percentage rose to ~15% and cell sorting was performed to sort the green-fluorescing cells from the non-fluorescing cells (Chapter 2.4.23). However not enough cells were able to be expanded within the timeframe following the cell sort, before the green cells became normal again and transient transfection had worn off. If RNA had been

extracted from these cells with such a low green fluorescing overall percentage and analysed by qPCR, there would not have been enough RNA derived from transfected cells that were exhibiting *EIF2S3*_WT and mutant expression respectively, as ~85% of them would be expressing endogenous *EIF2S3* only. Therefore, if the constructs were not being expressed to a high enough degree, the subsequent assays, such as insulin secretion (only able to be performed in MIN6 cells) and apoptosis assays, would not reflect the true effect of the *EIF2S3* (p.P432S) mutant.

5.3. Discussion

5.3.1. Cell line choice and insulin secretion assay

I wanted to functionally investigate the involvement of eIF2 γ in an insulin secretory context by manufacturing an *EIF2S3*/eIF2 γ knockout cell line (Chapter 2.4), to assess the role of eIF2 γ protein in insulin secretion in the pancreas. Initially MIN6 cells were considered as a sensible choice of cell line as they have been extensively and routinely used in different laboratories, especially by Professor Peter Jones' group in the Diabetes and Nutritional Sciences Division at Kings College London. Additionally, since the phenotype of the patients encompassed a pancreatic phenotype, the fact that these cells are pancreatic beta cells derived from transgenic mice (insulinomas) suggested that they were ideal in investigating the role of eIF2 γ on pancreatic function, such as insulin secretion from these cells. However, unfortunately, all original stocks of MIN6 cells at Kings College were found to be highly infected with mycoplasma and were initially unable to be used in functional studies. Furthermore, MIN6 cells are not commercially available, thus making another cell line choice inevitable. At this stage, there were no other common pancreatic beta cell lines to choose from that had been as widely used as MIN6 cells in practice. Therefore, I thought it best to research possible human cell lines of a similar nature as opposed

to mouse or other species, as this would be more relevant and may reflect a more accurate representation of what may occur in a human pancreas if *EIF2S3* was knocked out. Consequently human 1.1B4 pancreatic cells (PHE) were chosen; which are a hybrid cell line formed from the electrofusion of a primary culture of human pancreatic islets with PANC-1, in which the latter are human pancreatic ductal carcinoma cells. 1.1B4 cells have been reported to secrete insulin and have been extensively characterized through previous studies in Professor Peter Flatt's laboratory in Northern Ireland (Vasu et al., 2013, McCluskey et al., 2011, Guo-Parke et al., 2012), specifically involving insulin secretion assays. This cell line is formally identified by PHE to have applications in the study of pancreatic cell biology, which may be stimulated to become pure insulin-secreting cells, supporting this cell line as a suitable choice for this study. An extra benefit of this cell line is that it is commercially available and had been analysed before dispatch for mycoplasma, as well as on arrival in our laboratory; with testing being negative on both occasions. Therefore, I decided to perform a stable knockdown of the *EIF2S3* gene through the packaging of lentivirus and subsequent transduction (Chapter 2.4) in 1.1B4 cells. Interestingly, the patients in Pedigree 8 initially presented with hyperinsulinism which contributed to their hypoglycaemia, with later reduction in insulin secretion and glucose impairment in the three affected boys. It is therefore difficult to predict the effect of *EIF2S3* knock-down and also the *EIF2S3* p.P432S variant on insulin secretion. However one hypothesis would be that as it is known that insulin promotes protein synthesis through the activation of eIF2B (Proud, 2006) (Figure 5.4), perhaps when eIF2 γ is faulty as proposed in the patients carrying the *EIF2S3* (p.P432S), there is an increase in the feedback loop mechanism that normally occurs within the cell, that promotes insulin secretion. Therefore the patients may be producing too much insulin, which is reflected in their hyperinsulinism phenotype, as not enough eIF2B is being promoted to stimulate formation of the ternary complex, due to the p.P432S variant in their eIF2 γ . Therefore their pancreatic beta cells continue to stimulate more insulin release

to promote the protein synthesis pathway. Finding a human cell line that actually secreted insulin would have been ideal, however it has to be pointed out that even if this was possible, measuring endogenous insulin secretion *in vitro* may not have reflected physiological levels. Other factors may influence insulin secretion at different times, and as the dose of *in vivo* promoters and inhibitors of such pathways are unknown, *in vitro* analysis has its limitations as to whether it is reflecting what is actually occurring within the cell.

5.3.2. EIF2S3 expression

The human expression profile generated in this study is consistent with the tissues that are affected in the patients in Pedigree 8. Initial studies showed *EIF2S3* expression in the hypothalamo-pituitary axis, essentially in the developing hypothalamus and Rathke's pouch at CS20, equivalent to 49 days into development. Transcripts were also noted in the AP and PP, however not throughout the whole of the pituitary tissue at CS23, equivalent to 56 days into development (Figure 4.16A-B). These findings suggest that the phenotype in Pedigree 8 could stem from either the hypothalamus or the pituitary gland. Further studies investigated expression in the human pancreas due to the presence of a pancreatic phenotype in Pedigree 8. *EIF2S3* expression was noted in specific cells in the pancreatic tissue of a 13-week old foetus (Figure 4.16E-F). Professor Tom Jacques, a pathologist at GOSH, was consulted with respect to the specific aspects of pancreas expression. He concluded that it appears to be in the exocrine component and in the Islets of Langerhans. It is likely that the expression is observed in those regions that contain beta cell progenitors. Expression was also observed in the nasal epithelium (Figure 4.16C) and areas of the eye (Figure 4.16D); however the patients had no overt eye

phenotype. Nevertheless, it will be important to monitor the affected males in the long-term with respect to the development of an eye phenotype.

5.3.3. EIF2S3/eIF2 γ

The *EIF2S3* (p.P432S) variant segregates fully with the affected patients and the maternal ancestral line within the three generations of Pedigree 8, descending from the heterozygous asymptomatic grandmother (Figure 5.1). This variant is not located in any of the three known GTP-binding regions, but rather in the C-terminal domain of the eIF2 γ (Figure 5.4), a region of unknown function. Based on the discovery of the *EIF2S3* (p.P432S) variant in Pedigree 8 and the human expression profile of *EIF2S3*, an *EIF2S3* KO human cell line was generated using a LV transduction approach, to investigate the role of *EIF2S3/eIF2 γ* . Unfortunately, the *EIF2S3* knock-down cell population was unable to be verified at the protein level, as a reliable antibody was unavailable, as indicated by the western blots performed in this study. Moreover, there are no previously published studies reporting the use of any human anti-*EIF2S3* antibody in the literature and therefore no reliable data demonstrating that an antibody specific to eIF2 γ exists. Further work using the anti-*EIF2S3* antibody, may perform immunostaining on human embryonic sections of the brain, to further clarify whether this particular antibody is functional in a different experimental assay to western blot analysis.

Aside from the studies described earlier in yeast and zebrafish performed in previous studies (Borck et al., 2012, Moortgat et al., 2016), there has not been any other functional work performed that investigates the role of human *EIF2S3/eIF2 γ* , and no further mutations have been identified in *EIF2S3*, making it difficult to plan functional assays in this highly unexplored area. Previous work has shown that murine *Eif2s3y* suppresses the pluripotency state of murine embryonic stem cells, and promotes their

proliferation (Li et al., 2016). In mice, *Eif2s3y* on the Y chromosome is homologous to *Eif2s3x* on the X chromosome. However, it should be made clear that there is no human *EIF2S3Y* gene, and thus no *EIF2S3* homologue on the Y chromosome exists as it does in the mouse. Instead, *EIF2S3* has a homologue on chromosome 12 namely *EIF2S3L* which encodes the eukaryotic translation initiation factor 2 subunit 3-like protein. During spermatogenesis when meiosis in males is occurring, genes on the X chromosome are silenced, a process termed meiotic sex chromosome inactivation (MSCI) (McKee and Handel, 1993). As several essential housekeeping genes are located in the X chromosome, mammals have evolved to give rise to duplicated retroposed copies of genes with important functions, and have integrated them into autosomal locations. These gene copies, termed retrogenes, are only expressed at the time that their X-encoded parental genes are inactivated and thus are only expressed in the germ line in the testes during meiosis (Shiao et al., 2007, Betran et al., 2002, Turner, 2015). The *EIF2S3L* gene on chromosome 12 is only expressed in the testes, and therefore strongly suggests that *EIF2S3* is one of these essential genes on the X chromosome, as it has this retrogene copy in the autosome. This relates to the apoptosis data in this study, which showed higher cell death in the *EIF2S3* KO cells compared to controls, thus suggesting that the presence of *EIF2S3* is critical for cell proliferation and maintenance.

Yamauchi *et al.* have shown that spermatogenesis can occur in male mice with the Y chromosome contribution limited to only two genes: *Sry*, the testis determining factor, and *Eif2s3y*, the latter being the murine Y chromosome homologue of *Eif2s3x* (Yamauchi et al., 2014). Further studies by this group replaced *Sry* and *Eif2s3y* through transgenic activation of their homologues *Sox9*; which in mice is on chromosome 11 as opposed to the X chromosome in humans, and *Eif2s3x* on the X chromosome, and showed that spermatogenesis and reproduction still occurred in the mice. Thus the presence of just these two specific genes were able to substitute

the Y chromosome in mice (Yamauchi et al., 2016). This study demonstrates the critical role of *Eif2s3x* in reproduction, which complements the findings in this study of the high cell death observed in cells lacking *EIF2S3*. Due to eIF2 γ being an initiation factor, it plays an essential key role in initiating protein synthesis within the cell (Yatime et al., 2007). Therefore in its absence, this fundamental pathway of protein synthesis may not be able to be achieved to a high enough standard to maintain cell survival. The highly significant difference in apoptosis observed between the *EIF2S3* KO population and control cells observed in my studies, supports this hypothesis. In line with these findings, the *EIF2S3* (p.P432S) variant in our patients is therefore predicted to be a partial loss of function mutation, which is not deleterious enough for the patients to die but is pathogenic enough for them to manifest the disorder described. However further functional analysis is necessary to show the significance of the variant and the mechanism affected. The recent publication by Moortgat *et al* supports my observations by reporting pedigrees with certain similar phenotypic features, who are carrying what are described as pathogenic *EIF2S3* mutations, in which two out of the three male patients died. My study has unique and novel aspects, firstly the human embryonic expression data presented here had not previously been analysed in depth in a hypothalamo-pituitary and pancreatic context in the literature. As discussed, Pedigree 8 still has a unique phenotype for a family harbouring an *EIF2S3* variant, as the patients elicit a more severe hypopituitary phenotype, but a milder neurological phenotype compared to previous reports. Intellectual disability with the presence of microcephaly and epilepsy has been the main phenotypic focus in previous patients up until now. All previous reported patients had a thin corpus callosum on MRI; also observed in our patients. However three previously reported patients also had enlarged lateral ventricles (Borck et al., 2012); not present in Pedigree 8. In contrast, our patients have a small anterior pituitary on MRI as opposed to a normal structural pituitary and stalk in Moortgat *et al*'s study, and no mention of any structurally abnormal pituitary in Borck *et al*'s publication. Both previous reports

describe patients with GHD, however the authors did not provide any endocrine values; Borck *et al* simply stated that low growth hormone levels were observed in the two brothers, and treatment with GH resulted in some catch-up growth in one of them (Borck *et al.*, 2012). The patients in Pedigree 8 have GHD and TSHD, suggesting that the *EIF2S3* (p.P432S) variant may be affecting protein synthesis in both the somatotrophs and thyrotrophs, as opposed to previous *EIF2S3* variants that suggest affects in only the somatotroph cells of the pituitary. The mechanism causing this is unknown although a proline to serine substitution is likely to affect protein folding, and thus be detrimental to the protein structure of eIF2 γ . As we know it is expressed in the pituitary, it may be decreasing the occurrence of protein synthesis to a higher degree than previous mutations (thus causing the severe short stature), which extends across more cell types such as in the thyrotrophs. Patients in both pedigrees in Moortgat *et al*'s study had hypoglycaemia, however again there were no endocrine values presented. The microcephaly and ID observed in these patients may be primary, or secondary to brain damage caused by the hypoglycaemia. With this in mind, it cannot be ruled out that the microcephaly and ID in the patients described by Borck *et al* may in part have been a consequence of previous hypoglycaemia that went undetected. Although our patients in Pedigree 8 are similar to this report in having hypoglycaemia, they remain unique in having an unusual pancreatic phenotype that fluctuates between hyperinsulinaemic hypoglycaemia and hyperglycaemia, which has not been previously reported. Therefore this glucose dysregulation seen in our patients suggests a critical role for *EIF2S3* in pancreatic function, as well as in hypothalamo-pituitary function. A comparison of the patient phenotypes described in the two previously published studies, and the patients in this study, are presented in Appendix 6. Finally, aside from the expression findings and clinical aspects, the *EIF2S3* (p.P432S) remains completely novel, is in a highly conserved region of the gene, and has never appeared in a patient nor in a control individual before. The two previously reported *EIF2S3* mutations, p.I259M and

p.L465Sfs*4 both lie within the C-terminal domain, and were concluded to be pathogenic following zebrafish morpholino studies (Moortgat et al., 2016). This suggests that our p.P432S variant, also lying within the C-terminus, may also be pathogenic, however causing a different phenotype. A clear defined role for the C-terminal domain in eIF2 γ remains to be established. As discussed, the variant is most likely to affect protein folding and therefore structure. Therefore the mechanism affected would potentially be protein-protein interaction, thus the binding ability of eIF2 γ to other subunits and proteins would be altered, which in turn would influence protein synthesis.

Unfortunately this study did not have time to delve into other avenues of investigating what the overexpression of *EIF2S3*WT and the p.P432S mutant would do to a human or mouse pancreatic cell. If sufficient transfection had been achieved in 1.1B4 or MIN6 cells in this study, and both inserts were being expressed at sufficient levels (validated by qPCR), then cells would have been analysed for cell death using the caspase assay protocol, and analysed for insulin secretion using the ELISA method. Insulin secretion could only be measured using the MIN6 cell line, since the 1.1B4 cells did not secrete insulin, as discussed (Figure 5.9). Therefore functional assays still need to be performed to clarify whether the p.P432S variant is pathogenic and how it is contributing towards the phenotype in Pedigree 8.

5.4. Future work investigating the function of eIF2y

5.4.1. Transfection assays

Given more time, there are other approaches that can be applied to attempt a higher transfection efficiency of the *EIF2S3_WT* and *EIF2S3* (p.P432S) constructs. These include non-viral physical methods such as electroporation, microinjection, impalefection, hydrostatic pressure or lipofection. I would most likely begin with electroporation in the next instance on 1.1B4 or MIN6 cells as this is the next most common method used on hard-to-transfect cells. This technology creates small pores in cell membranes in which constructs can enter, by applying an electrical pulse. Nucleofector technology (Lonza) is a new improved version of electroporation in which high transfection efficiencies may be reached using lower substrate amounts, with only a moderate impact on cell viability. However, attempting transfection with the current Fugene or lipofectamine method on an alternative pancreatic beta cell line, to see if they are more efficient in incorporating the plasmid into their genome, is a potential option.

The *EIF2S3* insert was cloned into the LV-IRES plasmid specifically in order to be packaged into a viable lentivirus. The fact that this was not possible for various unknown reasons suggests that there may be a better plasmid into which the WT and mutant *EIF2S3* can be cloned, that may be more suitable for the transfection method as opposed to being chosen for transduction. In addition, given the fact that LV-IRES *EIF2S3* constructs did not elucidate successful LV packaging as anticipated, one cannot rule out the possibility that there may be other underlying faults with this plasmid that may affect other methods, thus making it a poor choice with which to continue to attempt transfection. Re-cloning the inserts into a different plasmid that expresses GFP, or cloning GFP into the original pCMV-SPORT6 plasmid that already contained the *EIF2S3* cDNA, would yield alternative constructs to the LV-IRES vector

which can then be transfected into cells. Alternatively, co-transfecting GFP with the pCMV-SPORT6 containing the *EIF2S3* cDNA is another route that can be taken.

5.4.2. Luciferase assays

As mentioned previously, ribosomes typically initiate translation at an AUG start codon. Mutations that weaken Met-tRNAⁱ binding to eIF2 or stimulate eIF2 GTPase activity have been found to enhance initiation at a UUG codon and confer a suppressor of initiation (Sui⁻) phenotype (Hinnebusch, 2011). In the previous study describing the p.I222T mutation in a patient with ID, the authors conducted an experiment showing that cells that express WT eIF2 γ show a greatly reduced expression of firefly luciferase reporter with a UUG start codon than Renilla-luciferase with an AUG codon, producing a low UUG/AUG initiation ratio (Borck et al., 2012), which is consistent with what happens *in vivo* usually with the AUG codon being selected. When the p.V281T/p.V281K yeast equivalent mutations were analysed by Borck *et al* in their study, there was an increased UUG/AUG initiation ratio by 2-3 fold. Overexpression of eIF2 β in the presence of p.V281T/p.V281K mutations, partially/fully respectively, restored the WT ratio in cells expressing the eIF2 γ mutants (Borck et al., 2012). Therefore this complex start codon selection assay may be exploited to investigate the p.P432S variant, which may possibly allow further investigation of the p.P432S variant and reveal whether a defect in AUG start codon selection is the mechanism that is affected. Interestingly, the investigators who performed these assays stated that they were unable to express recombinant forms of mammalian eIF2 γ , and were only able to mutate the corresponding Val281 residue in yeast eIF2 γ for functional analysis. The authors do not elaborate on the problems they faced with expressing mammalian eIF2 γ , indicating that they may have had the

same challenges in which I have been confronted with, e.g. with limited transfection efficiency.

Insulin rapidly activates protein synthesis by activating eIF2B GDP/GTP exchange, thus promoting formation of the ternary complex; eIF2 γ -GTP- Met-tRNAⁱ. Therefore if successful transfection of our *EIF2S3_WT* and *EIF2S3* (p.P432S) constructs can be achieved via any of the methods or cell lines discussed (section 5.4.1) then insulin could be used as a stimulant in the luciferase assays analysing UUG/AUG start codons. When these cells are expressing eIF2 γ WT and eIF2 γ mutant protein, firefly luciferase with the UUG start codon and Renilla-luciferase with the AUG start codon can then be measured directly from lysates following the Dual-Luciferase reporter assay system protocol (Promega). Basal activity can be initially analysed with the naturally occurring insulin in the cells, which would stimulate eIF2 activity endogenously. Insulin-stimulated activity generated by applying insulin into adjacent wells in the assay plate could essentially be measured simultaneously. The comparison of start codon selection in this context can then be compared between WT and mutant populations to observe the UUG/AUG start codon selection ratio in both cell populations at basal level, as well as after the addition of insulin. The latter will analyse whether the addition of insulin increases start codon selection in the mutant cells in a similar fashion to WT cells.

5.4.3. Binding assays

In addition, co-transfecting constructs containing the genes encoding the eIF2 α and β subunits (*EIF2S1* and *EIF2S2*), with the eIF2 γ WT and p.P432S variant constructs respectively, using a pull-down co-immunoprecipitation method with a His-tag, could essentially look for specific binding qualities of the individual subunits; α , β , γ , and also compare differences between the eIF2 γ WT with the p.P432S variant. Previous studies by Borck *et al* describe a similar method that looked at the yeast equivalent residue to the human eIF2 γ (p.I222T) variant that they identified (Borck et al., 2012). Given that the p.P432S variant is not in a known GTP-binding domain of eIF2 γ , unlike the p.I222T variant, some would say that p.P432S may possibly not affect binding at all. However given the rudimentary knowledge about the C-terminal domain, and that the variant is predicted to alter protein folding and structure, it is beneficial to study effects on protein-protein interaction for significant binding differences between the WT and p.P432S proteins, in combination with the published p.I222T mutation (Borck et al., 2012) which can be used as a control. Conducting this assay may further clarify the role of the C-terminus in human eIF2 γ .

There are other initiation factors involved in the promotion of protein synthesis in similar ways to eIF2, such as eIF3 which is comprised of 13 subunits and participates in the majority of steps leading to translation initiation (des Georges et al., 2015). One of these roles, as mentioned in section 5.1.2., is to bind to the 40S ribosomal subunit in order to keep the 40S and 60S subunits separate from each other, which allows the association of the ternary complex with the 40S ribosomal subunit (Hershey, 2015). Previous studies that sought to identify which components directly contacted residues in the eIF3 core, uncovered a direct bridge link between the globular domain of eIF3d to the eIF2 α (des Georges et al., 2015). This is just an example of how the initiation factors may work together to initiate protein synthesis. Therefore binding assays may uncover subtle differences between the eIF2 γ WT and the p.P432S

variant in respect to its ability to bind to closely related protein partners as well as more distant and unknown proteins in other pathways.

5.4.4. Mouse-models

In vitro studies are useful for characterising a gene and a particular variant within it to investigate how it may be contributing to a particular disease, but only to a certain extent. Alternatively, *in vivo* investigation using animal models would provide better analysis of the actual biology of a given disease in ways that *in vitro* assays are unable to. Coincidentally, it has just come to light that Dr James Turner's research group at the Francis Crick Institute has attempted to create a CRISPR-generated *Eif2s3x* (the *EIF2S3* mouse homologue) knock-out (KO) mouse. The CRISPR-Cas9 technique is namely the clustered regularly interspaced short palindromic repeats (CRISPR)-Cas9, which refers to the immune system in bacteria. This naturally occurring process in prokaryotes has been manipulated and developed into a gene editing technique that can target particular sequences of DNA to inactivate whole genes or to edit them (Wiedenheft et al., 2009, Doudna and Charpentier, 2014). It can alter as little as one base pair, enabling specific gene variants identified in patients to be inserted into organisms (Walsh and Hochedlinger, 2013). Following the inactivation of *Eif2s3x* in the mouse via CRISPR-Cas9, Dr Turner's group were unable to create mutant XY embryonic stem (ES) cell clones in the *Eif2s3x* KO mice (unpublished data), suggesting that *Eif2s3x* is critical for ES maintenance. Then, after injecting mouse zygotes, despite consistently recovering male and female mutants at the blastocyst stage, no mutants were recovered at birth, including female heterozygous mutants. Therefore the male mutants die consistent with the XY ES cells, and it appears that the targeting strategy that they performed was so efficient that it was able to kill both alleles in the females, again causing lethality. This is supported by their analysis of

XX blastocysts from which they failed to recover any WT alleles. These data are consistent with the findings in my study as the *EIF2S3* KO 1.1B4 cell line had a highly significant increased cell death compared to controls, mirroring Dr Turner's findings in unsustainable life in *Eif2s3x* KO mice. We plan on collaborating with Dr Turner on this project and investigating *Eif2s3x* KO mice in the context of the pituitary and pancreas respectively. In addition, there may also be the possibility of creating an *Eif2s3x* (p.P432S) mutant mouse model using the CRISPR-Cas9 method. This will enable the analysis of any *in vivo* consequences of the p.P432S variant, with particular focus on the tissues affected in the patient. Initially the growth of the *Eif2s3x* KO and the *Eif2s3x* (p.P432S) mutant mouse models can be analysed. This will be followed by dissection of the hypothalamus, pituitary and pancreas, which can be visualised structurally for comparison with a WT mouse. The number, distribution and localisation of molecular markers, such as Sox2, Sox3, Lhx3, Lhx4 and Prop1 for example, may be analysed in both the hypothalamus and the pituitary at different stages of development. This will be implemented by fluorescent antibody staining, to see if there is a reduction in Sox2 positive cells in the mutant compared to the WT mouse for example. With these available working murine antibodies, this technique could look at co-expression of the known molecular markers in specific cell types of the pituitary, such as the somatotroph cells to see if there is correlation with hormone deficiencies that are seen in the patient. The pancreas in these mutants can also be investigated in a similar way to observe the appearance, number, distribution and localisation of pancreatic islets and their beta cells. Furthermore, molecular markers specific to the developing pancreas can be analysed, such as Ins1, Pdx1, NeuroD1, Ngn3 and MafA for example. In addition, insulin secreted from the beta cells and glucagon secreted from the alpha cells can be measured to look at different aspects and cell types of the pancreas *in vivo*.

Chapter 6

General Discussion

6.1. Summary of findings

In this study I have demonstrated both a Sanger sequencing and an exome sequencing approach to uncover novel variants and candidate genes in patients with congenital hypopituitarism (CH) and related phenotypes. The former was achieved by screening Pedigree 1 for *LHX4* and identifying the first novel homozygous mutation, *LHX4* (p.T126M), in two siblings with a lethal form of hypopituitarism (Gregory et al., 2015b). The latter was achieved by submitting seven unrelated pedigrees to GOSgene for exome sequencing and identifying novel variants in the following novel genes: *CTPS2* (p.F166L) in Pedigree 2, *RNPC3* (p.L483F) and *PRMT6* (p.P350R) in Pedigrees 3-6, *FASN* (p.A2132V) and *APEX2* (p.M422V) in Pedigree 7, and *eIF2 γ* (p.P432S) in Pedigree 8. An *EIF2S3* KO human cell line was established in this study, using an shRNA LV technique, which showed a significantly higher level of caspase activity compared to controls. This increased apoptosis in the KO cells suggests that *EIF2S3* is crucial in sustaining cell viability. Although detailed functional analysis of the p.P432S variant was not completed within the timeframe of this study, these data, together with the hypothalamo-pituitary and pancreatic expression profile established in this study, suggest that p.P432S may cause a partial loss of function leading to a moderately severe phenotype. Molecular modelling together with the functional study of genes and the effect of particular mutations is extremely important to enable conclusions to be drawn about how certain phenotypes arise. However despite functional analysis performed in certain studies, often it is not possible to characterise the mechanisms affected by particular mutations through *in vitro* studies. This was the case when analysing the *LHX4* (p.T126M) homozygous variant in this study, in which transactivation of α GSU and PRL were not affected. As discussed, despite there being more target genes to analyse in this assay such as TSH β , POU1F1 and FSH β , it is not certain that these are genuine physiological targets of *LHX4*. Therefore, although I was not able to show how the p.T126M

mutation altered LHX4 function, the molecular modelling together with the strong genetic evidence, animal conservation, and previous studies performed in mice, strongly suggests pathogenicity of this homozygous variant. Therefore even though it is ideal to show functional significance of a variant, it is not always possible, and sometimes it is more valuable to accumulate all the facts, including segregation within the family, molecular modelling and previous studies, in order to hypothesise whether a particular mutation is pathogenic or not. The molecular basis of congenital hypopituitarism remains to be established in the majority of the families in our large cohort of >2000 CH patients. This indicates that there is a significant number of novel genes and regions of interest that are yet to be discovered, and both scientists and clinicians can collaborate and identify these novel mechanisms in order to understand more about the embryogenesis and development of the hypothalamo-pituitary axis.

6.2. Future Work

The expression profiles of *CTPS2*, *RNPC3*, *PRMT6*, *FASN* and *APEX2* have been analysed and discussed in Chapter 4. The variants identified in these genes in Pedigrees 2-7 will be functionally analysed in future studies using appropriate assays. Clinical investigation is essential and needs to take place regularly for all patients described in this study, to further characterise their phenotypes, and to get a clear picture of how their disorders are manifesting and changing with age. We would like to make murine transgenic models for all of these genes, as well as models harbouring the actual variants, using the CRISPR-Cas9 method. These *in vivo* models can then be compared to the normal mice for phenotypic differences, ranging from their size and the presence of other physical manifestations, through to molecular markers and hormone levels. The expression of *RNPC3* analysed in this study, together with the previous report by Argente *et al* describing *RNPC3* mutations

associated with IGHD, led me to hypothesise that the *RNPC3* (p.L483F) variant is responsible for the GHD observed in the patients in Pedigrees 3-6. However functional analysis is needed to confirm this and to characterise the actual mechanism that is affected in these patients by either or both of the variants in *RNPC3* and *PRMT6* respectively. Additionally, the ovarian phenotype remains unexplained, and may be due to either the *RNPC3* or the *PRMT6* variant. We have already begun to create mouse models for *Rnpc3* and *Prmt6* with our collaborators at The Francis Crick Institute, London. Dr Karine Rizzoti and colleagues will knock out the *Rnpc3* and *Prmt6* separately in the mouse, as well as simultaneously, to try to characterise the role of each gene in the developing mouse. If these mutants do not survive, then a conditional knock out of each gene in the pituitary gland of the mouse will be generated. In addition the *Rnpc3* (p.L483F) and *Prmt6* (p.P350R) variants will be introduced separately and in combination with each other to create a mouse model reflective of the patients' genotype (Pedigrees 3-6). Currently this group are analysing expression of both *Rnpc3* and *Prmt6* in embryonic murine hypothalamo-pituitary axis tissue as well as the ovaries, which can then be compared with the human expression profile performed in this study. We have obtained fibroblast cells from one of the affected female patients in Turkey that harbour the homozygous variants in *RNPC3* and *PRMT6*, and their unaffected sister that has a normal genotype. The RNA in these cells will be extracted and sequenced in a technique referred to as RNA-seq, also known as whole transcriptome shotgun sequencing. Transcriptomics can look at all parts of the transcript including mRNAs, non-coding RNAs and small RNAs, to enable analysis of the transcriptional structure of genes and their splicing patterns. In the RNA-seq technique, a population of RNA is converted into a library of cDNA fragments and then sequenced in a high-throughput manner to obtain short sequences, with reads typically 30-40 bp long. These can then be aligned to a reference sequence, or assembled to form a genome-scale transcription map that consists of both the transcriptional structure and the level of expression for each gene

(Wang et al., 2009). This method was carried out in the previous study by Argente *et al* in a lab in Finland which quantified the splicing efficiency and intron retention of U12-type introns with respect to U2-type introns per gene, and normalized by gene expression. The authors established 21 genes with significantly decreased U12/U2 ratios in patient cells compared to controls (Argente et al., 2014). Therefore we plan on sending the patient fibroblast cells to Finland for RNA-seq, as this lab have experience in analysing the data in this context using this complex technique. The U12/U2 ratio in their optimised assay can then be measured and the gene expression of known U12-spliced genes can be analysed. This scrutiny of the transcript containing the *RNPC3* (p.L483F) and *PRMT6* (p.P350R) variants can potentially uncover any defects in the mRNA processing of the minor spliceosome that are giving rise to the tissue-specific consequences seen in the patient. For example, in the somatotroph cells of the pituitary, that may be causing the IGHD seen in Pedigrees 3-6. In addition to analysing gene expression of the known U12-spliced genes associated with IGHD, previously identified by the authors, they could also analyse gene expression of U12-spliced genes known to be associated with the ovary. This can look for splicing abnormalities that may be giving rise to the ovarian failure seen in the patient. Furthermore the authors may be able to look back at their RNA sequencing data from the patients with the bilallelic *RNPC3* mutations (Argente et al., 2014), to look at splicing in ovarian-specific genes. The authors would most likely not have analysed these specific genes previously, due to their patients not having been diagnosed with ovarian failure, and thus were not considered relevant to the study. The mouse models together with the RNA sequencing results will help pinpoint the mechanism affected in the patients in Pedigree 3-7. Human ovarian embryonic tissue at >10pcw stage will be obtained from HDBR to analyse *RNPC3* and *PRMT6* expression in the ovary. This will establish whether expression is apparent in the developing fallopian tube or related structures of the female reproductive system, or alternatively in the paramesonephric duct, as discussed in Chapter 4. Furthermore,

RNPC3 expression analysis of the developing pituitary will be repeated, as the Rathke's pouch tissue in this study was damaged and despite results hinting at positive *RNPC3* staining in this area (Figure 4.9 A-C), *in situ* hybridisation needs to be repeated for this to be concluded.

To investigate the role of CTPS2 further we would like to generate a conditional *Ctps2* mouse knock out in the hypothalamo-pituitary axis, which will help characterize the role of *Ctps2* in the context of this region. Furthermore, a *Ctps2*(F166L) mouse model, reflecting the genotype of the patient would be beneficial, to recapitulate the effect of the variant in the mouse. Additionally, it may be possible to collaborate with Martin E *et al* to perform functional assays based on their analysis of the *CTPS1* gene (Martin et al., 2014). CTP formation depends on enzymes CTPS1 and CTPS2, whose respective roles remain unknown (Kassel et al., 2010). However the activity of these CTP synthases is thought to be a potentially important step for DNA synthesis in lymphocytes (van den Berg et al., 1995). This previous report identified a loss of function homozygous mutation (rs145092287) in *CTPS1* that caused a novel and life-threatening immunodeficiency. This disease was characterized by an impaired capacity of activated T and B cells to proliferate in response to antigen receptor-mediated activation (Martin et al., 2014), previously discussed in Chapter 4.2.3. The splice mutation identified in this patient was found to have decreased ERK1/2 phosphorylation, and CD25 and CD69 upregulation in CTPS1-deficient T-cells compared to controls. Firstly, fibroblast cells from the patient harbouring the CTPS2 (p.F166L) in Pedigree 2 can be obtained and *CTPS2* expression can be compared with control cells. In addition, based on the functional assays described in this previous study, and with the help of the immunology lab here at the ICH, proximal T-cell activation signals, and late responses, may be investigated in fibroblast cells obtained from the patient, and compared to controls. Furthermore, B cells could be activated in these cells, with anti-BCR and CpG, and IL-4 and CD40L for example,

and monitored for the upregulation of CTPS2, using similar optimised previously performed methods that monitored CTPS1 upregulation. These data may give critical insights into the impact of the mutation on protein function. However, these assays obviously have particular focus on immune cells, and as our patient in Pedigree 2 has not been diagnosed with an immunodeficiency, they may not reveal the mechanism affected by the CTPS2 (p.F166L). Although, the immune system of this patient may need to be further investigated. It cannot be completely ruled out that immune cells specifically in the pituitary and related tissues where *CTPS2* expression was identified (Figure 4.3), may be affected and indirectly contribute to the phenotype. However, the complex phenotype of the patient in Pedigree 2 is likely due to an as yet undetermined mechanism, unrelated to immune cells, initiated by the p.F166L missense substitution in CTPS2. In this case, the mouse model may be able to shed light on the underlying mechanism, hence it may be wise to begin with this *in vivo* study in the first instance.

Finally, based on the expression profiles of both *FASN* and *APEX2* in Chapter 4 of this study, it is hypothesised that the unique phenotype observed in the patient from Pedigree 7 is most likely to be hypothalamic. This hypothesis is based on the high *FASN* transcript expression observed in the hypothalamus in several stages during embryogenesis. This is opposed to only partial expression noted in Rathke's pouch at the early stage of CS16, in which transcripts are otherwise absent from the developing pituitary gland (Figures 4.11). *APEX2* transcript expression was completely absent in the developing hypothalamus and pituitary at all stages analysed. Recent clinical investigation of the patient identified an increased concentration of triglycerides, which will now be routinely monitored. The patient is due to have metabolic tests performed as an inpatient to analyse his fat metabolism, as well as an oral glucose tolerance test and diagnostic fast, which may show an abnormal impact on insulin secretion. His elevated triglyceride concentration

suggests a potential association of the phenotype with defective fatty acid synthesis due to the *FASN* mutation. These data together with the fact that *FASN* (p.A2132V) is a *de novo* variant, indicate that it is most likely to be mutated *FASN* that is giving rise to the phenotype seen in the patient (Pedigree 7). In addition, loss of *Fasn* in murine models generated in previous studies have a more severe phenotype compared to the *Apex2* mouse models (discussed in Chapter 4.4.3 and 4.4.5). The conditional *Fasn* murine knock out in NSPCs impairs adult neurogenesis (Knobloch et al., 2013). Murine null mutant *Fasn*^{-/-} embryos die before implantation, with *Fasn*^{+/-} heterozygotes dying at various stages of development *in utero*, suggesting that *Fasn* haploinsufficiency is incompatible with survival (Chirala et al., 2003). *Apex2*-null mice exhibit a growth retardation phenotype, with moderate dyshaematopoiesis, a severe defect in lymphopoiesis, and an accumulation of thymocytes and mitogen-stimulated splenocytes in G2/M phase. The authors concluded that APEX2 was implicated as an essential regulator of efficient cell cycle progression of proliferating lymphocytes (Ide et al., 2004). Therefore, firstly, we plan on collaborating with Dr Sally Camper in Michigan in making a hypothalamic conditional *Fasn* knock out mouse. In addition we hope to generate a *Fasn* (p.A2132V) mouse model specific to the variant identified in the patient. These mice can then be phenotypically analysed in different ways such as in size, presence of other phenotypic features, and hormone levels, and compared to controls. We have recently obtained skin fibroblasts from the patient, and in collaboration with Professor Peter Clayton at ICH and Professor Robert Semple at Addenbrooks, we plan to investigate the lipid pathway in more detail. We will also measure the FAS levels in these patient cells, which will indicate whether the increased triglycerides are directly associated with increased FAS, which would suggest that the mutation identified is a dominant activating mutation. It cannot be ruled out that the APEX2 (p.M422V) variant is contributing to the hypothalamo-pituitary phenotype observed in the patient. Alternatively this variant may potentially be responsible for the phenotype seen in other tissues, such as the sensorineural

hearing loss, which is echoed by the *APEX2* expression noted in the utricle of the developing ear (Figures 4.13 C-D) as discussed in Chapter 4.4.6. Further expression studies will entail obtaining human embryonic tissue from the spleen to analyse expression of *APEX2*, as well as *FASN*, due to the patient from Pedigree 7 having splenomegaly. This condition may stem from the *APEX2* (p.M422V) variant, especially as *Apex2*-null mice display an accumulation of splenocytes (white blood cells situated in the spleen). Discussions about generating an *Apex2* (p.M422V) mouse model will possibly take place at a later stage after the *Fasn* (p.A2132V) has been investigated.

6.3. Genetic screening methods

Obviously every study has its limitations, for example human error when screening for variants in known causative genes. As every nucleotide is analysed by eye following direct sequencing analysis, crucial variants may be overlooked occasionally, perhaps missing the pathogenic mutation that is causing the disease phenotype. Despite being the more expensive option, whole exome sequencing (WES) can overcome this hurdle to an extent by picking up all potential variants in the coding region of a patient in the analysis. However, some may argue that the Sanger sequencing approach may actually result in being more costly, depending on the number of genes needed to be screened and number of patients in whom screening was to be performed. Thus using a lot of manpower in the analysis of just a handful of genes. Multi-gene panel tests are a step up from individual gene screening that enable the sequencing of several known causative genes simultaneously, providing a method to identify mutations using both a rapid and cost effective strategy. However, panel testing still only looks at a limited number of known genes, when there may be a multitude that have previously been implicated in the literature to

cause that specific disorder, such as in HH for example. In such cases where the list of potential mutated known genes is so large, any, or more than one gene, could be mutated in any given patient thus making it difficult to choose which of the genes to put on the panel test. Therefore WES is most likely to be the most efficient option for patients such as these, as both known, implicated and novel candidate genes may be assessed instantaneously. A limitation of WES however can be the filtering process, in which human error may occasionally overlook a pathogenic mutation by analysing the data in the wrong context. For example, if the database parameters are set to search the exome for *de novo* variants, and the data are not additionally analysed separately using parameters set to look for variants of autosomal dominant inheritance, then a heterozygous mutation may be overlooked. Therefore in this study the genetic data for each family submitted to GOSgene for exome sequencing was analysed using all alternative parameters, so as to be sure not to miss any potentially pathogenic mutations (Appendix 2). A general overview of the filtering process for exome sequencing data used by GOSgene is shown in Appendix 2. Therefore I am confident that the variants identified and discussed in the pedigrees in this study are the most likely candidates generated through the filtering process, and that all other polymorphic and benign variants have been disregarded, thus leaving the only potential variants that are likely contributing to the phenotype e.g. *RNPC3* (p.L483F) and *PRMT6* (p.P350R) in Pedigrees 3-6. However, future work will need to investigate the role of these genes in the pituitary and related tissues, and the effects of the variants on their function, to help show significance of these variants before any conclusions about their contribution towards the phenotype is made. Furthermore, exome sequencing only considers variants in the coding region, and splicing variants up to two bases into the intron at either end of the exon. Therefore the presence of an additional intronic variant in any of the pedigrees described cannot be completely ruled out, despite it being an unlikely occurrence. Additionally epigenetics is another factor that may influence the severity of a phenotype, which again also cannot be

ruled out in an individual. Epigenetics refers to modifications in heritable genetic information other than changes in the DNA sequence, such as DNA methylation and histone modification that alter gene expression (Holliday, 1989). Whole genome sequencing (WGS) would be the most beneficial and efficient option for the identification of variants if there were unlimited resources. This method can interrogate all parts of the genome potentially revealing single-nucleotide variants (SNVs), indels, structural variants (SVs) and copy number variants (CNVs) in both the ~1% part of the protein coding sequences, and the remaining ~99% of the non-coding sequence (Ng and Kirkness, 2010). The 100,000 genomes project launched by Genomics England in 2012, aims to sequence 100,000 whole genomes of patients and their families with rare diseases and cancer by 2017 (www.genomicsengland.co.uk). The genomic sequence data can be matched with patient medical records, and interpreted in order to investigate the cause, diagnosis and treatment of disease. This large resource of genomic data will build a platform in characterising rare diseases and cancers, which will benefit future generations and many different areas of research. We have contributed to a percentage of this project by providing DNA from certain unique families with pituitary disorders, and hope that this will shed light on some of the extremely rare cases in our cohort. Despite these patients submitted for WGS, either via the 100,000 genomes project or elsewhere, this remains an option only for the analysis of a very small number of unique pedigrees, as it is impossible to perform for all of the pedigrees within our large cohort. Therefore WES remains the preferred choice as it costs significantly less than WGS due to it being confined to just the cDNA. Although WES constitutes such a low percentage of the entire genome due to this, it still contains the majority of pathogenic mutations identified to date (Rabbani et al., 2014).

6.4. Control databases

Control databases that are referred to when verifying a novel genetic variant can often be a concern. These databases can sometimes be ambiguous and lack information regarding the control samples themselves. They often fail to provide information as to how the individuals that were screened were classified as controls, and the criteria that was used for this. Nevertheless, they often state the number of controls within each ethnicity, enabling more relevant comparisons between DNA samples of similar ancestry. However, there are limitations here too, as individual control sub-cohorts are often small in number, and often do not define the descent of their controls sufficiently; such as when termed as 'European', which may consist of a multitude of ethnic backgrounds. Genotypes of Turkish descent will differ drastically from those of Swedish descent for example, and websites often generalise these as the same group and fail to subcategorize it. Prior to the ExAC browser (www.exac.broadinstitute.org) becoming one of the main control reference databases, control cohorts were also very limited in their number of patients too, for example in the 1000genomes database (www.1000genomes.org). One thousand individuals is not a very large number when verifying whether a variant is potentially pathogenic or not purely based on its absence from a database containing this number of patients. Prior to referring to databases, studies used to simply screen ~100 individual patients from the same ethnic origin as the patient that possessed the variant. Despite the direct ethnicity match, this is still a rather small number to be used as evidence to make rational conclusions regarding pathogenicity. It is interesting to consider how many times a novel variant in the literature has been concluded as potentially pathogenic and/or had unnecessary functional analysis performed on in the past, purely based on this referral to a small number of controls. The accumulation of samples in the ExAC browser has improved the variant verification process by increasing the number of control samples to ~100,000 alleles, in which all

polymorphisms present in samples are listed along with their frequency within this population. The additional information of whether a particular variant is present in heterozygous, homozygous or hemizygous form is also apparent. If one has identified a homozygous variant for example, the fact that it is only present in heterozygous form in a control patient indicates that it could be recessive and may be worth pursuing functionally. The importance of indicating the sex of the control individual by distinguishing whether a variant on an X-linked gene is heterozygous or hemizygous (on the male X chromosome) for example, and not just stating the presence of the variant 'on one patient allele', is obviously also vital in deciphering whether a variant is worth pursuing. For example, if the ExAC browser purely stated that the APEX2 (p.M422V) variant was present and did not mention that it had been identified in heterozygous form, then I would not have been sure that it had not been found in hemizygous form in a male control individual, as it is in the patient in Pedigree 7. Other control databases have not always had this information, which raises the question of how many novel homozygous variants have been excluded as being pathogenic, due to the database not stating whether it was heterozygous or not. Even though in my opinion the ExAC database is one of the best control databases commercially accessible, it still has an element of ambiguity that is similar to most other control databases. The large cohort of controls has been compiled from smaller cohorts of individuals that have been sequenced as part of various disease-specific and population genetic studies, where individuals affected by severe paediatric diseases have been excluded (www.exac.broadinstitute.org). Despite the removal of these patients with severe diseases, these cohorts are still derived from the general population that may suffer from a range of common polygenic diseases, and so cannot truly be termed as normal controls. This is a similar case to the National Heart Lung and Blood Institute (NHLBI) database, consisting of 6,500 subjects (www.nhlbi.nih.gov/), which GOSgene use as a control resource. The NHLBI collects the genotypes of patients with common diseases, therefore in my opinion it is not

completely impossible that one of the many variants that give rise to one of these common diseases may also be associated with a rarer disease when present in isolation. Even though the research area of the different groups that have contributed to the ExAC database are listed on their website, there is no detailed clinical information available for each sample. Therefore one cannot be sure that a certain 'control' sample does not have a mild undetected or developing phenotype that is linked to the disease in the patient being studied. Thus, some may say that this would not be a true comparison to controls. Therefore discretion needs to be drawn upon here, for example if the variant in the patient appears once or twice in the ExAC database, it may still be worth pursuing with functional studies. Hence why GOSgene set parameters for variants to have an occurrence rate of $<0.5\%$ in control databases, when analysing exome sequencing data.

6.5. Variable penetrance

Variable penetrance is when a heterozygous mutation is inherited from an asymptomatic parent but yet its presence in the progeny causes a disease phenotype. This has been reported to be the case in many publications and the concept has long been a subject of controversy, where many people firmly believe that such a variant cannot possibly be pathogenic simply due to its presence in the normal parent. This belief is that there must be another mutation so far undetected elsewhere in the genome that is working alongside such a variant to elicit the phenotype; termed digenic inheritance. However, this may not always be the case, and the argument against the sceptics is that in many publications the researchers have demonstrated that the mutation may lead to functional compromise, and has implications for pathogenicity that specifically fit with the patient phenotype. This suggests that perhaps a specific level of gene expression or dosage of the protein is needed for the phenotype to occur, and thus infers that each individual is different in this way, even when within the same family. Also, it cannot be ruled out that there may be another variant present in the parent, which influences gene dosage or has a positive effect that counteracts the pathogenic mutation, in which the child does not possess. From a wider perspective, variable penetrance casts an element of doubt on referring to control databases when validating a variant as potentially pathogenic or not. As mentioned, the presence of an identified patient variant in the same state (e.g. heterozygous) on a control database, often rules it out for further analysis. However, what if a heterozygous variant with variable penetrance is present in one of these control samples as it is in an asymptomatic parent? Therefore the same concept as previously mentioned applies; despite the presence of a variant amongst controls, it is the frequency of it that is crucial. This decision is the fine line between whether we may find the reason for a patient's disorder, or whether it remains a mystery.

6.6. Human embryonic sections

Human embryonic sections were analysed for expression in this study due to our unique access to the HDBR, rather than mouse embryonic sections. Even though the latter are more routinely used in other laboratories as they are more readily available, expression of a murine gene does not directly relate to human expression. Species may obviously differ from one another in terms of gene expression. Therefore I chose to analyse expression in normal human embryos in a hypothalamo-pituitary context, which had not been analysed by any other laboratory up until now. Essentially five different stages that span embryonic development were available: CS16, CS19, CS20 and CS23, equivalent to 39, 46, 49 and 56 days into development respectively (www.ehd.org/virtual-human-embryo/), and late 8pcw. Carefully processed hypothalamo-pituitary sections were obtained at these stages to observe specific expression, in addition to other sections of tissues affected in the respective patient who harboured the variant in the gene being analysed. As one can imagine, sectioning embryos is an intricate process, and maintaining the integrity of the tissues can be challenging (unpublished, HDBR), especially in smaller tissues such as the pituitary and the ovary. This delicate process with these precious embryos makes the success of both the sectioning and the expression assay vital, as human embryos are in short supply. There is little room for error in this field, and if the section is cut incorrectly or is damaged in the process, there is no rapid replacement at hand. Furthermore, human embryos more often than not peel off and do not stick down onto the slide as accurately as mouse embryos do (unpublished, HDBR), meaning that expression cannot always be visualised in some areas of the section with absolute precision. I found this a problem at times in this study as many of the sections obtained from HDBR had been damaged and were peeling off in this way, with some of the smaller structures of the brain not intact. For example, when looking at *RNPC3*,

although expression could be noted, areas of Rathke's pouch tissue had been lost and I was not able to repeat the experiment using an alternative sample.

6.7. Genetic counselling

Genetic counselling was given to all the pedigrees discussed in this study after identification of the respective genetic variants. Genetic counselling refers to how families are advised about the consequences of an inherited disorder, and the probability of developing a disorder or passing it on to future generations. Often people ask how finding the potential genetic cause for a patient's disease will actually help the patient. Some people would rather not know if they or their child harbour a mutation, and many choose not to find out which parent they inherited it from. Following genome or exome screening, one can choose not to be told whether they harbour variants known to contribute to common diseases. Therefore upon consent of the patient, researchers do not divulge such information to patients, and only inform them of a novel or known mutation that potentially contributes to their particular rare disease. If a novel potential variant is identified, then genetic counselling helps families understand what it may mean, for example how functional studies would most likely have to be carried out in order to further investigate whether it is pathogenic or actually benign. This is what would have had to have been explained to most of the families in this study. In a different context, genetic counselling can help give families advice as to what their options are with regard to family planning or options of *in vitro* fertilisation (IVF). It is now possible to screen and filter fertilised eggs before implantation that do not contain the pathogenic disease-causing mutation; a process known as pre-implantation genetic diagnosis (PGD), so that the child does not develop the disease that his or her sibling has (Vermeesch et al., 2016, Findlay, 2000). This stops further inheritance of the pathogenic mutation and prevents future

generations manifesting the disease, thus improving their quality of life. This is a highly controversial topic which has split the opinion of many (Eskandarani, 2009); however, simply selecting an embryo that does not contain the mutation is not by any means changing any part of the genetic code. It is simply an alternative genotype of the parents that will give rise to a baby without that particular disease. Despite this, I believe that it should remain a restricted service that is only carried out for the prevention of severe diseases. It should not be extended to parents' preference of gender or traits that they want their children to have, such as height or colouring, where certain variants may be included or excluded to result in these preferences. This information should remain anonymous and only the mutation in question should be excluded. Religious or ethical principles divide many where genetics is concerned (Fasouliotis and Schenker, 1998), with many believing that we should let nature take its course at all costs and not meddle with genetics as it is artificially influencing the gene pool. On rare occasions, genetic counselling may extend to discussing the possibility of gene therapy for the patient, which exists and differs in many countries for certain diseases (Kim et al., 2008). Options for this would currently only be if the family consented to being recruited to a clinical trial, if there is one that exists for their disease. It is a long way off from being routinely performed, and only certain clinical trials have been accepted both ethically and socially in specific disease areas in the UK. A recent example is the trial on maternal gene therapy of severe early-onset fetal growth restriction (Sheppard et al., 2016), which could potentially be the first trial of gene therapy during pregnancy. Phase 2b clinical trials have recently been undertaken for cystic fibrosis (CF). The respective patients have been recruited from 18 sites in the UK, and were given either a nebulised gene–liposome complex; a non-viral *CFTR* gene therapy delivered directly to the lungs, or a saline dose (placebo) every 28 days for 1 year. These trials noted a significant, albeit modest, treatment effect of the gene therapy in the CF patients, associated with a stabilisation of lung function versus the placebo, at 12 months follow up (Alton et al., 2015). Further

improvements in efficacy and consistency of response to this form of gene therapy is needed before it is considered for clinical care. Thus clinical trials have now progressed into the next phase in this study. Gene therapy in Duchenne muscular dystrophy, using adeno-associated viral delivery methods, is also being developed and has been accepted for clinical trials (Bowles et al., 2012). Another example is gene therapy for immunodeficiency disorders, such as X-linked severe combined immune deficiency (XSCID), whereby restoring gene expression in autologous hematopoietic stem cells has been shown to be an effective method of treatment. Thus resulting in the production of T-lymphocytes and subsequent immune reconstitution (Cavazzana-Calvo et al., 2000, Gaspar et al., 2004). However despite these revolutionary advancements serious complications have frequently occurred, such as 5 out of a total of 20 subjects developing leukaemia-like T lymphoproliferative disorder 2-5 years after XSCID gene therapy (Hacein-Bey-Abina et al., 2003a, Hacein-Bey-Abina et al., 2003b). Adverse effects of treatment such as these highlight the need for the development of new strategies to improve, not only the success rate, but most importantly the safety of gene therapy, such as accurate gene targeting (Kildebeck et al., 2012). Gene therapy is essentially the introduction of normal genes into patient cells in place of missing or defective ones, or the silencing of a particular gene using complex drugs, in order to correct genetic disorders. This treatment can potentially take place at any age, ranging from prenatally to being performed in an adult patient. Many research groups are fighting for the right to perform this procedure for a range of diseases to improve the quality of life for many families, however this also remains a highly controversial topic. The conventional rule is that only somatic cells should be genetically altered by gene therapy, and not germ cells that contain heritable information (Lanphier et al., 2015). However Ireland and Italy have recently permitted the genetic code of germ cells to be altered in an individual if and when gene therapy for a particular disease is possible. This means that there could potentially be no control over these modifications being incorporated into the gene

pool, and that they will become uncontrollable permanent fixtures in the DNA of future generations. Even though a long drawn out process of clinical trials always needs to be performed to allow any such treatment to be available to patients, there is always still a slim chance of adverse effects or consequences that will only come to light in the years to come. That is why in my opinion it is extremely important for genetic modifications to remain within the individual that has been treated. However, the fact that one country may have one law that confines gene therapy to somatic cells, and another may not, is a very worrying concept. It only takes one country to not abide by this rule for the future of the human race to potentially be affected by any unknown consequences of gene therapy. With regard to the patients investigated in this study, gene therapy would obviously not be an option at present, as extensive functional work would have to be undertaken on the variant in question. Only then could a strong grant proposal be written that, if accepted, would be followed by vigorous clinical trials before even having a chance of becoming an option for patients. However, it is not an impossible goal for the future with technology rapidly progressing year after year. The more we as scientists and clinicians can do to identify and characterize mutations in our area of research, the more options will then arise for patients. I believe that the more knowledge we have about a specific field, the more options we have to fight to change it for the better.

Appendices

Appendix 1

A

Construct transfected into HEK293T cells	Average luciferase/total protein 1 st assay	Average luciferase/total protein 2 nd assay	Average luciferase/total protein 3 rd assay	AVERAGE LUCIFERASE/TOTAL PROTEIN	STD DEV OF AVERAGE MEAN
EV	103.38	67.28	99.58	90.08	19.83
wtLHX4	3651.98	4685.17	6434.75	4923.97	1406.67
T126M	4391.96	5075.28	7072.48	5513.24	1392.89

B

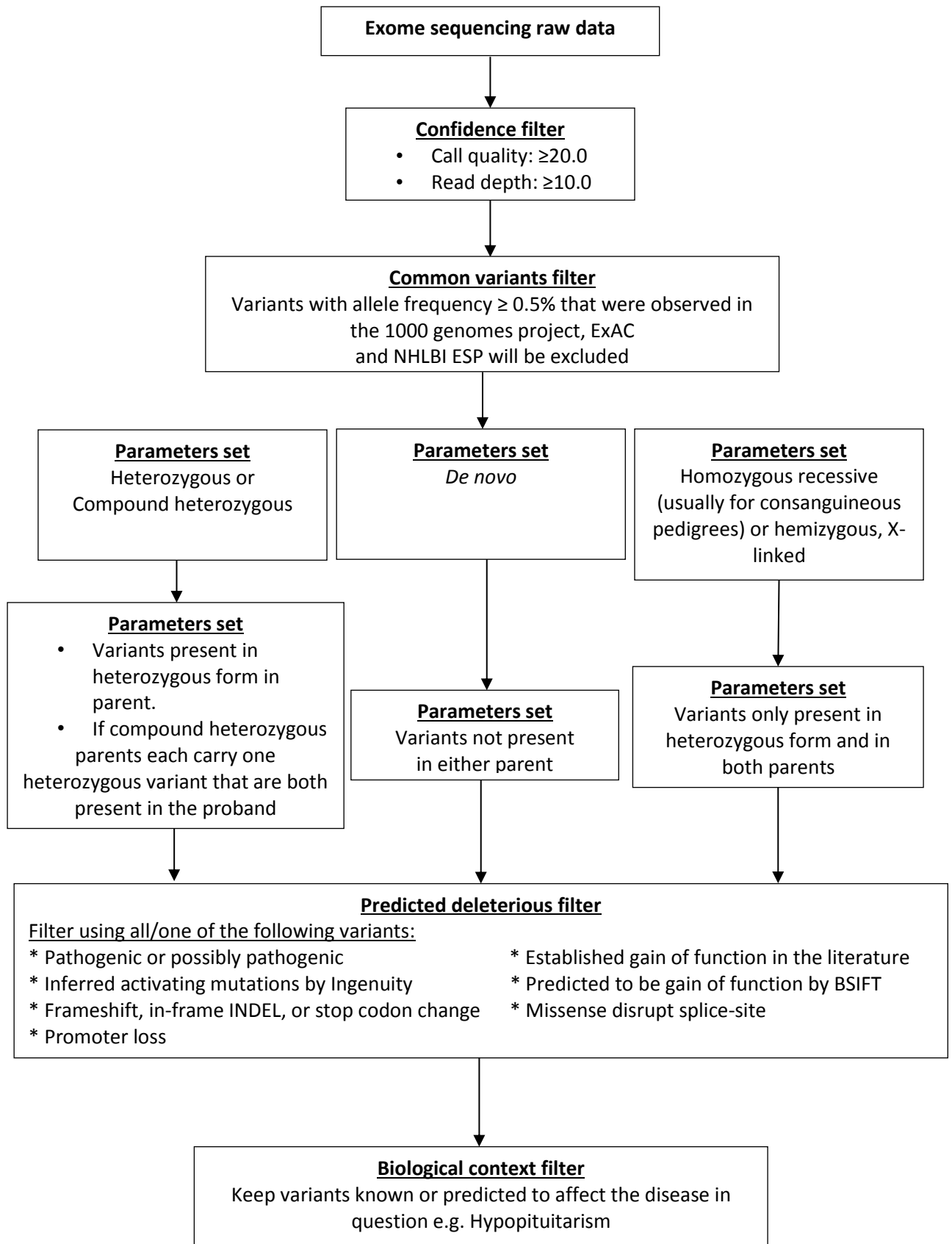
Construct transfected into HEK293T cells	Average luciferase 1 st assay	Average luciferase 2 nd assay	Average luciferase 3 rd assay	AVERAGE MEAN	STD DEV OF AVERAGE MEAN	T-TEST p value	Significance
EV	1	1	1	1	0		
wtlhx4	4.48	3.15	5.70	4.44	1.28	0.012675	*
wtLHX4	10.58	7.42	12.87	10.29	2.74		
wtlhx4 + pou1f1	28.18	20.83	41.04	30.01	10.23		
pou1f1	3.79	3.42	3.84	3.68	0.23		
POU1F1	4.52	3.85	5.81	4.73	0.99		
t126m	4.48	2.76	4.52	3.92	1.01	0.006792	**
T126M	10.65	6.17	11.93	9.58	3.02		
t126m + pou1f1	36.02	22.66	42.10	33.60	9.95		

C

Construct transfected into HEK293T cells	Average luciferase 1 st assay	Average luciferase 2 nd assay	Average luciferase 3 rd assay	AVERAGE MEAN	STD DEV OF AVERAGE MEAN	T-Test p value	Significance
EV	1	1	1	1	0		
wtlhx4	3.18	3.62	5.85	4.22	1.43	0.000351	***
wtLHX4	8.22	7.72	15.73	10.56	4.49		
pou1f1	3.45	3.25	3.29	3.33	0.10		
POU1F1	4.57	4.15	4.65	4.46	0.27		
wtlhx4 +pou1f1	26.83	29.72	34.23	30.26	3.73		
r84c	1.76	1.98	2.62	2.12	0.45	0.001696	**
R84C	3.01	3.35	5.66	4.01	1.44		
wtlhx4 + r84c	5.89	6.20	10.51	7.53	2.59		
r84c + pou1f1	14.27	16.17	20.95	17.13	3.44	0.010974	*

Appendix 1: Transactivation assays investigating the *LHX4* (p.T126M) variant. (A-C) Each table represents results from three separate luciferase assays performed in triplicate. **(A)** Transfection of HEK293T cells with *LHX4* WT and the *LHX4* (p.T126M) mutant construct, to investigate the effect of *LHX4* on the α GSU promoter. Luciferase values were normalised to total protein. This relates to Figure 3.7 A in this study. **(B-C)** Transfection of constructs into HEK293T cells to investigate the effect of WT and mutant *LHX4* on the prolactin promoter. Luciferase values were normalised to *Renilla* luciferase values. These tables relate to Figure 3.7 B and C respectively. EV, empty vector; WT, wild-type; STD DEV; standard deviation.

Appendix 2



Appendix 2: Flowchart showing the exome sequencing data filtering process.

This criteria was used to identify novel variants and regions of interest in Pedigrees 2-7. The parameter settings may be altered accordingly to analyse the data in different contexts e.g. to search for *de novo* or compound heterozygous variants respectively. All possible parameter settings were used to analyse all exome data. ExAC, Exome Aggregation Consortium; NHLBI ESP, National Heart Lung and Blood Institute Exome Sequencing Project; BSIFT, Bi-directional Sorting Intolerant from Tolerant.

Appendix 3

A. De novo filter for Pedigree 2

Position	Reference Allele	Sample Allele	Variation Type	Gene Region	Gene Name	Transcript	Protein Variant	Patient genotype	Parent genotypes	Comment	ExAC database
Chr11_13 0332577	A	C	SNV	Exonic	ADAMTS 15	NM_139055	p.T482P	Het	Not present	BAM – poor call	Het: 91/ 241,052; 40/ 106,064 in European Hom: 0
Chr12_13 2628391	G	C	SNV	Exonic	DDX51	NM_175066	p.P123R	Het	Not present	BAM - poor call	Present in old version of ExAC, but was filtered out as this site has poor coverage
ChrX_167 11551	G	T	SNV	Exonic	CTPS2	NM_001144 002	p.F166L	Het	Not present	BAM OK and confirmed by Sanger sequencing	Not present in ExAC

B. Homozygous recessive filter for Pedigrees 3-6

Position	Reference Allele	Sample Allele	Variation Type	Gene Region	Gene Name	Transcript	Protein Variant	Patient/s genotype	Parent genotypes	Comment	ExAC database
Chr1_1040 93650	A	T	SNV	Exonic	RNPC3	NM_017619	p.L483F	Hom	Het in both	BAM OK and confirmed by Sanger sequencing	Not present in ExAC
Chr1_1076 00386	C	G	SNV	Exonic	PRMT6	NM_018137	p.P350R	Hom	Het in both	BAM OK and confirmed by Sanger sequencing	Not present in ExAC

C(i). De novo filter for Pedigree 7

Position	Reference Allele	Sample Allele	Variation Type	Gene Region	Gene Name	Transcript	Protein Variant	Patient/s genotype	Parent genotypes	Comment	ExAC database
Chr2_1481312	A	G	SNV	Exonic	TPO	NM_000547	p.N425S	Het	Het in father	BAM OK	Not present in ExAC
Chr3_1.96E+08	GGCGCG	-	Del	Exonic	FBXO45	NM_001105573	p.G25_A26del	Het	Het in both	Failed QC - within unstable repeats	Not present in ExAC
Chr5_55256258	-	TCACTCCAG	Dup	Exonic	IL6ST	NM_002184	p.D312_S314dup	Het	Not present	Failed QC - within unstable repeats	Not present in ExAC
Chr17_7751862	CAC	-	Del	Exonic	KDM6B	NM_001080424	p.T762del	Het	Not present	Failed QC - within unstable repeats	Not present in ExAC
Chr17_80039488	G	A	SNV	Exonic	FASN	NM_004104	p.A2132V	Het	Not present	BAM OK and confirmed by Sanger sequencing	Not present in ExAC

C(ii). X-linked filter for Pedigree 7

Position	Reference Allele	Sample Allele	Variation Type	Gene Region	Gene Name	Transcript	Protein Variant	Patient/s genotype	Parent genotypes	Comment	ExAC database
ChrX_55033575	A	G	SNV	Exonic	APEX2	NM_014481	p.M422V	Hemi	Het in mother	BAM OK and confirmed by Sanger sequencing	Het: 1/86,652; 8405 in African Hemi: 0
ChrX_1.34E+08	G	A	SNV	Exonic	ZNF449	NM_152695	p.R324Q	Hemi	Het in mother	BAM OK and confirmed by Sanger sequencing	Het:20/87355 Hemi: 5/87355

Appendix 3: Exome sequencing filtering results from Pedigrees 2-7. These tables present the variants generated from the exome sequencing filtering process performed by GOSgene. The exome data was filtered using all possible options of parameter settings that are illustrated in Appendix 2. Parameter settings that did not generate any potential variants are not shown. The tables displayed in this figure present all potential variants that were filtered using appropriate parameters for that given pedigree/s. The text highlighted in red represents variants that were ruled out as candidates. **A:** The *de novo* filter for Pedigree 2 revealed the variants listed in this table. The variants in *ADAMTS15* and *DDX51* were excluded due to the BAM file having a poor call; indicating that the exome regions containing these variants were not clearly covered by the software due to homologous regions elsewhere in the genome. In addition the *ADAMTS15* variant was present multiple times in heterozygous form in the ExAC database. This left the *CTPS2* (p.F166L) variant as the remaining candidate generated from the exome sequencing data analysis. **B:** The homozygous recessive filter for the consanguineous Pedigrees 3-6 revealed only two variants; *RNPC3* (p.L483F) and *PRMT6* (p.P350R), present in the six affected patients in homozygous form, and the one unaffected father in heterozygous form, that had exome sequencing performed, suggesting a founder effect from this geographically isolated population. **C(i):** The *de novo* filter for Pedigree 7 revealed the variants listed in this table. The variant in the *TPO* gene was excluded due to it being present in heterozygous form in the unaffected father. The variants in *FBXO45*, *IL6ST* and *KDM6B* failed the QC due to them being located within unstable repeats that have not been mapped accurately and are poorly represented by the software. In addition, the variant in *FBXO45* was present in both unaffected parents in heterozygous form. This left the *FASN* (p.A2132V) variant as the remaining candidate generated from the *de novo* filter. **C(ii):** The X-linked filter for Pedigree 7 also revealed two variants. The variant in *ZNF449* was excluded due to its multiple presence on the ExAC database, leaving the *APEX2* (p.M422V) variant as the remaining candidate generated from the X-linked filter, as it only appeared once in the ExAC database in heterozygous

and not in hemizygous form. Therefore both *FASN* (p.A2132V) and *APEX2* (p.M422V) variants are potential disease-causing candidates in Pedigree 7. There is no data shown from Pedigree 8 as only the X-chromosome was sequenced, revealing only one candidate gene; *EIF2S3* (p.P432S). SNV, single nucleotide variant; BAM, binary alignment map; del, deletion; dup, duplication; QC, quality control.

Appendix 4

Pedigree	Consanguineous	Ethnicity	Variant identified	Protein prediction model	Mode of inheritance	Age of patient at presentation	Main diagnosis	Endocrine deficits	Accompanying phenotypes
2	No	Afro-Caribbean	<u>CTPS2</u> ChrX: 16711551 c.498C>A, p.F166L	Polyphen2: Probably damaging SIFT: Tolerated	<i>De novo</i> Heterozygous	23 years	Congenital pan-hypopituitarism	GH, TSH, ACTH, LH and FSH	Left microtia; an absent pinna Severe conductive hearing loss Ciliary dyskinesia Complete situs inversus with dextrocardia Hypoplasia of the mandible Severe eczema Learning difficulties Left facial nerve palsy with left sided hemiparesis
3-6	Yes	Turkish	<u>RNPC3</u> Chr1: 104093650 c.1449A>T, p.L483F	<u>RNPC3</u> Polyphen2: Probably damaging SIFT: Damaging	Autosomal recessive (Both homozygous)	-	-GHD in all patients	GH	-

			<u>PRMT6</u> Chr1: 107600386 c.1049C>G, p.P350R	<u>PRMT6</u> Polyphen2: Benign SIFT: Tolerated			-Primary ovarian failure in the females		
7	No	African (mother) White European (father)	<u>FASN</u> Chr17: 80039488 c.6395C>T, p.A2132V <u>APEX2</u> ChrX: 55033575 c.1264A>G, p.M422V	<u>FASN</u> Polyphen2: Probably damaging SIFT: Damaging <u>APEX2</u> Polyphen2: Benign SIFT: Tolerated	<i>De novo</i> (Heterozygous) Autosomal recessive (Hemizygous) Inherited from asymptomatic heterozygous mother.	19 years	Congenital panhypopituitar ism	GH, TSH, ACTH, LH and FSH	Short stature Dysmorphic features Developmental delay Sensorineural deafness Hypoparathyroidism Retinal dystrophy Reynaud's syndrome Splénomegaly Aortic regurgitation

Appendix 4: Genotypes and phenotypes of patients in Pedigrees 2-7. The table summarises the parental ethnic origins, and the protein prediction model results from databases Polyphen and SIFT, for each variant in patients from Pedigrees 2-7 discussed in Chapter 4 in this study.

Appendix 5

A

Cell population	Average mean luciferase 1st assay	Average mean luciferase 1st assay	Average mean luciferase 1st assay	Average mean luciferase of triplicates	Standard Deviation	2-tailed unpaired T-Test Basal activity v cyto addition	2-tailed unpaired T-Test NS basal v KO basal	2-tailed unpaired T-Test NT basal v KO basal	2-tailed unpaired T-Test NS cyto v KO cyto	2-tailed unpaired T-Test NT cyto v KO cyto
Clone 4 Cyto	2019	2695	2151	2288	358.31	0.0067	1.612E-04	4.232E-05	0.0021	0.0020
Clone 4 Basal	1156	1275	1177	1203	63.52					
Non silencing Cyto	767	352	285	468	261.10	0.2628				
Non silencing Basal	373	211	189	258	100.49					
Non-transduced Cyto	833	773	667	758	84.06	0.0009				
Non-transduced Basal	265	161	264	230	59.76					

B

	Contrast	Std. Err.	Tukey		Tukey	
			t	P> t	[95% Conf. Interval]	
group1						
NS vs Clone 4	-1382.889	59.22111	-23.35	0.0000	-1526.114	-1239.663
NT vs Clone 4	-1253.889	59.22111	-21.17	0.0000	-1397.114	-1110.663
NT vs NS	129	59.22111	2.18	0.0853	-14.22554	272.2255
group2						
basal vs cyto	-609.5185	48.35384	-12.61	0.0000	-706.7404	-512.2966
group1#group2						
(NT#basal) vs (Clone 4#cyto)	-2063	83.7513	-24.63	0.0000	-2311.565	-1814.435
(NS#basal) vs (Clone 4#cyto)	-2030.889	83.7513	-24.25	0.0000	-2279.454	-1782.324
(NS#cyto) vs (Clone 4#cyto)	-1820.556	83.7513	-21.74	0.0000	-2069.121	-1571.991
(NT#cyto) vs (Clone 4#cyto)	-1530.444	83.7513	-18.27	0.0000	-1779.009	-1281.879
(Clone 4#basal) vs (Clone 4#cyto)	-1085.667	83.7513	-12.96	0.0000	-1334.232	-837.1016
(NT#basal) vs (Clone 4#basal)	-977.3333	83.7513	-11.67	0.0000	-1225.898	-728.7683
(NS#basal) vs (Clone 4#basal)	-945.2222	83.7513	-11.29	0.0000	-1193.787	-696.6572
(NS#cyto) vs (Clone 4#basal)	-734.8889	83.7513	-8.77	0.0000	-983.4539	-486.3238
(NT#basal) vs (NT#cyto)	-532.5556	83.7513	-6.36	0.0000	-781.1206	-283.9905
(NT#cyto) vs (Clone 4#basal)	-444.7778	83.7513	-5.31	0.0000	-693.3428	-196.2127
(NT#basal) vs (NS#cyto)	-242.4444	83.7513	-2.89	0.0597	-491.0095	6.120611
(NS#basal) vs (NS#cyto)	-210.3333	83.7513	-2.51	0.1411	-458.8984	38.23172
(NT#basal) vs (NS#basal)	-32.11111	83.7513	-0.38	0.9989	-280.6762	216.4539
(NT#cyto) vs (NS#cyto)	290.1111	83.7513	3.46	0.0136	41.54606	538.6762
(NT#cyto) vs (NS#basal)	500.4444	83.7513	5.98	0.0000	251.8794	749.0095

Appendix 5: Raw mean average data and statistical tests of apoptosis assays. (A): Apoptosis assays measuring cell death in *EIF2S3* KO cells compared to controls. The table shows the average normalised luciferase values from the three apoptosis assays performed in triplicate wells. Caspase 3/7 activity is measured with and without (basal) the addition of cytokine treatment. This table relates to the average mean graph in Figure 5.11 in Chapter 5. Cyto; cytokine, Clone 4; *EIF2S3* Knock out 1.1B4 cell line. **(B): Pairwise comparisons of data from apoptosis assays based on a fitted two-way ANOVA model with Tukey adjustment for multiple testing.** Comparisons of Clone 4 with both the NT and NS control populations were significantly different both at basal and with cytokine treatment. There was no significant difference between NS basal and NS after cytokine treatment, which is consistent with the two-tailed unpaired T-test analysis. There was no significant difference between both controls at basal level as shown in the table.

Appendix 6

<u>Borck et al. 2012 Mol Cell</u>	<u>Moortgat et al. 2016 AJMG</u>	<u>This study – Pedigree 8</u>
<i>EIF2S3</i> , p.I222T in the highly conserved GTP-binding (G) domain	<i>EIF2S3</i> , p.I259M and p.I465Sfs*4 in two unrelated pedigrees in the C-terminal domain	<i>EIF2S3</i> , p.P432S in the C-terminal domain
<u>Three males: 2 brothers and maternal uncle</u> <ul style="list-style-type: none"> • Intellectual disability (moderate to severe) • Microcephaly • Short stature with GHD in two patients • Facial dysmorphic features • Epilepsy • Thin corpus callosum on MRI • Enlarged lateral ventricles on MRI 	<u>Three males: 2 brothers, 1 unrelated male</u> <ul style="list-style-type: none"> • Severe intellectual disability • Microcephaly • GHD • Hypoglycaemia • Epilepsy • Thin corpus callosum on MRI • Normal pituitary and stalk on MRI • Global white matter loss on MRI 	<u>Three males: 2 brothers and maternal male cousin</u> <ul style="list-style-type: none"> • Central hypothyroidism • GHD • Unique pancreatic phenotype: fluctuation between hyperinsulinaemic hypoglycaemia and hyperglycaemia • Small anterior pituitary on MRI • Thin corpus callosum on MRI
<u>Unique additional features:</u> <ul style="list-style-type: none"> • Cleft lip/palate • Behavioural problems • Postpubertal microgenitalism • Obesity 	<u>Unique additional features:</u> <ul style="list-style-type: none"> • Spastic quadriplegia • Convergent strabismus • Delayed puberty • Genital abnormalities • Micrognathia (undersized jaw) • Hypotonia • Global reduction of white matter on MRI 	<u>Unique additional features:</u> <ul style="list-style-type: none"> • Developmental delay • Behavioural problems • Micropenis • Undescended testes • Severe eczema • Convergent squint • Generalised white matter loss on MRI • Ventricular asymmetry on MRI

Appendix 6: Clinical phenotypes of male patients with *EIF2S3* mutations from three separate studies. Clinical phenotypes are from previous reports by Borck *et al* and Moortgat *et al* respectively, and from this current study. Not all unique additional features listed under each study were present in every patient described; each male within the study had various combinations of these features.

References

- AL-MAJED, H. T., JONES, P. M., PERSAUD, S. J., SUGDEN, D., HUANG, G. C., AMIEL, S. & WHITEHOUSE, B. J. 2004. ACTH stimulates insulin secretion from MIN6 cells and primary mouse and human islets of Langerhans. *J Endocrinol*, 180, 155-66.
- ALATZOGLOU, K. S., ANDONIADOU, C. L., KELBERMAN, D., BUCHANAN, C. R., CROLLA, J., ARRIAZU, M. C., ROUBICEK, M., MONCET, D., MARTINEZ-BARBERA, J. P. & DATTANI, M. T. 2011a. SOX2 haploinsufficiency is associated with slow progressing hypothalamo-pituitary tumours. *Hum Mutat*, 32, 1376-80.
- ALATZOGLOU, K. S., AZRIYANTI, A., ROGERS, N., RYAN, F., CURRY, N., NOAKES, C., BIGNELL, P., HALL, G. W., LITTOOIJ, A. S., SAUNDERS, D., THOMAS, P., STEWART, H. & DATTANI, M. T. 2014a. SOX3 deletion in mouse and human is associated with persistence of the craniopharyngeal canal. *J Clin Endocrinol Metab*, 99, E2702-8.
- ALATZOGLOU, K. S. & DATTANI, M. T. 2009. Genetic forms of hypopituitarism and their manifestation in the neonatal period. *Early Hum Dev*, 85, 705-12.
- ALATZOGLOU, K. S., KELBERMAN, D., COWELL, C. T., PALMER, R., ARNHOLD, I. J., MELO, M. E., SCHNABEL, D., GRUETERS, A. & DATTANI, M. T. 2011b. Increased transactivation associated with SOX3 polyalanine tract deletion in a patient with hypopituitarism. *J Clin Endocrinol Metab*, 96, E685-90.
- ALATZOGLOU, K. S., KULAR, D. & DATTANI, M. T. 2015. Autosomal Dominant Growth Hormone Deficiency (Type II). *Pediatr Endocrinol Rev*, 12, 347-55.
- ALATZOGLOU, K. S., WEBB, E. A., LE TISSIER, P. & DATTANI, M. T. 2014b. Isolated growth hormone deficiency (GHD) in childhood and adolescence: recent advances. *Endocr Rev*, 35, 376-432.
- ALO, P. L., VISCA, P., MAZZAFERRO, S., SERPIERI, D. E., MANGONI, A., BOTTI, C., MONACO, S., CARBONI, M., ZARACA, F., TROMBETTA, G. & DI TONDO, U. 1999. Immunohistochemical study of fatty acid synthase, Ki67, proliferating cell nuclear antigen, and p53 expression in hyperplastic parathyroids. *Ann Diagn Pathol*, 3, 287-93.
- ALSALEEM, M., SAADEH, L., MISRA, A. & MADANI, S. 2016. Neonatal isolated ACTH deficiency (IAD): a potentially life-threatening but treatable cause of neonatal cholestasis. *BMJ Case Rep*, 2016.
- ALTON, E. W., ARMSTRONG, D. K., ASHBY, D., BAYFIELD, K. J., BILTON, D., BLOOMFIELD, E. V., BOYD, A. C., BRAND, J., BUCHAN, R., CALCEDO, R., CARVELLI, P., CHAN, M., CHENG, S. H., COLLIE, D. D., CUNNINGHAM, S., DAVIDSON, H. E., DAVIES, G., DAVIES, J. C., DAVIES, L. A., DEWAR, M. H., DOHERTY, A., DONOVAN, J., DWYER, N. S., ELGMATI, H. I., FEATHERSTONE, R. F., GAVINO, J., GEA-SORLI, S., GEDDES, D. M., GIBSON, J. S., GILL, D. R., GREENING, A. P., GRIESENBACH, U., HANSELL, D. M., HARMAN, K., HIGGINS, T. E., HODGES, S. L., HYDE, S. C., HYNDMAN, L., INNES, J. A., JACOB, J., JONES, N., KEOGH, B. F., LIMBERIS, M. P., LLOYD-EVANS, P., MACLEAN, A. W., MANVELL, M. C., MCCORMICK, D., MCGOVERN, M., MCLACHLAN, G., MENG, C., MONTERO, M. A., MILLIGAN, H., MOYCE, L. J., MURRAY, G. D., NICHOLSON, A. G., OSADOLOR, T., PARRA-LEITON, J., PORTEOUS, D. J., PRINGLE, I. A., PUNCH, E. K., PYTEL, K. M., QUITTNER, A. L., RIVELLINI, G., SAUNDERS, C. J., SCHEULE, R. K., SHEARD, S., SIMMONDS, N. J., SMITH, K., SMITH, S. N., SOUSSI, N., SOUSSI, S., SPEARING, E. J., STEVENSON, B. J., SUMNER-JONES, S. G., TURKKILA, M., URETA, R. P., WALLER, M. D., WASOWICZ, M. Y., WILSON, J. M. & WOLSTENHOLME-HOGG, P. 2015. Repeated nebulisation of non-viral CFTR gene therapy in patients with cystic fibrosis: a randomised, double-blind, placebo-controlled, phase 2b trial. *Lancet Respir Med*, 3, 684-91.

- ANDERSEN, B., PEARSE, R. V., 2ND, JENNE, K., SORNSON, M., LIN, S. C., BARTKE, A. & ROSENFELD, M. G. 1995. The Ames dwarf gene is required for Pit-1 gene activation. *Dev Biol*, 172, 495-503.
- ANG, S. L., JIN, O., RHINN, M., DAIGLE, N., STEVENSON, L. & ROSSANT, J. 1996. A targeted mouse *Otx2* mutation leads to severe defects in gastrulation and formation of axial mesoderm and to deletion of rostral brain. *Development*, 122, 243-52.
- ARGENTE, J., FLORES, R., GUTIERREZ-ARUMI, A., VERMA, B., MARTOS-MORENO, G. A., CUSCO, I., OGHABIAN, A., CHOWEN, J. A., FRILANDER, M. J. & PEREZ-JURADO, L. A. 2014. Defective minor spliceosome mRNA processing results in isolated familial growth hormone deficiency. *EMBO Mol Med*, 6, 299-306.
- ARNHOLD, I. J., FRANCA, M. M., CARVALHO, L. R., MENDONCA, B. B. & JORGE, A. A. 2015. Role of *GLI2* in hypopituitarism phenotype. *J Mol Endocrinol*, 54, R141-50.
- ASHKENAZI-HOFFNUNG, L., LEBENTHAL, Y., WYATT, A. W., RAGGE, N. K., DATEKI, S., FUKAMI, M., OGATA, T., PHILLIP, M. & GAT-YABLONSKI, G. 2010. A novel loss-of-function mutation in *OTX2* in a patient with anophthalmia and isolated growth hormone deficiency. *Hum Genet*, 127, 721-9.
- AVILION, A. A., NICOLIS, S. K., PEVNY, L. H., PEREZ, L., VIVIAN, N. & LOVELL-BADGE, R. 2003. Multipotent cell lineages in early mouse development depend on *SOX2* function. *Genes Dev*, 17, 126-40.
- BAHAR, A., AKHA, O., KASHI, Z. & VESGARI, Z. 2011. Hyperprolactinemia in association with subclinical hypothyroidism. *Caspian J Intern Med*, 2, 229-33.
- BANCALARI, R. E., GREGORY, L. C., MCCABE, M. J. & DATTANI, M. T. 2012. Pituitary gland development: an update. *Endocr Dev*, 23, 1-15.
- BAUMANN, G. 1999. Mutations in the growth hormone releasing hormone receptor: a new form of dwarfism in humans. *Growth Horm IGF Res*, 9 Suppl B, 24-9; discussion 29-30.
- BAUMANN, G. & MAHESHWARI, H. 1997. The Dwarfs of Sindh: severe growth hormone (GH) deficiency caused by a mutation in the GH-releasing hormone receptor gene. *Acta Paediatr Suppl*, 423, 33-8.
- BAXTER, R. C. & DAI, J. 1994. Purification and characterization of the acid-labile subunit of rat serum insulin-like growth factor binding protein complex. *Endocrinology*, 134, 848-52.
- BEARNE, S. L., HEKMAT, O. & MACDONNELL, J. E. 2001. Inhibition of Escherichia coli CTP synthase by glutamate gamma-semialdehyde and the role of the allosteric effector GTP in glutamine hydrolysis. *Biochem J*, 356, 223-32.
- BENDAVID, C., DUPE, V., ROCHARD, L., GICQUEL, I., DUBOURG, C. & DAVID, V. 2010. Holoprosencephaly: An update on cytogenetic abnormalities. *Am J Med Genet C Semin Med Genet*, 154c, 86-92.
- BETRAN, E., THORNTON, K. & LONG, M. 2002. Retroposed new genes out of the X in Drosophila. *Genome Res*, 12, 1854-9.
- BIANCO, S. D. & KAISER, U. B. 2009. The genetic and molecular basis of idiopathic hypogonadotropic hypogonadism. *Nat Rev Endocrinol*, 5, 569-76.
- BIGOS, S. T. & CARNES, T. D. 1982. Isolated ACTH deficiency presenting as severe hypercalcemia. *Am J Med Sci*, 284, 24-30.
- BIN-ABBAS, B., CONTE, F. A., GRUMBACH, M. M. & KAPLAN, S. L. 1999. Congenital hypogonadotropic hypogonadism and micropenis: effect of testosterone treatment on adult penile size why sex reversal is not indicated. *J Pediatr*, 134, 579-83.
- BIRKENFELD, A. L., LEE, H. Y., MAJUMDAR, S., JURCZAK, M. J., CAMPOREZ, J. P., JORNAYVAZ, F. R., FREDERICK, D. W., GUIGNI, B., KAHN, M., ZHANG, D., WEISMANN, D., ARAFAT, A. M., PFEIFFER, A. F., LIESKE, S., OYADOMARI, S., RON, D., SAMUEL, V. T. & SHULMAN, G. I. 2011. Influence of the hepatic eukaryotic initiation factor 2alpha

- (eIF2 α) endoplasmic reticulum (ER) stress response pathway on insulin-mediated ER stress and hepatic and peripheral glucose metabolism. *J Biol Chem*, 286, 36163-70.
- BIRNBERG, N. C., LISSITZKY, J. C., HINMAN, M. & HERBERT, E. 1983. Glucocorticoids regulate proopiomelanocortin gene expression in vivo at the levels of transcription and secretion. *Proc Natl Acad Sci U S A*, 80, 6982-6.
- BOCQUET, B., MARZOUKA, N. A., HEBRARD, M., MANES, G., SENECHAL, A., MEUNIER, I. & HAMEL, C. P. 2013. Homozygosity mapping in autosomal recessive retinitis pigmentosa families detects novel mutations. *Mol Vis*, 19, 2487-500.
- BOEHM, U., BOULOUX, P. M., DATTANI, M. T., DE ROUX, N., DODE, C., DUNKEL, L., DWYER, A. A., GIACOBINI, P., HARDELIN, J. P., JUUL, A., MAGHNIE, M., PITTELOUD, N., PREVOT, V., RAIVIO, T., TENA-SEMPERE, M., QUINTON, R. & YOUNG, J. 2015. Expert consensus document: European Consensus Statement on congenital hypogonadotropic hypogonadism--pathogenesis, diagnosis and treatment. *Nat Rev Endocrinol*, 11, 547-64.
- BOISCLAIR, Y. R., RHOADS, R. P., UEKI, I., WANG, J. & OOI, G. T. 2001. The acid-labile subunit (ALS) of the 150 kDa IGF-binding protein complex: an important but forgotten component of the circulating IGF system. *J Endocrinol*, 170, 63-70.
- BORCK, G., SHIN, B. S., STILLER, B., MIMOUNI-BLOCH, A., THIELE, H., KIM, J. R., THAKUR, M., SKINNER, C., ASCHENBACH, L., SMIRIN-YOSEF, P., HAR-ZAHAV, A., NURNBERG, G., ALTMULLER, J., FROMMOLT, P., HOFMANN, K., KONEN, O., NURNBERG, P., MUNNICH, A., SCHWARTZ, C. E., GOTHELF, D., COLLEAUX, L., DEVER, T. E., KUBISCH, C. & BASEL-VANAGAITE, L. 2012. eIF2 γ mutation that disrupts eIF2 complex integrity links intellectual disability to impaired translation initiation. *Mol Cell*, 48, 641-6.
- BOTTNER, A., KELLER, E., KRATZSCH, J., STOBBE, H., WEIGEL, J. F., KELLER, A., HIRSCH, W., KIESS, W., BLUM, W. F. & PFAFFLE, R. W. 2004. PROP1 mutations cause progressive deterioration of anterior pituitary function including adrenal insufficiency: a longitudinal analysis. *J Clin Endocrinol Metab*, 89, 5256-65.
- BOULWARE, S. D., TAMBORLANE, W. V., MATTHEWS, L. S. & SHERWIN, R. S. 1992. Diverse effects of insulin-like growth factor I on glucose, lipid, and amino acid metabolism. *Am J Physiol*, 262, E130-3.
- BOWLES, D. E., MCPHEE, S. W., LI, C., GRAY, S. J., SAMULSKI, J. J., CAMP, A. S., LI, J., WANG, B., MONAHAN, P. E., RABINOWITZ, J. E., GRIEGER, J. C., GOVINDASAMY, L., AGBANDJE-MCKENNA, M., XIAO, X. & SAMULSKI, R. J. 2012. Phase 1 gene therapy for Duchenne muscular dystrophy using a translational optimized AAV vector. *Mol Ther*, 20, 443-55.
- BRODER, M. S., CHANG, E., CHEREPANOV, D., NEARY, M. P. & LUDLAM, W. H. 2016. IDENTIFICATION OF POTENTIAL MARKERS FOR CUSHING DISEASE. *Endocr Pract*, 22, 567-74.
- BRODSKY, M. C. & GLASIER, C. M. 1993. Optic nerve hypoplasia. Clinical significance of associated central nervous system abnormalities on magnetic resonance imaging. *Arch Ophthalmol*, 111, 66-74.
- BROWN, S. A., WARBURTON, D., BROWN, L. Y., YU, C. Y., ROEDER, E. R., STENGLER-RUTKOWSKI, S., HENNEKAM, R. C. & MUENKE, M. 1998. Holoprosencephaly due to mutations in ZIC2, a homologue of Drosophila odd-paired. *Nat Genet*, 20, 180-3.
- BRUNERT, D. & TSUNO, Y. 2016. Cell-Type-Specific Modulation of Sensory Responses in Olfactory Bulb Circuits by Serotonergic Projections from the Raphe Nuclei. 36, 6820-35.

- BURKOVICS, P., SZUKACSOV, V., UNK, I. & HARACSKA, L. 2006. Human Ape2 protein has a 3'-5' exonuclease activity that acts preferentially on mismatched base pairs. *Nucleic Acids Res*, 34, 2508-15.
- BYLUND, M., ANDERSSON, E., NOVITCH, B. G. & MUHR, J. 2003. Vertebrate neurogenesis is counteracted by Sox1-3 activity. *Nat Neurosci*, 6, 1162-8.
- CAMPER, S. A., SAUNDERS, T. L., KATZ, R. W. & REEVES, R. H. 1990. The Pit-1 transcription factor gene is a candidate for the murine Snell dwarf mutation. *Genomics*, 8, 586-90.
- CAPRA, V., SEVERINO, M., ROSSI, A., NOZZA, P., DONEDA, C., PERRI, K., PAVANELLO, M., FIORIO, P., GIMELLI, G., TASSANO, E. & DI BATTISTA, E. 2014. Pituitary deficiency and congenital infiltrating lipomatosis of the face in a girl with deletion of chromosome 1q24.3q31.1. *Am J Med Genet A*, 164a, 495-9.
- CARIBONI, A. & MAGGI, R. 2006. Kallmann's syndrome, a neuronal migration defect. *Cell Mol Life Sci*, 63, 2512-26.
- CASTINETTI, F., SAVEANU, A., REYNAUD, R., QUENTIEN, M. H., BUFFIN, A., BRAUNER, R., KAFFEL, N., ALBAREL, F., GUEDJ, A. M., EL KHOLY, M., AMIN, M., ENJALBERT, A., BARLIER, A. & BRUE, T. 2008. A novel dysfunctional LHX4 mutation with high phenotypical variability in patients with hypopituitarism. *J Clin Endocrinol Metab*, 93, 2790-9.
- CAVAZZANA-CALVO, M., HACEIN-BEY, S., DE SAINT BASILE, G., GROSS, F., YVON, E., NUSBAUM, P., SELZ, F., HUE, C., CERTAIN, S., CASANOVA, J. L., BOUSSO, P., DEIST, F. L. & FISCHER, A. 2000. Gene therapy of human severe combined immunodeficiency (SCID)-X1 disease. *Science*, 288, 669-72.
- CHAKRABARTI, A. & MAITRA, U. 1992. Release and recycling of eukaryotic initiation factor 2 in the formation of an 80 S ribosomal polypeptide chain initiation complex. *J Biol Chem*, 267, 12964-72.
- CHIRALA, S. S., CHANG, H., MATZUK, M., ABU-ELHEIGA, L., MAO, J., MAHON, K., FINEGOLD, M. & WAKIL, S. J. 2003. Fatty acid synthesis is essential in embryonic development: fatty acid synthase null mutants and most of the heterozygotes die in utero. *Proc Natl Acad Sci U S A*, 100, 6358-63.
- COGAN, J. D. & PHILLIPS, J. A., 3RD 2006. GH1 gene deletions and IGHD type 1A. *Pediatr Endocrinol Rev*, 3 Suppl 3, 480-8.
- COHEN, L. E. 2012. Genetic disorders of the pituitary. *Curr Opin Endocrinol Diabetes Obes*, 19, 33-9.
- COLVIN, S. C., MULLEN, R. D., PFAEFFLE, R. W. & RHODES, S. J. 2009. LHX3 and LHX4 transcription factors in pituitary development and disease. *Pediatr Endocrinol Rev*, 6 Suppl 2, 283-90.
- CONRAD, B., KRIEBEL, J. & HETZEL, W. D. 1978. Hereditary bimanual synkinesis combined with hypogonadotropic hypogonadism and anosmia in four brothers. *J Neurol*, 218, 263-74.
- CORREA, F. A., TRARBACH, E. B., TUSSET, C., LATRONICO, A. C., MONTENEGRO, L. R., CARVALHO, L. R., FRANCA, M. M., OTTO, A. P., COSTALONGA, E. F., BRITO, V. N., ABREU, A. P., NISHI, M. Y., JORGE, A. A., ARNHOLD, I. J., SIDIS, Y., PITTELOUD, N. & MENDONCA, B. B. 2015. FGFR1 and PROKR2 rare variants found in patients with combined pituitary hormone deficiencies. *Endocr Connect*, 4, 100-7.
- COUTURE, C., SAVEANU, A., BARLIER, A., CAREL, J. C., FASSNACHT, M., FLUCK, C. E., HOUANG, M., MAES, M., PHAN-HUG, F., ENJALBERT, A., DROUIN, J., BRUE, T. & VALLETTE, S. 2012. Phenotypic homogeneity and genotypic variability in a large series of congenital isolated ACTH-deficiency patients with TPIT gene mutations. *J Clin Endocrinol Metab*, 97, E486-95.

- CROISSANDEAU, G., GROUSELLE, D., LI, J. Y., ROCHE, M., PEILLON, F. & LE DAFNIET, M. 1994. Hypothyroidism increases TRH and TRH precursor levels in rat anterior pituitary. *Biochem Biophys Res Commun*, 201, 1248-54.
- DALLMAN, M. F. 2005. Adrenocortical function, feedback, and alphabet soup. *Am J Physiol Endocrinol Metab*, 289, E361-2.
- DASEN, J. S., MARTINEZ BARBERA, J. P., HERMAN, T. S., CONNELL, S. O., OLSON, L., JU, B., TOLLKUHNN, J., BAEK, S. H., ROSE, D. W. & ROSENFELD, M. G. 2001. Temporal regulation of a paired-like homeodomain repressor/TLE corepressor complex and a related activator is required for pituitary organogenesis. *Genes Dev*, 15, 3193-207.
- DATEKI, S., FUKAMI, M., UEMATSU, A., KAJI, M., ISO, M., ONO, M., MIZOTA, M., YOKOYA, S., MOTOMURA, K., KINOSHITA, E., MORIUCHI, H. & OGATA, T. 2010. Mutation and gene copy number analyses of six pituitary transcription factor genes in 71 patients with combined pituitary hormone deficiency: identification of a single patient with LHX4 deletion. *J Clin Endocrinol Metab*, 95, 4043-7.
- DATTANI, M. T. 2004. Novel insights into the aetiology and pathogenesis of hypopituitarism. *Horm Res*, 62 Suppl 3, 1-13.
- DATTANI, M. T., MARTINEZ-BARBERA, J. P., THOMAS, P. Q., BRICKMAN, J. M., GUPTA, R., MARTENSSON, I. L., TORESSON, H., FOX, M., WALES, J. K., HINDMARSH, P. C., KRAUSS, S., BEDDINGTON, R. S. & ROBINSON, I. C. 1998. Mutations in the homeobox gene HESX1/Hesx1 associated with septo-optic dysplasia in human and mouse. *Nat Genet*, 19, 125-33.
- DAVIS, S. W., CASTINETTI, F., CARVALHO, L. R., ELLSWORTH, B. S., POTOK, M. A., LYONS, R. H., BRINKMEIER, M. L., RAETZMAN, L. T., CARNINCI, P., MORTENSEN, A. H., HAYASHIZAKI, Y., ARNHOLD, I. J., MENDONCA, B. B., BRUE, T. & CAMPER, S. A. 2010. Molecular mechanisms of pituitary organogenesis: In search of novel regulatory genes. *Mol Cell Endocrinol*, 323, 4-19.
- DE MORSIER, G. 1956. [Studies on malformation of cranio-encephalic sutures. III. Agenesis of the septum lucidum with malformation of the optic tract]. *Schweiz Arch Neurol Psychiatr*, 77, 267-92.
- DELHASE, M., CASTRILLO, J. L., DE LA HOYA, M., RAJAS, F. & HOOGHE-PETERS, E. L. 1996. AP-1 and Oct-1 transcription factors down-regulate the expression of the human PIT1/GHF1 gene. *J Biol Chem*, 271, 32349-58.
- DES GEORGES, A., DHOTE, V., KUHN, L., HELLEN, C. U., PESTOVA, T. V., FRANK, J. & HASHEM, Y. 2015. Structure of mammalian eIF3 in the context of the 43S preinitiation complex. *Nature*.
- DI LORENZO, A., YANG, Y., MACALUSO, M. & BEDFORD, M. T. 2014. A gain-of-function mouse model identifies PRMT6 as a NF-kappaB coactivator. *Nucleic Acids Res*, 42, 8297-309.
- DIACZOK, D., DIVALL, S., MATSUO, I., WONDISFORD, F. E., WOLFE, A. M. & RADOVICK, S. 2011. Deletion of Otx2 in GnRH neurons results in a mouse model of hypogonadotropic hypogonadism. *Mol Endocrinol*, 25, 833-46.
- DIACZOK, D., ROMERO, C., ZUNICH, J., MARSHALL, I. & RADOVICK, S. 2008. A novel dominant negative mutation of OTX2 associated with combined pituitary hormone deficiency. *J Clin Endocrinol Metab*, 93, 4351-9.
- DMITRIEV, S. E., STOLBOUSHKINA, E. A., TEREININ, I. M., ANDREEV, D. E., GARBER, M. B. & SHATSKY, I. N. 2011. Archaeal translation initiation factor aIF2 can substitute for eukaryotic eIF2 in ribosomal scanning during mammalian 48S complex formation. *J Mol Biol*, 413, 106-14.
- DODE, C., TEIXEIRA, L., LEVILLIERS, J., FOUVEAUT, C., BOUCHARD, P., KOTTLER, M. L., LESPINASSE, J., LIENHARDT-ROUSSIE, A., MATHIEU, M., MOERMAN, A., MORGAN, G., MURAT, A., TOUBLANC, J. E., WOLCZYNSKI, S., DELPECH, M., PETIT, C., YOUNG, J. &

- HARDELIN, J. P. 2006. Kallmann syndrome: mutations in the genes encoding prokineticin-2 and prokineticin receptor-2. *PLoS Genet*, 2, e175.
- DOROFTEI, N. A., DE RUDDER, C., DE VISSCHER, N. & HANON, F. 2016. Isolated ACTH deficiency in a patient with empty sella as revealed by severe hyponatremia. *Acta Clin Belg*, 1-4.
- DOUCHI, T., NAKAE, M., YAMAMOTO, S., IWAMOTO, I., OKI, T. & NAGATA, Y. 2001. A woman with isolated prolactin deficiency. *Acta Obstet Gynecol Scand*, 80, 368-70.
- DOUDNA, J. A. & CHARPENTIER, E. 2014. Genome editing. The new frontier of genome engineering with CRISPR-Cas9. *Science*, 346, 1258096.
- DUBOURG, C., LAZARO, L., PASQUIER, L., BENDAVID, C., BLAYAU, M., LE DUFF, F., DUROU, M. R., ODENT, S. & DAVID, V. 2004. Molecular screening of SHH, ZIC2, SIX3, and TGIF genes in patients with features of holoprosencephaly spectrum: Mutation review and genotype-phenotype correlations. *Hum Mutat*, 24, 43-51.
- DUNCAN, P. J. & SHIPSTON, M. J. 2016. BK Channels and the Control of the Pituitary. *Int Rev Neurobiol*, 128, 343-68.
- EDERY, P., MARCAILLOU, C., SAHBATOU, M., LABALME, A., CHASTANG, J., TOURAINE, R., TUBACHER, E., SENNI, F., BOBER, M. B., NAMPOOTHIRI, S., JOUK, P. S., STEICHEN, E., BERLAND, S., TOUTAIN, A., WISE, C. A., SANLAVILLE, D., ROUSSEAU, F., CLERGET-DARPOUX, F. & LEUTENEGGER, A. L. 2011. Association of TALS developmental disorder with defect in minor splicing component U4atac snRNA. *Science*, 332, 240-3.
- EHLERS ET AL., H., L, 2013. Gonadotropin-releasing Hormone (GnRH) and the GnRH Receptor (GnRHR). *Glob. libr. women's med*.
- EL-ANDALOUSSI, N., VALOVKA, T., TOUEILLE, M., STEINACHER, R., FOCKE, F., GEHRIG, P., COVIC, M., HASSA, P. O., SCHAR, P., HUBSCHER, U. & HOTTIGER, M. O. 2006. Arginine methylation regulates DNA polymerase beta. *Mol Cell*, 22, 51-62.
- ENDRIZZI, J. A., KIM, H., ANDERSON, P. M. & BALDWIN, E. P. 2004. Crystal structure of Escherichia coli cytidine triphosphate synthetase, a nucleotide-regulated glutamine amidotransferase/ATP-dependent amidoligase fusion protein and homologue of anticancer and antiparasitic drug targets. *Biochemistry*, 43, 6447-63.
- ESKANDARANI, H. A. 2009. Pre-implantation genetic diagnosis in the Gulf Cooperative Council countries: utilization and ethical attitudes. *Hum Reprod Genet Ethics*, 15, 68-74.
- FALARDEAU, J., CHUNG, W. C., BEENKEN, A., RAIVIO, T., PLUMMER, L., SIDIS, Y., JACOBSON-DICKMAN, E. E., ELISEENKOVA, A. V., MA, J., DWYER, A., QUINTON, R., NA, S., HALL, J. E., HUOT, C., ALOIS, N., PEARCE, S. H., COLE, L. W., HUGHES, V., MOHAMMADI, M., TSAI, P. & PITTELOUD, N. 2008. Decreased FGF8 signaling causes deficiency of gonadotropin-releasing hormone in humans and mice. *J Clin Invest*, 118, 2822-31.
- FASOULIOTIS, S. J. & SCHENKER, J. G. 1998. Preimplantation genetic diagnosis principles and ethics. *Hum Reprod*, 13, 2238-45.
- FILGES, I., BISCHOF-RENNER, A., ROTHLSBERGER, B., POTTHOFF, C., GLANZMANN, R., GUNTARD, J., SCHNEIDER, J., HUBER, A. R., ZUMSTEG, U., MINY, P. & SZINNAI, G. 2012. Panhypopituitarism presenting as life-threatening heart failure caused by an inherited microdeletion in 1q25 including LHX4. *Pediatrics*, 129, e529-34.
- FINDLAY, I. 2000. Pre-implantation genetic diagnosis. *Br Med Bull*, 56, 672-90.
- FLYNN, A. & PROUD, C. G. 1996. The role of eIF4 in cell proliferation. *Cancer Surv*, 27, 293-310.
- FRAIETTA, R., ZYLBERSTEJN, D. S. & ESTEVES, S. C. 2013. Hypogonadotropic hypogonadism revisited. *Clinics (Sao Paulo)*, 68 Suppl 1, 81-8.

- FRANTZ, G. D., WEIMANN, J. M., LEVIN, M. E. & MCCONNELL, S. K. 1994. Otx1 and Otx2 define layers and regions in developing cerebral cortex and cerebellum. *J Neurosci*, 14, 5725-40.
- FREEMAN, M. E., KANYICKA, B., LERANT, A. & NAGY, G. 2000. Prolactin: structure, function, and regulation of secretion. *Physiol Rev*, 80, 1523-631.
- GARCIA, M., FERNANDEZ, A. & MORENO, J. C. 2014. Central hypothyroidism in children. *Endocr Dev*, 26, 79-107.
- GASPAR, H. B., PARSLEY, K. L., HOWE, S., KING, D., GILMOUR, K. C., SINCLAIR, J., BROUNS, G., SCHMIDT, M., VON KALLE, C., BARINGTON, T., JAKOBSEN, M. A., CHRISTENSEN, H. O., AL GHONAIUM, A., WHITE, H. N., SMITH, J. L., LEVINSKY, R. J., ALI, R. R., KINNON, C. & THRASHER, A. J. 2004. Gene therapy of X-linked severe combined immunodeficiency by use of a pseudotyped gammaretroviral vector. *Lancet*, 364, 2181-7.
- GASTON-MASSUET, C., MCCABE, M. J., SCAGLIOTTI, V., YOUNG, R. M., CARRENO, G., GREGORY, L. C., JAYAKODY, S. A., POZZI, S., GUALTIERI, A., BASU, B., KONIORDOU, M., WU, C. I., BANCALARI, R. E., RAHIKKALA, E., VEIJOLA, R., LOPPONEN, T., GRAZIOLA, F., TURTON, J., SIGNORE, M., MOUSAVY GHARAVY, S. N., CHAROLIDI, N., SOKOL, S. Y., ANDONIADOU, C. L., WILSON, S. W., MERRILL, B. J., DATTANI, M. T. & MARTINEZ-BARBERA, J. P. 2016. Transcription factor 7-like 1 is involved in hypothalamo-pituitary axis development in mice and humans. *Proc Natl Acad Sci U S A*, 113, E548-57.
- GOLDSMITH, S., LOVELL-BADGE, R. & RIZZOTI, K. 2016. SOX2 is sequentially required for progenitor proliferation and lineage specification in the developing pituitary. *Development*, 143, 2376-88.
- GORBENKO DEL BLANCO, D., ROMERO, C. J., DIACZOK, D., DE GRAAFF, L. C., RADOVICK, S. & HOKKEN-KOELEGA, A. C. 2012. A novel OTX2 mutation in a patient with combined pituitary hormone deficiency, pituitary malformation, and an underdeveloped left optic nerve. *Eur J Endocrinol*, 167, 441-52.
- GRECHUKHINA, O., ENGLISH, D. P., MILLER, D. & RATNER, E. 2016. Challenging Case of Postmenopausal Bleeding and Complete Urogenital Duplication. *Am J Case Rep*, 17, 331-6.
- GREGORY, L. C., ALATZOGLOU, K. S., MCCABE, M. J., HINDMARSH, P. C., SALDANHA, J. W., ROMANO, N., LE TISSIER, P. & DATTANI, M. T. 2016. Partial loss of function of the GHRH Receptor leads to mild Growth Hormone Deficiency. *J Clin Endocrinol Metab*, jc20162254.
- GREGORY, L. C., GASTON-MASSUET, C., ANDONIADOU, C. L., CARRENO, G., WEBB, E. A., KELBERMAN, D., MCCABE, M. J., PANAGIOTAKOPOULOS, L., SALDANHA, J. W., SPOUDEAS, H. A., TORPIANO, J., ROSSI, M., RAINE, J., CANHAM, N., MARTINEZ-BARBERA, J. P. & DATTANI, M. T. 2015a. The role of the sonic hedgehog signalling pathway in patients with midline defects and congenital hypopituitarism. *Clin Endocrinol (Oxf)*, 82, 728-38.
- GREGORY, L. C., HUMAYUN, K. N., TURTON, J. P., MCCABE, M. J., RHODES, S. J. & DATTANI, M. T. 2015b. Novel Lethal Form of Congenital Hypopituitarism Associated With the First Recessive LHX4 Mutation. *J Clin Endocrinol Metab*, 100, 2158-64.
- GRIPP, K. W., WOTTON, D., EDWARDS, M. C., ROESSLER, E., ADES, L., MEINECKE, P., RICHIERI-COSTA, A., ZACKAI, E. H., MASSAGUE, J., MUENKE, M. & ELLEDGE, S. J. 2000. Mutations in TGIF cause holoprosencephaly and link NODAL signalling to human neural axis determination. *Nat Genet*, 25, 205-8.
- GUCLU, M., CANDER, S., KIYICI, S., VATANSEVER, E., HACIHASANOGLU, A. B. & KISAKOL, G. 2015. Serum macroprolactin levels in pregnancy and association with thyroid autoimmunity. *BMC Endocr Disord*, 15, 31.

- GUO-PARKE, H., MCCLUSKEY, J. T., KELLY, C., HAMID, M., MCCLENAGHAN, N. H. & FLATT, P. R. 2012. Configuration of electrofusion-derived human insulin-secreting cell line as pseudoislets enhances functionality and therapeutic utility. *J Endocrinol*, 214, 257-65.
- HACEIN-BEY-ABINA, S., VON KALLE, C., SCHMIDT, M., LE DEIST, F., WULFFRAAT, N., MCINTYRE, E., RADFORD, I., VILLEVAL, J. L., FRASER, C. C., CAVAZZANA-CALVO, M. & FISCHER, A. 2003a. A serious adverse event after successful gene therapy for X-linked severe combined immunodeficiency. *N Engl J Med*, 348, 255-6.
- HACEIN-BEY-ABINA, S., VON KALLE, C., SCHMIDT, M., MCCORMACK, M. P., WULFFRAAT, N., LEBOULCH, P., LIM, A., OSBORNE, C. S., PAWLIUK, R., MORILLON, E., SORENSEN, R., FORSTER, A., FRASER, P., COHEN, J. I., DE SAINT BASILE, G., ALEXANDER, I., WINTERGERST, U., FREBOURG, T., AURIAS, A., STOPPA-LYONNET, D., ROMANA, S., RADFORD-WEISS, I., GROSS, F., VALENSI, F., DELABESSE, E., MACINTYRE, E., SIGAUX, F., SOULIER, J., LEIVA, L. E., WISSLER, M., PRINZ, C., RABBITTS, T. H., LE DEIST, F., FISCHER, A. & CAVAZZANA-CALVO, M. 2003b. LMO2-associated clonal T cell proliferation in two patients after gene therapy for SCID-X1. *Science*, 302, 415-9.
- HADI, M. Z., GINALSKI, K., NGUYEN, L. H. & WILSON, D. M., 3RD 2002. Determinants in nuclease specificity of Ape1 and Ape2, human homologues of Escherichia coli exonuclease III. *J Mol Biol*, 316, 853-66.
- HASTINGS, M. L., RESTA, N., TRAUM, D., STELLA, A., GUANTI, G. & KRAINER, A. R. 2005. An LKB1 AT-AC intron mutation causes Peutz-Jeghers syndrome via splicing at noncanonical cryptic splice sites. *Nat Struct Mol Biol*, 12, 54-9.
- HAYES, F., DWYER, A. & PITTELOUD, N. 2000. Hypogonadotropic Hypogonadism (Hh) and Gonadotropin Therapy. In: DE GROOT, L. J., BECK-PECCOZ, P., CHROUSOS, G., DUNGAN, K., GROSSMAN, A., HERSHMAN, J. M., KOCH, C., MCLACHLAN, R., NEW, M., REBAR, R., SINGER, F., VINIK, A. & WEICKERT, M. O. (eds.) *Endotext*. South Dartmouth (MA): MDText.com, Inc.
- HE, H., LIYANARACHCHI, S., AKAGI, K., NAGY, R., LI, J., DIETRICH, R. C., LI, W., SEBASTIAN, N., WEN, B., XIN, B., SINGH, J., YAN, P., ALDER, H., HAAN, E., WIECZOREK, D., ALBRECHT, B., PUFFENBERGER, E., WANG, H., WESTMAN, J. A., PADGETT, R. A., SYMER, D. E. & DE LA CHAPELLE, A. 2011. Mutations in U4atac snRNA, a component of the minor spliceosome, in the developmental disorder MOPD I. *Science*, 332, 238-40.
- HERMESZ, E., MACKEM, S. & MAHON, K. A. 1996. Rpx: a novel anterior-restricted homeobox gene progressively activated in the prechordal plate, anterior neural plate and Rathke's pouch of the mouse embryo. *Development*, 122, 41-52.
- HERR, W. & CLEARY, M. A. 1995. The POU domain: versatility in transcriptional regulation by a flexible two-in-one DNA-binding domain. *Genes Dev*, 9, 1679-93.
- HERSHEY, J. W. 2015. The role of eIF3 and its individual subunits in cancer. *Biochim Biophys Acta*, 1849, 792-800.
- HILLIER, S. G. 2001. Gonadotropic control of ovarian follicular growth and development. *Mol Cell Endocrinol*, 179, 39-46.
- HINNEBUSCH, A. G. 2011. Molecular mechanism of scanning and start codon selection in eukaryotes. *Microbiol Mol Biol Rev*, 75, 434-67, first page of table of contents.
- HOLLIDAY, R. 1989. DNA methylation and epigenetic mechanisms. *Cell Biophys*, 15, 15-20.
- HONG, M. & KRAUSS, R. S. 2013. Rescue of holoprosencephaly in fetal alcohol-exposed Cdon mutant mice by reduced gene dosage of Ptch1. *PLoS One*, 8, e79269.
- HOUSSET, M., SAMUEL, A., ETTAICHE, M., BEMELMANS, A., BEBY, F., BILLON, N. & LAMONERIE, T. 2013. Loss of Otx2 in the adult retina disrupts retinal pigment epithelium function, causing photoreceptor degeneration. *J Neurosci*, 33, 9890-904.
- HU, J., CHE, L., LI, L., PILO, M. G., CIGLIANO, A., RIBBACK, S., LI, X., LATTE, G., MELA, M., EVERT, M., DOMBROWSKI, F., ZHENG, G., CHEN, X. & CALVISI, D. F. 2016. Co-activation of

- AKT and c-Met triggers rapid hepatocellular carcinoma development via the mTORC1/FASN pathway in mice. *Sci Rep*, 6, 20484.
- HUANG, H. K., YOON, H., HANNIG, E. M. & DONAHUE, T. F. 1997. GTP hydrolysis controls stringent selection of the AUG start codon during translation initiation in *Saccharomyces cerevisiae*. *Genes Dev*, 11, 2396-413.
- HUGHES, J. N., AUBERT, M., HEATLIE, J., GARDNER, A., GECZ, J., MORGAN, T., BELSKY, J. & THOMAS, P. Q. 2016. Identification of an IGSF1-specific deletion in a five generation pedigree with X-linked Central Hypothyroidism without macroorchidism. *Clin Endocrinol (Oxf)*.
- HUTTON ET AL., P. L. 2009. Sox Gene Expression. *Developmental Neurobiology*. Elsevier.
- HUTTON, S. R. & PEVNY, L. H. 2011. SOX2 expression levels distinguish between neural progenitor populations of the developing dorsal telencephalon. *Dev Biol*, 352, 40-7.
- IDE, Y., TSUCHIMOTO, D., TOMINAGA, Y., NAKASHIMA, M., WATANABE, T., SAKUMI, K., OHNO, M. & NAKABEPPU, Y. 2004. Growth retardation and dyslymphopoiesis accompanied by G2/M arrest in APEX2-null mice. *Blood*, 104, 4097-103.
- IGUCHI, G., OKIMURA, Y., TAKAHASHI, T., MIZUNO, I., FUMOTO, M., TAKAHASHI, Y., KAJI, H., ABE, H. & CHIHARA, K. 1999. Cloning and characterization of the 5'-flanking region of the human growth hormone-releasing hormone receptor gene. *J Biol Chem*, 274, 12108-14.
- IWAMA, S., WELT, C. K., ROMERO, C. J., RADOVICK, S. & CATUREGLI, P. 2013. Isolated prolactin deficiency associated with serum autoantibodies against prolactin-secreting cells. *J Clin Endocrinol Metab*, 98, 3920-5.
- JAYAKODY, S. A., ANDONIADOU, C. L., GASTON-MASSUET, C., SIGNORE, M., CARIBONI, A., BOULOUX, P. M., LE TISSIER, P., PEVNY, L. H., DATTANI, M. T. & MARTINEZ-BARBERA, J. P. 2012. SOX2 regulates the hypothalamic-pituitary axis at multiple levels. *J Clin Invest*, 122, 3635-46.
- JIN, J. M. & YANG, W. X. 2014. Molecular regulation of hypothalamus-pituitary-gonads axis in males. *Gene*, 551, 15-25.
- JOUSTRA, S. D., SCHOENMAKERS, N., PERSANI, L., CAMPI, I., BONOMI, M., RADETTI, G., BECK-PECCOZ, P., ZHU, H., DAVIS, T. M., SUN, Y., CORSSMIT, E. P., APPELMAN-DIJKSTRA, N. M., HEINEN, C. A., PEREIRA, A. M., VAREWIJCK, A. J., JANSSEN, J. A., ENDERT, E., HENNEKAM, R. C., LOMBARDI, M. P., MANNENS, M. M., BAK, B., BERNARD, D. J., BREUNING, M. H., CHATTERJEE, K., DATTANI, M. T., OOSTDIJK, W., BIERMASZ, N. R., WIT, J. M. & VAN TROTSBURG, A. S. 2013. The IGSF1 deficiency syndrome: characteristics of male and female patients. *J Clin Endocrinol Metab*, 98, 4942-52.
- KASSEL, K. M., AU DA, R., HIGGINS, M. J., HINES, M. & GRAVES, L. M. 2010. Regulation of human cytidine triphosphate synthetase 2 by phosphorylation. *J Biol Chem*, 285, 33727-36.
- KAUPPILA, A. 1997. Isolated prolactin deficiency. *Curr Ther Endocrinol Metab*, 6, 31-3.
- KAUPPILA, A., MARTIKAINEN, H., PUISTOLA, U., REINILA, M. & RONNBERG, L. 1988. Hypoprolactinemia and ovarian function. *Fertil Steril*, 49, 437-41.
- KEITH, B., ADELMAN, D. M. & SIMON, M. C. 2001. Targeted mutation of the murine arylhydrocarbon receptor nuclear translocator 2 (Arnt2) gene reveals partial redundancy with Arnt. *Proc Natl Acad Sci U S A*, 98, 6692-7.
- KELBERMAN, D. & DATTANI, M. T. 2007a. Genetics of septo-optic dysplasia. *Pituitary*, 10, 393-407.
- KELBERMAN, D. & DATTANI, M. T. 2007b. Hypothalamic and pituitary development: novel insights into the aetiology. *Eur J Endocrinol*, 157 Suppl 1, S3-14.
- KELBERMAN, D. & DATTANI, M. T. 2008. Septo-optic dysplasia - novel insights into the aetiology. *Horm Res*, 69, 257-65.

- KELBERMAN, D. & DATTANI, M. T. 2009. Role of transcription factors in midline central nervous system and pituitary defects. *Endocr Dev*, 14, 67-82.
- KELBERMAN, D., DE CASTRO, S. C., HUANG, S., CROLLA, J. A., PALMER, R., GREGORY, J. W., TAYLOR, D., CAVALLO, L., FAIENZA, M. F., FISCHETTO, R., ACHERMANN, J. C., MARTINEZ-BARBERA, J. P., RIZZOTI, K., LOVELL-BADGE, R., ROBINSON, I. C., GERRELLI, D. & DATTANI, M. T. 2008. SOX2 plays a critical role in the pituitary, forebrain, and eye during human embryonic development. *J Clin Endocrinol Metab*, 93, 1865-73.
- KELBERMAN, D., RIZZOTI, K., AVILION, A., BITNER-GLINDZICZ, M., CIANFARANI, S., COLLINS, J., CHONG, W. K., KIRK, J. M., ACHERMANN, J. C., ROSS, R., CARMIGNAC, D., LOVELL-BADGE, R., ROBINSON, I. C. & DATTANI, M. T. 2006. Mutations within Sox2/SOX2 are associated with abnormalities in the hypothalamo-pituitary-gonadal axis in mice and humans. *J Clin Invest*, 116, 2442-55.
- KELBERMAN, D., RIZZOTI, K., LOVELL-BADGE, R., ROBINSON, I. C. & DATTANI, M. T. 2009. Genetic regulation of pituitary gland development in human and mouse. *Endocr Rev*, 30, 790-829.
- KILDEBECK, E., CHECKETTS, J. & PORTEUS, M. 2012. Gene therapy for primary immunodeficiencies. *Curr Opin Pediatr*, 24, 731-8.
- KIM, S., PENG, Z. & KANEDA, Y. 2008. Current status of gene therapy in Asia. *Mol Ther*, 16, 237-43.
- KIMBALL, S. R. 1999. Eukaryotic initiation factor eIF2. *Int J Biochem Cell Biol*, 31, 25-9.
- KIMBALL, S. R., HEINZINGER, N. K., HORETSKY, R. L. & JEFFERSON, L. S. 1998. Identification of interprotein interactions between the subunits of eukaryotic initiation factors eIF2 and eIF2B. *J Biol Chem*, 273, 3039-44.
- KNOBLOCH, M., BRAUN, S. M., ZURKIRCHEN, L., VON SCHOULTZ, C., ZAMBONI, N., ARAUZO-BRAVO, M. J., KOVACS, W. J., KARALAY, O., SUTER, U., MACHADO, R. A., ROCCIO, M., LUTOLF, M. P., SEMENKOVICH, C. F. & JESSBERGER, S. 2013. Metabolic control of adult neural stem cell activity by Fasn-dependent lipogenesis. *Nature*, 493, 226-30.
- KRUDE, H., BIEBERMANN, H., LUCK, W., HORN, R., BRABANT, G. & GRUTERS, A. 1998. Severe early-onset obesity, adrenal insufficiency and red hair pigmentation caused by POMC mutations in humans. *Nat Genet*, 19, 155-7.
- LAMACZ, M., TONON, M. C., LOUISET, E., CAZIN, L. & VAUDRY, H. 1991. [The intermediate lobe of the pituitary, model of neuroendocrine communication]. *Arch Int Physiol Biochim Biophys*, 99, 205-19.
- LAMI, F., CARLI, D., FERRARI, P., MARINI, M., ALESI, V., IUGHETTI, L. & PERCESEPE, A. 2013. Holoprosencephaly: report of four cases and genotype-phenotype correlations. *J Genet*, 92, 97-101.
- LAMOLET, B., PULICHINO, A. M., LAMONERIE, T., GAUTHIER, Y., BRUE, T., ENJALBERT, A. & DROUIN, J. 2001. A pituitary cell-restricted T box factor, Tpit, activates POMC transcription in cooperation with Pitx homeoproteins. *Cell*, 104, 849-59.
- LANPHIER, E., URNOV, F., HAECKER, S. E., WERNER, M. & SMOLENSKI, J. 2015. Don't edit the human germ line. *Nature*, 519, 410-1.
- LAYMAN, L. C. 2007. Hypogonadotropic hypogonadism. *Endocrinol Metab Clin North Am*, 36, 283-96.
- LI, H., COLLADO, M., VILLASANTE, A., MATHEU, A., LYNCH, C. J., CANAMERO, M., RIZZOTI, K., CARNEIRO, C., MARTINEZ, G., VIDAL, A., LOVELL-BADGE, R. & SERRANO, M. 2012. p27(Kip1) directly represses Sox2 during embryonic stem cell differentiation. *Cell Stem Cell*, 11, 845-52.
- LI, H., WITTE, D. P., BRANFORD, W. W., ARONOW, B. J., WEINSTEIN, M., KAUR, S., WERT, S., SINGH, G., SCHREINER, C. M., WHITSETT, J. A. & ET AL. 1994. Gsh-4 encodes a LIM-

- type homeodomain, is expressed in the developing central nervous system and is required for early postnatal survival. *Embo j*, 13, 2876-85.
- LI, N., MU, H., ZHENG, L., LI, B., WU, C., NIU, B., SHEN, Q., HE, X. & HUA, J. 2016. EIF2S3Y suppresses the pluripotency state and promotes the proliferation of mouse embryonic stem cells. *Oncotarget*, 7, 11321-31.
- LIPPE, B., KAPLAN, S. A. & LAFRANCHI, S. 1979. Septo-optic dysplasia and maternal age. *Lancet*, 2, 92-3.
- LITT, M., QIU, Y. & HUANG, S. 2009. Histone arginine methylations: their roles in chromatin dynamics and transcriptional regulation. *Biosci Rep*, 29, 131-41.
- LIU, Y., FAN, M., YU, S., ZHOU, Y., WANG, J., YUAN, J. & QIANG, B. 2002. cDNA cloning, chromosomal localization and expression pattern analysis of human LIM-homeobox gene LHX4. *Brain Res*, 928, 147-55.
- LUTHER, M. J., HAUGE-EVANS, A., SOUZA, K. L., JORNS, A., LENZEN, S., PERSAUD, S. J. & JONES, P. M. 2006. MIN6 beta-cell-beta-cell interactions influence insulin secretory responses to nutrients and non-nutrients. *Biochem Biophys Res Commun*, 343, 99-104.
- MARKMILLER, S., CLOONAN, N., LARDELLI, R. M., DOGGETT, K., KEIGHTLEY, M. C., BOGLEV, Y., TROTTER, A. J., NG, A. Y., WILKINS, S. J., VERKADE, H., OBER, E. A., FIELD, H. A., GRIMMOND, S. M., LIESCHKE, G. J., STAINIER, D. Y. & HEATH, J. K. 2014. Minor class splicing shapes the zebrafish transcriptome during development. *Proc Natl Acad Sci U S A*, 111, 3062-7.
- MARTIN, E., PALMIC, N., SANQUER, S., LENOIR, C., HAUCK, F., MONGELLAZ, C., FABREGA, S., NITSCHKE, P., ESPOSTI, M. D., SCHWARTZENTRUBER, J., TAYLOR, N., MAJEWSKI, J., JABADO, N., WYNN, R. F., PICARD, C., FISCHER, A., ARKWRIGHT, P. D. & LATOUR, S. 2014. CTP synthase 1 deficiency in humans reveals its central role in lymphocyte proliferation. *Nature*, 510, 288-92.
- MAURIN, A. C., BENANI, A., LORSIGNOL, A., BRENACHOT, X., PARRY, L., CARRARO, V., GUISSARD, C., AVEROUS, J., JOUSSE, C., BRUHAT, A., CHAVEROUX, C., B'CHIR, W., MURANISHI, Y., RON, D., PENICAUD, L. & FAFOURNOUX, P. 2014. Hypothalamic eIF2alpha signaling regulates food intake. *Cell Rep*, 6, 438-44.
- MCCABE, M. J., ALATZOGLOU, K. S. & DATTANI, M. T. 2011a. Septo-optic dysplasia and other midline defects: the role of transcription factors: HESX1 and beyond. *Best Pract Res Clin Endocrinol Metab*, 25, 115-24.
- MCCABE, M. J., BANCALARI, R. E. & DATTANI, M. T. 2014. Diagnosis and evaluation of hypogonadism. *Pediatr Endocrinol Rev*, 11 Suppl 2, 214-29.
- MCCABE, M. J. & DATTANI, M. T. 2014. Genetic aspects of hypothalamic and pituitary gland development. *Handb Clin Neurol*, 124, 3-15.
- MCCABE, M. J., GASTON-MASSUET, C., TZIAFERI, V., GREGORY, L. C., ALATZOGLOU, K. S., SIGNORE, M., PUELLES, E., GERRELLI, D., FAROOQI, I. S., RAZA, J., WALKER, J., KAVANAUGH, S. I., TSAI, P. S., PITTELOU, N., MARTINEZ-BARBERA, J. P. & DATTANI, M. T. 2011b. Novel FGF8 mutations associated with recessive holoprosencephaly, craniofacial defects, and hypothalamo-pituitary dysfunction. *J Clin Endocrinol Metab*, 96, E1709-18.
- MCCABE, M. J., HU, Y., GREGORY, L. C., GASTON-MASSUET, C., ALATZOGLOU, K. S., SALDANHA, J. W., GUALTIERI, A., THANKAMONY, A., HUGHES, I., TOWNSHEND, S., MARTINEZ-BARBERA, J. P., BOULOUX, P. M. & DATTANI, M. T. 2015. Novel application of luciferase assay for the in vitro functional assessment of KAL1 variants in three females with septo-optic dysplasia (SOD). *Mol Cell Endocrinol*, 417, 63-72.
- MCCARTNEY, C. R. 2010. Maturation of sleep-wake gonadotrophin-releasing hormone secretion across puberty in girls: potential mechanisms and relevance to the pathogenesis of polycystic ovary syndrome. *J Neuroendocrinol*, 22, 701-9.

- MCCLUSKEY, J. T., HAMID, M., GUO-PARKE, H., MCCLENAGHAN, N. H., GOMIS, R. & FLATT, P. R. 2011. Development and functional characterization of insulin-releasing human pancreatic beta cell lines produced by electrofusion. *J Biol Chem*, 286, 21982-92.
- MCKEE, B. D. & HANDEL, M. A. 1993. Sex chromosomes, recombination, and chromatin conformation. *Chromosoma*, 102, 71-80.
- MCNAY, D. E., TURTON, J. P., KELBERMAN, D., WOODS, K. S., BRAUNER, R., PAPADIMITRIOU, A., KELLER, E., KELLER, A., HAUF, N., KRUDE, H., SHALET, S. M. & DATTANI, M. T. 2007. HESX1 mutations are an uncommon cause of septooptic dysplasia and hypopituitarism. *J Clin Endocrinol Metab*, 92, 691-7.
- MEHTA, A., HINDMARSH, P. C., MEHTA, H., TURTON, J. P., RUSSELL-EGGITT, I., TAYLOR, D., CHONG, W. K. & DATTANI, M. T. 2009. Congenital hypopituitarism: clinical, molecular and neuroradiological correlates. *Clin Endocrinol (Oxf)*, 71, 376-82.
- MENDONCA, B. B., OSORIO, M. G., LATRONICO, A. C., ESTEFAN, V., LO, L. S. & ARNHOLD, I. J. 1999. Longitudinal hormonal and pituitary imaging changes in two females with combined pituitary hormone deficiency due to deletion of A301,G302 in the PROP1 gene. *J Clin Endocrinol Metab*, 84, 942-5.
- MING, J. E. & MUENKE, M. 2002. Multiple hits during early embryonic development: digenic diseases and holoprosencephaly. *Am J Hum Genet*, 71, 1017-32.
- MOORTGAT, S., DESIR, J., BENOIT, V., BOULANGER, S., PENDEVILLE, H., NASSOGNE, M. C., LEDERER, D. & MAYSTADT, I. 2016. Two novel EIF2S3 mutations associated with syndromic intellectual disability with severe microcephaly, growth retardation, and epilepsy. *Am J Med Genet A*.
- MORTENSEN, A. H., MACDONALD, J. W., GHOSH, D. & CAMPER, S. A. 2011. Candidate genes for panhypopituitarism identified by gene expression profiling. *Physiol Genomics*, 43, 1105-16.
- MOUDEN, C., DUBOURG, C., CARRE, W., ROSE, S., QUELIN, C., AKLOUL, L., HAMDY-ROZE, H., VIOT, G., SALHI, H., DARNAULT, P., ODENT, S., DUPE, V. & DAVID, V. 2016. Complex mode of inheritance in holoprosencephaly revealed by whole exome sequencing. *Clin Genet*, 89, 659-68.
- NARANDA, T., SIRANGELO, I., FABBRI, B. J. & HERSHEY, J. W. 1995. Mutations in the NKXD consensus element indicate that GTP binds to the gamma-subunit of translation initiation factor eIF2. *FEBS Lett*, 372, 249-52.
- NEWBERN, K., NATRAJAN, N., KIM, H. G., CHORICH, L. P., HALVORSON, L. M., CAMERON, R. S. & LAYMAN, L. C. 2013. Identification of HESX1 mutations in Kallmann syndrome. *Fertil Steril*, 99, 1831-7.
- NG, P. C. & KIRKNESS, E. F. 2010. Whole genome sequencing. *Methods Mol Biol*, 628, 215-26.
- PAIN, V. M. 1996. Initiation of protein synthesis in eukaryotic cells. *Eur J Biochem*, 236, 747-71.
- PAVITT, G. D. & PROUD, C. G. 2009. Protein synthesis and its control in neuronal cells with a focus on vanishing white matter disease. *Biochem Soc Trans*, 37, 1298-310.
- PAVITT, G. D., RAMAIAH, K. V., KIMBALL, S. R. & HINNEBUSCH, A. G. 1998. eIF2 independently binds two distinct eIF2B subcomplexes that catalyze and regulate guanine-nucleotide exchange. *Genes Dev*, 12, 514-26.
- PEREZ MILLAN, M. I., BRINKMEIER, M. L., MORTENSEN, A. H. & CAMPER, S. A. 2016. PROP1 triggers epithelial-mesenchymal transition-like process in pituitary stem cells. *Elife*, 5.
- PFAEFFLE, R. W., HUNTER, C. S., SAVAGE, J. J., DURAN-PRADO, M., MULLEN, R. D., NEEB, Z. P., EIHOZLER, U., HESSE, V., HADDAD, N. G., STOBBE, H. M., BLUM, W. F., WEIGEL, J. F. & RHODES, S. J. 2008. Three novel missense mutations within the LHX4 gene are

- associated with variable pituitary hormone deficiencies. *J Clin Endocrinol Metab*, 93, 1062-71.
- PFÄFFLE, R. & KLAMMT, J. 2011. Pituitary transcription factors in the aetiology of combined pituitary hormone deficiency. *Best Pract Res Clin Endocrinol Metab*, 25, 43-60.
- PFÄFFLE, R. W., BLANKENSTEIN, O., WULLER, S. & KENTRUP, H. 1999. Combined pituitary hormone deficiency: role of Pit-1 and Prop-1. *Acta Paediatr Suppl*, 88, 33-41.
- PFÄFFLE, R. W., DIMATTIA, G. E., PARKS, J. S., BROWN, M. R., WIT, J. M., JANSEN, M., VAN DER NAT, H., VAN DEN BRANDE, J. L., ROSENFELD, M. G. & INGRAHAM, H. A. 1992. Mutation of the POU-specific domain of Pit-1 and hypopituitarism without pituitary hypoplasia. *Science*, 257, 1118-21.
- PLAWNER, L. L., DELGADO, M. R., MILLER, V. S., LEVEY, E. B., KINSMAN, S. L., BARKOVICH, A. J., SIMON, E. M., CLEGG, N. J., SWEET, V. T., STASHINKO, E. E. & HAHN, J. S. 2002. Neuroanatomy of holoprosencephaly as predictor of function: beyond the face predicting the brain. *Neurology*, 59, 1058-66.
- POLIZZI, A., PAVONE, P., IANNETTI, P., MANFRE, L. & RUGGIERI, M. 2006. Septo-optic dysplasia complex: a heterogeneous malformation syndrome. *Pediatr Neurol*, 34, 66-71.
- POTOK, M. A., CHA, K. B., HUNT, A., BRINKMEIER, M. L., LEITGES, M., KISPERT, A. & CAMPER, S. A. 2008. WNT signaling affects gene expression in the ventral diencephalon and pituitary gland growth. *Dev Dyn*, 237, 1006-20.
- PROUD, C. G. 2006. Regulation of protein synthesis by insulin. *Biochem Soc Trans*, 34, 213-6.
- QUAYNOR, S. D., BOSLEY, M. E., DUCKWORTH, C. G., PORTER, K. R., KIM, S. H., KIM, H. G., CHORICH, L. P., SULLIVAN, M. E., CHOI, J. H., CAMERON, R. S. & LAYMAN, L. C. 2016. Targeted next generation sequencing approach identifies nineteen new candidate genes in normosmic hypogonadotropic hypogonadism and Kallmann Syndrome. *Mol Cell Endocrinol*.
- RABBANI, B., TEKIN, M. & MAHDIEH, N. 2014. The promise of whole-exome sequencing in medical genetics. *J Hum Genet*, 59, 5-15.
- RAIVIO, T., AVBELJ, M., MCCABE, M. J., ROMERO, C. J., DWYER, A. A., TOMMISKA, J., SYKIOTIS, G. P., GREGORY, L. C., DIACZOK, D., TZIAFERI, V., ELTING, M. W., PADIDELA, R., PLUMMER, L., MARTIN, C., FENG, B., ZHANG, C., ZHOU, Q. Y., CHEN, H., MOHAMMADI, M., QUINTON, R., SIDIS, Y., RADOVICK, S., DATTANI, M. T. & PITTELOUD, N. 2012. Genetic overlap in Kallmann syndrome, combined pituitary hormone deficiency, and septo-optic dysplasia. *J Clin Endocrinol Metab*, 97, E694-9.
- REISINE, T., ROUGON, G., BARBET, J. & AFFOLTER, H. U. 1985. Corticotropin-releasing factor-induced adrenocorticotropin hormone release and synthesis is blocked by incorporation of the inhibitor of cyclic AMP-dependent protein kinase into anterior pituitary tumor cells by liposomes. *Proc Natl Acad Sci U S A*, 82, 8261-5.
- REYNAUD, R., JAYAKODY, S. A., MONNIER, C., SAVEANU, A., BOULIGAND, J., GUEDJ, A. M., SIMONIN, G., LECOMTE, P., BARLIER, A., RONDARD, P., MARTINEZ-BARBERA, J. P., GUIOCHON-MANTEL, A. & BRUE, T. 2012. PROKR2 variants in multiple hypopituitarism with pituitary stalk interruption. *J Clin Endocrinol Metab*, 97, E1068-73.
- RIZZOTI, K., BRUNELLI, S., CARMIGNAC, D., THOMAS, P. Q., ROBINSON, I. C. & LOVELL-BADGE, R. 2004. SOX3 is required during the formation of the hypothalamo-pituitary axis. *Nat Genet*, 36, 247-55.
- ROESSLER, E., DU, Y. Z., MULLOR, J. L., CASAS, E., ALLEN, W. P., GILLESSEN-KAESBACH, G., ROEDER, E. R., MING, J. E., RUIZ I ALTABA, A. & MUENKE, M. 2003. Loss-of-function mutations in the human GLI2 gene are associated with pituitary anomalies and holoprosencephaly-like features. *Proc Natl Acad Sci U S A*, 100, 13424-9.

- ROMERO, C. J., PINE-TWADDELL, E. & RADOVICK, S. 2011. Novel mutations associated with combined pituitary hormone deficiency. *J Mol Endocrinol*, 46, R93-r102.
- ROSENFELD, J. A., BALLIF, B. C., MARTIN, D. M., AYLSWORTH, A. S., BEJJANI, B. A., TORCHIA, B. S. & SHAFFER, L. G. 2010. Clinical characterization of individuals with deletions of genes in holoprosencephaly pathways by aCGH refines the phenotypic spectrum of HPE. *Hum Genet*, 127, 421-40.
- RYTHER, R. C., MCGUINNESS, L. M., PHILLIPS, J. A., 3RD, MOSELEY, C. T., MAGOULAS, C. B., ROBINSON, I. C. & PATTON, J. G. 2003. Disruption of exon definition produces a dominant-negative growth hormone isoform that causes somatotroph death and IGHD II. *Hum Genet*, 113, 140-8.
- SAJEDI, E., GASTON-MASSUET, C., ANDONIADOU, C. L., SIGNORE, M., HURD, P. J., DATTANI, M. & MARTINEZ-BARBERA, J. P. 2008a. DNMT1 interacts with the developmental transcriptional repressor HESX1. *Biochim Biophys Acta*, 1783, 131-43.
- SAJEDI, E., GASTON-MASSUET, C., SIGNORE, M., ANDONIADOU, C. L., KELBERMAN, D., CASTRO, S., ETCHEVERS, H. C., GERRELLI, D., DATTANI, M. T. & MARTINEZ-BARBERA, J. P. 2008b. Analysis of mouse models carrying the I26T and R160C substitutions in the transcriptional repressor HESX1 as models for septo-optic dysplasia and hypopituitarism. *Dis Model Mech*, 1, 241-54.
- SALVATORI, R., FAN, X., MULLIS, P. E., HAILE, A. & LEVINE, M. A. 2002. Decreased expression of the GHRH receptor gene due to a mutation in a Pit-1 binding site. *Mol Endocrinol*, 16, 450-8.
- SEGAL, T. Y., MEHTA, A., ANAZODO, A., HINDMARSH, P. C. & DATTANI, M. T. 2009. Role of gonadotropin-releasing hormone and human chorionic gonadotropin stimulation tests in differentiating patients with hypogonadotropic hypogonadism from those with constitutional delay of growth and puberty. *J Clin Endocrinol Metab*, 94, 780-5.
- SHARP, P. A. & BURGE, C. B. 1997. Classification of introns: U2-type or U12-type. *Cell*, 91, 875-9.
- SHENG, H. Z., MORIYAMA, K., YAMASHITA, T., LI, H., POTTER, S. S., MAHON, K. A. & WESTPHAL, H. 1997. Multistep control of pituitary organogenesis. *Science*, 278, 1809-12.
- SHEPPARD, M., SPENCER, R. N., ASHCROFT, R. & DAVID, A. L. 2016. Ethics and social acceptability of a proposed clinical trial using maternal gene therapy to treat severe early-onset fetal growth restriction. *Ultrasound Obstet Gynecol*, 47, 484-91.
- SHIAO, M. S., KHIL, P., CAMERINI-OTERO, R. D., SHIROISHI, T., MORIWAKI, K., YU, H. T. & LONG, M. 2007. Origins of new male germ-line functions from X-derived autosomal retrogenes in the mouse. *Mol Biol Evol*, 24, 2242-53.
- SHOHREH, R., SHERAFAT-KAZEMZADEH, R., JEE, Y. H., BLITZ, A. & SALVATORI, R. 2011. A novel frame shift mutation in the GHRH receptor gene in familial isolated GH deficiency: early occurrence of anterior pituitary hypoplasia. *J Clin Endocrinol Metab*, 96, 2982-6.
- SINGH, S., TOKHUNTS, R., BAUBET, V., GOETZ, J. A., HUANG, Z. J., SCHILLING, N. S., BLACK, K. E., MACKENZIE, T. A., DAHMANE, N. & ROBBINS, D. J. 2009. Sonic hedgehog mutations identified in holoprosencephaly patients can act in a dominant negative manner. *Hum Genet*, 125, 95-103.
- SLAVIN, T. P., NIELL-SWILLER, M., SOLOMON, I., NEHORAY, B., RYBAK, C., BLAZER, K. R. & WEITZEL, J. N. 2015. Clinical Application of Multigene Panels: Challenges of Next-Generation Counseling and Cancer Risk Management. *Front Oncol*, 5, 208.
- SLOOP, K. W., PARKER, G. E., HANNA, K. R., WRIGHT, H. A. & RHODES, S. J. 2001. LHX3 transcription factor mutations associated with combined pituitary hormone deficiency impair the activation of pituitary target genes. *Gene*, 265, 61-9.

- SOBRIER, M. L., NETCHINE, I., HEINRICHS, C., THIBAUD, N., VIE-LUTON, M. P., VAN VLIET, G. & AMSELEM, S. 2005. Alu-element insertion in the homeodomain of HESX1 and aplasia of the anterior pituitary. *Hum Mutat*, 25, 503.
- SOBRIER, M. L., TSAI, Y. C., PEREZ, C., LEHEUP, B., BOUCEBA, T., DUQUESNOY, P., COPIN, B., SIZOVA, D., PENZO, A., STANGER, B. Z., COOKE, N. E., LIEBHABER, S. A. & AMSELEM, S. 2016. Functional characterization of a human POU1F1 mutation associated with isolated growth hormone deficiency: a novel etiology for IGHD. *Hum Mol Genet*, 25, 472-83.
- SOLOMON, B. D., MERCIER, S., VELEZ, J. I., PINEDA-ALVAREZ, D. E., WYLLIE, A., ZHOU, N., DUBOURG, C., DAVID, V., ODENT, S., ROESSLER, E. & MUENKE, M. 2010. Analysis of genotype-phenotype correlations in human holoprosencephaly. *Am J Med Genet C Semin Med Genet*, 154c, 133-41.
- SOLOMON, N. M., ROSS, S. A., MORGAN, T., BELSKY, J. L., HOL, F. A., KARNES, P. S., HOPWOOD, N. J., MYERS, S. E., TAN, A. S., WARNE, G. L., FORREST, S. M. & THOMAS, P. Q. 2004. Array comparative genomic hybridisation analysis of boys with X linked hypopituitarism identifies a 3.9 Mb duplicated critical region at Xq27 containing SOX3. *J Med Genet*, 41, 669-78.
- SONG, S., SLIWERSKA, E., EMERY, S. & KIDD, J. M. 2017. Modeling Human Population Separation History Using Physically Phased Genomes. *Genetics*, 205, 385-395.
- STEINMULLER, R., STEINBERGER, D. & MULLER, U. 1998. MEHMO (mental retardation, epileptic seizures, hypogonadism and -genitalism, microcephaly, obesity), a novel syndrome: assignment of disease locus to xp21.1-p22.13. *Eur J Hum Genet*, 6, 201-6.
- STEVANOVIC, M., LOVELL-BADGE, R., COLLIGNON, J. & GOODFELLOW, P. N. 1993. SOX3 is an X-linked gene related to SRY. *Hum Mol Genet*, 2, 2013-8.
- SUN, Y., BAK, B., SCHOENMAKERS, N., VAN TROTSBURG, A. S., OOSTDIJK, W., VOSHOL, P., CAMBRIDGE, E., WHITE, J. K., LE TISSIER, P., GHARAVY, S. N., MARTINEZ-BARBERA, J. P., STOKVIS-BRANTSMA, W. H., VULSMA, T., KEMPERS, M. J., PERSANI, L., CAMPI, I., BONOMI, M., BECK-PECCOZ, P., ZHU, H., DAVIS, T. M., HOKKEN-KOELEGA, A. C., DEL BLANCO, D. G., RANGASAMI, J. J., RUIVENKAMP, C. A., LAROS, J. F., KRIEK, M., KANT, S. G., BOSCH, C. A., BIERMASZ, N. R., APPELMAN-DIJKSTRA, N. M., CORSSMIT, E. P., HOVENS, G. C., PEREIRA, A. M., DEN DUNNEN, J. T., WADE, M. G., BREUNING, M. H., HENNEKAM, R. C., CHATTERJEE, K., DATTANI, M. T., WIT, J. M. & BERNARD, D. J. 2012. Loss-of-function mutations in IGSF1 cause an X-linked syndrome of central hypothyroidism and testicular enlargement. *Nat Genet*, 44, 1375-81.
- TAJIMA, T., HATTORI, T., NAKAJIMA, T., OKUHARA, K., TSUBAKI, J. & FUJIEDA, K. 2007. A novel missense mutation (P366T) of the LHX4 gene causes severe combined pituitary hormone deficiency with pituitary hypoplasia, ectopic posterior lobe and a poorly developed sella turcica. *Endocr J*, 54, 637-41.
- TAJIMA, T., YORIFUJI, T., ISHIZU, K. & FUJIEDA, K. 2010. A novel mutation (V101A) of the LHX4 gene in a Japanese patient with combined pituitary hormone deficiency. *Exp Clin Endocrinol Diabetes*, 118, 405-9.
- TAKAGI, M., ISHII, T., INOKUCHI, M., AMANO, N., NARUMI, S., ASAKURA, Y., MUROYA, K., HASEGAWA, Y., ADACHI, M. & HASEGAWA, T. 2012. Gradual loss of ACTH due to a novel mutation in LHX4: comprehensive mutation screening in Japanese patients with congenital hypopituitarism. *PLoS One*, 7, e46008.
- TAKAGI, M., NARUMI, S., HAMADA, R., HASEGAWA, Y. & HASEGAWA, T. 2014. A novel KAL1 mutation is associated with combined pituitary hormone deficiency. *Hum Genome Var*, 1, 14011.
- TAN, W. L., BHATTACHARYA, B., LOH, M., BALASUBRAMANIAN, I., AKRAM, M., DONG, D., WONG, L., THAKKAR, B., SALTO-TELLEZ, M., SOO, R. A., FICHTNER, I., IACOPETTA, B.

- & SOONG, R. 2011. Low cytosine triphosphate synthase 2 expression renders resistance to 5-fluorouracil in colorectal cancer. *Cancer Biol Ther*, 11, 599-608.
- TARANOVA, O. V., MAGNESS, S. T., FAGAN, B. M., WU, Y., SURZENKO, N., HUTTON, S. R. & PEVNY, L. H. 2006. SOX2 is a dose-dependent regulator of retinal neural progenitor competence. *Genes Dev*, 20, 1187-202.
- TATSUMI, K., MIYAI, K., NOTOMI, T., KAIBE, K., AMINO, N., MIZUNO, Y. & KOHNO, H. 1992. Cretinism with combined hormone deficiency caused by a mutation in the PIT1 gene. *Nat Genet*, 1, 56-8.
- TECH, K. & GERSHON, T. R. 2015. Energy metabolism in neurodevelopment and medulloblastoma. *Transl Pediatr*, 4, 12-9.
- THOMAS, P. & BEDDINGTON, R. 1996. Anterior primitive endoderm may be responsible for patterning the anterior neural plate in the mouse embryo. *Curr Biol*, 6, 1487-96.
- THOMAS, P. Q., DATTANI, M. T., BRICKMAN, J. M., MCNAY, D., WARNE, G., ZACHARIN, M., CAMERON, F., HURST, J., WOODS, K., DUNGER, D., STANHOPE, R., FORREST, S., ROBINSON, I. C. & BEDDINGTON, R. S. 2001. Heterozygous HESX1 mutations associated with isolated congenital pituitary hypoplasia and septo-optic dysplasia. *Hum Mol Genet*, 10, 39-45.
- TING, N. S., KAO, P. N., CHAN, D. W., LINTOTT, L. G. & LEES-MILLER, S. P. 1998. DNA-dependent protein kinase interacts with antigen receptor response element binding proteins NF90 and NF45. *J Biol Chem*, 273, 2136-45.
- TOPALOGU, A. K. & KOTAN, L. D. 2016. Genetics of Hypogonadotropic Hypogonadism. *Endocr Dev*, 29, 36-49.
- TORRE, D. L. & FALORNI, A. 2007. Pharmacological causes of hyperprolactinemia. *Ther Clin Risk Manag*, 3, 929-51.
- TSUCHIMOTO, D., SAKAI, Y., SAKUMI, K., NISHIOKA, K., SASAKI, M., FUJIWARA, T. & NAKABEPPU, Y. 2001. Human APE2 protein is mostly localized in the nuclei and to some extent in the mitochondria, while nuclear APE2 is partly associated with proliferating cell nuclear antigen. *Nucleic Acids Res*, 29, 2349-60.
- TURANKAR, S., SONONE, K. & TURANKAR, A. 2013. Hyperprolactinaemia and its comparison with hypothyroidism in primary infertile women. *J Clin Diagn Res*, 7, 794-6.
- TURNER, J. M. 2015. Meiotic Silencing in Mammals. *Annu Rev Genet*, 49, 395-412.
- TURTON, J. P., REYNAUD, R., MEHTA, A., TORPIANO, J., SAVEANU, A., WOODS, K. S., TIULPAKOV, A., ZDRAVKOVIC, V., HAMILTON, J., ATTARD-MONTALTO, S., PARASCANDALO, R., VELLA, C., CLAYTON, P. E., SHALET, S., BARTON, J., BRUE, T. & DATTANI, M. T. 2005. Novel mutations within the POU1F1 gene associated with variable combined pituitary hormone deficiency. *J Clin Endocrinol Metab*, 90, 4762-70.
- VAN DEN BERG, A. A., VAN LENTHE, H., KIPP, J. B., DE KORTE, D., VAN KUILENBURG, A. B. & VAN GENNIP, A. H. 1995. Cytidine triphosphate (CTP) synthetase activity during cell cycle progression in normal and malignant T-lymphocytic cells. *Eur J Cancer*, 31a, 108-12.
- VAN DER KNAAP, M. S., LEEGWATER, P. A., KONST, A. A., VISSER, A., NAIDU, S., OUDEJANS, C. B., SCHUTGENS, R. B. & PRONK, J. C. 2002. Mutations in each of the five subunits of translation initiation factor eIF2B can cause leukoencephalopathy with vanishing white matter. *Ann Neurol*, 51, 264-70.
- VASU, S., MCCLENAGHAN, N. H., MCCLUSKEY, J. T. & FLATT, P. R. 2013. Cellular responses of novel human pancreatic beta-cell line, 1.1B4 to hyperglycemia. *Islets*, 5, 170-7.
- VERMEESCH, J. R., VOET, T. & DEVRIENDT, K. 2016. Prenatal and pre-implantation genetic diagnosis. *Nat Rev Genet*, 17, 643-656.

- WAGNER, J. K., EBLE, A., HINDMARSH, P. C. & MULLIS, P. E. 1998. Prevalence of human GH-1 gene alterations in patients with isolated growth hormone deficiency. *Pediatr Res*, 43, 105-10.
- WAKIL, S. J. 1989. Fatty acid synthase, a proficient multifunctional enzyme. *Biochemistry*, 28, 4523-30.
- WALLIS, D. E., ROESSLER, E., HEHR, U., NANNI, L., WILTSHIRE, T., RICHIERI-COSTA, A., GILLESSEN-KAESBACH, G., ZACKAI, E. H., ROMMENS, J. & MUENKE, M. 1999. Mutations in the homeodomain of the human SIX3 gene cause holoprosencephaly. *Nat Genet*, 22, 196-8.
- WALSH, R. M. & HOCHEDLINGER, K. 2013. A variant CRISPR-Cas9 system adds versatility to genome engineering. *Proc Natl Acad Sci U S A*, 110, 15514-5.
- WANG, Z., GERSTEIN, M. & SNYDER, M. 2009. RNA-Seq: a revolutionary tool for transcriptomics. *Nat Rev Genet*, 10, 57-63.
- WARD, R. D., RAETZMAN, L. T., SUH, H., STONE, B. M., NASONKIN, I. O. & CAMPER, S. A. 2005. Role of PROP1 in pituitary gland growth. *Mol Endocrinol*, 19, 698-710.
- WEBB, E. A., ALMUTAIR, A., KELBERMAN, D., BACCHELLI, C., CHANUDET, E., LESCAI, F., ANDONIADOU, C. L., BANYAN, A., ALSAWAID, A., ALRIFAI, M. T., ALAHMESH, M. A., BALWI, M., MOUSAVY-GHARAVY, S. N., LUKOVIC, B., BURKE, D., MCCABE, M. J., KASIA, T., KLETA, R., STUPKA, E., BEALES, P. L., THOMPSON, D. A., CHONG, W. K., ALKURAYA, F. S., MARTINEZ-BARBERA, J. P., SOWDEN, J. C. & DATTANI, M. T. 2013. ARNT2 mutation causes hypopituitarism, post-natal microcephaly, visual and renal anomalies. *Brain*, 136, 3096-105.
- WEBB, E. A. & DATTANI, M. T. 2010. Septo-optic dysplasia. *Eur J Hum Genet*, 18, 393-7.
- WIEDENHEFT, B., ZHOU, K., JINEK, M., COYLE, S. M., MA, W. & DOUDNA, J. A. 2009. Structural basis for DNase activity of a conserved protein implicated in CRISPR-mediated genome defense. *Structure*, 17, 904-12.
- WIERNAN, M. E., PAWLOWSKI, J. E., ALLEN, M. P., XU, M., LINSEMAN, D. A. & NIELSEN-PREISS, S. 2004. Molecular mechanisms of gonadotropin-releasing hormone neuronal migration. *Trends Endocrinol Metab*, 15, 96-102.
- WILLIAMSON, K. A., HEVER, A. M., RAINGER, J., ROGERS, R. C., MAGEE, A., FIEDLER, Z., KENG, W. T., SHARKEY, F. H., MCGILL, N., HILL, C. J., SCHNEIDER, A., MESSINA, M., TURNPENNY, P. D., FANTES, J. A., VAN HEYNINGEN, V. & FITZPATRICK, D. R. 2006. Mutations in SOX2 cause anophthalmia-esophageal-genital (AEG) syndrome. *Hum Mol Genet*, 15, 1413-22.
- WONG, J., FARLIE, P., HOLBERT, S., LOCKHART, P. & THOMAS, P. Q. 2007. Polyalanine expansion mutations in the X-linked hypopituitarism gene SOX3 result in aggresome formation and impaired transactivation. *Front Biosci*, 12, 2085-95.
- WOODS, K. S., CUNDALL, M., TURTON, J., RIZOTTI, K., MEHTA, A., PALMER, R., WONG, J., CHONG, W. K., AL-ZYUOD, M., EL-ALI, M., OTONKOSKI, T., MARTINEZ-BARBERA, J. P., THOMAS, P. Q., ROBINSON, I. C., LOVELL-BADGE, R., WOODWARD, K. J. & DATTANI, M. T. 2005. Over- and underdosage of SOX3 is associated with infundibular hypoplasia and hypopituitarism. *Am J Hum Genet*, 76, 833-49.
- WWW.1000GENOMES.ORG.
- WWW.EHD.ORG/VIRTUAL-HUMAN-EMBRYO/.
- WWW.EMAZE.COM.
- WWW.EVS.GS.WASHINGTON.EDU/EVS/.
- WWW.EXAC.BROADINSTITUTE.ORG.
- WWW.FIPAPATIENTS.ORG.
- WWW.GENOMICSENGLAND.CO.UK.
- WWW.INFORMATICS.JAX.ORG.
- WWW.NCBI.NLM.NIH.GOV.

WWW.NCBI.NLM.NIH.GOV/SNP/.

WWW.NHLBI.NIH.GOV/.

WWW.USMANSCIENCE.COM.

- YAMADA, M. & MORI, M. 2008. Mechanisms related to the pathophysiology and management of central hypothyroidism. *Nat Clin Pract Endocrinol Metab*, 4, 683-94.
- YAMAUCHI, Y., RIEL, J. M., RUTHIG, V. A., ORTEGA, E. A., MITCHELL, M. J. & WARD, M. A. 2016. Two genes substitute for the mouse Y chromosome for spermatogenesis and reproduction. *Science*, 351, 514-6.
- YAMAUCHI, Y., RIEL, J. M., STOYTCHIEVA, Z. & WARD, M. A. 2014. Two Y genes can replace the entire Y chromosome for assisted reproduction in the mouse. *Science*, 343, 69-72.
- YATIME, L., MECHULAM, Y., BLANQUET, S. & SCHMITT, E. 2007. Structure of an archaeal heterotrimeric initiation factor 2 reveals a nucleotide state between the GTP and the GDP states. *Proc Natl Acad Sci U S A*, 104, 18445-50.
- YIN, X., LI, Y., XU, G., AN, W. & ZHANG, W. 2009. Ghrelin fluctuation, what determines its production? *Acta Biochim Biophys Sin (Shanghai)*, 41, 188-97.
- ZARGAR, A. H., MASOODI, S. R., LAWAY, B. A., SHAH, N. A. & SALAHUDIN, M. 1997. Familial puerperal alactogenesis: possibility of a genetically transmitted isolated prolactin deficiency. *Br J Obstet Gynaecol*, 104, 629-31.
- ZHAO, E., LI, J., XIE, Y., JIN, W., ZHANG, Z., CHEN, J., ZENG, L., YIN, G., QIAN, J., WU, H., YING, K., ZHAO, R. C. & MAO, Y. 2003. Cloning and identification of a novel human RNPC3 gene that encodes a protein with two RRM domains and is expressed in the cell nucleus. *Biochem Genet*, 41, 315-23.
- ZIMMERMAN, E. A. & ANTUNES, J. L. 1976. Organization of the hypothalamic-pituitary system: current concepts from immunohistochemical studies. *J Histochem Cytochem*, 24, 807-15.
- ZUFFEREY, R., DONELLO, J. E., TRONO, D. & HOPE, T. J. 1999. Woodchuck hepatitis virus posttranscriptional regulatory element enhances expression of transgenes delivered by retroviral vectors. *J Virol*, 73, 2886-92.